Lancaster University

Characterising the role of the Amyloid Precursor Protein and Glucagon-like peptide-1 analogues in Age-Related Macular Degeneration

Fatima Sultan BSc (Hons)

Supervised by Dr Edward Parkin

This thesis is submitted in fulfilment of the degree of

Masters by Research in Biomedical Science

I, Fatima Sultan, confirm that the work presented in this thesis is my own work and has not been submitted in substantially the same form for the award of a higher degree elsewhere. Where information has been derived from other sources, I confirm this has been indicated in the thesis.

August 2021

Acknowledgments

I would like to thank my supervisor Dr. Ed Parkin for his continuous guidance and support during both the lab work and the writing up phase of my thesis. Without his continuous encouragement and motivation, this work would have never been accomplished.

I would also like to thank my family, my fiancé and all my friends who were always beside me to provide support in all means until this accomplishment was completed.

Thank you. I couldn't have done it without you!

Abstract

Age-related macular degeneration (AMD) is a progressive retinal neurodegenerative disorder characterised, in some forms of the disease, by the loss of photoreceptors and the underlying retinal pigment epithelium (RPE) in the macula due to the accumulation of extracellular deposits known as "drusen". A major component of drusen deposits is the Alzheimer's disease (AD)-related amyloid beta (Aβ)-peptide, a 4kDa peptide derived from the larger amyloid precursor protein (APP) through sequential cleavage by enzymes known as β- and γ-secretases. Alternatively, in the 'non-amyloidogenic' pathway, APP can be processed by a third enzyme, α-secretase, which cleaves within the Aβ region of the protein thereby preventing the production of toxic peptides as well as producing a larger soluble fragment, sAPPα, known for its neuroprotective and neurotrophic properties.

The current project aims to characterise the role played by APP and its proteolytic fragments in AMD using human retinal pigment epithelial cells (ARPE-19) and UV-A light (a known AMD risk factor) as the stressor. In addition, a group of diabetes drugs known as Glucagon Like Peptide-1 (GLP-1) analogues that have previously been purported to reduce neuronal death in AD and Parkinson's Disease (PD) have been tested for their ability to protect ARPE-19 cells against stress-inducing reagents relative to AMD (UV-A light, hydrogen peroxide and Aβ-peptides).

The results of the current study demonstrate that endogenous cell-associated full-length APP expression was depleted in ARPE-19 cells following UV-A irradiation. Furthermore, β-secretase but not α-secretase processing of the protein was reduced. Small interfering RNA-mediated depletion of endogenous APP or γ-secretase (but not α- or β-secretase) inhibition ablated the detrimental effect of UV-A on cell viability. In contrast, α-secretase and, possibly, γ-secretase but not β-secretase activity appeared to promote the longer-term proliferation of ARPE-19 cells in the absence of UV-A irradiation. Furthermore, two of the GLP-1 analogues tested, liraglutide and lixisenatide, were able to restore cell viability after UV-A exposure.

Collectively, these data indicate clear links between the expression/proteolysis of APP and the proliferation and resistance of ARPE-19 cells to UV-A irradiation. Whilst these effects are clearly differential, the data warrant further investigation of the role played by APP in AMD. Furthermore, the protective effects against UV-A shown by liraglutide and lixisenatide warrant further investigation of the molecular mechanisms involved with a view to identifying new drug targets for the prevention or treatment of retinal neurodegenerative diseases such as AMD.

Abbreviations

Aβ, amyloid-beta.

AcD, acidic domain.

AD, Alzheimer's disease.

ADAM, a disintegrin and metalloprotease.

AICD, APP intracellular domain.

AMD, age-related macular degeneration.

APH-1, anterior pharynx defective 1.

APP, amyloid precursor protein.

BACE1, beta-site APP-cleaving enzyme 1.

BCA, bicinchoninic acid.

BRB, blood-retinal barrier.

BSA, bovine serum albumin.

CAM, cell adhesion molecule.

CNV, choroidal neovascularisation.

CSF, cerebrospinal fluid.

CTF, C-terminal fragment.

CuBD, copper binding domain.

DMEM, Dulbecco's modified eagle medium.

DMSO, dimethyl sulfoxide.

DPP-4, dipeptidylpeptidase-4.

DTT, dithiothreitol.

ECL, enhanced chemiluminescence.

EGF, epidermal growth factor.

EGFR, epidermal growth factor receptor.

ERK1/2, extracellular signal-regulated kinases 1 and 2.

FBS, Foetal Bovine Serum.

GA, geographic atrophy.

GFLD, growth factor-like domain.

GLP-1, glucagon like peptide-1.

GLP-1R, glucagon like peptide-1 receptor.

HBD, heparin-binding domain.

HEK, human embryonic kidney.

ROS, reactive oxygen species.

hfRPE, human fetal retinal pigment epithelium.

hNSCs, human neural stem cells.

HRP, horse radish peroxidase.

HTT, huntingtin.

KPI, Kunitz-type protease inhibitor.

LB, liquid broth.

LTP, long-term potentiation.

MMP, matrix metalloprotease.

NGF, nerve growth factor.

ONH, optic nerve head.

PD, Parkinson's disease.

PEDF, pigment epithelium-derived factor.

PEN-2, presenilin enhancer 2.

PI3K, phosphatidylinositol 3-kinase.

PKB, protein kinase B.

PKC, protein kinase C.

PS1 and PS2, presenilin1 and 2.

PVDF, polyvinylidene fluoride.

RGC, retinal ganglion cells.

RPE, retinal pigment epithelium.

sAPPα, soluble APPα fragment.

sAPPβ, soluble APPβ fragment.

sAPP, secreted/soluble APP.

SD, standard deviation.

SDS-PAGE, Sodium Dodecyl Sulphate-Polyacrylamide Gel Electrophoresis.

siRNA, small interfering RNA.

SK, seborrheic keratosis.

T2DM, type-2 diabetes mellitus.

TACE, tumour necrosis factor-α converting enzyme.

TEMED, N,N,N',N'-Tetramethylethylenediamine.

TM, transmembrane.

TNFα, Tumour Necrosis Factor-α.

VEGF, vascular endothelial growth factor.

vPDT, verteporfin photosensitiser.

ZMP, zinc metalloprotease.

Table of Contents

Chapter 1

Literature Review

1.1. Introduction

Age-related macular degeneration (AMD) is an ocular disease classified under the umbrella of neurodegenerative diseases (Kaarniranta *et al.*, 2011). AMD pathology is characterised by extracellular deposits in the retina known as "drusen" which consist of amyloid-beta (Aβ) as a major component, a peptide well known in Alzheimer's Disease (AD) pathology to form extracellular aggregates known as "senile plaques" leading to neurotoxicity and synaptic loss in the brains of AD patients (Luibl *et al.*, 2006).

The purpose of the current project was to characterise the role of the amyloid precursor protein (APP) and its metabolites in AMD using retinal pigment epithelial cells (ARPE-19) which has a direct link to the pathology of AMD and the formation of drusen deposits.

Moreover, a group of diabetes drugs known as Glucagon Like Peptide-1 (GLP-1) analogues that have already shown promise for the treatment of neurodegenerative diseases such as AD and Parkinson's disease (PD) (Gejl *et al.*, 2016; Foltynie and Aviles-Olmos, 2014) were tested here for their ability to protect retinal derived cells against stress-inducing reagents relative to AMD pathology.

1.2. Age-related Macular Degeneration (AMD)

Age-related macular degeneration (AMD) is a progressive and currently incurable retinal disease caused by a deterioration of the macula; the central part of the retina responsible for detailed central vision (Parmet *et al.*, 2006). Loss of central vision can hinder normal daily activities such as reading, driving and recognising faces (Fig. 1.1).

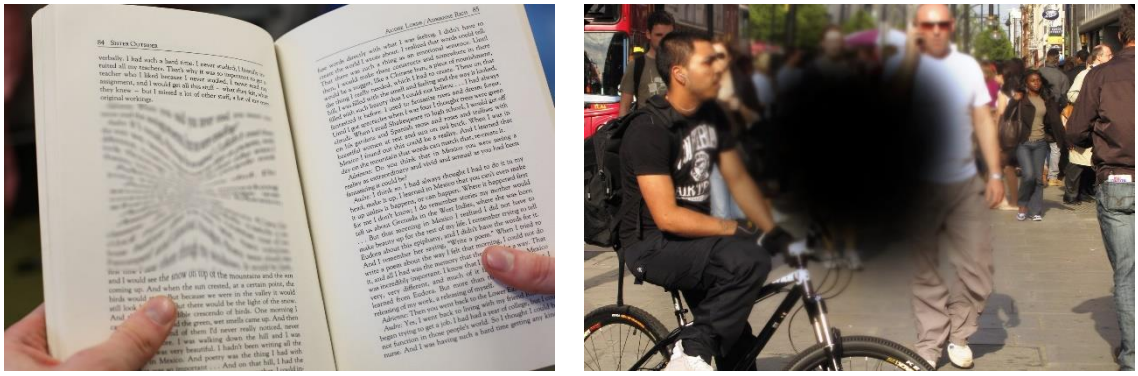

Figure 1.1. Loss of central vision in AMD affects daily activities. (Adapted from https://www.nhs.uk)

AMD is classified into early and late stages. Early AMD can develop into dry (atrophic) or wet (exudative) forms. Dry AMD is more prevalent and is associated with "drusen" deposits, small specks of yellowish white material, in the macula underneath the retina (Salvi *et al.*, 2006). Accumulation of these deposits leads to the gradual destruction of the retinal pigment epithelium (RPE) and the photoreceptors in the macular region (Mathenge, 2014). This manifests clinically with symptoms of blurred central vision that deteriorates gradually over time (Parmet *et al.*, 2006).

Wet AMD is less common; it accounts for approximately 15 % of AMD cases (Parmet *et al.*, 2006). However, the symptoms are severe and progress rapidly which makes it responsible for 90% of acute vision loss due to AMD (Hernández-Zimbrón *et al.*, 2018). Wet AMD is characterised by abnormal choroidal vessels developing underneath the macula and leaking blood and fluid. This eventually results in the formation of a central fibrous sub-retinal scar leading to a sudden decline in central visual acuity (Mathenge, 2014; Salvi *et al.*, 2006). A common symptom of wet AMD is straight lines appearing wavy or distorted (Parmet *et al.*, 2006).

1.2.1. Epidemiology

AMD is the leading cause of irreversible blindness in people aged 50 and older in developed countries and the third leading cause of visual disability globally (Pascolini and Mariotti, 2012). It has a global prevalence of 8.7% (Wong *et al.*, 2014) affecting 170 million people worldwide (Pennington

and DeAngelis, 2016). It is projected that the number of AMD patients will rise to 288 million in 2040 with the increased aging population (Wong *et al.*, 2014).

A systematic literature review by Wong *et al*. (2014) based on numerus epidemiological studies on AMD found a significant difference in prevalence between various ethnic groups and geographical regions (Fig. 1.2). It was shown that the prevalence of any age-related macular degeneration was higher in European ancestry populations (12.3 %) compared to Asian and African populations (7.4 % and 7.5 %, respectively) with the geographic atrophy subtype being more prevalent in Europeans (1.11 %) than in Asians (0.21 %), Africans (0.14 %) or Hispanics (0.16 %). In terms of geographical regions, the disease was also less prevalent in Asia compared to Europe and North America.

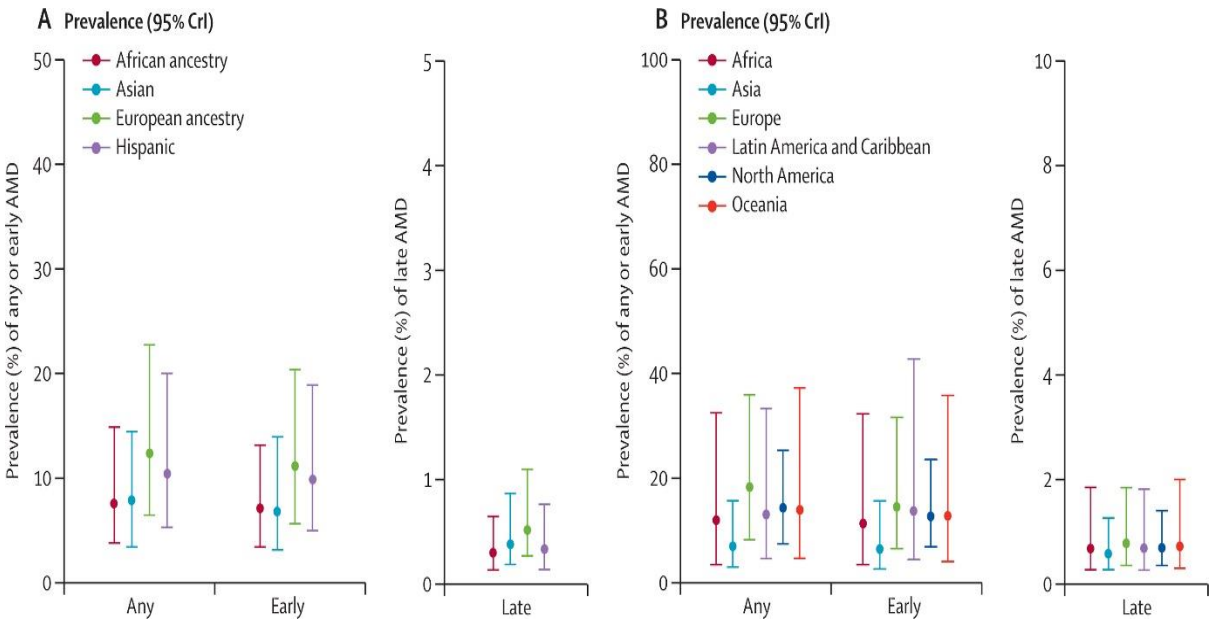

Figure 1.2. Prevalence of Age-related Macular Degeneration illustrated by ethnic group (A) and geographical region (B). (Wong *et al.*, 2014)

In contrast, other studies in African and Asian populations have demonstrated that AMD is a major contributor to blindness and visual disability in these countries (Mathenge *et al.*, 2012; Gupta *et al.*, 2007; Krishnan *et al.*, 2010).

A meta-analysis by Owen *et al.* (2012) applied to the UK population data of 2007-2009 found that the overall prevalence of late AMD in people aged 50 and older was 2.4 %. This equates to 513 000 cases which was estimated to increase by 71 000 new cases per year reaching 679 000 by 2020. The prevalence of geographic atrophy and neovascular AMD subtypes were 1.3 % and 1.2%, respectively, in the same age group (≥ 50).

This disease has a substantial impact on the physical and mental health of the aging population and their families and the numbers presented above reflect the substantial global and national burden of AMD especially with the exponential increase in the aged population.

1.2.2. Risk factors

Strong risk factors for AMD include advanced age, family history, genetic factors and smoking (Salvi *et al.*, 2006). Smoking is the most consistent risk factor particularly in people who have one or more of the AMD susceptibility genes (Mathenge, 2014). This is because smoking decreases the levels of antioxidant micronutrients in blood plasma, alters choroidal circulation (Evans, 2001) and exposes the macula to high levels of oxidative stress which might lead to inflammation inducing a vicious cycle resulting in the development of AMD and loss of central vision (Hernández-Zimbrón *et al.*, 2018).

Exposure to sunlight, especially blue light and UV light, is considered a possible risk factor in the development of AMD (Fletcher *et al.*, 2008; Vojniković *et al.*, 2007; Plestina-Borjan and Klinger-Lasić, 2007) although the evidence is still controversial (Zhou *et al.*, 2018). Epidemiologic evidence suggests that excessive light exposure is associated with increased risk of AMD (Chalam *et al.*, 2011). This is due to photochemical damage by the blue light and short wavelength radiation (UV-A radiation of 315-400 nm) that is able to penetrate the eye protective structures into the retina (Glickman, 2011). This induces significant oxidative stress to the retinal pigment epithelium and leads to the formation

of lipoprotein aggregates in Bruch's membrane and drusen deposits resulting finally in the destruction of photoreceptors in the macula and AMD development (Nowak *et al.*, 2005).

Other risk factors associated with the disease include hypertension, cardiovascular risk factors, increased body mass index, hyperopia (farsightedness), female gender and being from a non-Hispanic white ethnicity (Salvi *et al.*, 2006; Age-Related Eye Disease Study Research Group, 2000). Several studies have also associated diabetes mellitus as a risk factor for AMD (Chen *et al.*, 2014; Hahn *et al.*, 2013; Topouzis *et al.*, 2009; Choi *et al.*, 2011).

1.2.3. Pathology of the disease

Although the aetiology and pathogenesis of AMD are largely unclear, it is considered a multifactorial disease involving complex interactions between genetic and environmental factors (Ding *et al.*, 2009). The disease pathology is characterised by degeneration of the RPE, Bruch's membrane, the retinal photoreceptors and in some cases (the wet form) changes to the choroidal capillaries (Ding *et al.*, 2009) (Fig. 1.3).

Normal ageing processes occur in the human eye and these involve morphological changes to RPE cells, thickening of Bruch's membrane and the internal limiting membrane, which separates the neuronal retinal cells from the vitreous body, reduction in retinal neuronal elements and the presence of few small hard drusen (< 63 μm in diameter) (Elshatory *et al.,* 2019; Bonilha, 2008).

Drusen are insoluble extracellular aggregates localised beneath the basement membrane of RPE cells and towards the inner collagenous layer of Bruch's membrane (Fig 1.3A) (Rattner and Nathans, 2006). They appear in AMD as clusters of yellow-white deposits in the macular region and become more prominent as the overlying RPE becomes thinner with disease progression (Fig. 1.3B). Clinically, they are classified into hard and soft drusen based on their morphology. Hard drusen are normal in the ageing eye and not necessarily a sign of AMD if present in low numbers. They look like small yellowish punctate deposits less than 63 μm in size (Ding *et al.*, 2009). Soft drusen, however, are more of a serious risk factor for the development of AMD. They are paler in colour, larger in size and

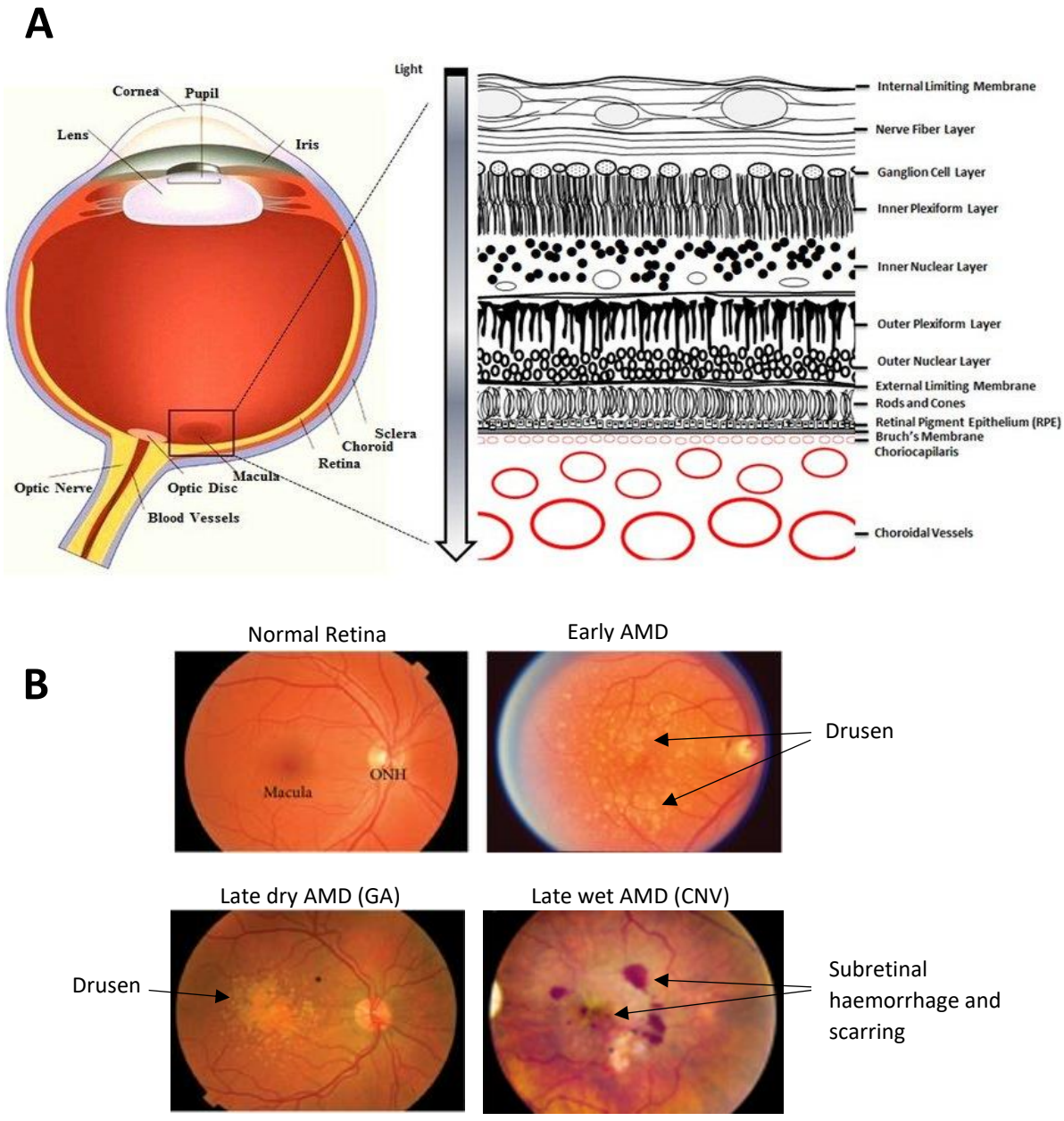

Figure 1.3. The structure of the eye and development of age-related macular degeneration (AMD) pathology. (A) A schematic diagram depicting a cross section of the eye showing the various structures and the macular region at the posterior segment of the eye. The enlarged diagram on the right shows the arrangement of retinal layers with RPE cells forming the blood-retinal barrier (BRB) at the bottom which separates the retina from the choroidal capillaries and vessels underneath. **(B) Fundus photographs of the various clinical stages of AMD in comparison to normal retina.** The normal retina shows a healthy macula and the optic nerve head (ONH). In early-stage AMD yellow extracellular drusen deposits accumulate around the macular region. Late dry AMD or Geographic Atrophy (GA) shows a large area of drusen accumulation at the macula with pigmentary changes of hypopigmentation indicating RPE cell death and hyperpigmentation (darkening) at the periphery of hypopigmented areas indicating RPE cell proliferation. Late wet AMD or choroidal neovascularisation (CNV) is characterised by choroidal vessels invading areas in the retina afflicted by drusen leading to subretinal haemorrhage and scaring. (Diagram and photos adapted from Ambati and Fowler, 2012; Gao *et al.*, 2015; Shahandeh *et al.*, 2015).

have a more diffuse appearance and blurry edges (Ding *et al.*, 2009). The molecular components of hard and soft drusen are similar. They contain lipids, lipoproteins, glycoproteins, ubiquitin, inflammatory molecules such as complements and immunoglobulins and the Alzheimer's disease amyloid beta (Aβ) (Anderson *et al.*, 2004; Mullins *et al.*, 2000; Hageman *et al.*, 2001).

Early stages of AMD involve thickening of Bruch's membrane, the accumulation of lipofuscin in the RPE cells and high amounts of drusen accumulation beneath the RPE (Ding *et al.*, 2009) (Fig. 1.4 A-C). A study by Young (1987) demonstrated that AMD is initiated in the RPE cells by the accumulation of lipofuscin. These are sacs of non-degradable residues originating from the breakdown of photoreceptor outer segments or from incomplete digestion of abnormal molecules within the RPE which accumulate throughout an individual's life span. When RPE cells become engorged with lipofuscin, they start expelling their content into Bruch's membrane where they accumulate in the form of drusen and basal laminar deposits (Young, 1987).

Clinically, early AMD is characterised by the presence of numerous intermediate drusen (larger than 63 μm in diameter but smaller than 125 μm) or pigmentary abnormalities (NICE guideline, 2018). When these changes develop into larger drusen (≥ 125 μm) or soft drusen with pigmentary abnormalities, the risk of progression into late AMD increases (NICE guideline, 2018; Klein *et al.*, 2002)

Late AMD is manifested in two main forms; late dry AMD (also known as geographic atrophy) and late wet (neovascular) AMD (Green, 1996). Geographic atrophy is characterised by large areas of hypopigmentation in the macula indicating RPE cell loss (Fig. 1.3B). This is accompanied by hyperpigmentation alterations which correspond to areas of RPE cell proliferation in order to compensate for cell loss (de Jong, 2006). RPE cell loss is followed by the gradual deterioration of the overlying retinal photoreceptors which depend on the RPE for metabolic and trophic support (Fig. 1.4D). Outer retinal layers including the outer plexiform and inner nuclear layer may also be affected leading to their degradation (Ding *et al.*, 2009). This eventually leads to retinal thinning and a progressive decline in visual acuity.

The hallmark of late-stage wet AMD is choroidal neovascularisation (CNV) wherein immature blood vessels sprouting from the choroidal vessels invade the areas distorted by drusen accumulation (Fig. 1.4E). These blood vessels penetrate Bruch's membrane growing into the subretinal space and the outer retina (Ambati and Fowler, 2012). They leak blood and fluid resulting in the formation of subretinal scars of fibrous tissue (Fig. 1.3B) which is associated clinically with acute decline in central vision and eventually central blindness (Ambati and Fowler, 2012; Mathenge, 2014).

Notably, there is a significant overlap between the two forms of AMD in terms of the underlying pathophysiology and it is possible, in some cases, that dry AMD develops into the neovascular AMD (Ambati and Fowler, 2012).

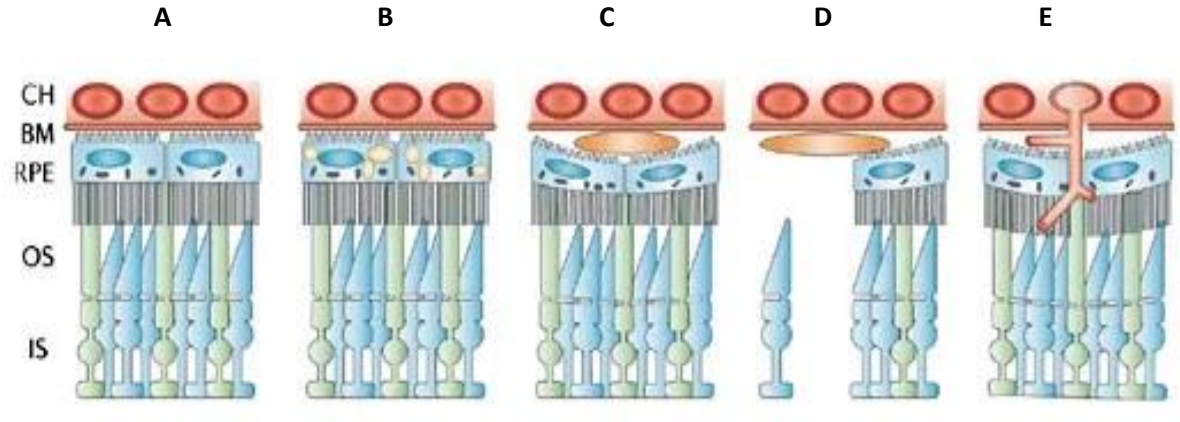

Figure 1.4. A schematic illustration of the various stages of AMD pathology at a cellular level. (A) The normal retina and retinal pigment epithelium (RPE). **(B)** Accumulation of lipofuscin in RPE cells. **(C)** A druse deposit separating the RPE cell basement membrane from Bruch's membrane (BM). **(D)** Degradation of the RPE and the overlying rods and cones photoreceptors due to drusen accumulation. **(E)** Choroidal neovascularisation. CH, choroid; OS, outer segments; IS, inner segments. (Rattner and Nathans, 2006).

Inflammation plays a prominent role in the pathology of both dry and wet AMD (Kauppinen *et al.*, 2016). In healthy states, the eye is an immune privileged organ which means that the immune system is downregulated in its tissues (Streilein, 2003) with RPE cells playing a vital role in this downregulation by creating the outer blood-retinal barrier (BRB). They form a monolayer of adjacent

cells tightly connected by adherence and tight junctions thereby decreasing permeability to immune related cells and molecules as well as secreting immunosuppressive factors (Zhou and Caspi, 2010; Thumann *et al.*, 2013). As such, the degradation of RPE due to drusen accumulation and AMD pathology compromises the BRB leading to increased permeability to immune cells and inflammatory factors causing a breach to the immune privileged organ (Ambati *et al.*, 2013). The recruitment of immune cells and complement factors and initiation of inflammation in the retinal tissues leads to increased RPE cell damage and further compromise to the BRB promoting a vicious cycle that potentiates inflammation and further degradation of the RPE and photoreceptors (Nussenblatt and Ferris, 2007; Ambati *et al.*, 2013). Indeed elements of the immune system were observed in eye tissues affected by AMD including the macrophages, the complement cascade and microglia (Chen *et al.*, 2008). Moreover, studies confirmed the presence of inflammation related molecules in drusen deposits including complement components (Nozaki *et al.*, 2006), various immunoglobulins (Hageman *et al.*, 2001) and Aβ (Anderson *et al.*, 2004) the latter of which is also central to the inflammation process observed in AD (Gold and El Khoury, 2015).

1.2.4. Current treatments

Laser treatment such as laser photocoagulation has been used as primary treatment for wet AMD in order to limit the damage resulting from choroidal neovascularisation (Chakravarthy *et al.*, 2013). Photodynamic therapy with verteporfin photosensitiser (vPDT) was later introduced as a treatment for wet AMD (Chakravarthy *et al.*, 2013). However, these treatments carry some risks and only slow the progression of the disease instead of improving vision. Laser photocoagulation, in particular, has a high recurrence rate, reduced efficiency in improving vision acuity and could induce vision loss (Elshatory *et al.,* 2019).

The introduction of vascular endothelial growth factor (VEGF) inhibitors has revolutionised the treatment of exudative (wet) AMD. Some of the approved drugs include pegaptanib (Macugen), ranibizumab (Lucentis), bevacizumab (Avastin), and aflibercept (Eylea) (Elshatory *et al.,* 2019). These

are administered as intravitreal injections applied in several doses and have shown effectiveness in stabilising vision with significant improvement in visual acuity reported in many cases (Mathenge, 2014).

Currently, there is no approved treatment for dry AMD. However, studies and trials are in development specially for the treatment of advanced stage disease (geographic atrophy). Some of the factors suggested as useful targets for drug development include oxidative stress, lipofuscin accumulation, inflammation and mutations associated with the complement pathway (Zarbin and Rosenfeld, 2010).

The use of antioxidant and mineral supplementation such as xanthophyll and zinc supplements has been shown to decrease the risk of developing late AMD (Coleman *et al.*, 2008; Scripsema *et al.*, 2015). In addition, some of the non-pharmacological recommendations include smoking cessation, the use of protective eye glasses, low vision aid and rehabilitation to improve the quality of life of patients and promote independent living (Mathenge, 2014).

1.2.5. *In vitro* models of AMD

As discussed earlier, treatment options are currently available to slow the progression of the wet form of the disease whereas no clinical treatment is available to treat dry AMD. *In vitro* cellular models have been developed to study the physiology and pathology of the disease and to test the use of drugs for the treatment of AMD (Forest *et al.*, 2015).

Although *in vivo* models are viewed as more physiologically relevant tools to study any disease, they are unable to recapitulate all aspects of AMD (Forest *et al.*, 2015). Cell-culture based *in vitro* models are advantageous in the sense that they are defined systems with the ability to control and manipulate experimental conditions to get a better understanding of the intricate disease environment and interactions between different tissues, cells and molecules (Hornof *et al.*, 2005).

Primary cell cultures of human fetal retinal pigment epithelium hfRPE are particularly useful *in vitro* models of AMD as they exhibit morphological and physiological features such as displaying a uniformed size and shape, polarity, protein expression patterns and metabolic activity similar to that of the native tissue (Ablonczy *et al.*, 2011; Maminishkis *et al.*, 2006). However, primary cell cultures have slow growth patterns and often described as "finite" as they lose the ability to proliferate and expand after limited amounts of passages (Segeritz and Vallier, 2017). Moreover, the cost of isolating and culturing primary cultures is often high as they require good handling expertise and rely on the continuous supply of stocks (Segeritz and Vallier, 2017). They might also behave differently with every cell division if optimum conditions were not maintained (Ramos *et al.*, 2014).

Other cell types utilised in AMD research include stem cells-derived RPE and the immortalised ARPE-19 cell line (Forest *et al.*, 2015). ARPE-19 cells are a spontaneously arising human cell line established by selective trypsinisation of a primary RPE culture (Dunn *et al.*, 1996). They were shown to exhibit the characteristic structural and functional features of RPE cells *in vivo* (Dunn *et al.*, 1996). Having strong growth potential, ARPE-19 cells were considered highly valuable tools for studying RPE physiology and pathology including in AMD research (Dunn *et al.*, 1996). Cell lines such as ARPE-19 offer several advantages over primary cultures including being cost effective, easy to handle, provide unlimited and pure population of cells which ensures consistent sample and reproducible results (Kaur and Dufour, 2012). On the other hand, there are limitations to the use of immortal cell lines including the low accuracy and physiological relevance compared to primary cells (Kaur and Dufour, 2012). Also, care must be taken when using cell lines as they might not act identically to their primary cells after several passages (Kaur and Dufour, 2012). A study by Ablonczy *et al.* (2011) concluded that the primary fhRPE cells resemble a functionally normal RPE *in vivo*, while ARPE-19 cells demonstrate the properties of a pathologic or aged RPE which in a way sets a specific use in research to each of these cell types.

Disease modelling such as cell culture models of the ocular barriers (cornea, conjunctiva, blood–retinal barrier) are more advanced *in vitro* techniques that combine the use of retinal derived

cell cultures with other membranes and connective tissues to resemble the *in vivo* environment and aid the understanding of drug transport into ocular tissues, investigating pathological ocular conditions, and as an alternative to *in vivo* toxicity screening of drug compounds (Hornof *et al.*, 2005).

1.3. Amyloid beta-peptide and the amyloid precursor protein in AMD

As described earlier (section 1.2.3), the accumulation of drusen deposits is a hallmark of AMD disease pathology. These deposits comprise a plethora of proteins, lipids, and other inflammation-related materials including the Alzheimer's disease-associated Aβ-peptide (Anderson *et al.*, 2004; Luibl *et al.*, 2006; Dentchev *et al.*, 2003). Recent studies have found that Aβ is not only a major component of drusen deposits but is also associated with key stages in AMD progression and is now thought to be linked to its aetiology (Ratnayaka *et al.*, 2015; Ohno-Matsui, 2011; Johnson *et al.*, 2002).

Multiple Aβ reservoirs exist in the normal eye (Fig. 1.5) including those originating in the retinal ganglion cells (RGC) and RPE which serve as major sources of Aβ synthesis and secretion (Ratnayaka *et al.*, 2015). When examining the distribution of APP in different eye regions, Sambamurti *et al.* (2007) observed high levels of APP expression in the retina and RPE cells as well as very large quantities of secreted APP in the vitreous humour. It is likely that the RPE and RGC cells are responsible for the majority of APP and Aβ production and secretion in the outer and inner retina, respectively (Fig. 1.5) (Ohno-Matsui, 2011). The RGCs synthesise APP which is then rapidly transported in small vesicles into the optic nerve to reach the axonal plasma membrane and the synapses (Morin *et al.*, 1993; Kipfer-Kauer *et al.*, 2010). APP and Aβ expression was also found in the pial/dural tissues which are the meningeal layers surrounding the optic nerve (Goldblum *et al.*, 2007).

In fact, APP is thought to be required for the normal function of the rod and cone pathways as observed in an electroretinogram study of APP knockout mice (Ho *et al.*, 2012). However, Aβ burden increases with senescence due to increased synthesis and decreased clearance (Ratnayaka *et al.*, 2015). As with AD pathology, Aβ tends to aggregate and form extracellular deposits (drusen in AMD and senile plaques in AD). Aβ is located in drusen within substructural vesicular components named

amyloid vesicles which are co-localized with activated complement components (Johnson *et al.*, 2002). This indicates that Aβ aggregates could be the primary sites for complement activation and a key factor in driving local inflammation which leads to RPE atrophy, drusen biogenesis and AMD development.

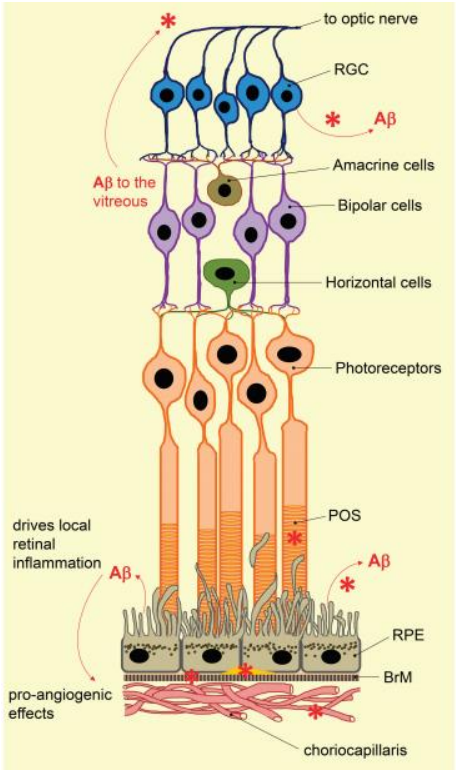

Figure 1.5. A schematic illustration of the various Aβ reservoirs (red asterisks) in the aging eye including locations of synthesis, secretion, and aggregation. RGC, retinal ganglion cells; RPE, retinal pigment epithelium; POS, photoreceptor outer segment; BrM, Bruch's Membrane. (Ratnayaka *et al.*, 2015)

A study by (Prasad *et al.*, 2017) demonstrated that intraocular injection of mice with Aβ-peptides induced the accumulation of drusen which were immunopositive for Aβ and complement proteins and led to degenerative changes in the retina mimicking AMD-like pathology. Conversely it has been shown that knocking down the Aβ-degrading enzyme neprilysin leads to the development of AMD-like pathology in mice including the degeneration of RPE cells and the development of drusen-like deposits (Ohno-Matsui, 2011). Several other studies have linked AD with AMD suggesting a common pathogenic mechanism between the two diseases and implicating Aβ toxicity in the retinal

degeneration observed in AMD (Ong *et al.*, 2019; Kaarniranta *et al.*, 2011; Ning *et al.*, 2008; Frost *et al.*, 2016). Ning *et al.* (2008) studied AMD development in the retina of a mouse model of AD and demonstrated a significant age-dependant deposition of Aβ in the nerve fibre layer and an overall increase in the expression of APP in the neuroretina including the RGC and the inner nuclear layer; a phenomenon that was accompanied by increased levels of inflammatory and apoptotic markers leading to the degeneration of the retina. Frost *et al.* (2016) found evidence to suggest an increased risk of AMD in AD patients. In a cohort study, the AD group showed a significantly greater proportion of participants with early AMD compared to the cognitively normal group (Frost *et al.*, 2016). Conversely, a study by Klaver *et al.* (1999) examining the relation between AMD and AD found evidence of an increased risk of developing AD in individuals with advanced AMD.

In addition to its role in dry AMD, Aβ was also found to play an important role in the development of CNV (the wet form of the disease) by increasing the expression of VEGF and decreasing the expression of pigment epithelium-derived factor (PEDF) secreted by RPE cells which acts as a potent antiangiogenic factor (Dawson *et al.*, 1999; Yoshida *et al.*, 2005; Koyama *et al.*, 2008).

1.3.1. APP structure and function

Aβ-peptides are derived from the amyloid precursor protein (APP) which is a transmembrane protein that plays major roles in several important cellular functions, most notably in the nervous system although it is ubiquitously expressed (Gralle and Ferreira, 2007). Although the precise physiological function of the protein remains to be fully elucidated, APP in the CNS is known to be involved in synaptogenesis and synaptic plasticity during development and in adulthood (Gralle and Ferreira, 2007). The protein acts as a contact receptor and a diffusible factor to drive tissue morphogenesis and restructuring (Gralle and Ferreira, 2007). During the early stages of neurodevelopment, APP serves as a cell adhesion molecule (CAM) which, together with other CAMs, facilitates migration of developing neurons from the ventricular zones to the appropriate layer in the cortex (Valiente and Marin, 2010). APP also collaborates with other proteins to generate neuronal axons with growth cones and direct them to form synapses at the correct targets (Lowery and Van

Vactor, 2009; Sosa *et al.*, 2017). A recent study has found that APP is located within the presynaptic active zone where it is involved in the regulation of synaptic vesicle lifespan, exo- and endocytosis, cytoskeletal rearrangement and mitochondrial activity highlighting the role of the protein within the presynapse (Laßek *et al.*, 2016).

The amyloid precursor protein is a single-pass (type 1) transmembrane glycoprotein with a large ectodomain and a shorter intracellular tail at the C-terminus (Sosa *et al.*, 2017). The APP ectodomain consists of four main domains; two of them are rigidly folded domains (named E1 and E2) and the other two, the acidic domain and the juxtamembrane region, are highly flexible and extended domains which connect E1 to E2 and the E2 to the single transmembrane helix, respectively (Fig. 1.6) (Coburger *et al.*, 2013). The globular E1 domain consists of two subdomains; the heparin-binding domain (HBD) (also called the growth-factor-like-domain, GFLD) which has been implicated in neurite outgrowth and the copper/metal-binding domain (CuBD). The helix-rich E2 domain is also subdivided into a heparin-binding site and metal-binding sites. It contains the RERMS amino acid sequence motif which is known to induce cell growth and neurite extension (Jin *et al.*, 1994). The APP intracellular domain has significant roles as a transcription factor regulating gene expression (Müller *et al.*, 2007), in apoptosis (Bertrand *et al.*, 2001) and in several other events related to the YENPTY sequence (Sosa *et al.*, 2017). This amino acid sequence is recognised by several adaptor proteins involved in cytoskeletal dynamics, cell adhesion, migration, and synaptogenesis (Sosa *et al.*, 2017; Muller *et al.*, 2008).

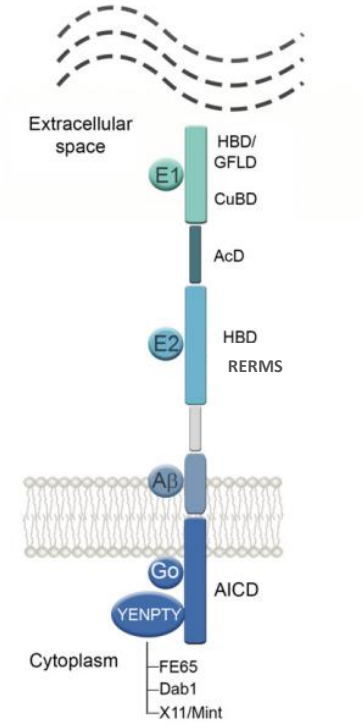

Figure 1.6. A schematic diagram of APP structure. APP consists of a large extracellular domain, a single transmembrane segment, and a short cytoplasmic tail. HBD, heparin-binding domain; GFLD, growth factor-like domain; CuBD, copper binding domain; AcD, acidic domain; AICD, APP intracellular domain. (Sosa *et al.*, 2017).

The *APP* gene is located on chromosome 21 and consists of 19 exons, three of which (exons 7, 8 and 15) can be alternatively spliced (De Strooper and Annaert, 2000) giving rise to at least 8 different isoforms (Bayer *et al.*, 1999). Three isoforms (APP_{695}, APP_{751} and APP_{770}) are the most common with APP_{695} being the predominantly expressed isoform in the CNS (Yoshikai *et al.*, 1990) and APP_{751} and APP_{770} being expressed more ubiquitously (Yoshida *et al.*, 2005; Wang *et al.*, 2011). The APP_{695} isoform lacks the Kunitz-type protease inhibitor (KPI) domain which exists in the other two splice variants (APP_{751} and APP_{770}), whereas APP_{770} contains an additional domain (the OX- 2 domain) which is absent in the other two isoforms (Chua *et al.*, 2013).

APP becomes post-translationally modified whilst trafficking through the secretory pathway in the endoplasmic reticulum and Golgi apparatus, by N-glycosylation and O-glycosylation, sulphation and phosphorylation as well as by proteolytic cleavage at the cell surface (Weidemann *et al.*, 1989; Walter and Haass, 2000).

1.3.2. APP proteolysis

The amyloid precursor protein is proteolytically processed in a rapid and highly complex manner by a range of enzymes (O'Brien and Wong, 2011; Sun *et al.*, 2015). However, broadly speaking, APP processing can be classified into the amyloidogenic pathway and the non-amyloidogenic pathways (Fig. 1.7). In the former, the protein is first cleaved by β-secretase at the N-terminus of the Aβ-domain (Fig. 1.7A) producing a soluble fragment (sAPPβ) and a C-terminal fragment (β-CTF or C99) (Fig. 1.7B). This is followed by γ-secretase cleavage at one of the sites between +40 and +44 (Aβ-peptide numbering) which leads to the generation of intact Aβ-peptides, most commonly Aβ40 and Aβ42 known to accumulate and form toxic aggregates in neurodegenerative diseases. Additionally, an APP intracellular domain (AICD) is produced following γ-secretase cleavage of β-CTF. Alternatively, APP can undergo non-amyloidogenic processing in which an α-secretase activity (Prakasam *et al.*, 2010) cleaves within the Aβ domain (between Lys16 and Leu17) thus producing a large soluble ectodomain (sAPPα) and a shorter C-terminal fragment (α-CTF or C83) (Fig. 1.7C). Subsequent cleavage of the α-CTF by γ-secretase generates an N-terminally truncated version of Aβ called p3 which is known to be less toxic and aggregation prone than Aβ (Dulin *et al.*, 2008). As with the amyloidogenic pathway, AICD is also produced by this latter cleavage and may function as a transcription factor (Multhaup *et al.*, 2015).

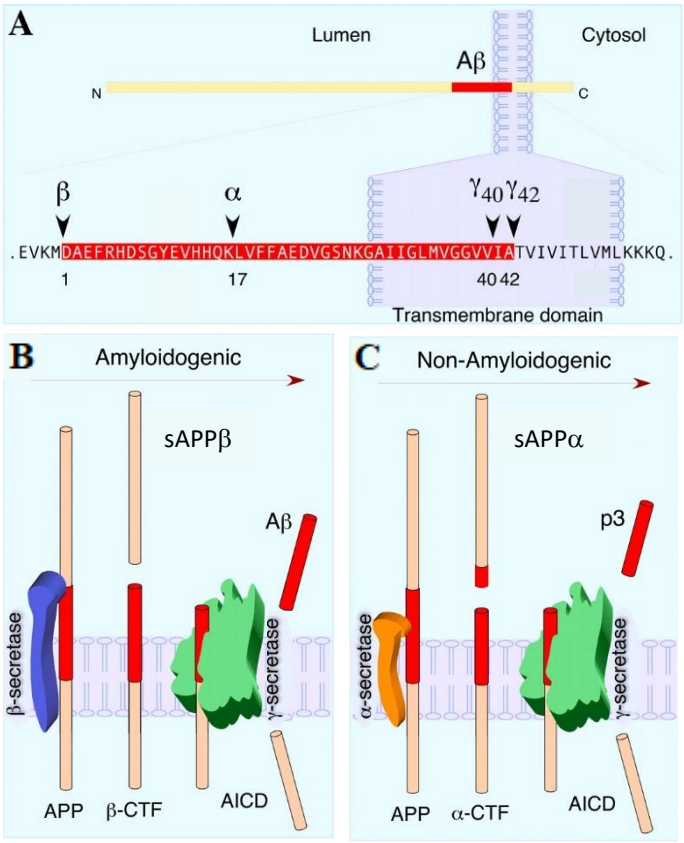

Figure 1.7. The proteolytic processing of the amyloid precursor protein (APP). (A) APP consisting of a large N-terminal ectodomain, a short intracellular C-terminus and a single transmembrane segment with Aβ domain coloured *red* and enlarged. The cleavage points of α-, β- and γ- secretases are also indicated with numbering starting from the N-terminus of the Aβ amino acid sequence. **(B)** Amyloidogenic processing of APP by β- and γ-secretases generating a soluble APPβ fragment (sAPPβ), intact Aβ and APP intracellular domain (AICD). **(C)** Non-amyloidogenic processing of APP by α- and γ- secretase cleavage yielding soluble APPα fragment (sAPPα), N-terminally truncated Aβ (p3) and AICD. CTF; C-terminal fragment. (Adapted from Thinakaran and Koo, 2008).

1.3.2.1. α- secretase

α-secretase cleavage is the predominant APP processing pathway outside the CNS and under normal physiological conditions (Sisodia *et al.*, 1990; De Strooper *et al.*, 2010). The ADAM (a disintegrin and metalloprotease) family of membrane-bound proteases are responsible for the α-secretase cleavage of APP between Lys16 and Leu17 of the Aβ domain (Asai *et al.*, 2003) and their participation in this manner can be subdivided into constitutive and protein kinase C (PKC)-regulated α-secretase activities (LeBlanc *et al.*, 1998; Mills and Reiner, 1999). Constitutive α-secretase activity is largely attributed to ADAM10 (Lammich *et al.*, 1999; Postina *et al.*, 2004) while α-secretase activity mediated

by other members of the ADAM family (including ADAM9 and ADAM17/TACE (tumour necrosis factor-α converting enzyme) has been linked to regulated activity (Buxbaum *et al.*, 1998; Weskamp *et al.*, 2002; Koike *et al.*, 1999).

The ADAM family of zinc metalloproteinases have a common modular domain structure (Fig. 1.8A, (Zhang *et al.*, 2016)) and are glycoproteins consisting of distinct extracellular domains starting with a signal peptide at the N-terminus that directs the protein to the secretory pathway. This is followed by a pro-domain which maintains enzyme inactivity as well as acting as an intramolecular chaperone ensuring the protein is folded into the correct tertiary structure (Edwards *et al.*, 2008). The pro-domain is removed in the mature protein (Roghani *et al.*, 1999). Further domains are the catalytic or metalloprotease domain which is a globular structure comprising two subdomains and the active site which contains the Zinc atom (Fig. 1.8B, (Edwards *et al.*, 2008)), a disintegrin domain (related to their interaction with integrin receptors in cell adhesion (Bridges and Bowditch, 2005)), a cysteine-rich domain and an epidermal growth factor-like (EGF-like) domain (Lammich *et al.*, 1999; De Strooper *et al.*, 2010). Notably, ADAM10 and ADAM17 lack the EGF-like domain (Janes *et al.*, 2005). Additionally, there is a transmembrane domain and a cytoplasmic tail which has a role in several ADAM family members in specifying binding sites for signal transducing proteins (Seals and Courtneidge, 2003). Such adapter protein interaction with the cytoplasmic tail of the ADAM could impact its maturation, trafficking, membrane localisation, interaction with cytoskeletal proteins or affect its proteolytic activity (White *et al.,* 2005).

There are 38 *adam* genes described in a variety of species, 21 of which were found in humans (Edwards *et al.*, 2008; Brocker *et al.*, 2009). Several ADAMs (including ADAMs 2, 7, 18, 20, 21, 29 and 30) are primarily expressed in the testis and associated tissues (Seals and Courtneidge, 2003). Other members (including ADAMs 8, 9, 10, 11, 12, 15, 17, 19, 22, 23, 28 and 33) are more broadly expressed including in the central nervous system (Sagane *et al.*, 1999; Seals and Courtneidge, 2003).

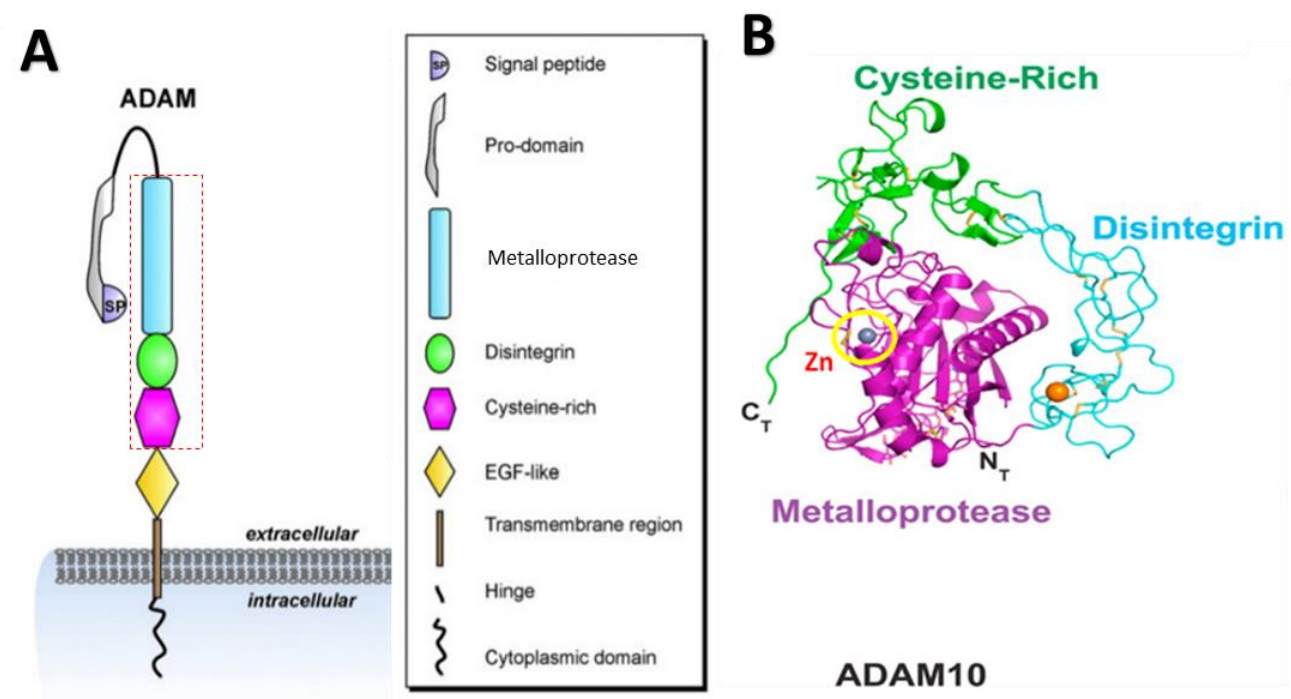

Figure 1.8. The structure of the ADAM family of zinc metalloproteinases with focus on ADAM10. (A) A schematic diagram of the domain organisation of the ADAM family. ADAM (a disintegrin and metalloproteinase) general structure includes a large extracellular domain which consists of a signal peptide followed by a pro-domain, a metalloprotease domain, a disintegrin domain, a cysteine-rich domain and an epidermal growth factor-like (EGF-like) domain, a transmembrane region and a cytoplasmic domain. Domains are not drawn to scale. The red dashed-line box contains the portion enlarged in the ADAM10 diagram (Panel B). **(B) The architecture of the mature ADAM10 ectodomain.** The active site of ADAM10 is characterised by the presence of a zinc atom (the grey sphere)**.** (Adapted from Zhang *et al.*, 2016; Seegar *et al.*, 2017).

α-secretase cleavage occurs constitutively and can be stimulated above its constitutive levels which is referred to as the regulated α-secretase cleavage (Lichtenthaler, 2011). Various ADAM family members were suggested as potential constitutive α-secretases based on *in vitro* studies showing the candidate protease can cleave APP-derived synthetic peptides and APP α-secretase cleavage increased as a result of its over-expression (Lichtenthaler, 2011; Allinson *et al.*, 2003; Deuss *et al.*, 2008). ADAM10, ADAM9 and ADAM17 were the most studied ADAM family members and were all suggested as constitutive α-secretases (Koike *et al.*, 1999; Lammich *et al.*, 1999; Slack *et al.*, 2001; Asai *et al.*, 2003). Furthermore, Tanabe *et al.* (2007) suggested that ADAM19 is closely associated with constitutive α-secretase activity. This was confirmed by observing increased levels of sAPPα when

ADAM19 was overexpressed in HEK293 cells. Moreover, constitutive sAPPα levels were reduced by 21% as a result of silencing ADAM19 with RNAi in human glioblastoma A172 cells (Tanabe *et al.*, 2007). However, the same study argued that ADAM19 may not be the main α-secretase in neurons given the minor effect on sAPPα levels when the protease was silenced. Also, ADAM19 was not able to cleave isolated APP derived peptides *in vitro* indicating that ADAM19 might contribute to constitutive α-secretase activity through the activation of other ADAMs (Tanabe *et al.*, 2007). Additionally, ADAM8 was investigated as a potential α-secretase by Naus *et al.* (2006) who demonstrated that it could cleave APP derived peptides in HEK cells at a similar efficacy to that of ADAM10. However, ADAM8 cleaves APP between His14 and Gln15 (Aβ numbering) which is slightly different to the known α-cleavage site (between Lys16 and Leu17 of the Aβ domain) (Amour *et al.*, 2002; Naus *et al.*, 2006). ADAM33 was also studied with regards to its α-secretase activity by Zou *et al.* (2004) who found that it was able to cleave APP derived peptides. However, the later study also found that, similar to ADAM8, ADAM33 cleaves APP at His14↓Gln15 (Aβ numbering) and with low efficiency indicating that it might not be a physiologically relevant α-secretase. Moreover, in cell-based co-transfection experiments ADAM33 acted as a negative regulator of APP shedding by decreasing levels of its secreted forms (Zou *et al.*, 2004).

ADAM9 was originally thought to be responsible, at least in part, for α-secretase cleavage of APP due to its ability to increase phorbol ester-regulated sAPPα generation when co-expressed in COS cells (Koike *et al.*, 1999; Hotoda *et al.*, 2002). However, Roghani *et al.* (1999) showed that ADAM9 was able to cleave an APP derived peptide at the His14↓Gln15 site withing the Aβ region but not at the regular α- site (Lys16↓Leu17) cleaved by ADAM10. Moreover, hippocampal neurons derived from ADAM9 knockout mice showed unaltered levels of APP cleavage products p3 and Aβ-peptides compared to wild-type neurons arguing against a major role of this ADAM family member in constitutive α-secretase shedding (Weskamp *et al.*, 2002). Later studies demonstrated that ADAM9 is not directly involved in APP α-secretase shedding but instead it acts indirectly through an effect on

ADAM10 (Cissé *et al.*, 2005; Parkin and Harris, 2009). Cissé *et al.* (2005) showed that ADAM9 was unable to rescue sAPPα generation in fibroblasts lacking ADAM10, however, it did enhance sAPPα production in the same cells when co-expressed with ADAM10. In fact, several studies suggest that ADAM9 and ADAM15 are involved in the shedding of ADAM10 from the cell surface (Parkin and Harris, 2009; Cissé *et al.*, 2005; Tousseyn *et al.*, 2009), a process that leads to the generation of a C-terminal fragment from ADAM10 which acts as a signal transducing molecule involved in gene regulation (Tousseyn *et al.*, 2009). Although, it is not clear how this process contributes to α-secretase shedding, it is thought to eventually increases the processing of APP through the non-amyloidogenic pathway and, therefore, enhance sAPPα production (Gough *et al.*, 2011).

Regarding ADAM17, it was concluded that this protease is important for the regulated but not the constitutive α-secretase cleavage given that embryonic fibroblasts derived from ADAM17 knockout mice showed deficiency in phorbol-ester regulated α-secretase activity while constitutive APP shedding was unaffected (Buxbaum *et al.*, 1998). Similarly, only regulated but not basal APP secretion was affected when human primary neuron cultures were treated with an inhibitor specific to ADAM17 (Blacker *et al.*, 2002). On the other hand, data from several *in vitro* cell culture studies suggested that ADAM17 could be involved in both constitutive and regulated α-secretase activity, however, in a cell-type dependant manner (Slack *et al.*, 2001; Hiraoka *et al.*, 2007; Asai *et al.*, 2003; Gough *et al.*, 2011). Furthermore, by studying the kinetics of APP cleavage by ADAM17 Mohan *et al.* (2002) found that this ADAM family member cleaves TNFα (Tumour Necrosis Factor-α) much more efficiently than other substrates including APP which is cleaved slowly and at much higher enzyme concentrations.

In light of what was discussed in the literature regarding the roles of the various ADAMs in α-secretase activity and by using novel reagents and methods, it was concluded that ADAM10 is the physiologically relevant constitutive α-secretase in primary neurons (Kuhn *et al.*, 2010; Jorissen *et al.*, 2010). Using an antibody specific to the α-cleavage site Kuhn *et al.* (2010) found that ADAM10

knockdown, but not ADAM9 or 17, resulted in the complete abolishment of α-secretase processing of APP in various cell lines and in primary murine neurons and other proteases were unable to compensate. Moreover, Jorissen *et al.* (2010) confirmed that α-secretase processing was severely suppressed in neurons derived from *Adam10* conditional knock-out mice.

In order to analyse the roles of the different ADAMs in α-secretase activity and to differentiate between α-secretase and the secretases/sheddases of other membrane proteins, specific inhibitors were designed to target their active sites. One of the early inhibitors used in this respect was batimastat and other related hydroxamic acid-based zinc metalloprotease (ZMP) inhibitors (Parkin *et al.*, 2002; Parvathy *et al.*, 1998; Gearing *et al.*, 1994). Hydroxamic acid-based inhibitors are highly potent ligands that bind directly to the Zn ion in the active site of the enzyme (Fischer *et al.*, 2019; Verma, 2012). They were originally designed as matrix metalloprotease (MMP) inhibitors, however, having strong Zn^{2+}-chelating moieties led to them being broad spectrum inhibitors not only of MMPs but also of members of the ADAM family of endoproteases (Vandenbroucke and Libert, 2014; Fingleton, 2008). In fact, these compounds were the tool used originally to characterise the properties of α-secretase cleavage (Hooper *et al.*, 1997). Using batimastat and other related hydroxamic acid-based ZMP inhibitors, Parvathy *et al.* (1998) found that these compounds were able to inhibit α-secretase shedding of APP but not β-secretase activity which proved that α-secretase is in fact a zinc metalloprotease. Moreover, the early finding by Sisodia (1992) that it is a requirement for APP to be localised to the plasma membrane in order for it to be processed at the alpha cleavage site was further confirmed by Parvathy *et al.* (1999) using a cell impermeable hydroxamic acid-based ZMP inhibitor and showing that this compound was able to nearly completely inhibit sAPPα production, thus proving that α-secretase is a plasma membrane-associated metalloprotease.

1.3.2.2. β- secretase

BACE1 (beta-site APP-cleaving enzyme 1) is a transmembrane aspartyl protease and the primary β-secretase for the generation of Aβ in the brain (Cai *et al.*, 2001). Another homologue, BACE 2, exists which shares 64% amino acid homology with BACE1 (De Strooper *et al.*, 2010). BACE2 has limited β-secretase activity in cells but cleaves APP more efficiently near the α-secretase cleavage site at Phe20-Ala21 and also at Phe19-Phe20 of the Aβ domain (Yan *et al.*, 2001). However, unlike BACE1, BACE2 is not selective for APP and has a lower expression level in the brain (De Strooper *et al.*, 2010). Studies have also confirmed the expression of BACE1 in the neuronal retina and RPE cells (Yoshida *et al.*, 2005; Prakasam *et al.*, 2010). The enzyme is active at low pH which might explain its localisation in acidic intracellular compartments such as the trans-Golgi network and the endosomes (Vassar *et al.*, 1999; Kinoshita *et al.*, 2003). It is thought that any APP escaping α-secretase cleavage at the cell surface is reinternalized in clathrin-coated pits which fuse with endosomes containing BACE 1 and γ-secretase leading to the generation of Aβ (O'Brien and Wong, 2011).

1.3.2.3. γ- secretase

γ-secretase is a high molecular weight complex composed of four main subunits; the presenilins (PS1 or PS2) which form the catalytic core, nicastrin, anterior pharynx defective 1 (APH-1), and presenilin enhancer 2 (PEN-2) (Fig. 1.9) (Zhang *et al.*, 2014). Presenilins are multi-transmembrane spanning proteins with nine transmembrane (TM) segments (Laudon *et al.*, 2005). TM6 and TM7 contain two highly conserved aspartate residues which are essential to the catalytic activity of the γ-secretase complex (Wolfe *et al.*, 1999). Mutations in PS1 and PS2 are linked to familial AD and are associated with the aberrant cleavage of APP favouring the production of the more aggregation prone Aβ42 compared to Aβ40 (Borchelt *et al.*, 1996). Presenilin mutations can also increase the amyloidogenic processing of APP by decreasing APP transport to the cell surface where non-amyloidogenic processing occurs (Cai *et al.*, 2003).

The other three components of the γ-secretase complex are accessory proteins which interact with the presenilins to form an active complex. Nicastrin is a type 1 transmembrane glycoprotein which acts as a substrate receptor within the complex by binding to the free N-terminus of previously shed transmembrane proteins (Shah *et al.*, 2005). In the case of APP, it binds the free N-terminus of CTFα or CTFβ after cleavage by α- or β- secretase, respectively (Zhang *et al.*, 2014). APH-1 and PEN-2 are multi-pass transmembrane proteins (De Strooper, 2003). APH-1 is thought to form an initial scaffolding complex with nicastrin (LaVoie *et al.*, 2003) while PEN-2 is involved in PS1 endoproteolysis in order to form an active heterodimer of its N- and C- terminal fragments (Luo *et al.*, 2003) in addition to having a role in stabilising the complex (Prokop *et al.*, 2004).

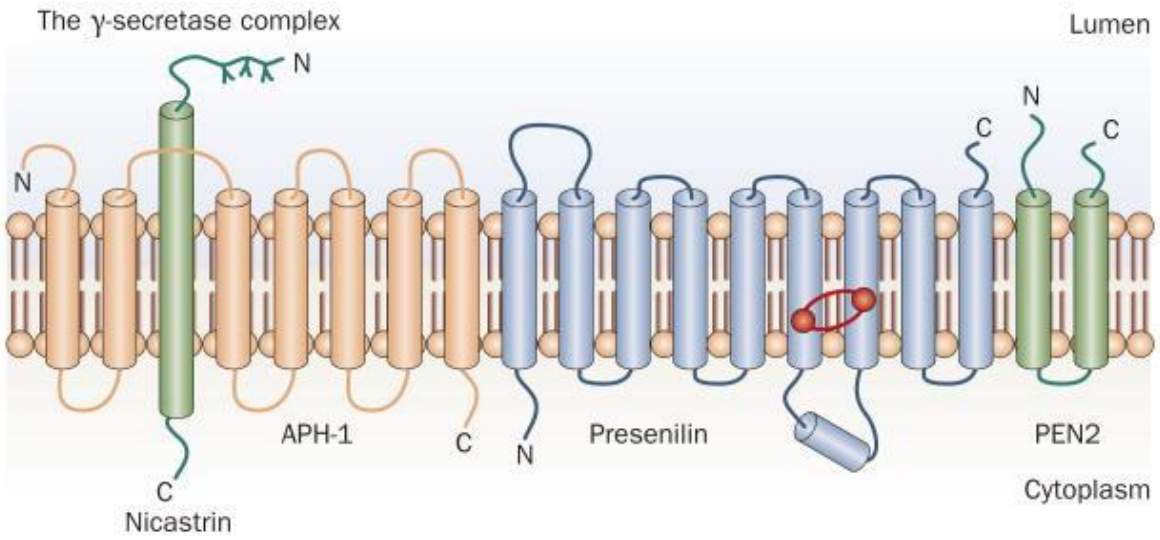

Figure 1.9. A schematic diagram of the subunits of γ-secretase complex. The γ-secretase complex responsible for the cleavage of APP CTFα and CTFβ to generate the p3 and Aβ fragments respectively, is a four-subunit aspartyl protease consisting of presenilin as its catalytic core (red dots indicate aspartate residues) alongside nicastrin, APH-1 and PEN-2 essential accessory proteins. APH-1, anterior pharynx defective 1; PEN-2, presenilin enhancer 2. (De Strooper *et al.*, 2010).

γ-secretase is essential for the intramembranous cleavage of a variety of type 1 transmembrane proteins including APP, Notch, E-cadherin and tyrosinase suggesting an important role for this secretase in several biological functions (De Strooper *et al.*, 1999; Marambaud *et al.*, 2002; Wang *et al.*, 2006; Haapasalo and Kovacs, 2011). The subunits of γ-secretase are expressed in various tissues including the retina and the RPE (Prakasam *et al.*, 2010). γ-secretase is expressed both at the cell surface where it complements α-secretase function and in endosomes and the trans-Golgi network where it complements β-secretase function leading to Aβ production (Frykman *et al.*, 2010; O'Brien and Wong, 2011).

1.4. sAPPα and sAPPβ in cell protection and proliferation

Saitoh *et al.* (1989) identified growth promoting properties of secreted APP (sAPP) fragments in fibroblasts *in vitro*. Other early literature demonstrated a correlation between low levels of sAPPα in the cerebrospinal fluid (CSF) and spatial memory defects in rats (Anderson *et al.*, 1999). Decreased sAPPα levels have also been demonstrated in the CSF of patients with familial AD compared to healthy subjects (Lannfelt *et al.*, 1995) and this has also been shown to correlate with cognitive impairment (Almkvist *et al.*, 1997) suggesting an important role for this proteolytic fragment in normal memory functioning and neuronal survival. Extensive research followed both *in vitro* and *in vivo* which found evidence of the trophic and proliferative roles of soluble APP (Fig. 1.10) in neuronal cell cultures (Araki *et al.*, 1991; Caillé *et al.*, 2004) and in non-neuronal cells where it acts as a growth or proliferative factor in addition to having other roles in the stimulation of cell motility and migration (Pietrzik *et al.*, 1998; Kirfel *et al.*, 2002; Quast *et al.*, 2003).

Another vital role for the soluble forms of APP (sAPPα and sAPPβ) lies in the regulation of neural differentiation and neurogenesis in adults as well as during development of the nervous system in embryonic stages (Caillé *et al.*, 2004; Hayashi *et al.*, 1994). *In vitro* treatment of human neural stem cells (hNSCs) with high doses of sAPPα/β induced the differentiation of hNSCs into an astrocytic lineage (Kwak *et al.*, 2006). During development, sAPPα/β has been shown to stimulate the

proliferation of embryonic neural stem cells (Hayashi *et al.*, 1994; Ohsawa *et al.*, 1999). Moreover, in adult neurogenesis, sAPPα/β cooperates with the epidermal growth factor (EGF) to regulate the proliferation of neural progenitor cells in the subventricular zone in mice (Caillé *et al.*, 2004). It stimulates the proliferation of EGF-responsive progenitors thus increasing the pool of progenitors (Caillé *et al.*, 2004). Acting in combination with nerve growth factor (NGF), sAPP fragments α and β stimulate neurite outgrowth in neuronal cell cultures (Milward *et al.*, 1992). Furthermore, *in vivo* studies have shown that exogenous administration of sAPPα/β or peptides encoding the trophic domains of the protein such as a 17-mer peptide spanning APP sequence 319-335 (APP_{695} numbering) or specifically the RERMS sequence (Fig. 1.10) can increase synaptic density in animal models leading to enhanced memory function (Meziane *et al.*, 1998; Mileusnic *et al.*, 2004; Roch *et al.*, 1994). Another study by Ring *et al.* (2007) demonstrated that sAPPα is sufficient to rescue the behavioural and physiological defects observed in APP knock-out mice. Moreover, the over-expression of ADAM10, the constitutive α-secretase in neurons, resulted in increased synaptogenesis in mice demonstrating the neurotrophic effects of sAPPα on cortical cholinergic, glutamatergic and GABAergic presynaptic bouton densities (Bell *et al.*, 2008).

Numerous studies have proven a neuroprotective role for sAPPα against various insults including ischemia (Smith-Swintosky *et al.*, 1994), neuronal damage following traumatic brain injury (Corrigan *et al.*, 2012; Plummer *et al.*, 2016), hypoglycaemia, glutamate and excitotoxic injury (Mattson *et al.*, 1993; Furukawa *et al.*, 1996a), Aβ induced oxidative injury (Goodman and Mattson, 1994), epoxomicin (a protease inhibitor) and UV irradiation (Copanaki *et al.*, 2010).

The sAPPα fragment can also ameliorate Aβ production through direct modulation of BACE1 activity (Obregon *et al.*, 2012) and reduces dendritic spine loss induced by Aβ oligomerisation (Tackenberg and Nitsch, 2019). Furthermore, sAPPα can modulate specific signalling pathways to inhibit tau phosphorylation (Deng *et al.*, 2015) thereby affecting the two main hallmarks of AD pathology (Habib *et al.*, 2017).

The afore-mentioned roles of sAPPα and sAPPβ in neuroproliferation, neuroprotection, neurogenesis, neuritogenesis and synaptic plasticity can be attributed to specific domains in the ectodomain of the APP molecule including the growth factor-like and heparin-binding domains in E1 and the RERMS sequence in E2 (Nhan *et al.*, 2015; Chasseigneaux and Allinquant, 2012) (Fig. 1.10). Those domains exist in both sAPPα and sAPPβ, however sAPPα was found to be up to 100-fold more potent than sAPPβ in protecting primary hippocampal neurons against glucose deprivation, Aβ toxicity and glutamate induced excitotoxicity (Barger and Harmon, 1997; Furukawa *et al.*, 1996b). This is explained by the presence of 16 additional amino acids at the C-terminus of sAPPα (compared to sAPPβ) which are thought to harbour part of a neuroprotective amino acid sequence residing in residues 591-612 (APP_{695} numbering) (Fig. 1.10) (Barger and Harmon, 1997; Furukawa *et al.*, 1996b). Additionally, residues 598-611 (APP_{695} numbering) are involved in LTP (long-term potentiation) enhancement and increased spatial memory performance, a property not shared by sAPPβ (Taylor *et al.*, 2008). On the other hand, sAPPβ and not sAPPα is part of a neuronal self-destruction pathway. It binds death receptor 6 inducing apoptosis and axonal pruning of peripheral neurons in the absence of growth factor (Nikolaev *et al.*, 2009).

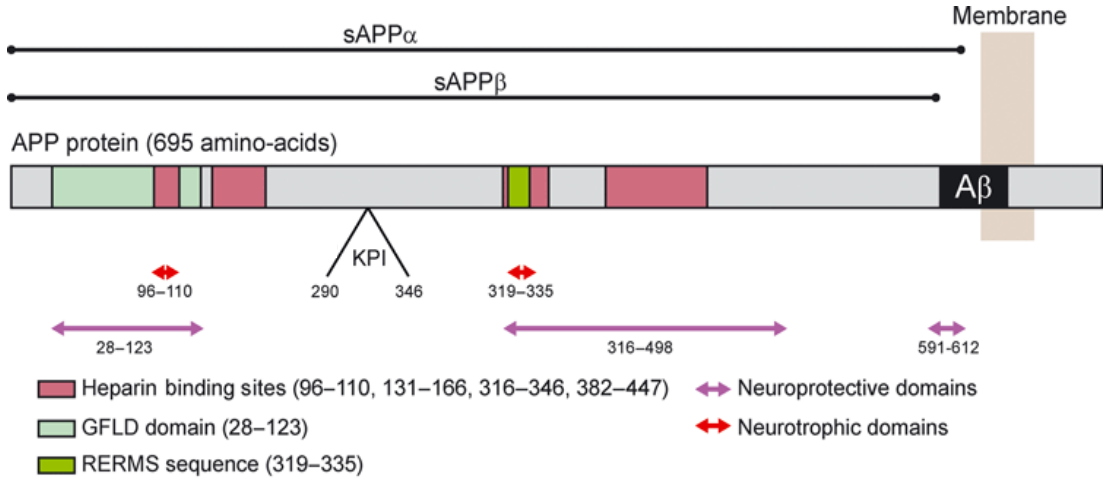

Figure 1.10. A schematic diagram of the various domains of soluble APP fragments and their known functions. Three neuroprotective domains are indicated by the purple arrows including the growth factor-like domain (GFLD) in E1 (28 – 123), amino acid sequence (316 – 498) in E2 and the C-terminal sequence only present in sAPPα (591 – 612). Neurotrophic domains (red arrows) involved in neurite outgrowth include the heparin binding site (HBS) (96 – 110) and the RERMS sequence (319 – 335). The position of the Kunitz-type protease inhibitor (KPI) that is present in APP_{751} and APP_{770} isoforms is indicated. Amino acid numbering is for APP_{695}. (Chasseigneaux and Allinquant, 2012).

1.5. UV light and APP expression/proteolysis

Only a few recent studies have discussed the effects of UV light exposure on APP expression and proteolysis. Almenar-Queralt *et al.* (2014) showed using mouse and human neuroblastoma SH-SY5Y cells that UV-irradiation leads to accelerated APP processing through the stimulation of secretase activity, particularly γ-secretase. This led to disrupted APP axonal transport as a consequence of impaired delivery of APP-containing vesicles to the synapse. These results indicated that damage-induced APP processing as a consequence of altered protein axonal trafficking concomitantly resulted in the failure of synaptic maintenance and neuronal damage.

Another study concerning seborrheic keratosis (SK) (an age-related skin disease) demonstrated a relationship between UV damage and APP overexpression in the ageing skin leading to the onset of SK (Li *et al.*, 2018). It showed that APP expression was higher in UV-exposed skin compared to non-exposed skin areas and APP, along with its proteolytic products, were highly expressed in skin tissues afflicted by SK relative to paired adjacent normal skin.

Finally, Cuesta *et al.* (2009a) demonstrated that UV-C irradiation resulted in a p53-dependant decrease in intracellular APP levels. Moreover, the later study showed that treatment with thyroid hormone T3 led to the reversal of UV-induced decline in APP through a mechanism mediated by the tumour suppressor p53.

1.6. Glucagon like peptide-1 (GLP-1) and GLP-1 analogues

1.6.1. The GLP-1 hormonal system

Glucagon was discovered in 1923 (Kimball and Murlin, 1923) and is responsible for increasing blood glucose concentrations (hyperglycaemia) through glycogenolysis and gluconeogenesis in the liver (Exton and Park, 1968; Ramnanan *et al.*, 2011). However, later studies in the 1960s and 70s found glucagon-like material produced in the intestine derived from the glucagon precursor protein (an 18 kDa protein called proglucagon) but lacking the glucagon amino acid sequence and, therefore, having biological functions distinct from the hyperglycaemic effects of glucagon (Unger *et al.*, 1968; Murphy *et al.*, 1971; Patzelt *et al.*, 1979). Two peptides were identified and named glucagon-like peptide 1 and 2 (GLP-1 and GLP-2) (Bell *et al.*, 1983; Orskov *et al.*, 1987). GLP-1 (7-36 amide; a truncated version of GLP-1 (1-37)) was identified as the incretin hormone in humans, a hormone that stimulates insulin secretion from the endocrine pancreas (Kreymann *et al.*, 1987; Müller *et al.*, 2019).

GLP-1 is an endogenous hormone secreted by intestinal cells called “L-cells” in response to food intake (Buffa *et al.*, 1978). It stimulates glucose-dependant insulin secretion from β-cells in the pancreas (Meloni *et al.*, 2013). GLP-1 has a plethora of metabolic effects on various organs resulting in decreased food intake and enhanced gastric emptying, stimulation of pancreatic β-cell proliferation and survival, lowered glucagon secretion, increased sodium excretion (natriuresis) and diuresis in addition to cardioprotective and neuroprotective effects (Müller *et al.*, 2019) (Fig. 1.11).

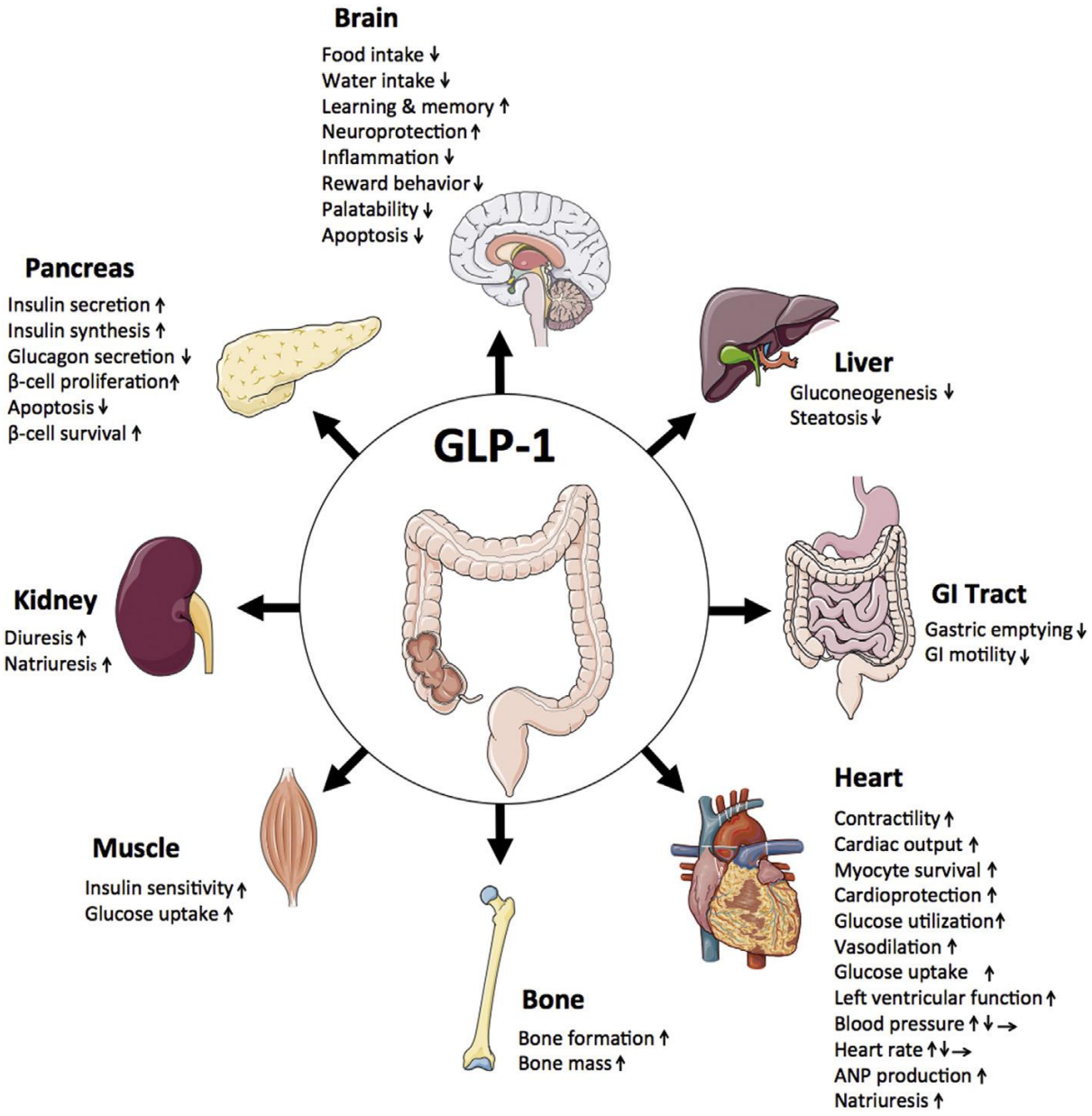

Figure 1.11. The direct and indirect effects of endogenous GLP-1 on metabolism in various tissues and organs. GLP-1 is produced by L cells in the intestine. Its effects, however, are not limited to food metabolism and modulating pancreatic secretion. Rather GLP-1 demonstrates direct and indirect effects on a plethora of body tissues and organs including the kidneys, heart and brain. (Müller *et al.*, 2019).

GLP-1 achieves its biological function through binding to its specific receptor named GLP-1R (Mayo *et al.*, 2003). This is a G protein-coupled receptor consisting of seven transmembrane domains of the Gαs type which act by stimulating adenylyl cyclase and increasing intracellular cAMP levels (Dillon *et al.*, 1993). GLP-1R was originally found to be present in the insulin-secreting cells of the

pancreas (Orskov and Nielsen, 1988). However, it is now known to be present in a variety of cells and tissues including the lungs, kidneys, stomach, intestine as well as the heart, muscles and the brain where it mediates the extra pancreatic effects of GLP-1 including neuroprotection (Wei and Mojsov, 1995; Alvarez *et al.*, 2005; Müller *et al.*, 2019).

Given the role played by the RPE cells in the formation of the BRB and in the pathophysiology of diabetic retinopathy, Puddu *et al.* (2013) investigated the expression and function of the GLP-1 and its receptor GLP-1R in the RPE cells. The study confirmed the expression of a functional GLP-1R in ARPE-19 cells at both mRNA and protein level (Puddu *et al.*, 2013). Moreover, the later study showed that GLP-1R was able to induce signal transduction pathways downstream within the ARPE-19 cells via the phosphorylation of protein kinase B (PKB) and extracellular signal-regulated kinases 1 and 2 (ERK1/2) which was dependant on the upstream activation of phosphatidylinositol 3-kinase (PI3K) and epidermal growth factor receptor (EGFR) (Puddu *et al.*, 2013). GLP-1R expression was also confirmed in the neural retina, specifically in the RGC, and the levels of GLP-1 were shown to be decreased in the retinas of diabetic mice (Shu *et al.*, 2019; Hebsgaard *et al.*, 2018).

1.6.2. GLP-1 analogues in the treatment of diabetes

Research has identified a myriad of metabolic effects of GLP-1 on various tissues and organs (Fig 1.11). In addition to its positive effects on pancreatic β-cells and glucose-dependant insulin stimulation which led to its great pharmacological value in the treatment of type-2 diabetes mellitus (T2DM), GLP-1 has demonstrated protective effects in the brain against neurodegeneration (Müller *et al.*, 2019). However, GLP-1 has a short half-life in plasma (1.5-5 min) (Hui *et al.*, 2002) and, consequently, several analogues with longer half-lives were developed and are currently on the market for the treatment of T2DM; these include exenatide (exendin-4), liraglutide, lixisenatide, albiglutide and dulaglutide (Hinnen, 2017).

1.6.2.1. Exendin-4

Exendin-4 was the first FDA approved GLP-1 analogue to be used as an add-on therapy for type 2 diabetes (Park, 2016; Perazella and Shirali, 2014). It was approved in the US in 2005 and became available in the UK in 2007 (Krentz, 2018). Exenatide is the synthetic form of exendin-4 which was originally isolated from the venom of *Heloderma suspectum*, a lizard inhabitant of the Southwestern US (Krentz, 2018). Exendin-4, the naturally occurring compound, was found to have a longer half-life compared to the endogenous GLP-1 hormone due to its resistance to degradation by dipeptidylpeptidase-4 (DPP-4) (Sekar *et al.*, 2016). The drug is sold under the trade name (Byetta) and is administered subcutaneously twice a day (Sekar *et al.*, 2016).

1.6.2.2. Liraglutide

Liraglutide is a long-acting human GLP-1 analogue and was the second drug approved for the treatment of T2DM in Europe in 2009 and in the United States in 2010 (Sekar *et al.*, 2016). It is a synthetic compound that shares 97% amino acid homology with the human GLP-1 (Sonia and Sharma, 2014). In addition to its effects on glucose-dependant insulin secretion, liraglutide was shown to improve several disease risk factors including blood pressure, lipid profile and body weight (Sonia and Sharma, 2014). The drug (sold under the trade name Victoza) is administered once daily as a subcutaneous injection (Day, 2018).

1.6.2.3. Lixisenatide

Lixisenatide is a more recently approved diabetes drug which has been marketed under the trade name Lyxumia since 2013 (Elkinson and Keating, 2013). Like liraglutide, lixisenatide is a once-daily subcutaneously administered drug (Ratner *et al.*, 2010). It has also been shown to have positive effects, additional to the lowering of blood glucose, including slowing gastric emptying and reducing body weight which are sustained even after treatment (Lorenz *et al.*, 2013; Barnett, 2011). Lixisenatide is better tolerated than exendin-4 and shows a lower incidence of side effects common to this class of drugs such as nausea, vomiting, diarrhoea and hypoglycaemia (Sekar *et al.*, 2016).

1.6.3. GLP-1 analogues in the treatment of neurodegenerative diseases

In vitro and *in vivo* studies have demonstrated neuroprotective effects related to GLP-1 receptor agonism in the context of a range of neurodegenerative conditions. In rat and human neuronal cell cultures, GLP-1 and exendin-4 were able to enhance differentiation and neurite outgrowth in combination with nerve growth factor (Perry *et al.*, 2002b). In addition, both of the former two molecules were able to protect hippocampal neuron cultures against insults characteristic of AD including glutamate excitotoxicity and associated apoptosis (Perry *et al.*, 2002a), iron and Aβ induced-toxicity (oxidative insult) (Perry *et al.*, 2003). It has also been shown that GLP-1 analogues can shift APP processing towards the non-amyloidogenic pathway possibly by enhancing ADAM10 maturation and activity (Ohtake *et al.*, 2014).

Huntington's disease is a neurodegenerative disease in which mutant huntingtin (HTT) protein accumulates forming toxic aggregates which impair autophagy and protein clearance mechanisms leading to oxidative stress and neuronal death. In a cell culture model of the disease, liraglutide was shown to enhance insulin sensitivity and increase cell viability (Chang *et al.*, 2018). The positive effects of liraglutide were found to be due to its ability to enhance antioxidant pathways leading to reduced oxidative stress as well as stimulating autophagy and clearance of HTT aggregates.

Studies on animal models have demonstrated promising results in relation to both AD and PD. In mice, ventricular infusions of exendin-4 protected dopaminergic cells against MPTP-induced toxicity and prevented the development of locomotor deficits characteristic of PD (Li *et al.*, 2009). GLP-1 receptor agonists were shown to ameliorate memory and learning defects in AD mouse models by protecting the hippocampus against neuronal and synaptic loss and preventing the disease-associated decline in synaptic plasticity (During *et al.*, 2003; Perry *et al.*, 2002a; McClean *et al.*, 2011). Liraglutide injections into AD mice reduced Aβ plaques and oligomers and the number of activated microglia whilst increasing the number of young neurons in the hippocampus (McClean *et al.*, 2011). Currently, only a few of these GLP-1 analogues are in clinical trials for the treatment of AD (Femminella *et al.*,

2019; Gejl *et al.*, 2016) or PD (Athauda *et al.*, 2017; Aviles-Olmos *et al.*, 2014; Foltynie and Aviles-Olmos, 2014).

Finally, and of particular relevance to the current project, GLP-1 receptor activation in the retina using the GLP-1 analogues liraglutide, lixisenatide or exenatide has been shown to demonstrate protective effects against diabetic retinal neurodegeneration (Hernandez *et al.*, 2016; Shu *et al.*, 2019).

1.7. Experimental aims in the current study

The overarching aims of the current project are to characterise the potential role of APP and its proteolytic fragments in AMD and to determine whether there is any place for the use of GLP-1 analogues in the treatment of the disease.

Given that UV-light is a possible risk factor for AMD (Vojniković *et al.*, 2007; Plestina-Borjan and Klinger-Lasić, 2007), it will be used as the stressor to treat human retinal pigment epithelial cells (ARPE-19) and the effects on cell viability will be monitored whilst examining possible changes in endogenous APP expression and proteolysis. Next the levels of APP and/or its fragments will be manipulated using small interfering RNA (siRNA) or inhibitors of the different secretase classes. The effects of full-length APP, sAPPα and sAPPβ on ARPE-19 cell viability/proliferation will also be investigated by co-culturing these cells with HEK293 cells stably over-expressing the proteins/protein fragments.

Finally, given the afore-mentioned neuroprotective effects of GLP-1 analogues against insults related to neurodegeneration including Aβ toxicity and oxidative stress, these compounds (exendin-4, liraglutide and lixisenatide) will be tested in order to determine whether they exhibit any protective effects in ARPE-19 cells exposed to a range of stress conditions (H_2O_2, Aβ and UV treatments).

Collectively, it is hoped that such experiments will provide us with a more comprehensive understanding of the molecular mechanisms involved in the pathology of AMD as well as providing evidence supporting the potential use of GLP-1 analogue drugs for the treatment or prevention of AMD.

Chapter 2

Materials and Methods

2. Materials and Methods

2.1. Materials

The human retinal pigment epithelial cell line (ARPE-19) and the human neuroblastoma cell line (SH-SY5Y) were purchased from ATCC (Teddington, UK). The human embryonic kidney cell line (HEK 293) was generously provided by Professor David Allsop (Lancaster University, Lancaster, UK). The production of the construct pIREShyg FL-APP_{695} has been described previously (Parkin *et al.,* 2007). pIREShyg $sAPP_{695}\alpha$ and pIREShyg $sAPP_{695}\beta$ constructs were generated by Dr. Edward Neale (Lancaster University, Lancaster, UK).

The rabbit polyclonal anti-Amyloid Precursor Protein C-Terminal antibody (APP-CT), mouse monoclonal anti-β-actin antibody, secondary goat anti-rabbit IgG (whole molecule)-peroxidase antibody and the secondary rabbit anti-mouse IgG (whole molecule)-peroxidase antibody were purchased from Sigma-Aldrich (Gillingham, UK). The mouse monoclonal anti-β-amyloid 1-16 antibody (clone 6E10), rabbit polyclonal anti-sAPPβ antibody and the mouse monoclonal anti-p53 antibody were purchased from BioLegend (San Diego, USA).

Human β-Amyloid (1-42) peptides were purchased from GenScript (Piscataway, USA). The selective ADAM10 inhibitor GI254023X and γ-secretase inhibitor begacestat (GSI-953) were purchased from Tocris (Bristol, UK). β-secretase inhibitor IV was purchase from Merck Millipore (Darmstadt, Germany) and batimastat was purchased from Sigma-Aldrich (Gillingham, UK). The GLP-1 analogues exendin-4, liraglutide and lixisenatide were produced by ChinaPeptides Co., Ltd (Shanghai, China). DharmaFECT™ Transfection reagent and siRNAs were purchased from Dharmacon™/GE Healthcare (Little Chalfont, UK).

Cell culture reagents were from Lonza (Basel, Switzerland) and all other laboratory reagents were from Sigma-Aldrich (Gillingham, UK) unless otherwise stated.

2.2. Methods

2.2.1. Cell Culture

ARPE-19 cells were cultured in Dulbecco's Modified Eagle Medium:F12 (DMEM:F12) basal medium whilst HEK293 and SH-SY5Y cells were cultured in Dulbecco's Modified Eagle Medium (DMEM) basal medium. All growth media were supplemented with 10% (v/v) Foetal Bovine Serum (FBS) (Thermofisher, Waltham, USA) and a penicillin/streptomycin mixture (penicillin 50 units/ml and streptomycin 50 units/ml). Cultures were grown at 37° C in a 5% (v/v) CO_2 environment with medium being changed every 2-3 days.

When passaging cells, spent medium was removed and replaced with 2 ml trypsin which, after ensuring complete cell coverage, was removed and replaced with a fresh 2 ml of trypsin. The flasks were then returned to the incubator until the cells had become detached. The cognate complete growth medium was then added to the trypsinised cells and the cell suspension was transferred into a 50 ml Falcon tube. Cells were then pelleted by centrifugation for 5 min at 500 *g* in an Allegra® X-22R Centrifuge (Beckman Coulter, Indianapolis, USA) prior to removing the supernatant. The pellet was then resuspended in an appropriate volume of complete growth medium as required for each experiment and new stock flasks were also seeded as required.

For long term storage, cells were frozen in liquid nitrogen. Here, a confluent T75 cm^2 flask of cells was trypsinised and pelleted as described previously and the cell pellet was resuspended in 1.5 ml of 10% (v/v) Dimethyl Sulfoxide (DMSO) in the culture growth medium appropriate for the specific cell type. The cell suspension was then transferred into a cryovial which was kept at -80° C for at least 48 h prior to being transferred into liquid nitrogen. In order to resurrect frozen cells, vials were thawed briefly at room temperature and the contents were then transferred into a 50 ml Falcon tube to which 20 ml of pre-warmed growth medium was added. The cells were then pelleted by centrifugation at 200 *g* for 3 min and the supernatant was discarded. The pellet was then routinely resuspended in 2

ml of growth medium before seeding 1 ml of this resuspension into each of two T75 cm^2 flasks containing 10 ml growth medium.

2.2.2. Cell drug treatments

Unless otherwise stated, the following treatments are described for small scale 96 well plate cultures. Volumes were scaled up accordingly for experiments using larger cell culture flasks. Here, a cell pellet obtained following the trypsinisation of a confluent T75 cm^2 flask of ARPE-19 cells (section 2.2.1.) was resuspended in growth medium (routinely 10 ml) and the cells were counted. Sufficient additional growth medium was then added to the cells such that the required number of cells would be achieved when 100 μl of the resuspension was added to 100 μl of growth medium (200 μl total) in the wells of a 96 well culture plate. The cells were then cultured until they reached confluence. Unless otherwise stated, the spent medium was then removed from the cells and they were washed *in situ* with 200 μl of UltraMEM before replacing this with a second 200 μl aliquot of the same medium to which test compounds were added as described below.

2.2.2.1. Hydrogen peroxide (H_2O_2)

The 30 % (v/v) H_2O_2 stock (Fisher Bioreagents, Loughborough, UK) (11.33 μl) was diluted with 5 ml of distilled water to give solution A. Adding 5 μl of solution A to 200 μl of medium on cells resulted in a final H_2O_2 concentration of 500 μM. Lower H_2O_2 culture concentrations were achieved simply by diluting solution A with the required volume of distilled water before adding 5 μl of each of these secondary dilutions to the cells. All solutions were filter-sterilised under aseptic conditions before addition to cell cultures.

2.2.2.2. GLP-1 analogues

All GLP-1 analogue stock solutions were prepared aseptically using filter -sterilized solutions. Exendin-4 (MW = 4186.6), provided as 1 mg of solid, was dissolved in 29.86 ml of 0.1 % (w/v) Bovine Serum Albumin (BSA) (Fisher Bioreagents, Loughborough, UK) to produce an 8 μM stock solution

which was aliquoted out and stored at -80° C. When required, 5μl of this solution was added to 200 μl of medium on cells in order to give a final drug concentration of approximately 200 nM.

Liraglutide (MW = 3751.202) was purchased as a 5 mg solid and dissolved in 16.66 ml of 0.1 % (w/v) BSA. This 80 μM stock solution was then aliquoted and frozen at -80° C. When required, an aliquot of the stock solution was diluted 10-fold with 0.1% (w/v) BSA and 5 μl of this secondary dilution was added to 200 μl of medium on cells in order to give a final drug concentration of approximately 200 nM.

Similarly, lixisenatide (MW = 4858) (5 mg) was dissolved in 12.91 ml of 0.1 % (w/v) BSA to achieve an 80 μM stock which was aliquoted and frozen. When required, an aliquot of the stock solution was diluted 10-fold with 0.1% (w/v) BSA and 5 μl of this secondary dilution was added to 200 μl of medium on cells in order to give a final drug concentration of approximately 200 nM.

Lower experimental concentrations of the GLP-1 analogues were achieved by serially diluting the secondary dilutions described above using 0.1% (w/v) BSA before adding to the cells.

2.2.2.3. Secretase inhibitors

The ADAM10 inhibitor, GI254023X (MW = 391.50), stock was prepared by dissolving 1 mg in 25.511 ml DMSO. The β-secretase inhibitor IV (MW = 578.72) stock was prepared by dissolving 1 mg in 17.3 ml DMSO and the gamma-secretase inhibitor, begacestat (MW =391.74), stock was prepared by dissolving 1 mg in 25.527 ml DMSO. Batimastat (MW 477.64) stock was prepared by dissolving 10 mg in 2.09 ml of DMSO. All stocks were aliquoted out and stored at -20° C. The stocks were diluted accordingly with DMSO such that adding 2 μl of these dilutions to 200 μl of culture medium yielded the required final inhibitor concentrations.

2.2.2.4. β-Amyloid (1-42) synthetic peptides

The supplied Aβ (1-42) peptide (0.5 mg) was dissolved in 22.15 μl of DMSO to generate a stock solution which was aliquoted and stored at -80° C. The addition of 2 μl of this solution to 200

μl of cell culture medium gave a 50 μM final concentration. Lower peptide concentrations (0-40 μM) were achieved by diluting the stock solution with DMSO before adding 2μl of the dilutions to cells.

2.2.3. UV-A treatment of cells

ARPE-19 cells (T25 cm^2 flasks) were grown to the required level of confluence before serum starving them for 6 h in UltraMEM. The UltraMEM was then removed and the cells were washed *in situ* with 10 ml of phenol red-free DMEM (Thermofisher, Waltham, USA) before adding a fresh 8 ml of the same medium. The cells were then exposed to UV-A for the required length of time. UV-A irradiation was provided by six Phillips TLR 36W tubes (Starna Ltd, Romford, UK) and cells were at a distance of 8 cm away from the light source. Flasks of cells were covered with Mylar film to block any contaminating wavelengths of the UV-B and UV-C spectrum (McFeat *et al.,* 2013). The measured output from the UV-A light source at the experiment conditions and settings was 46 Wm^{-2}. At 50 , 75 , 100 and 125 min exposure UV dosage was calculated as 105, 158, 210 and 263 kJm^{-2} respectively. During irradiation, the flasks were placed on custom size copper plates positioned on a water-cooled base which kept the temperature during irradiation relatively constant (in the range of 20-25° C). Following irradiation the cells were transferred back into UltraMEM (10 ml) and incubated at 37° C in 5 % (v/v) CO_2 for an 18 h post-irradiation recovery period.

2.2.4. MTS (3-(4,5-dimethylthiazol-2-yl)-5-(3-carboxymethoxyphenyl)-2-(4-sulfophnnnmnnnenyl)-2H-tetrazolium) cell viability assay

Following cell treatments, the spent culture medium was removed and the cells were rinsed with 200μl of UltraMEM. This was then replaced with a fresh 100 μl of UltraMEM to which 20 μl of Cell Titer 96®Aqueous One Solution Cell Proliferation Assay MTS reagent (Promega, Madison, USA) was added. Blanks were always included consisting of medium only wells with 20 μl of the MTS reagent. The microtiter plate was covered with foil and incubated at 37° C for 20 min (or until suitable colour development occurred) with occasional mixing by tapping the plate every 2-3 min. Absorbance was measured at 490nm using a Perkin Elmer Wallac Victor^2 Microplate Reader (Ramsey, USA).

2.2.5. Trypan Blue Assay

ARPE-19 cells were trypsinised and pelleted as described in section 2.2.1. and the cell pellet was resuspended in 5 ml of Phosphate Buffered Saline (PBS; 150 mM NaCl, 2 mM NaH_2PO_4 and 20 mM Na_2HPO_4 at pH 7.4). 20 μl of this cell suspension was transferred into an Eppendorf tube and mixed with a 20 μl of Trypan Blue. Following a 2 min incubation, 20 μl of the mixture was transferred into a haemocytometer and cells were counted in each of the nine grid squares under light microscope. Cell counts were averaged to find the number of cells in a volume of 0.1 μl. This was multiplied by 400 to find the cell count in the original 20 μl cell suspension sample taking into account the 1:1 dilution with Trypan Blue. Finally, the resulting number was multiplied by 250 to reveal the number of cells in the original 5 ml suspension. Once cell counts had been performed, the cell suspensions were centrifuged again at 500 rpm for 5 min and the supernatant PBS was discarded. The remaining cell pellets were frozen at -80° C pending preparation of cell lysate samples.

2.2.6. Harvesting and processing conditioned cell culture medium

Conditioned UltraMEM from cell cultures was collected and frozen at -80° C pending concentration. Once thawed, these samples (10 ml) were centrifuged at 3000 rpm in a Hettich Rotanta 460R centrifuge (Tuttlingen, Germany) for 5 min at 4° C to pellet any cell debris. A total of 8 ml of the supernatant was then transferred into a 10 kDa cut-off centrifugal concentrator (Millipore, Watford, UK) which had previously been equilibrated by spinning through 4 ml of distilled water for 10 min at 4000 rpm. The samples were then centrifuged at 3500 rpm until the volume was concentrated down to 250 μl. If the volume was accidently decreased further, the sample was diluted back to 250 μl using the filtrate that had already passed through the filter. The concentrated samples were then transferred to eppendorfs using a syringe and needle and frozen at -80° C pending Western blot analysis.

2.2.7. Harvesting cells and preparation of cell lysates

After removing the conditioned culture medium (see above), cells were rinsed with 10 ml of PBS which was then replaced with a fresh 10 ml of PBS. Cells were scraped from the base of the flask into the PBS using a cell scraper ensuring all cells were dislodged effectively. The cell suspension was then transferred to a 50 ml Falcon tube and the culture flask was rinsed with another 10 ml of PBS to collect residual cells; this was then combined in the same Falcon tube. Cell suspensions were centrifuged at 1000 rpm and 4° C for 5 min (Hettich Rotanta 460R centrifuge) before discarding the supernatants and freezing the cell pellets at -80° C until required to prepare cell lysates. In order to prepare lysates, the cell pellets were thawed and resuspended in 750 μl (ARPE-19 cells) or 1.5 ml (SH-SY5Y and HEK293 cells) of lysis buffer (50 mM Tris, 150 mM NaCl, 1% (v/v) IGEPAL, 0.1 % (w/v) sodium deoxycholate, and 5 mM EDTA, pH 7.4) containing protease inhibitor cocktail (Sigma-Aldrich, Gillingham, UK) or protease and phosphatase inhibitor cocktail (Thermofisher, Waltham, USA) at a ratio of 1:100 (inhibitor cocktail : lysis buffer). Samples were then sonicated on half power for 30 seconds using a probe sonicator (MSE, Crawley, UK). The sonicated samples were transferred into eppendorf tubes and centrifuged at 11,600 *g* for 10 min to pellet any insoluble material. Leaving the pellet undisturbed, all but the final 50 μl of the supernatant was transferred into a fresh eppendorf tube. Lysate protein concentrations were assayed using the bicinchoninic acid (BCA) protein assay (section. 2.2.8) and protein concentrations were equalised across different samples before freezing them in 50-100 μl aliquots at -80° C pending further analysis.

2.2.8. Bicinchoninic acid (BCA) protein assay

Bovine serum albumin (BSA) protein standards were prepared at 0, 0.2, 0.4, 0.6, 0.8 and 1 mg/ml. The standards (10 μl) and lysate samples (10 μl for ARPE-19 and 3 μl for SH-SY5Y and HEK293) were pipetted in duplicate into the wells of a 96-well microtiter plate. A working reagent consisting of BCA reagent (Pierce, Rockford, USA) and 4% (w/v) $CuSO_4.5H_2O$ (50:1, v/v) was prepared and 200 μl was added to all wells containing standards and samples. Samples and the working reagent were

mixed by gentle tapping of the plate before a 30 min incubation period at 37° C. Absorbance was measured at 562 nm using a Perkin Elmer Wallac Victor^2 Microplate Reader (Ramsey, USA).

After taking the average of the duplicate readings, a standard curve was produced using the values of the BSA protein standards and the protein concentrations in the lysate samples were extrapolated using the resultant regression equation. Samples were then equalised in terms of protein concentrations by adding lysis buffer to the more concentrated samples.

2.2.9. Sodium Dodecyl Sulphate-Polyacrylamide Gel Electrophoresis (SDS-PAGE)

SDS-PAGE was performed using 7-17 % and 5-20 % acrylamide gradient gels. Resolving gel solutions (Tables 2.1 and 2.2) were made up and the gels were poured using a gradient mixer. Once poured, the gels were covered with a thin layer of isopropanol to facilitate polymerisation and left to set for 30 min. The isopropanol was then removed and the stacking gel (Table. 2.3) was poured before immediately inserting the comb and leaving to set for a further 30 min.

Samples and low molecular weight markers (GE Healthcare, Little Chalfont, UK) were prepared by diluting 2:1 (v/v) with dissociation buffer (3.5 ml of 1 M Tris-HCl pH 6.8, 2.5 g SDS, 0.3085 g dithiothreitol (DTT), 5 ml glycerol, few drops of 0.5% (w/v) bromophenol blue solution, and dH_2O to make up to 25 ml) and boiling for 3 min. Gels were run in Tris/Glycine/SDS running buffer (supplied as 10x buffer containing 0.25 M Tris base, 1.92 M glycine, and 1% (w/v) SDS; Geneflow Ltd, Lichfield, UK) at 35 mA per gel for 45 min or until the dye front reached the base of the gel.

Table. 2.1. Components of 7-17 % acrylamide resolving gels.

Component	7 %	17%
Sucrose	-	0.37 g
Distilled H_2O	1.36 ml	-
1 M Tris-HCl, pH 8.8	1.39 ml	1.39 ml
10% (w/v) SDS	37 µl	37 µl
30% acrylamide bis-acrylamide stock solution (Severn Biotech Ltd, Kidderminster, UK)	0.88 ml	2.1

1.5% (w/v) ammonium persulphate	100µl	220µl
N,N,N',N'-Tetramethylethylenediamine (TEMED)	3µl	3µl

Table. 2.2. Components of 5-20 % acrylamide resolving gel.

Component	5%	20%
Sucrose	-	0.37 g
Distilled H_2O	1.64 ml	-
1 M Tris-HCl, pH 8.8	1.39 ml	-
1.5 M Tris-HCl, pH 8.8	-	0.93 ml
10% (w/v) SDS	37 µl	37 µl
30% acrylamide bis-acrylamide	0.63 ml	2.5 ml
1.5% (w/v) ammonium persulphate	71 µl	220 µl
N,N,N',N'-Tetramethylethylenediamine (TEMED)	3µl	3µl

Table. 2.3. Components of the stacking gel.

Component	Volume
30% acrylamide bis-acrylamide	1 ml
1 M Tris-HCl, pH 6.8	1.25 ml
Distilled H_2O	7.65 ml
1.5% (w/v) ammonium persulphate	0.5 ml
10% (w/v) SDS	100 µl
N,N,N',N'-Tetramethylethylenediamine (TEMED)	10 µl

2.2.10. Immunoblotting (Western Blotting)

Proteins resolved by SDS-PAGE were transferred to Immobilon-P polyvinylidene fluoride (PVDF) membrane (Merck Millipore, Darmstadt, Germany) by wet blotting. The membrane was first equilibrated by submerging in methanol for 10 sec, distilled water for 2 min and then in Towbin transfer buffer (20 mM Tris, 150 mM Glycine, methanol 20% (v/v) in dH_2O) for 20 min. Resolving gels were equilibrated briefly in transfer buffer for a maximum of 5 min before assembling the transfer sandwich which consisted of 4x blotting papers, gel, PVDF membrane and another 4x blotting papers

in a blotting cassette. All components of the transfer sandwich were equilibrated in transfer buffer and then proteins were wet-blotted at 115V for 1 h. Following transfer, the gel was discarded and the PVDF membrane was washed for 5 min with PBS before blocking for 1 h at room temperature in 5% (w/v) semi-skimmed milk in PBS containing 0.1% (v/v) Tween-20 (PBS-Tween) on a shaking platform. The membrane was then washed in PBS for 5 min before adding the primary antibody (Table. 2.4) and incubating overnight in a Falcon tube on a spiramix at 4° C (except for the anti β-actin antibody where the membranes were incubated for 2 h at RT). The primary antibody was then discarded and the membranes were rinsed for 1x 1 min and 2x 15min in PBS-Tween on a shaking platform. This was followed by incubation with the horse radish peroxidase (HRP)-conjugated secondary antibody (Table. 2.4) for 1 h at RT. All antibodies were dissolved in PBS + 0.1% (v/v) Tween-20 containing 2% (w/v) BSA. Finally, the membranes were rinsed for 1x 1 min and 2x 15 min with PBS prior to developing the blots.

Table. 2.4. Primary and secondary antibodies used and their concentrations.

Primary antibody	Dilution (v/v)	Secondary antibody	Dilution (v/v)
Rabbit polyclonal anti-APP-CT	1/5000	Goat anti-rabbit-HRP	1/4000
Mouse monoclonal anti-p53	1/4000	Rabbit anti-mouse-HRP	1/4000
Mouse monoclonal; anti-β-actin	1/5000	Rabbit anti-mouse-HRP	1/4000
Mouse monoclonal anti-β-amyloid 1-16 antibody (clone 6E10)	1/4000	Rabbit anti-mouse-HRP	1/4000
Rabbit polyclonal anti-sAPPβ	1/1000	Goat anti-rabbit-HRP	1/4000

In the darkroom, the PVDF membranes were then incubated for 2 min with 6 ml (3 ml of each solution supplied) of enhanced chemiluminescence (ECL) western blotting substrate (Pierce, Rockford, USA) with manual shaking. They were then placed between two acetate films and exposed to X-ray films in a developing cassette for variable exposure time periods depending on the antibody used. X-ray films were then developed manually.

Western blots were analysed by calculating the area of protein bands on the X-ray films using image J software. Cell lysate samples were equalised using BCA assay (section 2.2.8) before performing electrophoresis and western blotting. Equal amounts of protein were also confirmed by checking the actin blots by naked eye. Media samples were equalised by concentrating samples to equal volumes of 250 μl and results were corrected to account for observed changes in cell viability.

For the quantification of FL-APP blots, the areas of both mature and immature protein bands were combined and represented in the bar charts. This is because, depending on protein separation quality, it was not always possible to separate the two bands and calculate their areas separately. The acrylamide gels used were also unable to resolve individual CTFs of the α- and β-secretase cleavage. Moreover, smaller peptides such as Aβ species were not picked up on the 6E10 blot (used to blot media samples) as Aβ peptide (4 kDa) is below the detection ability of the acrylamide gradient gels utilised in the current study. Note that only 6E10 antibody can recognise the Aβ sequence (1-16). Furthermore, given that 10 kDa filters were used to concentrate media samples, it is most likely that Aβ peptides were filtered out.

2.2.11. Amido Black staining of membranes

After development, the PVDF membranes were removed from the acetate film and stained with Amido Black stain (0.1% (w/v) Amido Black, 1% (v/v) acetic acid, 40% (v/v) methanol in dH_2O) by submerging the membranes in the solution for 2 min until protein bands became visible. Membranes were then rinsed under tap water to remove excess stain and left to air-dry.

2.2.12. APP depletion using siRNA transfection

Endogenous APP was depleted in ARPE-19 cells using siRNA purchased from Dharmacon (Little Chalfont, UK):

Control/scramble siRNA: D-001810-10-05, ON-TARGETplus Non-targeting Pool, 5 nmol

APP siRNA: LQ-003731-00-0002, ON-TARGETplus Human APP (351) siRNA, set of four 2 nmol siRNA quantities.

The non-targeting (scramble) siRNA (5 nmol) was resuspended in 1 ml of RNase-free water and the APP siRNA (8 nmol total amount) was resuspended in 1.6 ml of RNase-free water to prepare 5 μM siRNA stock solutions which were aliquoted and stored at -20° C.

The required volume of siRNA (see individual figures) was then diluted to a total of 200 μl with UltraMEM in one Falcon tube whilst, in another, DharmaFECT transfection reagent (0.25 μl, unless otherwise stated) (Dharmacon Little Chalfont, UK) was diluted in UltraMEM to a total of 200 μl. The two solutions were incubated for 15 min at RT before combining them, mixing thoroughly by pipetting, and incubating for a further 20 min at RT. The combined sample (400 μl) was then made up to 2 ml with complete growth medium (DMEM:F12 + 10% (v/v) FCS) lacking antibiotics.

Cells were grown to 70 % confluence in 96-well plates and the spent medium was removed and replaced with 100 μl of the transfection mixture described above. Following a 24 h incubation, the transfection mixture was replaced with 200 μl of complete growth medium (containing antibiotics) in which cells were incubated for a further 72 h.

For larger scale cultures, volumes were scaled up accordingly.

2.2.13. Bacterial transformation

Competent XL-1 Blue *E. coli* cells (Stratagene, California, USA) were aliquoted out into 20 μl volumes in Eppendorf tubes on ice and β-mercaptoethanol (0.4 μl) was added to each tube before incubating on ice for 10 min swirling gently every 2 min. DNA (1μl) was added and the cells were incubated on ice for a further 30 min. The plasmids used consisted of the pIREShyg mammalian expression vector (Clontech Takara, Saint-Germain-en-Laye, France) containing coding DNA sequences corresponding to human FL-APP_{695}, $sAPP_{695}\alpha$ or $sAPP_{695}\beta$. After the 30 min incubation on ice, cells were heat shocked at 42° C for 45 sec then allowed to cool on ice for 2 min before adding 0.9 ml of liquid Luria Broth (LB) (Melford Ltd, Ipswich, UK) prewarmed to 37°C. The cells were then incubated for 30 min at RT with mixing on a carousel before centrifuging for 10 min at 2000 rpm in a bench-top microcentrifuge. 800 μl of the supernatant was discarded and the cells were resuspended

in the remaining 100 μl of liquid. The transformed cells were then plated onto antibiotic-containing agar plates and incubated overnight at 37° C. Agar plates were prepared by adding 7.5 g of agar to 500 ml LB broth. This was autoclaved and allowed to cool to 45° C for 1 h prior to adding 500 μl of 100 mg/ml filter-sterilised ampicillin. Plates were poured and left to set for at least 10 min at RT before plating the transformed bacteria.

2.2.14. Bacterial suspension cultures

Bacterial mini-cultures were grown by stabbing single colonies from the agar plate with a sterile pipette tip and inoculating 3 ml of LB broth containing 3 μl of filter-sterilised ampicillin. Cultures were grown overnight at 37° C in a BioSan Shaker-Incubator ES-20 at 250 rpm (Berlin, Germany). Bacterial midi-cultures were produced by inoculating 50 ml of LB broth (containing 50 μl ampicillin (100 mg/ml)) with 500 μl of mini-culture. Cultures were incubated overnight at 37° C in the bench top shaker-incubator.

2.2.15. DNA preparation

Bacterial midi-cultures were centrifuged for 20 min at 7300 rpm and 4° C using a JLA 25.50 rotor (Beckman Coulter, Indianapolis, USA). The supernatant was discarded and cell pellets were stored at -20° C for at least 24 h before use. Plasmid DNA purification was carried out using QIAGEN Plasmid Midi Kits (Hilden, Germany) following the manufacturer's protocol. Finally, the DNA pellet was re-dissolved in 250 μl of filter-sterilised dH_2O and quantified using a NanoDrop spectrophotometer (Thermo Fisher Scientific, Waltham, USA).

2.2.16. Plasmid linearization and DNA precipitation

Restriction enzyme digest mixture (Table. 2.5) was prepared for each plasmid and samples were incubated overnight at 37° C. The DNA was then precipitated by adding 1/10 volume of filter-sterilised 3 M sodium acetate, pH 5.2 to the 50 μl digested DNA. This was followed by the addition of two volumes of cold absolute ethanol, mixing and incubating at -20° C for 1 h. DNA samples were then centrifuged for 20 min at 14 000 rpm (4° C) in a benchtop microcentrifuge. The supernatant was

removed and 300 μl of cold 80 % (v/v) ethanol was added to the DNA pellet without resuspending. The DNA was then centrifuged again for 5 min under the same conditions. The supernatant was removed and the DNA was resuspended in 30 μl of sterile dH_2O in a sterile flow hood.

Table. 2.5. Components of restriction enzyme digest solutions.

Ingredient	Quantity
DNA	10 μg
Restriction enzyme (Ahd1)	0.5 μl
Acetylated BSA (10 μg/μl stock)	0.5 μl
10x restriction enzyme buffer	5 μl
dH_2O (filter-sterilized)	To make the volume up to 50 μl.

2.2.17. Stable transfection of mammalian cells

HEK293 cells were grown to confluence in T75 cm^2 flasks, harvested by trypsinisation (section 2.2.1) and the cell pellet was resuspended in 0.8 ml of complete growth medium. The 30 μl of previously linearized plasmid (section 2.2.16) was added to a 2 mm electroporation cuvette (Gene Pulser®/MicroPulser™ 0.4 cm gap; Bio-rad, Deeside, UK) to which the resuspended cells were transferred and mixed well with the DNA. Cells were stably transfected by electroporation in the ECM 630 electroporator (square wave, 120V, 25 ms, 2 mm path width; Bio-rad, Deeside, UK). Transfected cells were resuspended in 5 ml of complete growth medium prior to transferring them into another 10 ml of DMEM in a T75 cm^2 flask. A selection control flask with electroporated cells (but no plasmid) was also produced. The growth medium was replaced the following morning with a fresh 10 ml of the same medium. Once the cells reached approximately 60% confluence, 30 μl of the selection antibiotic hygromycin B (provided as a 50 mg/ml stock in PBS; Thermo Fisher Scientific, Waltham, USA) was added to the medium. The cells were then cultured as previously described (section 2.2.1) in the presence of antibiotic until all of the selection control cells had died. At this point the surviving transfected cells were split into two flasks and cultured once more in the presence of antibiotic until confluent. The successfully transfected cells were then either frozen in liquid nitrogen (section 2.2.1) or used for further experiments.

2.2.18. Co-culture of ARPE-19 and HEK293 cells

A transwell system consisting of a 24-well plate and ThinCert™ Cell Culture Inserts was purchased from Greiner Bio One (Stonehouse, UK). HEK293 cells were grown in the inserts (0.1-1.15 ml total medium volume) and ARPE-19 cells were seeded into the basal wells of the system (1.2 ml total medium volume). Both cell types were cultured in DMEM:F12 complete growth medium at the indicated volumes for 7 days before discarding the inserts and collecting ARPE-19 cells by trypsinisation (120 μl of trypsin added to each well). The trypsin was neutralized by the addition of 1.2 ml of growth medium and cells were pelleted in 1.5 ml Eppendorf tubes centrifuged at low speed (1500 rpm) for 5 min in a bench-top microcentrifuge. Cell pellets were resuspended in 360 μl of PBS and cell viability was determined using the Trypan blue assay (section 2.2.5) taking into account the volume differences compared to T25 cm^2 flasks.

2.2.19. Statistical analysis

Statistical analysis was conducted using IBM SPSS statistics software (version 28). Normal distribution was confirmed for the data using Shapiro Wilk's test then a Student's t-test or Welch's t-test was used for comparing two sets of data depends on the equality of variances (Levene's F-test) result. For comparing multiple groups of data, ANOVA and Tukey or Games-Howell post-hoc analysis were conducted (also depends on the equality of variances (Levene's F-test) result). Error bars represent the means ± standard deviation (SD). Figures show a representative immunoblot and the number of replicates and significance level for each experiment is indicated in the relevant figure legends. The n number represents sample replicates in the same experiment.

Chapter 3

Optimisation of the effects of UV-A on APP processing and viability in ARPE19 cells

3. Optimisation of the effects of UV-A on APP processing and viability in ARPE-19 cells

Although several protective mechanisms exist to block UV from reaching the retina including the cornea and the lens, a proportion of UV-A light (315-400nm) is still able to penetrate the retina and cause photochemical damage (Roberts, 2001; Glickman, 2011). Studies have shown an association between the severity of light exposure and the development and exacerbation of multiple age-related ocular diseases including AMD (Chalam *et al.*, 2011; Roberts, 2011). The specific mechanisms leading to AMD are largely unknown. However, the pathology of the disease involves degeneration of the retinal photoreceptors, RPE and Bruch's membrane (Ding *et al.*, 2009). One of the main characteristics of AMD is the formation and accumulation of subretinal pigment epithelial deposits named "drusen" which contain amyloid beta (generated from the amyloid precursor protein) as a major constituent (Ratnayaka *et al.*, 2015).

In the current study, we sought to determine the effects of UV-A light on the viability of human retinal pigment epithelial cells (ARPE-19) and to examine possible links to APP expression and proteolysis. Given the established link between UV light exposure and p53 levels (Ayala *et al.*, 2007; Latonen and Laiho, 2005; McFeat *et al.*, 2013) and the links between this latter protein and APP expression (Cuesta *et al.*, 2009b; Buizza *et al.*, 2013) we also examined any concomitant effects of UV-A on p53 levels in ARPE-19 cells. Furthermore, later experiments would examine any potentially protective effects of GLP-1 mimetics against UV-A in this cell line. As such it was essential that we determined an appropriate UV-A dosage that could be used to achieve significant but not total cell death.

3.1. Optimisation of UV-A effects on cell viability

Initially UV dosage effects on cell viability were examined with subsequent experiments using GLP-1 mimetics in mind. Previous publications have incorporated a pre-treatment period with GLP-1 mimetics in serum-free medium prior to stress exposure (Sharma *et al.*, 2014; Panagaki *et al.*, 2017). The induction of apoptosis and the associated effects of UV light on cell counts have also commonly been examined following a suitable recovery period following treatment (Gao and Talalay, 2004; Chou *et al.*, 2018). As such, the initial experiment conducted in the current study involved pre-incubating ARPE-19 cells for 6 h in UltraMEM before exchanging this for phenol red-free medium (to mitigate any UV absorption effects of phenol red) for various timed exposures to UV-A. The cells were then transferred into fresh UltraMEM for an 18 h recovery period prior to determining cell viability using Trypan blue counts as described in the Materials and Methods section. Note that 80% confluent cells were employed initially such that they would still be actively dividing during the extended treatment periods (Youn *et al.*, 2011).

The results (Fig. 3.1.) demonstrated that 50 min exposure of ARPE-19 cells to UV-A irradiation induced a moderate but significant decrease in viable cell count by 32.1 ± 2.0 % relative to the control cell cultures. However, longer UV-A treatment times of 75, 100 and 125 min led to dramatic decreases in the number of viable cells by 79.8 ± 4.0, 99.8 ± 0.3 and 100 ± 0 % respectively, relative to controls. Therefore, 50 min was chosen as the optimum UV-A treatment time to be used in the subsequent UV experiments.

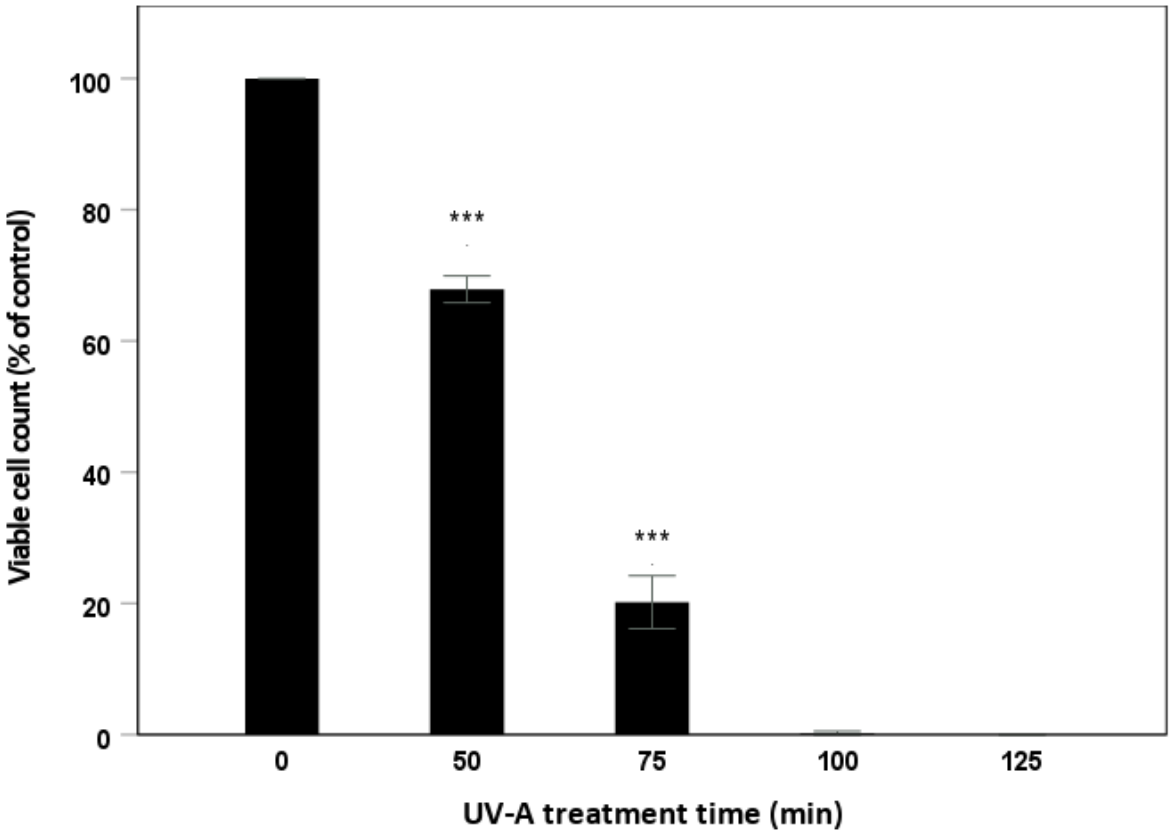

Figure 3.1. Trypan blue viable cell counts following UV-A irradiation of 80% confluent ARPE-19 cells and a subsequent 18 h post-irradiation recovery period. T25 cm^2 flasks of 80% confluent cells were preincubated for 6 h in UltraMEM and then transferred into phenol red-free DMEM during UV exposure for the indicated times. The cells were then transferred into UltraMEM for an 18 h recovery period. Viable cell numbers were then determined using the Trypan blue assay as described in the Materials and Methods. Results are expressed as a percentage of no UV exposure control cell cultures and are means ± S.D. (n=3). ***, $p \leq 0.001$.

3.2. The effects of UV-A light on p53 levels

Given the previously established links between UV-A exposure and apoptosis (Ayala *et al,.* 2007; Latonen & Laiho, 2005) and the links between p53 and APP expression (Cuesta *et al*., 2009; Buizza *et al.,* 2013) the relationship between UV-A light exposure and p53 protein levels was investigated in the current study. As such, lysates from ARPE-19 cells treated for 50 min with UV-A light were prepared and equal amounts of proteins were resolved by SDS-PAGE and immunoblotted using an anti-p53 antibody (see Materials and Methods). The results (Fig. 3.2.) showed a trend towards

an increase in p53 levels following UV exposure. However, the level of increase of 78.0 ± 58.5 % was highly variable between different samples and therefore it was statistically insignificant.

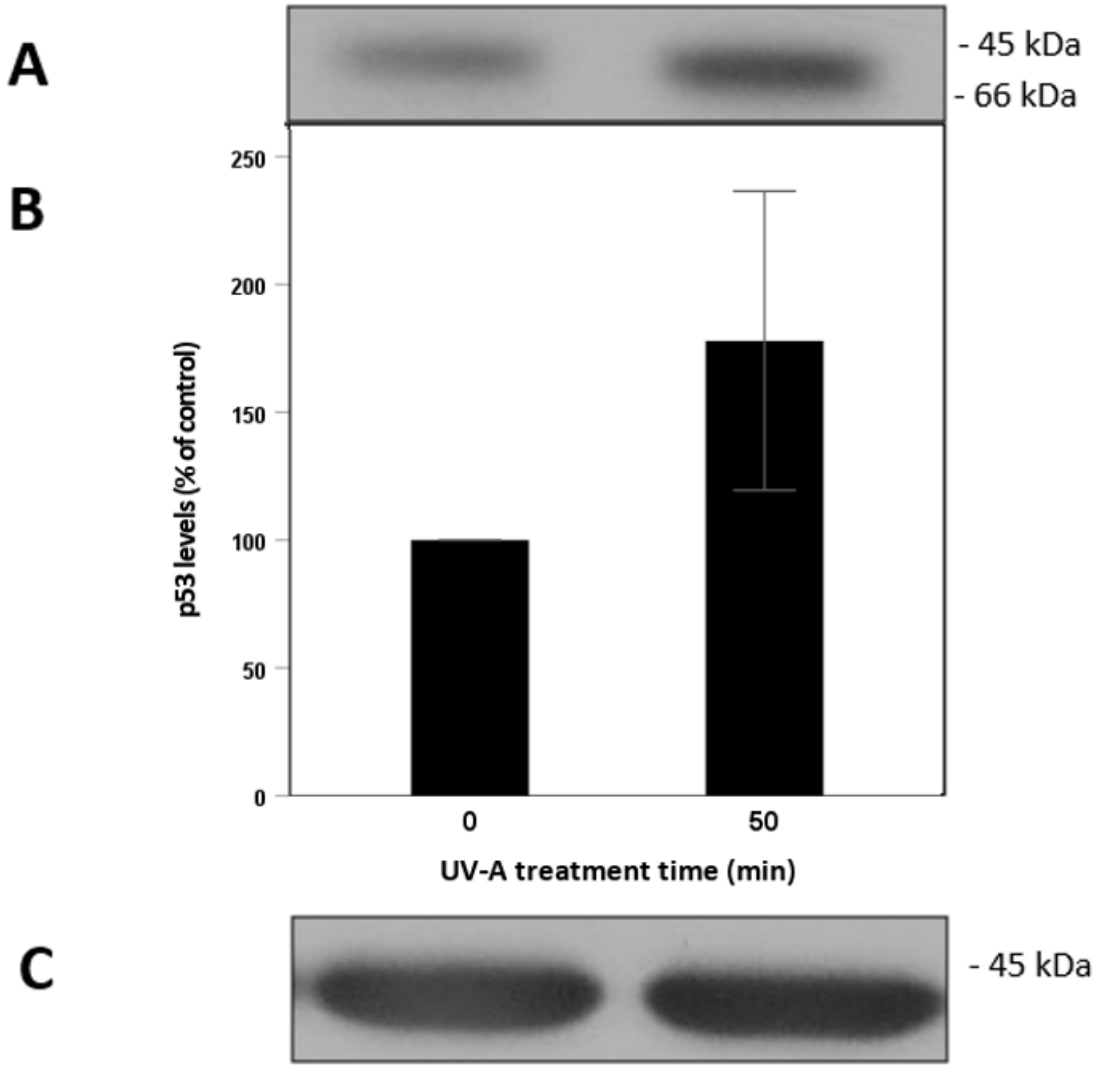

Figure 3.2. p53 levels following 50 min UV-A irradiation of 80% confluent ARPE-19 cells and a subsequent 18 h post-irradiation recovery period. T25 cm^2 flasks of 80% confluent cells were preincubated for 6 h in UltraMEM and then transferred into phenol red-free DMEM during UV exposure for 50 min. The cells were then transferred into UltraMEM for an 18 h recovery period. Cell lysates were then prepared and proteins were resolved by SDS-PAGE and immunoblotted as described in the Materials and Methods section. **(A)** Detection of p53 using the anti-p53 antibody. **(B)** Quantification of multiple p53 immunoblots by densitometric analysis. **(C)** Detection of actin using the anti-actin antibody. Results are expressed as a percentage of control cell culture p53 levels and are means ± S.D. (n=3).

3.3. The effects of UV-A light on APP expression and proteolysis

A previous study has shown the ability of UV light to decrease APP levels in SH-SY5Y cells and various other cell lines by accelerating its secretase-dependant processing (Almenar-Queralt *et al.*, 2014). Therefore, in the current study, we examined the effect of UV-A on APP expression and proteolysis in ARPE-19 cells. As such, lysate samples from the UV-A treatments described in the preceding section were also subjected to immunoblotting using the anti-APP C-terminal antibody (Fig. 3.3.). Various possible isoforms and maturation states of APP were detected (Fig. 3.3.A). Given that ARPE-19 cells are not neuronal cells, it is most likely that the heavier protein band shown in (Fig. 3.3.A) represents the mature forms of APP_{770} and/or APP_{751} and the lighter band indicates the immature form(s) of these isoforms. Furthermore, the absence of APP_{695} in ARPE-19 cells has previously been confirmed by comparing immunoblot patterns between mock- and APP_{695}-transfected ARPE-19 stable transfectants (Parkin *et al*. unpublished data). Notably, the APP immunoblots showed that the upper band appeared to decrease to a greater degree than the lower band following UV-A treatment indicating a possible increased processing of the mature protein following UV-A treatment. Quantification of multiple immunoblots (Fig. 3.3.B) showed that FL-APP expression decreased significantly (45.9 ± 23.1 %) following UV-A treatment.

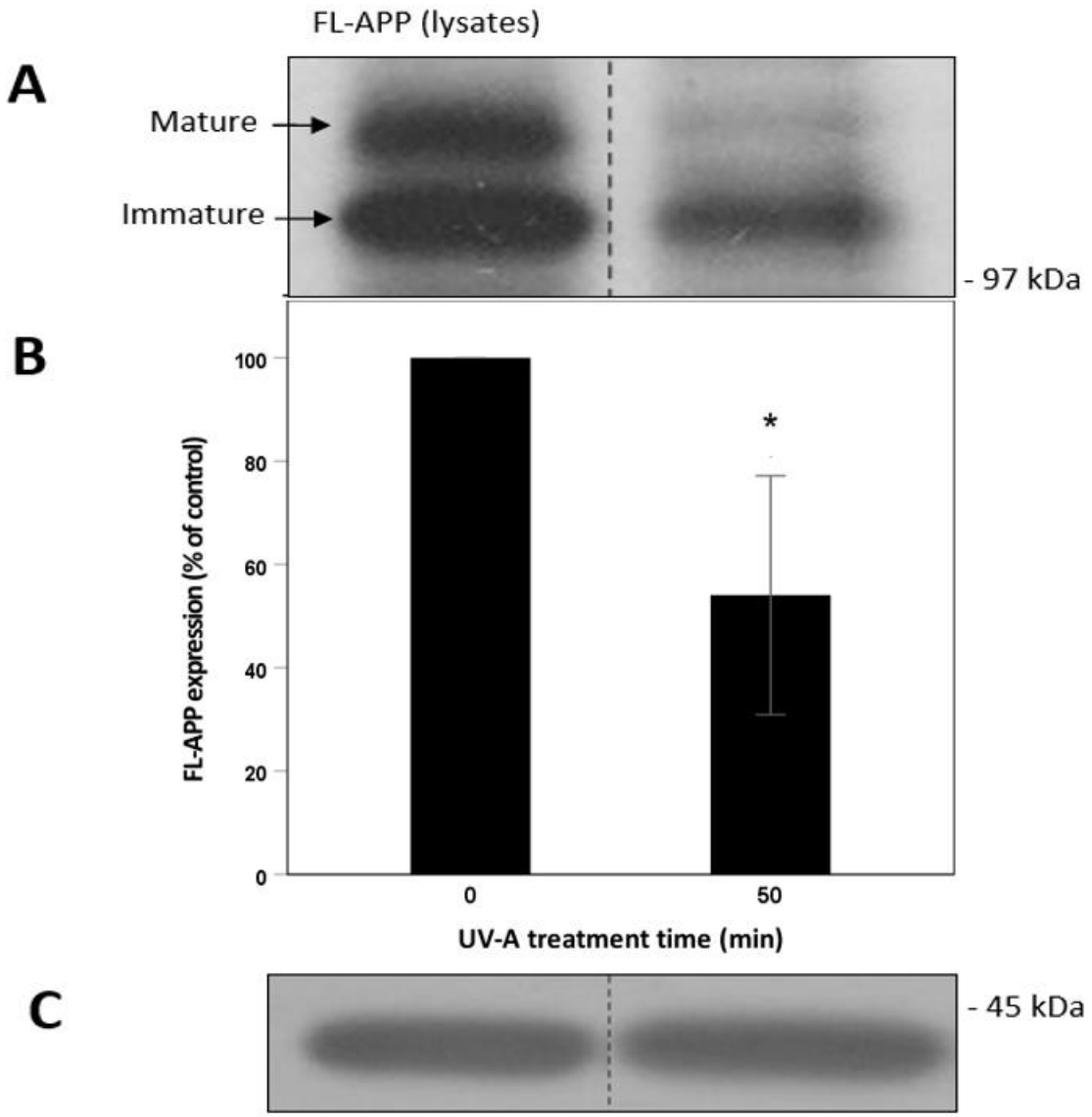

Figure 3.3. FL-APP expression following 50 min UV-A irradiation of 80% confluent ARPE-19 cells and a subsequent 18 h post-irradiation recovery period. T25 cm^2 flasks of 80% confluent cells were preincubated for 6 h in UltraMEM and then transferred into phenol red-free DMEM during UV exposure for 50 min. The cells were then transferred into UltraMEM for an 18 h recovery period. Cell lysates were then prepared and proteins were resolved by SDS-PAGE and immunoblotted as described in the Materials and Methods section. **(A)** Detection of mature and immature forms of FL-APP using the anti-APP C-terminal antibody. **(B)** Quantification of multiple APP immunoblots by densitometric analysis. **(C)** Detection of actin using the anti-actin antibody. Results are expressed as a percentage of control cell cultures and are means ± S.D. (n=3). *, $p \leq 0.05$. Dashed lines indicate where protein bands on the same immunoblot have been rearranged for illustrative purposes.

In order to examine the effects of UV-A irradiation on APP processing, medium samples of UV-treated cells were concentrated and equal volumes were resolved on SDS-PAGE (Materials and Methods). Medium samples were then immunoblotted using two different antibodies to examine the

concentrations of both soluble fragments produced by the amyloidogenic and non-amyloidogenic pathway.

First, the anti-APP 6E10 antibody which recognises amino acid residues 1-16 of the beta amyloid sequence (Pirttila *et al.*, 1994) was used in order to detect sAPPα. The results (Fig. 3.4A and B) showed that sAPPα levels decreased significantly (28.2 ± 11.0 %) following UV-A treatment. However, when results were corrected in order to account for observed changes in cell viability (Fig. 3.4.C), sAPPα levels showed no significant difference from the control levels.

Second, medium samples were immunoblotted using the anti-sAPPβ antibody that recognises the beta-secretase generated fragment sAPPβ. The results (Fig. 3.5A and B) revealed a significant decline in sAPPβ production (51.7 ± 9.8 %) following UV-A treatment. This decline persisted even after taking viability results into account (37.8 ± 12.9 % decrease following UV-A treatment, Fig. 3.5C).

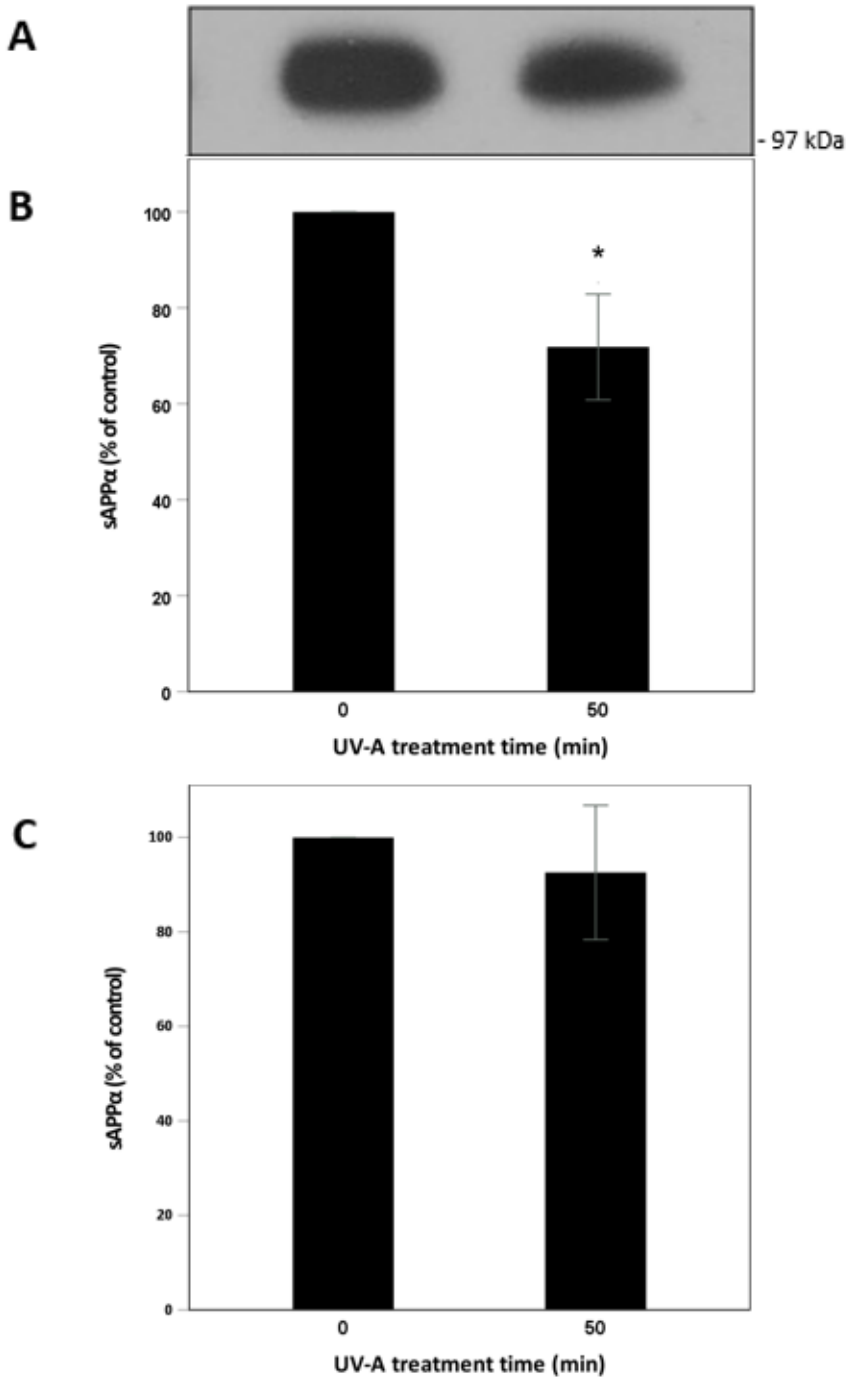

Figure 3.4. sAPPα production following 50 min UV-A irradiation of 80% confluent ARPE-19 cells and a subsequent 18 h post-irradiation recovery period. T25 cm^2 flasks of 80% confluent cells were preincubated for 6 h in UltraMEM and then transferred into phenol red-free DMEM during UV exposure for 50 min. The cells were then transferred into UltraMEM for an 18 h recovery period. Conditioned medium samples were concentrated as described in the Materials and Methods section and equal volumes were resolved by SDS-PAGE and immunoblotted (Materials and Methods). **(A)** Detection of sAPPα using the anti-APP 6E10 antibody. **(B)** Quantification of multiple immunoblots by densitometric analysis showing uncorrected results. **(C)** Quantification of multiple immunoblots by densitometric analysis showing results corrected for observed changes in cell viability. Results are expressed as a percentage of control cell cultures and are means ± S.D. (n=4). *, $p \leq 0.05$.

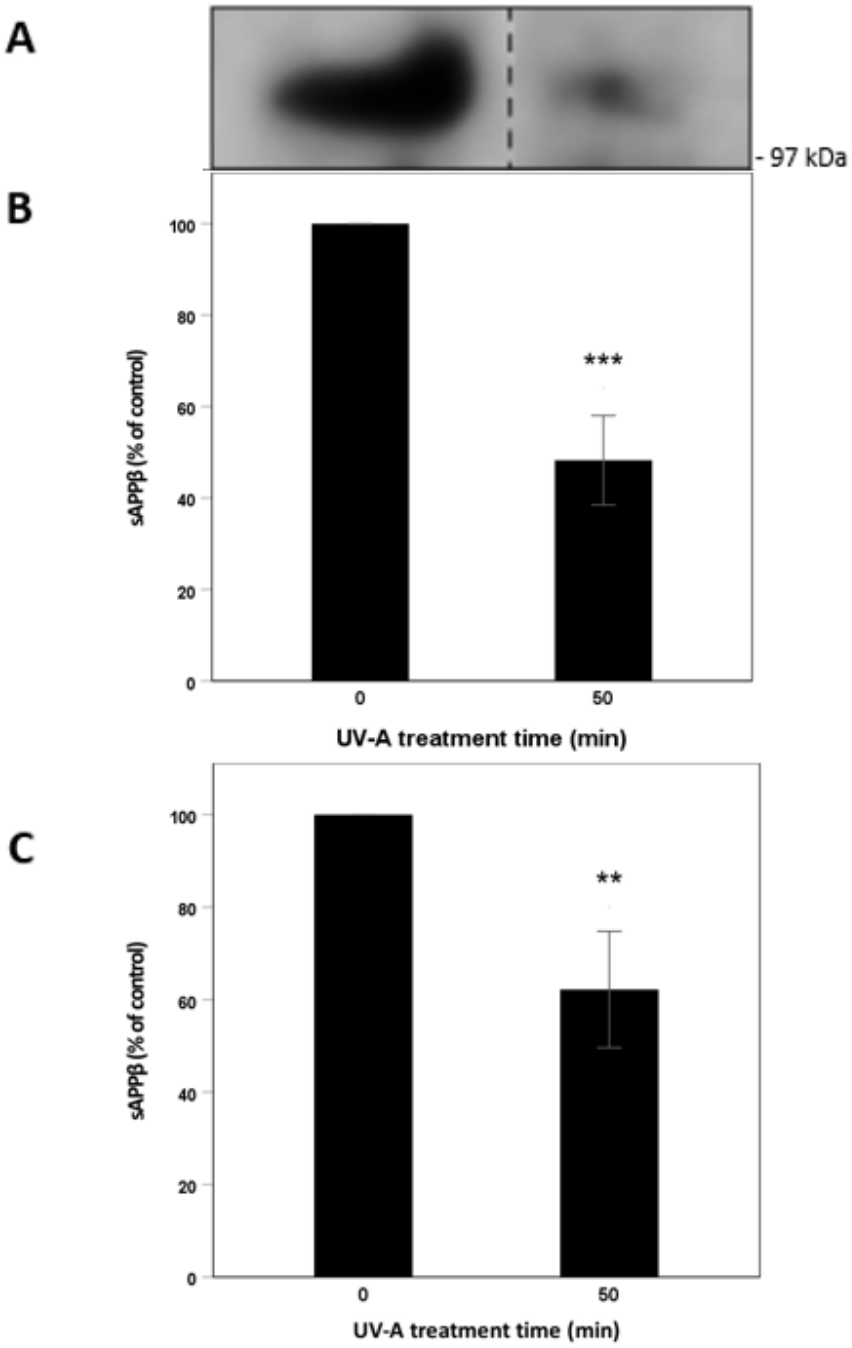

Figure 3.5. sAPPβ production following 50 min UV-A irradiation of 80% confluent ARPE-19 cells and a subsequent 18 h post-irradiation recovery period. T25 cm^2 flasks of 80% confluent cells were preincubated for 6 h in UltraMEM and then transferred into phenol red-free DMEM during UV exposure for 50 min. The cells were then transferred into UltraMEM for an 18 h recovery period. Conditioned medium samples were concentrated as described in the Materials and Methods section and equal volumes were resolved by SDS-PAGE and immunoblotted (Materials and Methods). **(A)** Detection of sAPPβ using the anti-sAPPβ antibody. **(B)** Quantification of multiple immunoblots by densitometric analysis showing uncorrected results. **(C)** Quantification of multiple immunoblots by densitometric analysis showing results corrected for observed changes in cell viability. Results are expressed as a percentage of control cell cultures and are means ± S.D. (n=3). **, $p \leq 0.01$; ***, $p \leq 0.001$. Dashed lines indicate where protein bands on the same immunoblot have been rearranged for illustrative purposes.

3.4. Summary

The aim of these experiments was to optimise UV-A treatment conditions in ARPE-19 cells by firstly determining an appropriate UV dosage that would lead to significant but not total cell death. This was essential considering subsequent experiments in which the effects of GLP-1 mimetics and various secretase inhibitors on UV-treated cells will be examined. It was shown that treatment of 80% confluent cells with 50 min of UV-A light reduced the viable cell count significantly by approximately 30% relative to the control cell cultures. The second aim was to study the effects of UV-A on p53 levels and APP expression and proteolysis in these cells. p53 levels were highly variable following UV-A exposure with a trend towards an increase. On the other hand, UV-A light lead to a significant decrease in FL-APP expression which was accompanied by a significant reduction in the production of the secreted APP fragment sAPPβ but not significant for sAPPα after correcting results to account for observed changes in cell viability.

Chapter 4

The effects of full-length APP and its proteolytic fragments on UV-mediated decreases in ARPE-19 cell viability

4. The effects of full-length APP and its proteolytic fragments on UV-mediated decreases in ARPE-19 cell viability

Full-length APP levels in ARPE-19 cell lysates were reduced following UV treatment in the current study (see Chapter 3, Fig. 3.3) and have also previously been shown to decrease in SH-SY5Y cells and various other cell lines following similar treatment (Almenar-Queralt *et al*., 2014). In the current study, there were also some UV-mediated changes in the generation of soluble APP fragments following UV treatment (see Chapter 3, Figs. 3.4 and 3.5) and similar decreases in soluble APP production have previously been inferred following a decrease in cell-associated APP C-terminal fragment levels after UV treatment (Almenar-Queralt *et al.*, 2014). Furthermore, the soluble APP (sAPPα) fragment generated via the non-amyloidogenic pathway is known to exert neuroprotective and neurotrophic functions linked to growth-factor-like properties (Plummer *et al.*, 2016; Gralle *et al.*, 2009; Wehner *et al.*, 2004); properties not shared by the sAPPβ fragment generated via the opposing amyloidogenic pathway (Copanaki *et al.*, 2010).

The data outlined above raise the possibility of APP being mechanistically linked to a cellular response to UV treatment. As such, in the current study, the effects of full-length APP and its metabolites, sAPPα and sAPPβ, on the proliferation and resistance to UV-A treatment of ARPE-19 cells were examined.

4.1. The effects of siRNA-mediated APP depletion on ARPE-19 cell viability following UV-A treatment

In order to explore what effects FL-APP might have on the response of ARPE-19 cells to UV-A exposure, an siRNA protein depletion strategy was initially employed. In this respect, it was first necessary to determine a suitable concentration of both DharmaFECT transfection reagent and APP siRNA that did not impact significantly on cell viability whilst still significantly depleting APP expression.

Initially, a range of DharmaFECT concentrations (as recommended in the manufacturer's protocol) were applied to 70% confluent ARPE-19 cells in 96-well plates in a final volume of 100 μl. Here, a mock transfection process lacking siRNA was performed (see Materials and Methods) such that the final DharmaFECT concentrations added to cells were 0, 0.5, 1, 2.5 and 5 μl/ml. The cells were then cultured for a total of 48 h and an MTS assay was subsequently performed in order to determine cell viability (see Materials and Methods). The results (Fig. 4.1) showed that viable cell numbers decreased by 10.6 ± 6.8 % at the highest concentration of DharmaFECT (5 μl/ml). However, a similar reduction in cell numbers was also apparent at the lowest DharmaFECT concentration of 0.5 μl/ml (10.1 ± 3.1 %). Given that the second highest compound concentration did not yield any reductions in cell viability even after 48 h, 2.5 μl/ml DharmaFECT was chosen as a suitable concentration to use in subsequent transfections.

Next, the toxicity of different concentrations of APP siRNA were determined whilst the final DharmaFECT concentration was kept constant at 2.5 μl/ml. In these experiments the preparation of DharmaFECT:siRNA complexes was performed (see Materials and Methods) and they were subsequently applied to 70% confluent cells for 24 h before changing the medium to complete growth medium and culturing the cells for a further 72 h before conducting an MTS assay. Note, here that the incubation time with DharmaFECT:siRNA complexes (24 h) was half that with DharmaFECT alone as detailed in the preceding paragraph. As such, no toxicity from the DhramaFECT alone would be expected. The results (Fig. 4.2.) showed that none of the siRNA concentrations resulted in any decreases in cell viability. As such, the highest concentration of APP siRNA (37.5 nM) was employed for future experiments in order to achieve the highest level of APP depletion.

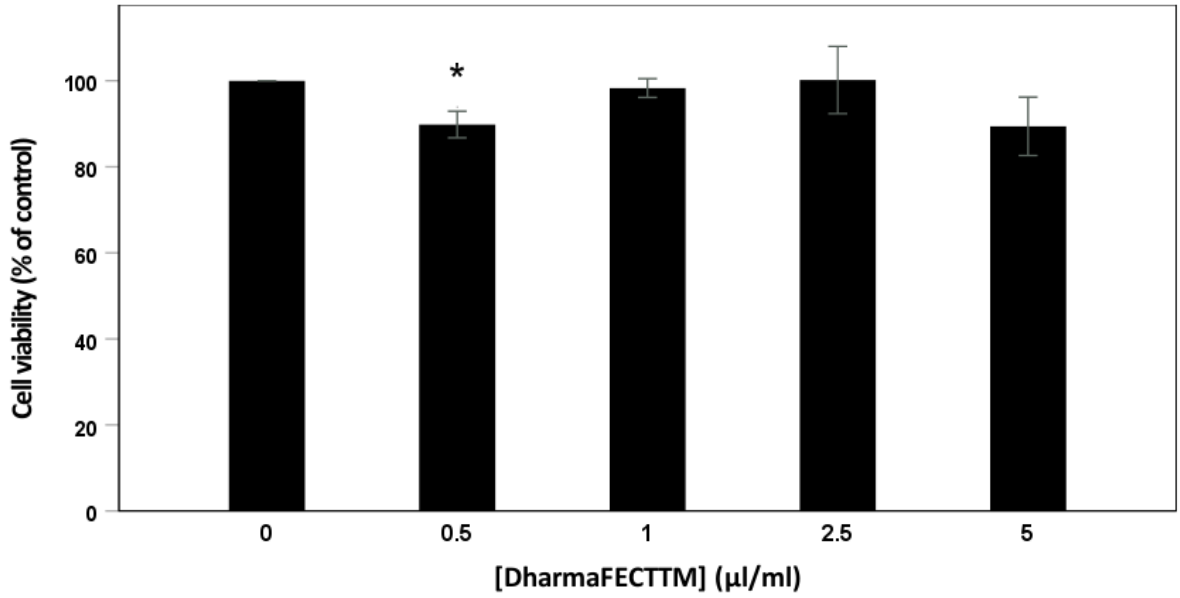

Figure 4.1. Cell viability following DharmaFECT treatment of ARPE-19 cell cultures. ARPE-19 cultures (70% confluent) were treated for 48 h with the indicated concentrations of DharmaFECT in 100 µl of a mixture of UltraMEM and DMEM:F12 media lacking antibiotics and then subjected to an MTS viability assay as described in the Materials and Methods section. Results are expressed as a percentage of no DharmaFECT control cell cultures and are means ± S.D. (n=4). *, $p \leq 0.05$.

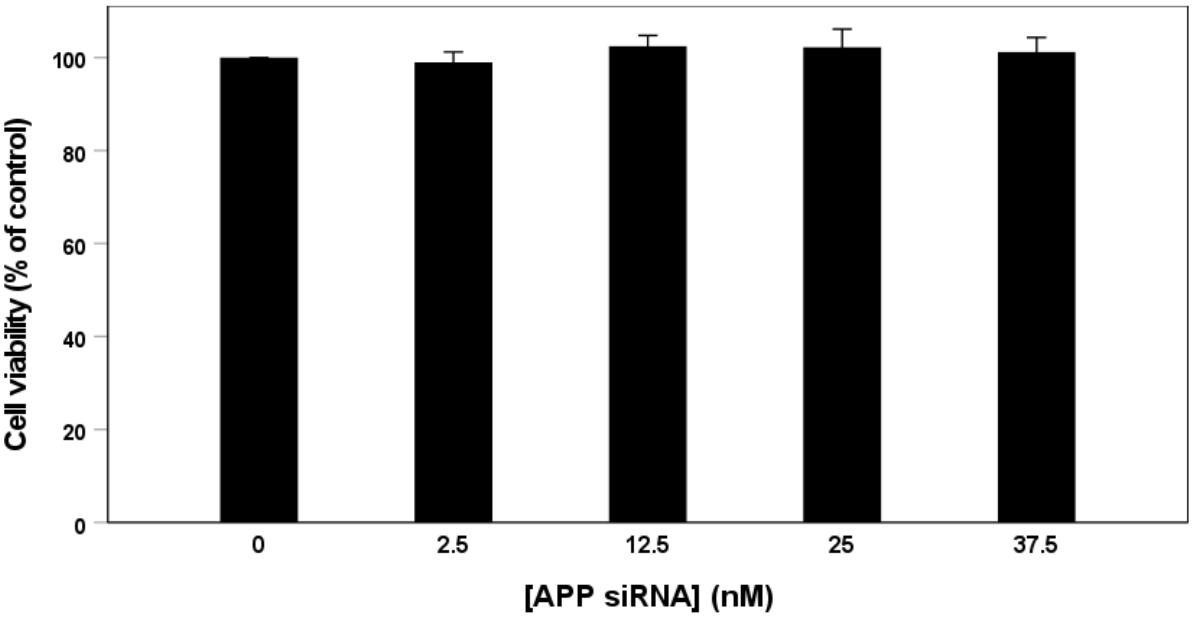

Figure 4.2. Cell viability following APP siRNA treatment of ARPE-19 cell cultures. ARPE-19 cultures (70% confluent) were treated for 24 h with DharmaFECT/siRNA complexes (final DharmaFECT concentration of 2.5 µl/ml) at the indicated final siRNA concentrations in 100 µl of a mixture of UltraMEM and DMEM:F12 media lacking antibiotics (see Materials and Methods). The medium was then replaced with fresh complete medium (DMEM:F12) and cells were incubated a further 72 h before performing an MTS cell viability assay (Materials and Methods). Results are expressed as a percentage of no siRNA control cell cultures and are means ± S.D. (n=6).

Having ascertained suitably non-toxic concentrations of both Dharmafect and siRNA to use (2.5 μl/ml final DharmaFECT concentration and 37.5 nM APP-siRNA) the effects of these conditions on APP levels and the resistance of ARPE-19 cells to UV-A irradiation were examined. In this experiment, 60% confluent T25cm^2 flasks of cells were employed such that they would be at 80% confluence following the initial 48 h siRNA transfection period (24 h with the complexes on the cells followed by a further 24 h after complex removal and replacement with complete growth medium). Medium was then exchanged for phenol red-free DMEM while cells were subjected to 50 min UV-A exposure (see Materials and Methods). The medium was then exchanged again for UltraMEM and the cells were cultured for an 18 h recovery period prior to determining cell viability using Trypan blue counts as described in the Materials and Methods section. Note that the incubation period was a total of approximately 24 h shorter than in the preceding experiment (Fig. 4.2) so should not have resulted in any appreciable toxicity from DharmaFECT:siRNA complexes alone. The results (Fig. 4.3.) revealed that UV treatment for 50 min caused a significant decrease in viable cell counts (by 25.4 ± 2.2 %) as seen previously (see Chapter 3, Fig. 3.1). The depletion of APP using siRNA did not affect the viability of cells without UV-A treatment. However, interestingly, depleting APP seemed to increase the resistance of cells to UV-A treatment restoring viability to 94.2 ± 4.1 % that of the control cultures.

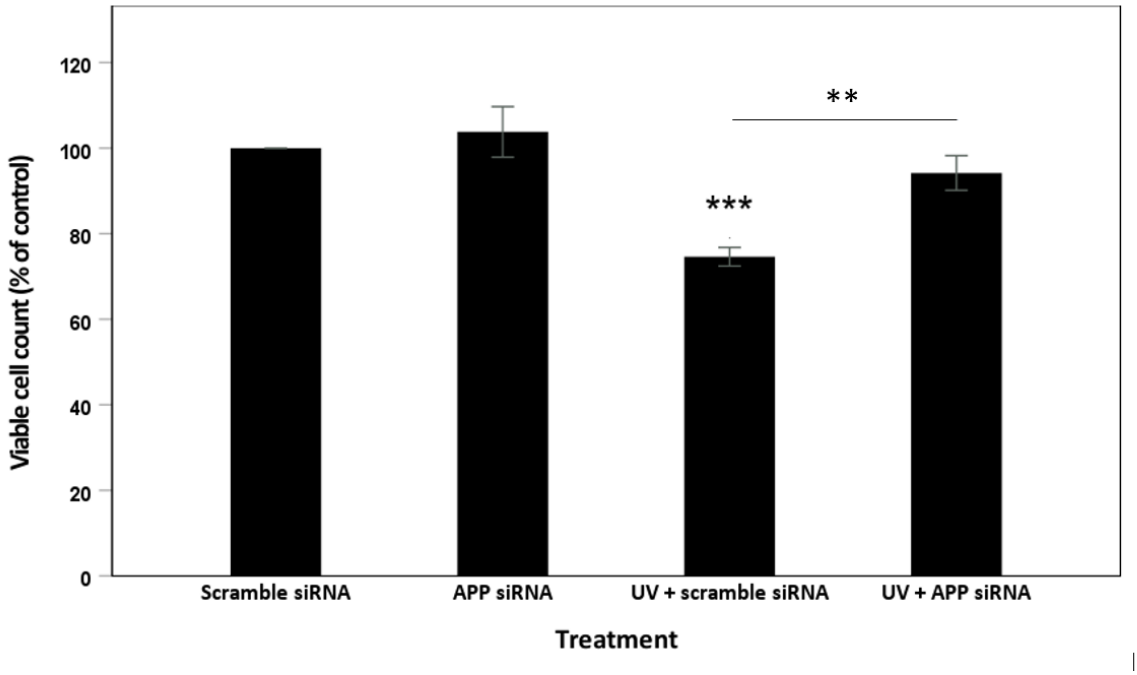

Figure 4.3. Viable cell numbers of ARPE-19 cell cultures following APP siRNA treatment combined with 50 min UV-A irradiation. T25 cm^2 flasks of 60% confluent cells were treated for 24 h with DharmaFECT/siRNA complexes (final DharmaFECT concentration of 2.5 μl/ml) and either APP or scramble siRNA at 37.5 nM (see Materials and Methods) in a mixture of UltraMEM and DMEM:F12 media lacking antibiotics. The medium was then replaced with fresh complete medium DMEM:F12 and cells were incubated further for 24 h before transferring them into phenol red-free DMEM during UV exposure for 50 min. The cells were then transferred into UltraMEM for an 18 h recovery period. Viable cell numbers were then determined using the Trypan blue assay as described in the Materials and Methods. Results are expressed as a percentage of control cell cultures and are means ± S.D. (n=3). **, $p \leq 0.01$; ***, $p \leq 0.001$.

Lysate samples from the APP siRNA and UV-A treatments described above were subjected to immunoblotting using the anti-APP C-terminal antibody. The results (Fig. 4.4A and C) showed a significant decrease in full-length APP levels following siRNA treatment (32.6 ± 4.3 %). Furthermore, APP levels were also decreased following UV-A treatment (in the absence of APP siRNA) as observed in the preceding results chapter (Fig. 3.3). Interestingly, these two effects seemed additive in terms of the decreased levels of APP in APP siRNA and UV-A treated cells. Similar results were observed in terms of the APP-CTF (Fig. 4.4B and C).

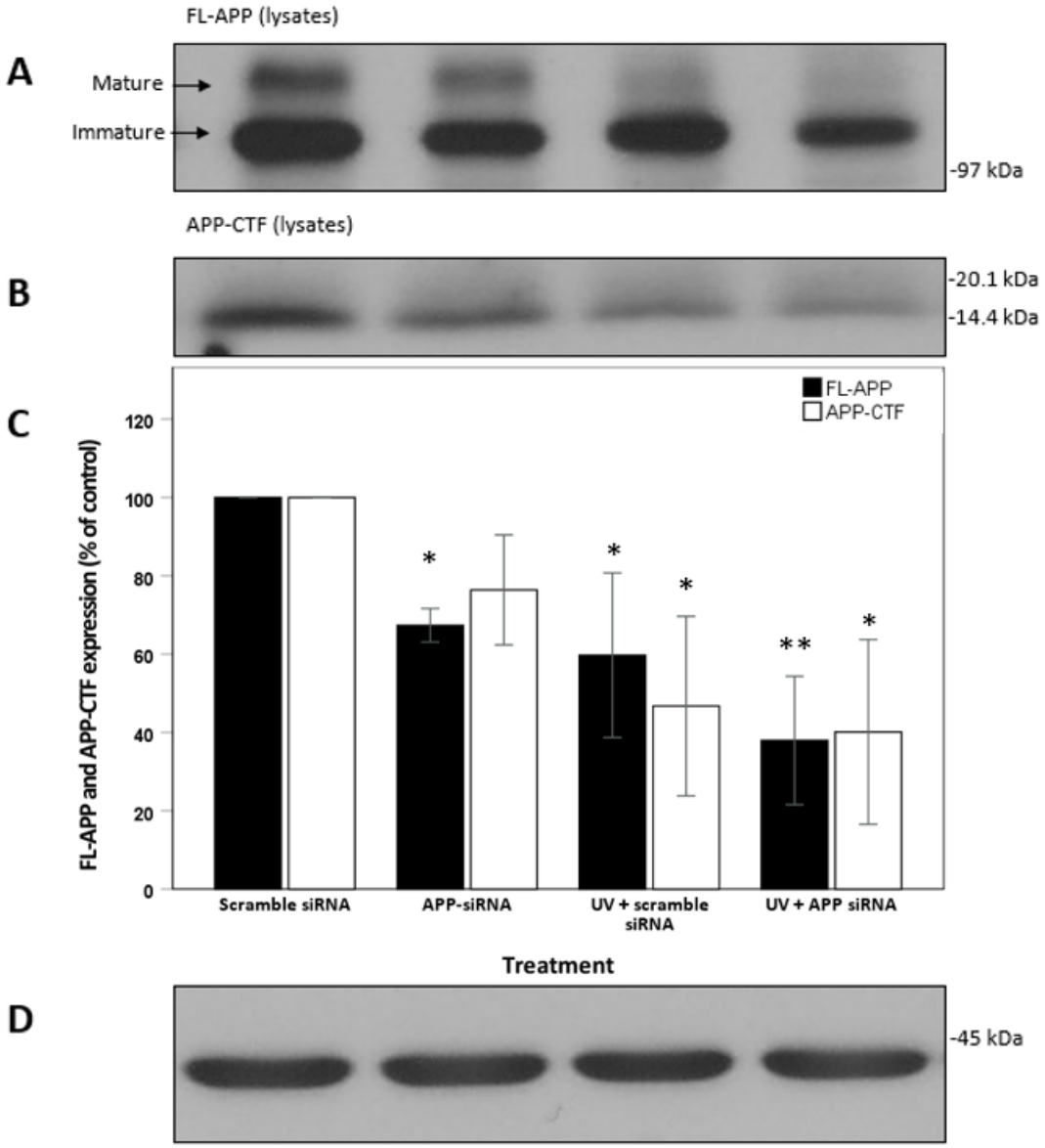

Figure 4.4. APP expression in ARPE-19 cells following APP siRNA treatment combined with 50 min UV-A irradiation. T25 cm^2 flasks of 60% confluent cells were treated for 24 h with DharmaFECT/siRNA complexes (final DharmaFECT concentration of 2.5 μl/ml) and either APP or scramble siRNA at 37.5 nM (see Materials and Methods) in a mixture of UltraMEM and DMEM:F12 media lacking antibiotics. The medium was then replaced with fresh complete medium DMEM:F12 and cells were incubated further for 24 h before transferring them into phenol red-free DMEM during UV exposure for 50 min. The cells were then transferred into UltraMEM for an 18 h recovery period. Cell lysates were then prepared and proteins were resolved by SDS-PAGE and immunoblotted as described in the Materials and Methods section. **(A)** Detection of mature and immature forms of FL-APP using the anti-APP C-terminal antibody. **(B)** Detection of APP-CTF using the anti-APP C-terminal antibody. **(C)** Quantification of multiple APP immunoblots by densitometric analysis. **(D)** Detection of actin using the anti-actin antibody. Results are expressed as a percentage of control cell cultures and are means ± S.D. (n=3). *, $p \leq 0.05$; **, $p \leq 0.01$, compared with the corresponding control.

The same lysates were then immunoblotted for p53 and the results (Fig. 4.5) showed a trend towards an increase in p53 levels following UV-A exposure. However, none of the changes reached statistical significance.

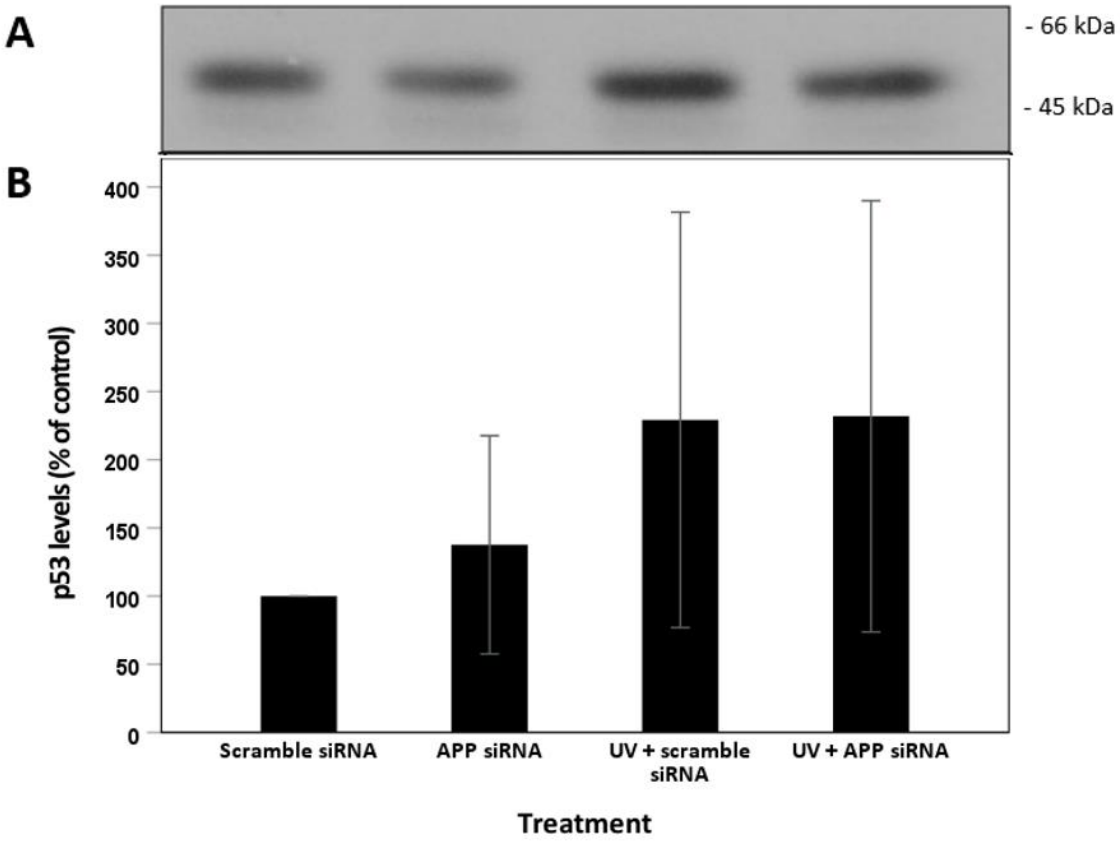

Figure 4.5. p53 levels in ARPE-19 cells following APP siRNA treatment combined with 50 min UV-A irradiation. T25 cm^2 flasks of 60% confluent cells were treated for 24 h with DharmaFECT/siRNA complexes (final DharmaFECT concentration of 2.5 μl/ml) and either APP or scramble siRNA at 37.5 nM (see Materials and Methods) in a mixture of UltraMEM and DMEM:F12 media lacking antibiotics. The medium was then replaced with fresh complete medium DMEM:F12 and cells were incubated further for 24 h before transferring them into phenol red-free DMEM during UV exposure for 50 min. The cells were then transferred into UltraMEM for an 18 h recovery period. Cell lysates were then prepared and proteins were resolved by SDS-PAGE and immunoblotted as described in the Materials and Methods section. **(A)** Detection of p53 using the anti-p53 antibody. **(B)** Quantification of multiple p53 immunoblots by densitometric analysis. Results are expressed as a percentage of control cell cultures and are means ± S.D. (n=3).

4.2. The effects of exogenous soluble APP fragments on the growth/viability of ARPE-19 cells

Given the results in the preceding section showing that depleting endogenous APP enhanced the resistance of ARPE-19 cells to UV-A treatment (Fig. 4.3), we next sought to determine the effects of increasing soluble APP fragment levels on the viability of ARPE-19 cells. To this end stable HEK cell transfectants over-expressing FL-APP_{695}, $sAPP_{695}\alpha$ or $sAPP_{695}\beta$ were generated and co-cultured with ARPE-19 cells in a transwell system followed by subsequent monitoring of ARPE-19 cell viability.

4.2.1. Confirmation of APP/APP fragment over-expression in HEK cell lines

HEK cell stable transfectants were generated as described in the Materials and Methods section using pIREShyg vector containing coding inserts corresponding to FL-APP_{695}, $sAPP_{695}\alpha$ or $sAPP_{695}\beta$ or an empty vector for the control cells. In order to verify transfection levels, confluent T75cm^2 flasks of transfected cells were incubated for 24 h in UltraMEM before harvesting cells and preparing lysates and concentrated conditioned medium (see Materials and Methods).

Equal amounts of protein from cell lysates were then immunoblotted using the anti-APP C-terminal antibody and the results (Fig. 4.6A) showed three bands, the lower two and most intense of which likely corresponded to mature and immature forms of FL-APP_{695} as these bands were far more prominent (increased by 118.8 ± 28.7%; Fig. 4.6C) in the FL-APP_{695}-transfected cell lysates. The upper most band in the anti-APP C-terminal antibody blots was the same in all four cell lysates and, therefore, likely corresponded to the endogenous $APP_{751/770}$ in HEK cells (Fig. 4.6A). Notably levels of APP-CTFs were massively increased in the FL-APP_{695}-transfected cell lysates (Fig. 4.6B); in fact endogenous levels of these fragments were below the levels of detectability in HEK cells and so could not be quantified relative to the mock-transfected cells.

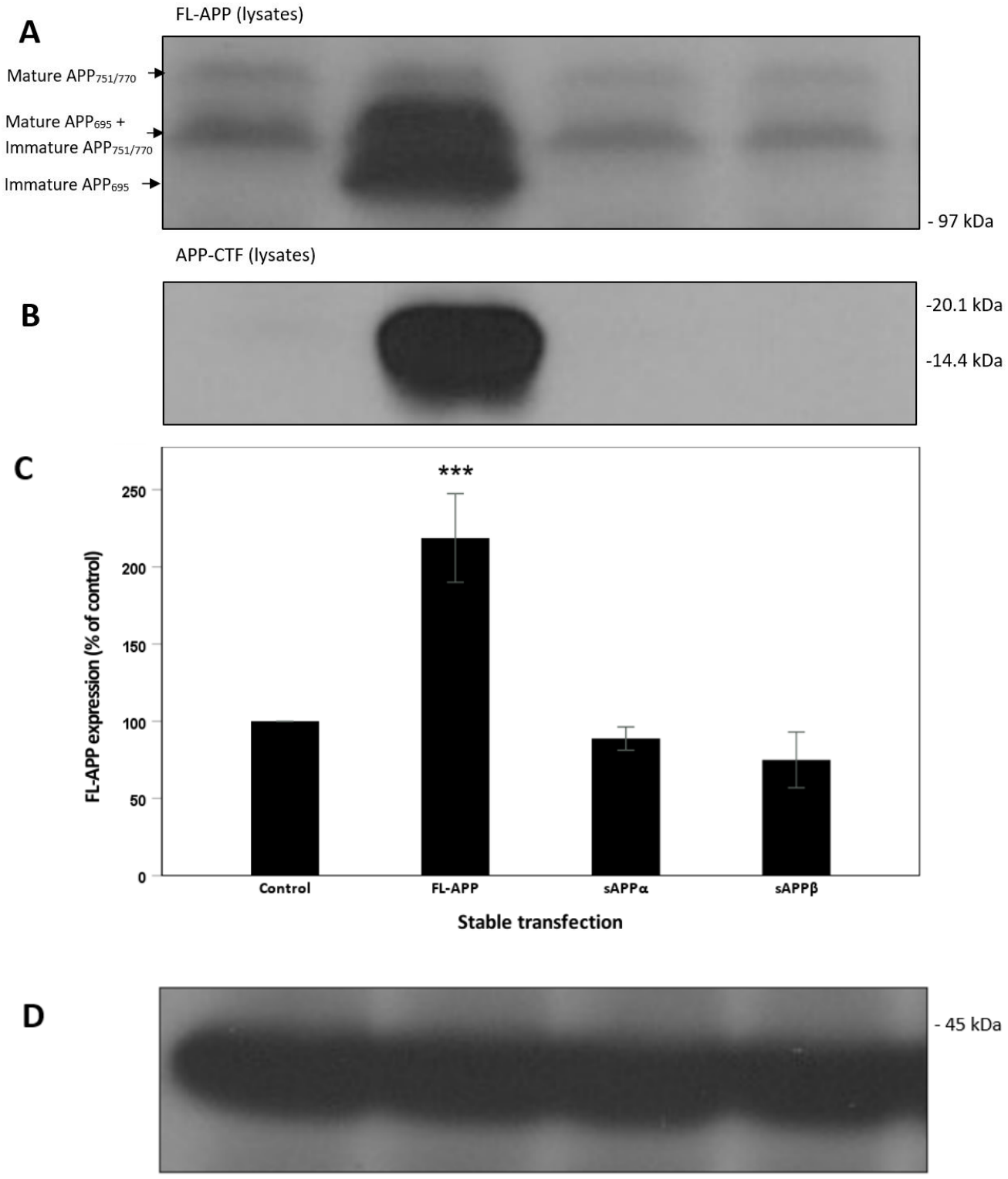

Figure 4.6. FL-APP and APP-CTF expression in HEK293 cell stable transfectant cell lysates. Stable transfectants were generated as described in the Materials and Methods section using pIREShyg vector containing coding inserts corresponding to FL-APP_{695}, $sAPP_{695}\alpha$ or $sAPP_{695}\beta$ or an empty vector for the control cells. Confluent T75cm^2 flasks of transfectants were then cultured in UltraMEM for 24 h before harvesting cells and preparing lysates (see Materials and Methods). Equal amounts of protein from lysates were then immunoblotted with the APP C-terminal antibody in order to detect **(A)** FL-APP and **(B)** APP-CTFs. **(C)** Quantification of multiple FL-APP immunoblots by densitometric analysis. **(D)** Detection of actin using the anti-actin antibody. Results are expressed as a percentage of control (mock-transfected) cell cultures and are means ± S.D. (n=3). ***, $p \leq 0.001$.

The concentrated conditioned medium samples (equal volumes) from the stable HEK transfectants were then immunoblotted using the 6E10 antibody in order to determine sAPPα levels. The results (Fig. 4.7A) showed prominent bands corresponding to sAPP$_{695}\alpha$ in medium from both FL-APP$_{695}$ and sAPP$_{695}\alpha$-transfected cells. At this level of blot exposure, there were no corresponding fragments detected in the mock- or sAPP$_{695}\beta$-transfected cells. Therefore, quantification of the results was performed relative to the FL-APP$_{695}$-transfected cells and showed 1.82 ± 0.34-fold more sAPP$_{695}\alpha$ in medium from cells expressing the soluble fragment compared to the full-length protein (Fig. 4.7B). It was only when the blots were over-exposed that endogenous sAPPα shed from cells became visible (Fig. 4.7C) and, although it is conceded that at this level of over-exposure the blots were most-likely not quantitative, it is estimated that the sAPPα generated by the FL-APP$_{695}$ and sAPP$_{695}\alpha$-transfected cells was 684.2 ± 72.3 % and 1082.5 ± 44.4 % higher, respectively, than the mock-transfected cells whereas levels produced by the sAPP$_{695}\beta$-transfected cells were unchanged (Fig. 4.7D).

Immunoblotting the same medium samples using the anti-sAPPβ antibody showed a protein band corresponding to sAPP$_{695}\beta$ in the medium from both FL-APP$_{695}$ and sAPP$_{695}\beta$-transfected cells (Fig. 4.8.A). Endogenous sAPPβ was not detectable even with longer blot exposure times. Quantification of multiple sAPPβ immunoblots (Fig. 4.8.B) revealed that levels of this fragment were 7.82 ± 2.37-fold higher in medium from the sAPP$_{695}\beta$-transfected HEK cells compared to those transfected with FL-APP$_{695}$.

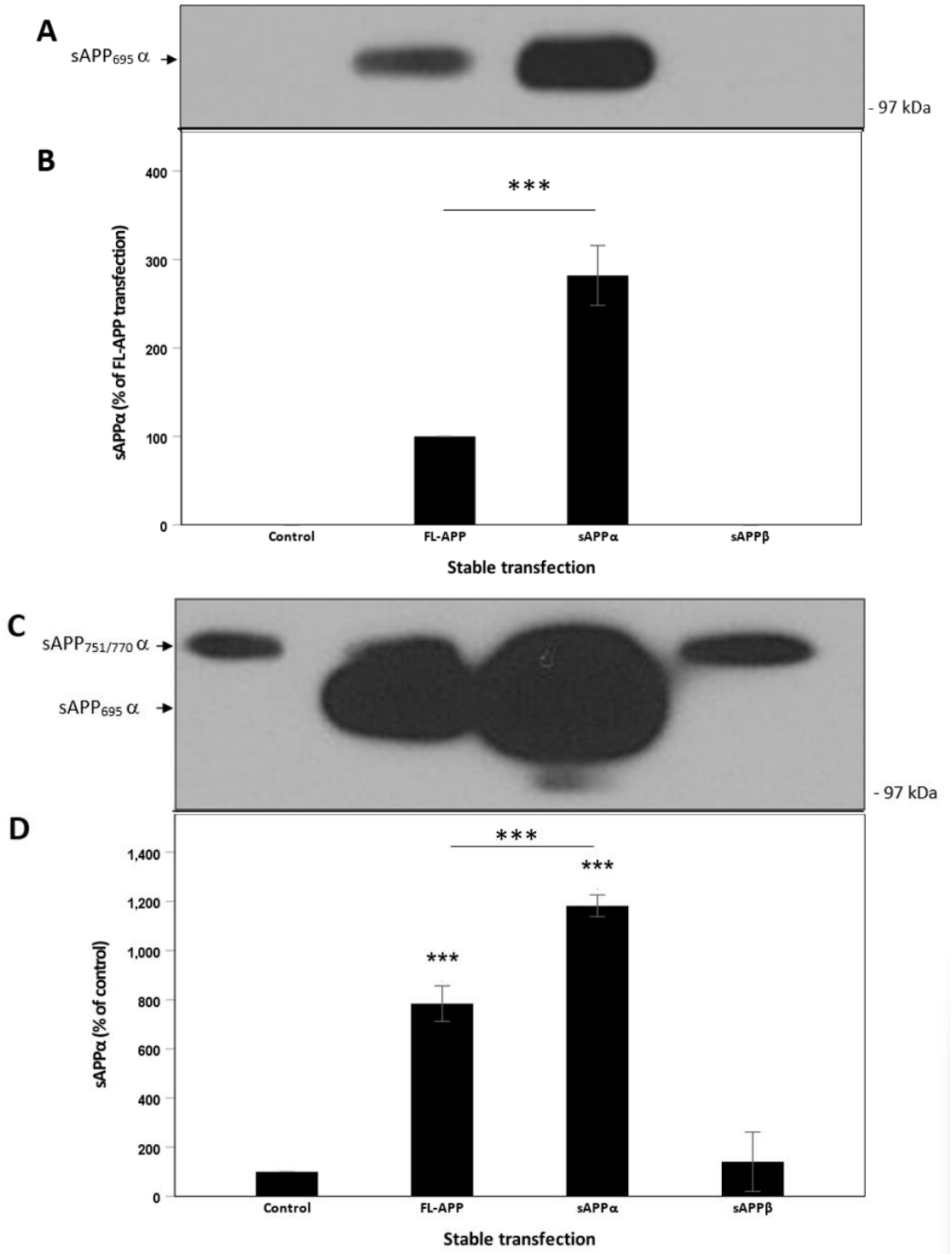

Figure 4.7. sAPPα production by HEK293 cell stable transfectants. Stable transfectants were generated as described in the Materials and Methods section using pIREShyg vector containing coding inserts corresponding to FL-APP_{695}, $sAPP_{695}\alpha$ or $sAPP_{695}\beta$ or an empty vector for the control cells. Confluent T75cm^2 flasks of transfectants were then cultured in UltraMEM for 24 h before harvesting cells and preparing concentrated conditioned medium samples (see Materials and Methods). Equal volumes of these samples were then immunoblotted with the 6E10 antibody in order to detect sAPPα. **(A)** Representative lower exposure 6E10 blot with **(B)** quantification of multiple immunoblots relative to the $sAPP_{695}\alpha$ generated by the FL-APP_{695}-transfected cells. **(C)** Representative over-exposure 6E10 blot and associated **(D)** quantification relative to mock-transfected controls. Results are means ± S.D. (n=2 or n=3). ***, $p \leq 0.001$.

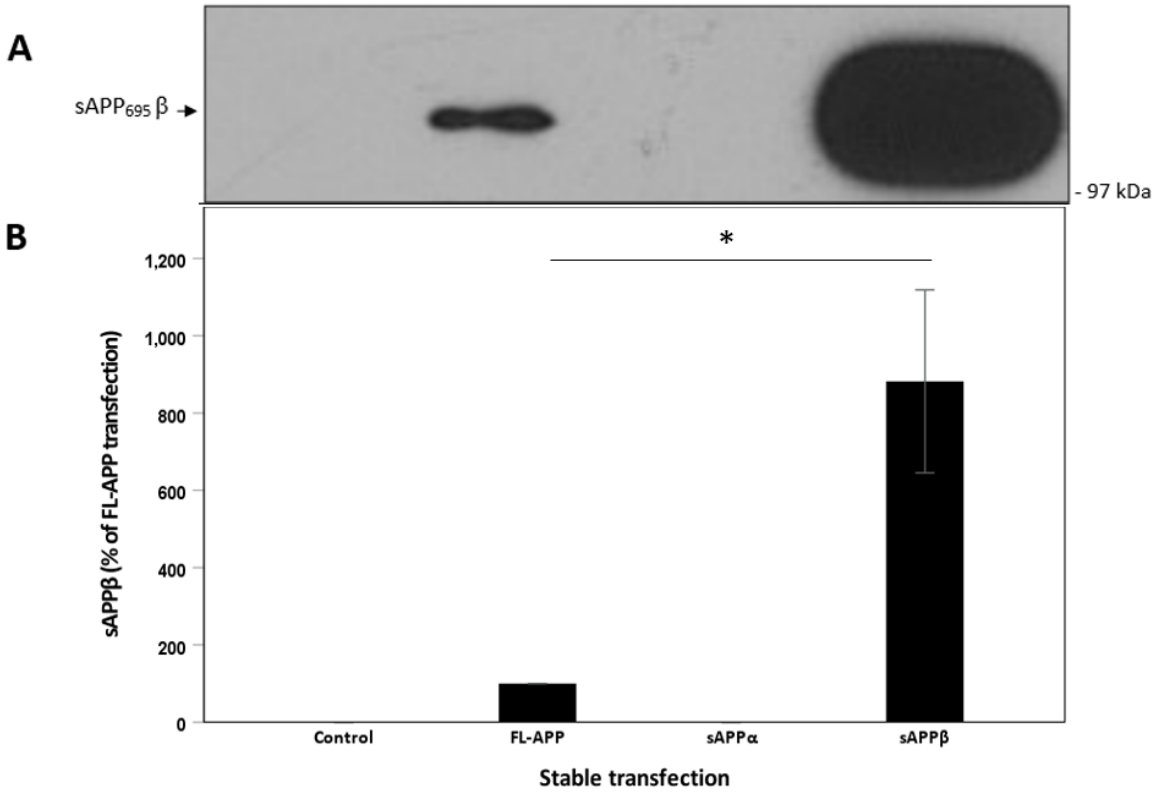

Figure 4.8. sAPPβ production by HEK293 cell stable transfectants. Stable transfectants were generated as desribed in the Materials and Methods section using pIREShyg vector containing coding inserts corresponding to FL-APP_{695}, $sAPP_{695}\alpha$ or $sAPP_{695}\beta$ or an empty vector for the control cells. Confluent T75cm^2 flasks of transfectants were then cultured in UltraMEM for 24 h before harvesting cells and preparing concentrated conditioned medium samples (see Materials and Methods). Equal volumes of these samples were then immunoblotted with the anti-sAPPβ antibody **(A)** and multiple immunoblots were quantified by densitometric analysis **(B).** Results are expressed as a percentage of sAPPβ production by cells transfected with FL-APP and are means ± S.D. (n=3). **, $p \leq 0.01$.

4.2.2. Lack of effect of APP transfections on p53 levels in HEK cells

Previous studies have demonstrated a relationship between p53 and APP expression levels (Cuesta *et al.*, 2009b; Buizza *et al.*, 2013). As such, cell lysate samples from the HEK293 stable transfectants in the current study were also subjected to immunoblotting using an anti-p53 antibody (see Materials and Methods). However, the results (Fig. 4.9) showed that overexpressing FL-APP or its soluble fragments had no effect on cellular p53 levels.

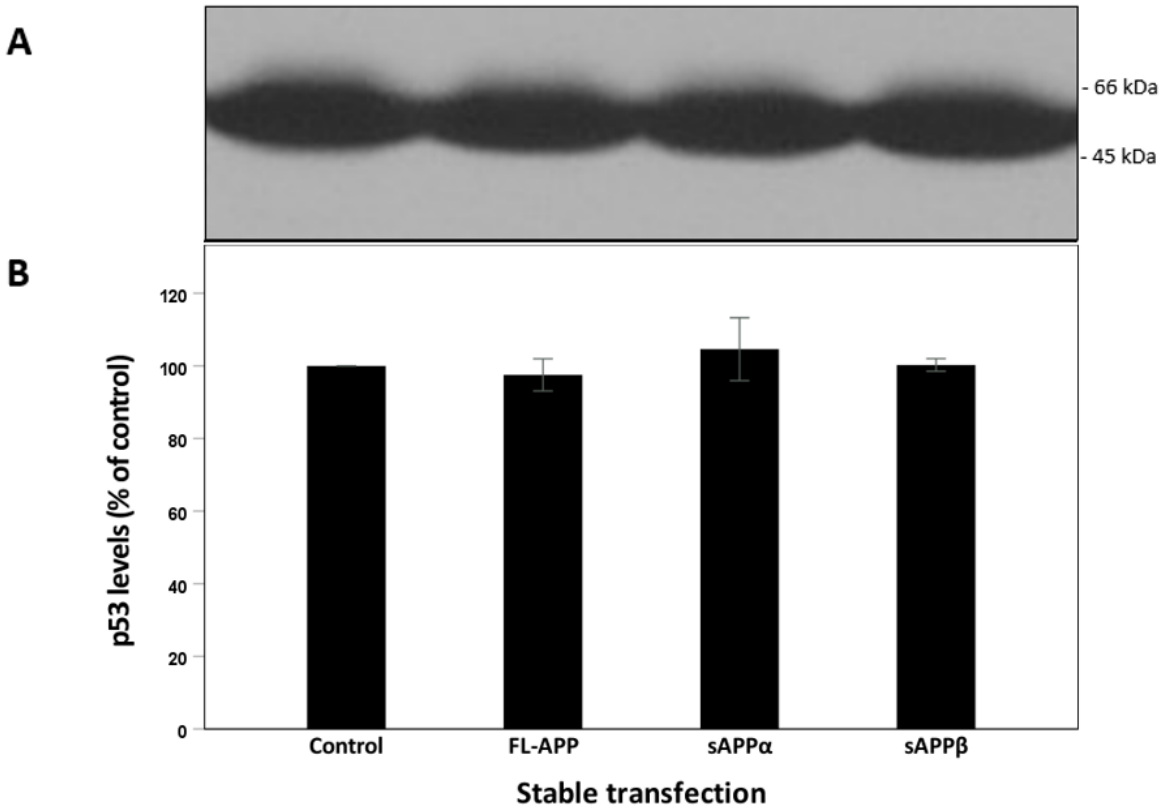

Figure 4.9. p53 levels in HEK293 cell stable transfectant cell lysates. Stable transfectants were generated as described in the Materials and Methods section using pIREShyg vector containing coding inserts corresponding to FL-APP_{695}, $sAPP_{695}\alpha$ or $sAPP_{695}\beta$ or an empty vector for the control cells. Confluent T75cm^2 flasks of transfectants were then cultured in UltraMEM for 24 h before harvesting cells and preparing lysates (see Materials and Methods). Equal amounts of protein from lysates were then immunoblotted with the p53 **(A)** and multiple immunoblots were quantified by densitometric analysis **(B).** Results are expressed as a percentage of control (mock-transfected) cell cultures and are means ± S.D. (n=3).

4.2.3. Co-culture of ARPE-19 and HEK293 APP stable transfectants

Having confirmed the over-expression of FL-APP_{695}, $sAPP_{695}\alpha$ and $sAPP_{695}\beta$ in the HEK cell stable transfectants, the next step was to examine the effects of co-culturing these cells in a transwell system on the proliferation of ARPE-19 cells. Initially it was necessary to determine appropriate numbers of each cell line to seed into the upper and lower chamber of the system.

The ARPE-19 cells would be seeded in the lower chamber and, ideally, should grow to confluence over a 7-day period to permit appropriate monitoring of cell proliferation. As such, a range of ARPE-19 cell numbers were seeded into the wells of a 24 well transwell plate and the time taken

for each well of cells to reach confluence was monitored by light microscopy. The results (Fig. 4.10) showed that wells seeded initially with 12250 cells reached confluence after 7 days.

As far as the HEK cells were concerned, they would ideally reach confluence in the upper chambers of the transwell plates very quickly in order to maximize soluble APP fragment production but, at the same time, not become so over-confluent that they died off before the end of a 7-day growth period. Seeding 150 000 HEK cells led to 70% confluence by about day 3 (data not shown) and the cells continued to proliferate reaching about 90% confluence by day 7 (Fig. 4.11). Cells seeded at higher densities had begun to die off by day 7 (data not shown). Therefore, 150,000 was chosen as the optimum number of HEK cells to seed in the subsequent transwell co-culture experiments with ARPE-19 cells.

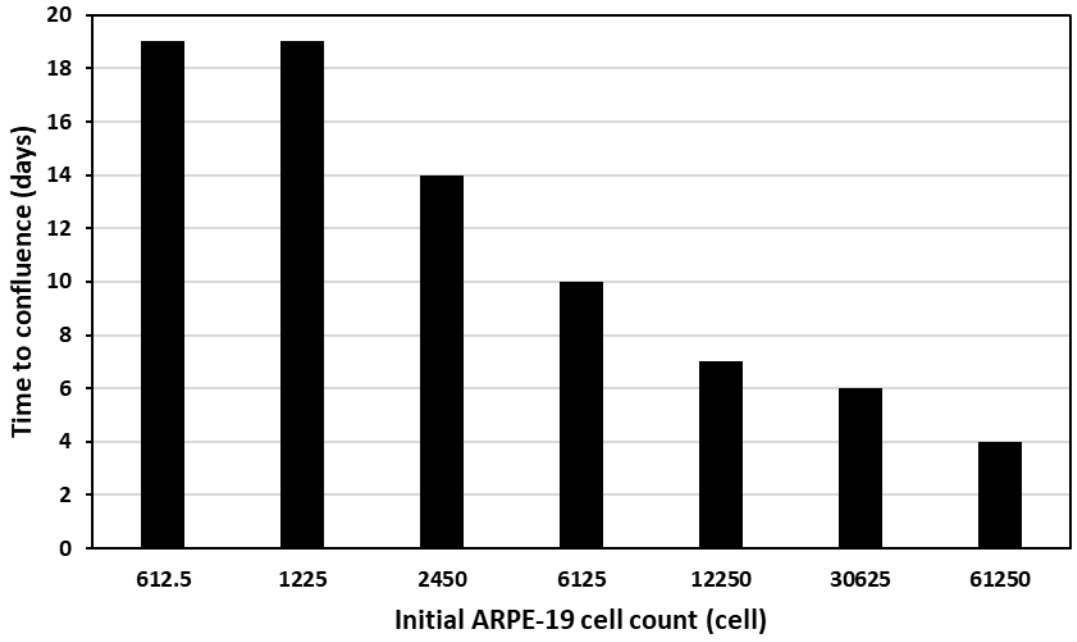

Figure 4.10. Time taken by ARPE-19 cells to reach 100% confluence as a function of the number of cells initially seeded. ARPE-19 cells were counted on a haemocytometer and seeded out in triplicate wells in a 24-well plate at the cell numbers indicated (X-axis). Cells were monitored daily by light microscopy in order to determine the approximate time taken to reach full confluence as indicated on the Y-axis. Results are the means of the three triplicate wells.

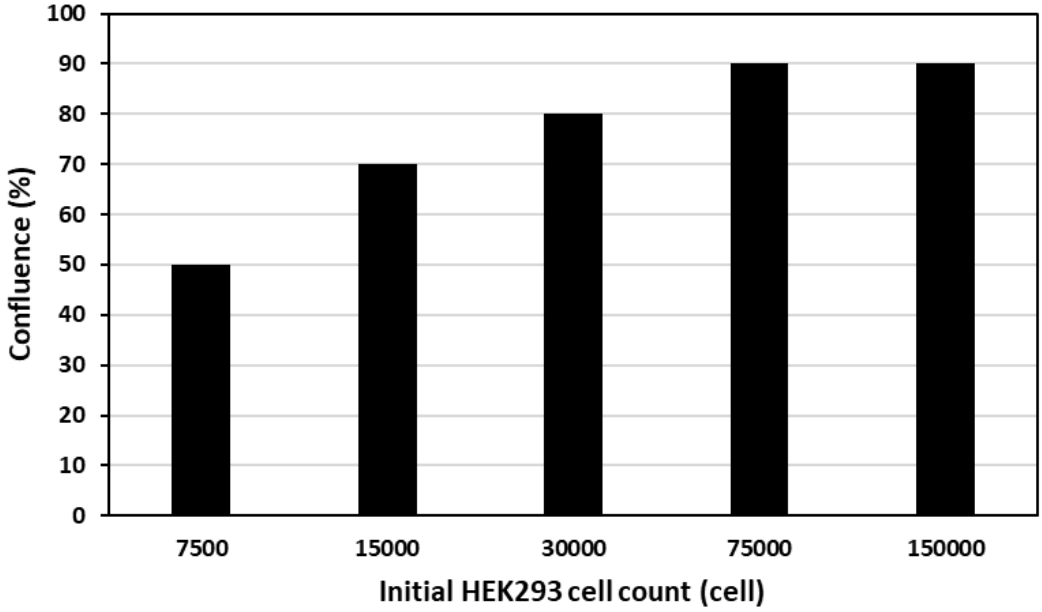

Figure 4.11. The level of confluence of HEK293 cells 7 days after seeding as a function of the number of cells initially seeded. HEK293 cells were counted on a haemocytometer and seeded out in triplicate wells in a 24-well plate at the cell numbers indicated (X-axis). Cells were monitored by light microscopy in order to determine their confluency. Results represent the percentage of confluence at day 7. Results are the means of the three triplicate wells.

Next, the effects of HEK cell transfectant co-culture on the proliferation of ARPE-19 cells were monitored. ARPE-19 cells (12250) were seeded into the lower chambers of the transwell system whilst 150 000 HEK cells expressing FL-APP_{695}, $sAPP_{695}\alpha$, $sAPP_{695}\beta$ or empty vector were seeded in the upper chambers. Both chambers contained complete growth medium (DMEM:F12) as both types of cells grew effectively in this medium. After 7 days the number of viable ARPE-19 cells in the lower chambers was determined by Trypan blue counts as described in the Materials and Methods section. The results (Fig. 4.12) demonstrated that culturing ARPE-19 cells in the presence of $sAPP_{695}\alpha$-transfected HEK293 cells led to a 55.8 ± 12.0 % increase in viable cell numbers compared to cells cultured in the presence

of mock-transfected HEK cells. Neither FL-APP$_{695}$ nor sAPP$_{695}\beta$ appeared to increase the viable ARPE-19 cell count.

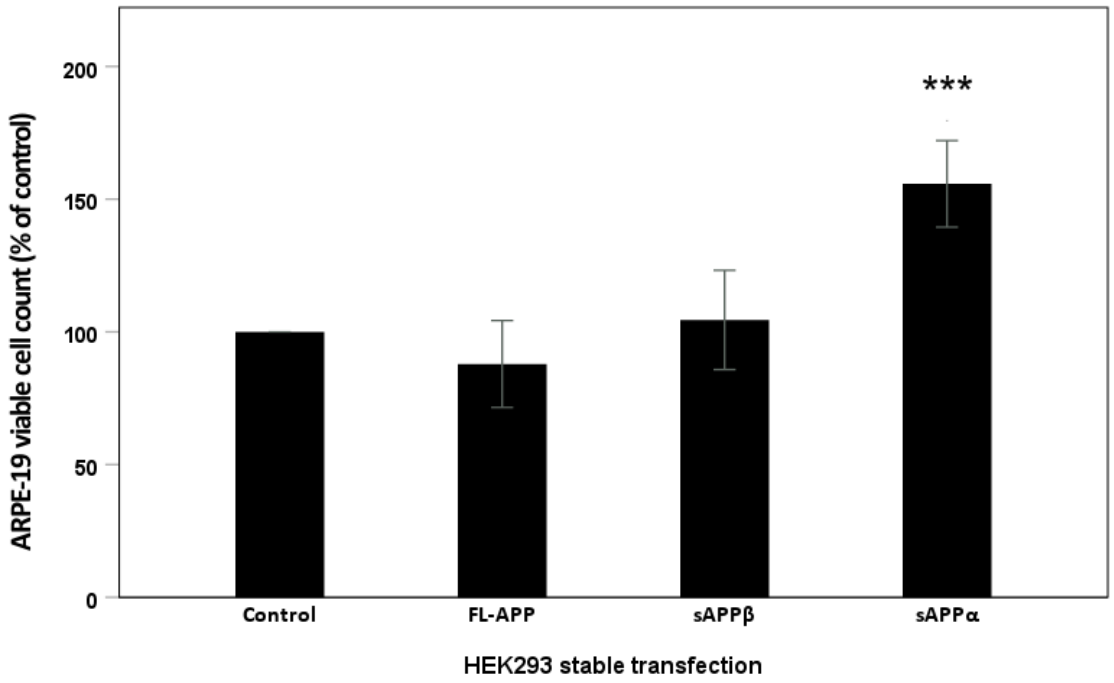

Figure 4.12. ARPE-19 viable cell counts following 7-day co-culture with HEK293 stable transfectants. ARPE-19 and the indicated HEK293 transfectants were seeded in the lower and upper chambers, respectively, of transwell plates. Both cell types were grown in the same DMEM:F12 medium for 7 days at which point the upper chambers/inserts were discarded and the ARPE-19 cells in the lower chambers were harvested by trypsinisation. Viable cell numbers were then determined using the Trypan blue assay as described in the Materials and Methods section. Results are expressed as a percentage of viable cell numbers in control cell cultures (i.e. AREPE-19 cells cultured in the presence of mock-transfected HEK293 cells) and are means ± S.D. (n=6). ***, $p \leq 0.001$.

4.3. Summary

The aim of these experiments was to examine the effects of FL-APP and its proteolytic fragments on the viability and proliferation of ARPE-19 cells in the presence and absence of UV-A light exposure. The results showed that depleting endogenous APP using APP-siRNA significantly increased the resistance of ARPE-19 cells to UV-A irradiation restoring viable cell counts to approximately control levels.

On the other hand, sAPPα produced exogenously by HEK cells enhanced viable ARPE-19 cell numbers in co-culture experiments. An effect that was not observed when the latter cell type was incubated with HEK293 cells over-expressing either FL-APP_{695} or $sAPP_{695}\beta$.

Finally, the manipulation of APP levels whether by siRNA-mediated depletion of the protein in ARPE-19 cells or by the stable overexpression of APP or its proteolytic fragments in HEK293 cells did not affect cellular p53 levels in the current study.

Chapter 5

The effects of secretase inhibitors on ARPE-19 cell proliferation and resistance to UV-A exposure

5. The effects of secretase inhibitors on ARPE-19 cell proliferation and resistance to UV-A exposure

The HEK/ARPE-19 co-culture experiments in the previous chapter showed that sAPPα enhanced the proliferation of the latter cell line (Fig. 4.12). However, other results showed that down regulating FL-APP using APP-siRNA enhanced the resistance of cells to UV-A irradiation (Fig. 4.3.). Therefore, it was possible that the proteolytic fragments of APP generated by the amyloidogenic and non-amyloidogenic pathways might have differential effects on ARPE-19 cells. In order to investigate this, the effects of secretase inhibitors on the proliferation and resistance to UV-A of ARPE-19 cells were examined.

5.1. Optimisation of α-secretase inhibitor concentrations

Studies have shown that ADAM10, a member of the ADAM family is the key constitutive α-secretase (Lammich *et al.*, 1999; Postina *et al.*, 2004) whereas ADAM17 is thought to be a regulated α-secretase (Buxbaum *et al.*, 1998). Therefore, initially we decided to use an inhibitor which might be somewhat more specific towards ADAM10. In this respect, GI254023X (Tocris, Bristol, UK) has distinct IC_{50} values with respect to ADAM10 (IC_{50} = 5.3 nM) and ADAM17 (IC_{50} = 541 nM) (Ludwig *et al.*, 2005). Initially, the effects of a range of inhibitor concentrations on APP metabolism in ARPE-19 cells were examined. Confluent cells were incubated for 24 h in UltraMEM in the presence of 0-100 nM GI254023X and cell lysates and concentrated conditioned medium samples were subsequently prepared as described in the Materials and Methods section. Following equalisation of protein concentrations, the lysates were immunoblotted with the anti-APP C-terminal antibody. The results (Fig. 5.1A and C) showed that GI254023X caused a slight accumulation of full-length APP in cell lysates that was only statistically significant at the concentration of 50 nM (increased by 17.6 ± 0.8%). On the other hand, APP-CTF levels actually decreased at 50nM (decreased by 11.9 ± 3.6 %). However, none of the changes in APP-CTF levels at any of the inhibitor's concentrations tested were statistically significant (Fig. 5.1B and C).

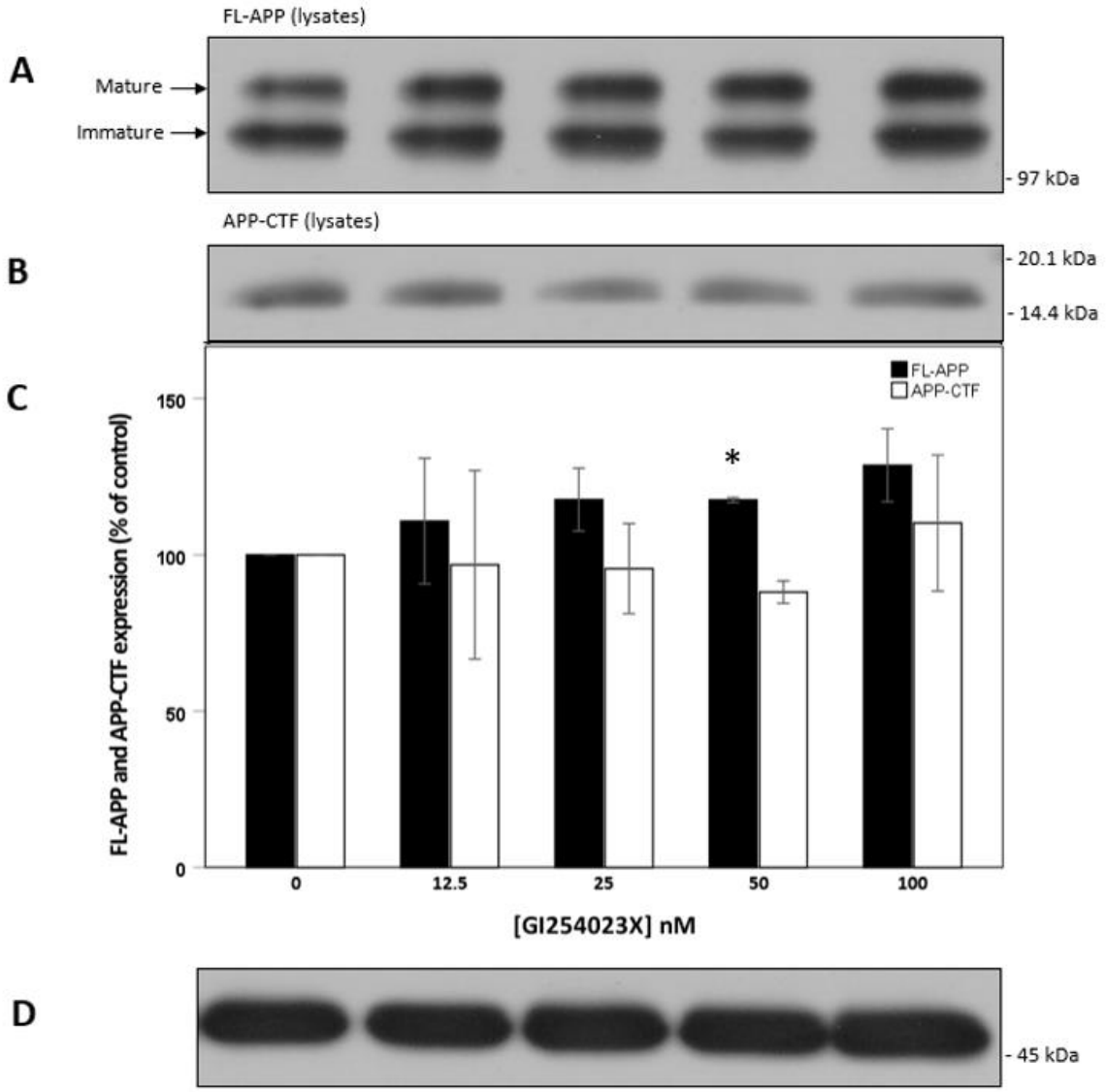

Figure 5.1. The effect of GI254023X on FL-APP and APP-CTF levels in cell lysates following 24 h treatment of confluent ARPE-19 cells. Confluent cells were transferred into UltraMEM and incubated in the absence or presence of the indicated drug concentrations for 24 h. Cell lysates were then prepared and equal protein amounts from each sample were immunoblotted (see Materials and Methods). **(A)** Detection of mature and immature forms of FL-APP using the anti-APP C-terminal antibody. **(B)** Detection of APP-CTF using the anti-APP C-terminal antibody. **(C)** Quantification of multiple APP immunoblots by densitometric analysis. **(D)** Detection of actin using the anti-actin antibody. Results are expressed as a percentage of no inhibitor control cell cultures and are means ± S.D. (n=3). *, $p \leq 0.05$.

Conditioned medium samples from the GI254023X-treated cells were then concentrated and equal volumes were subjected to immunoblotting using antibody 6E10 to detect sAPPα. The results (Fig. 5.2) showed no significant alteration in sAPPα levels in conditioned medium.

The lack of effect of GI254023X on sAPPα production by ARPE-19 cells was surprising given that the previously published IC_{50} value of the inhibitor with respect to ADAM10 was 5.3 nM (Ludwig *et al.*, 2005). This raised the possibility that APP might be constitutively cleaved by another member of the ADAM family in the cell line. In order to investigate this, we next tested the effects of a more general ADAM inhibitor, batimastat, on sAPPα secretion from ARPE-19 cells. Here, we extended the concentration range of inhibitor to include a higher, 500 nM, concentration. As in the previous experiment, confluent cells were incubated in UltraMEM for 24 h in the absence or presence of

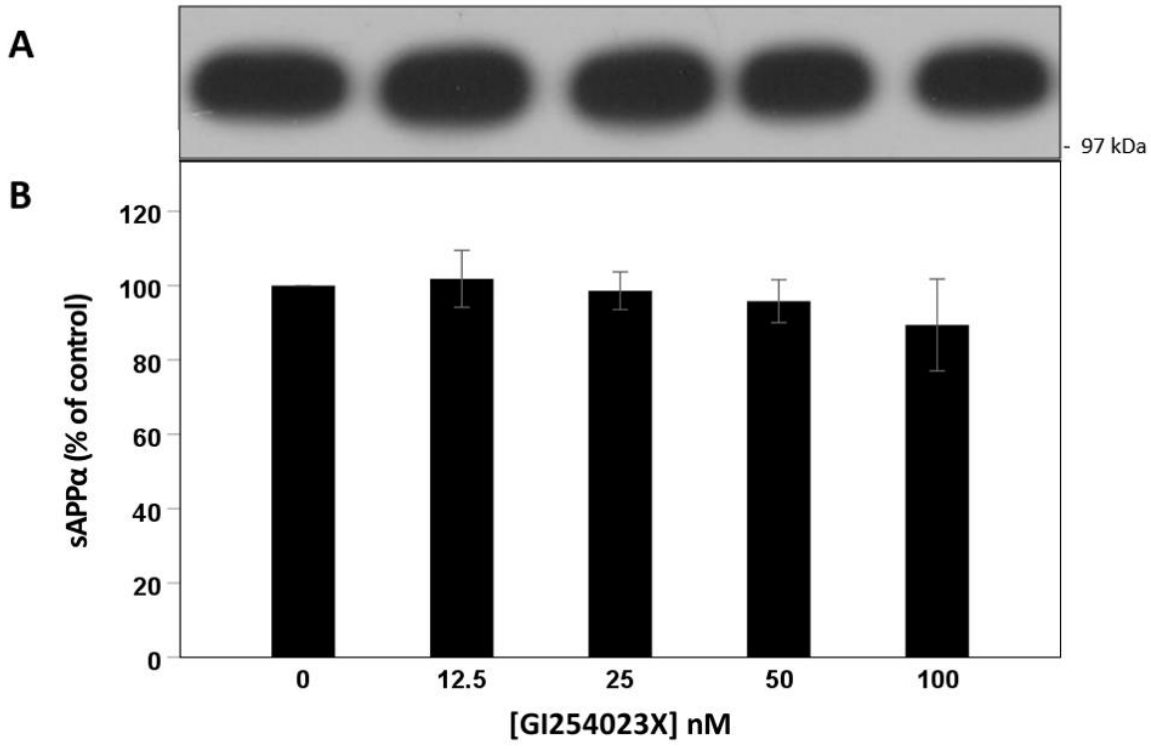

Figure 5.2. The effect of GI254023X on sAPPα levels in conditioned medium following 24 h treatment of confluent ARPE-19 cells. Confluent cells were transferred into UltraMEM and incubated in the absence or presence of the indicated drug concentrations for 24 h. Concentrated conditioned medium samples were then prepared and equal volumes from each sample were immunoblotted. **(A)** Detection of sAPPα using antibody 6E10. **(B)** Quantification of multiple 6E10 immunoblots by densitometric analysis. Results are expressed as a percentage of control cell cultures and are means ± S.D. (n=3).

inhibitor and equal protein from lysate samples was immunoblotted initially with the anti-APP C-terminal antibody. The results (Fig. 5.3) showed no major changes in either FL-APP or APP-CTF levels.

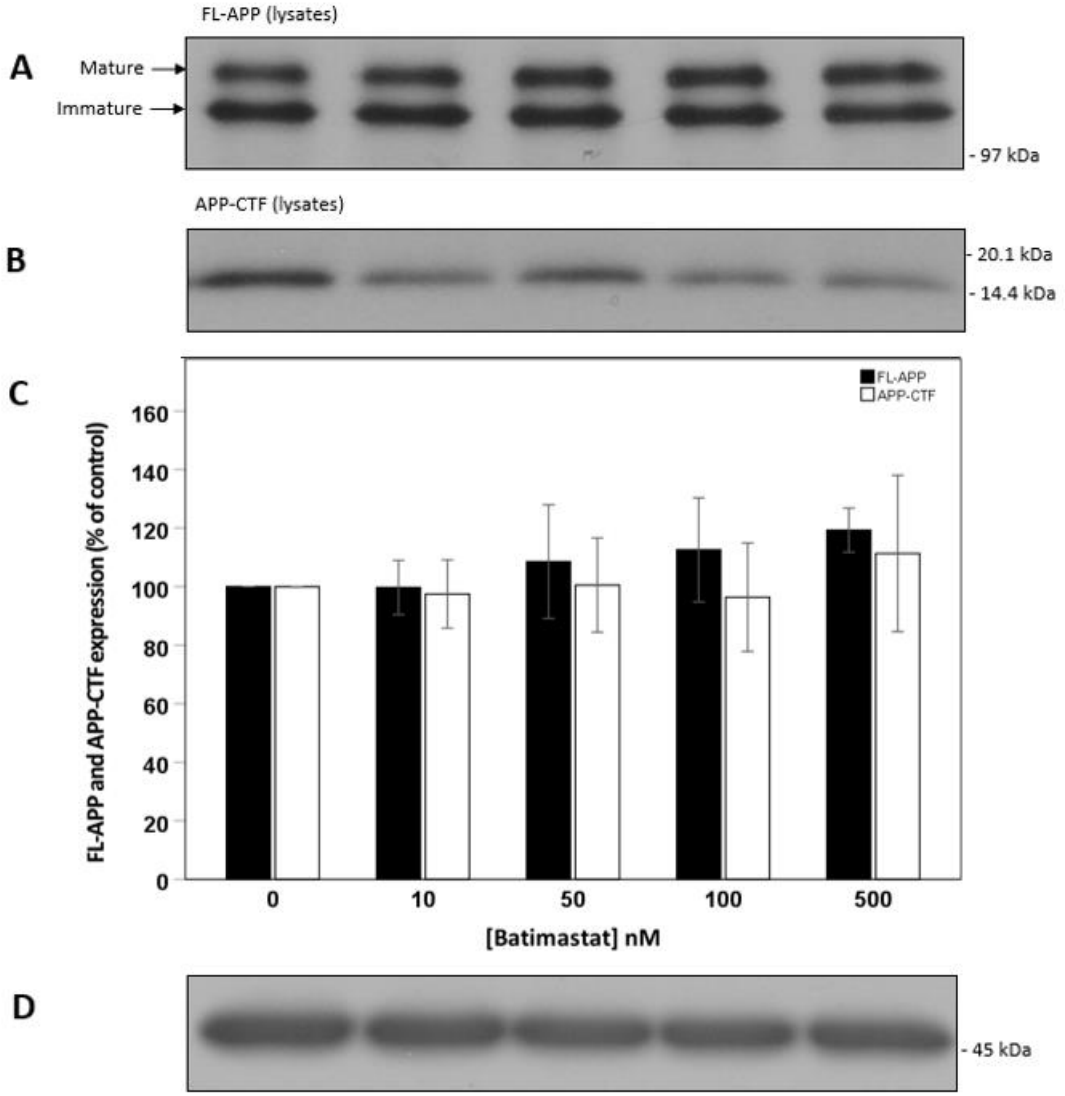

Figure 5.3. The effect of batimastat on FL-APP and APP-CTF levels in cell lysates following 24 h treatment of confluent ARPE-19 cells. Confluent cells were transferred into UltraMEM and incubated in the absence or presence of the indicated drug concentrations for 24 h. Cell lysates were then prepared and equal protein amounts from each sample were immunoblotted (see Materials and Methods). **(A)** Detection of mature and immature forms of FL-APP using the anti-APP C-terminal antibody. **(B)** Detection of APP-CTF using the anti-APP C-terminal antibody. **(C)** Quantification of multiple APP immunoblots by densitometric analysis. **(D)** Detection of actin using the anti-actin antibody. Results are expressed as a percentage of no inhibitor control cell cultures and are means ± S.D. (n=3).

Next, medium samples from batimastat treated cells were concentrated and equal volumes were immunoblotted with the 6E10 antibody in order to detect sAPPα. As for GI254023X previously, the results (Fig. 5.4.) showed no changes in sAPPα levels in the medium from batimastat-treated cells.

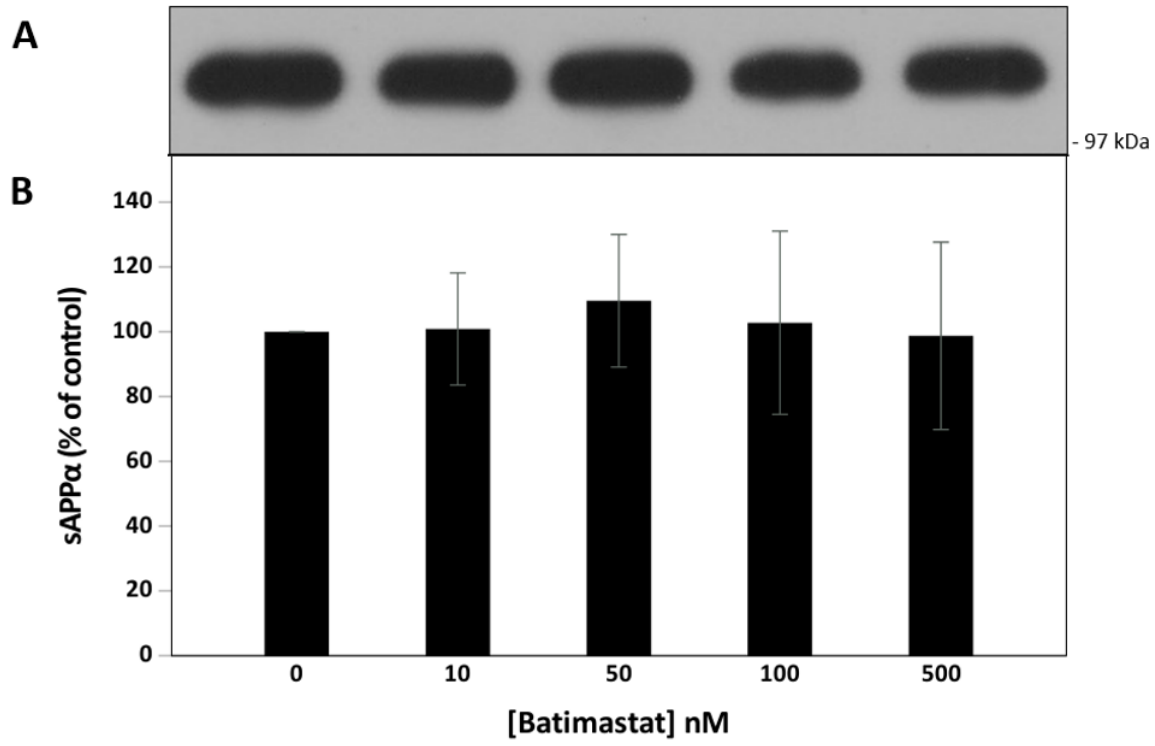

Figure 5.4. The effect of batimastat on sAPPα levels in conditioned medium following 24 h treatment of confluent ARPE-19 cells. Confluent cells were transferred into UltraMEM and incubated in the absence or presence of the indicated drug concentrations for 24 h. Concentrated conditioned medium samples were then prepared and equal volumes from each sample were immunoblotted. **(A)** Detection of sAPPα using antibody 6E10. **(B)** Quantification of multiple 6E10 immunoblots by densitometric analysis. Results are expressed as a percentage of control cell cultures and are means ± S.D. (n=3).

Given that neither batimastat nor GI254023X inhibited sAPPα production by ARPE-19 cells, it was postulated that the mechanisms underlying generation of this fragment might differ from previously studied cell lines. As such, the effects of two of the higher concentrations of the inhibitors on sAPPα shedding by the neuroblastoma cell line, SH-SY5Y, were examined. Here, confluent cells were transferred to UltraMEM and incubated in the absence or presence of 50 nM GI254023X or 100 nM batimastat for 24 h. Lysate samples were then prepared and immunoblotted with the APP C-terminal antibody. The results (Fig. 5.5) showed no drug-induced changes in either FL-APP or APP-CTFs

in SH-SY5Y cells. Levels of sAPPα in conditioned medium were then examined using antibody 6E10 (Fig. 5.6) and showed a trend towards a decrease following both treatments of 50 nM GI254023X and 100 nM batimastat (by approximately 30 and 25 % respectively) although these changes were not statistically significant.

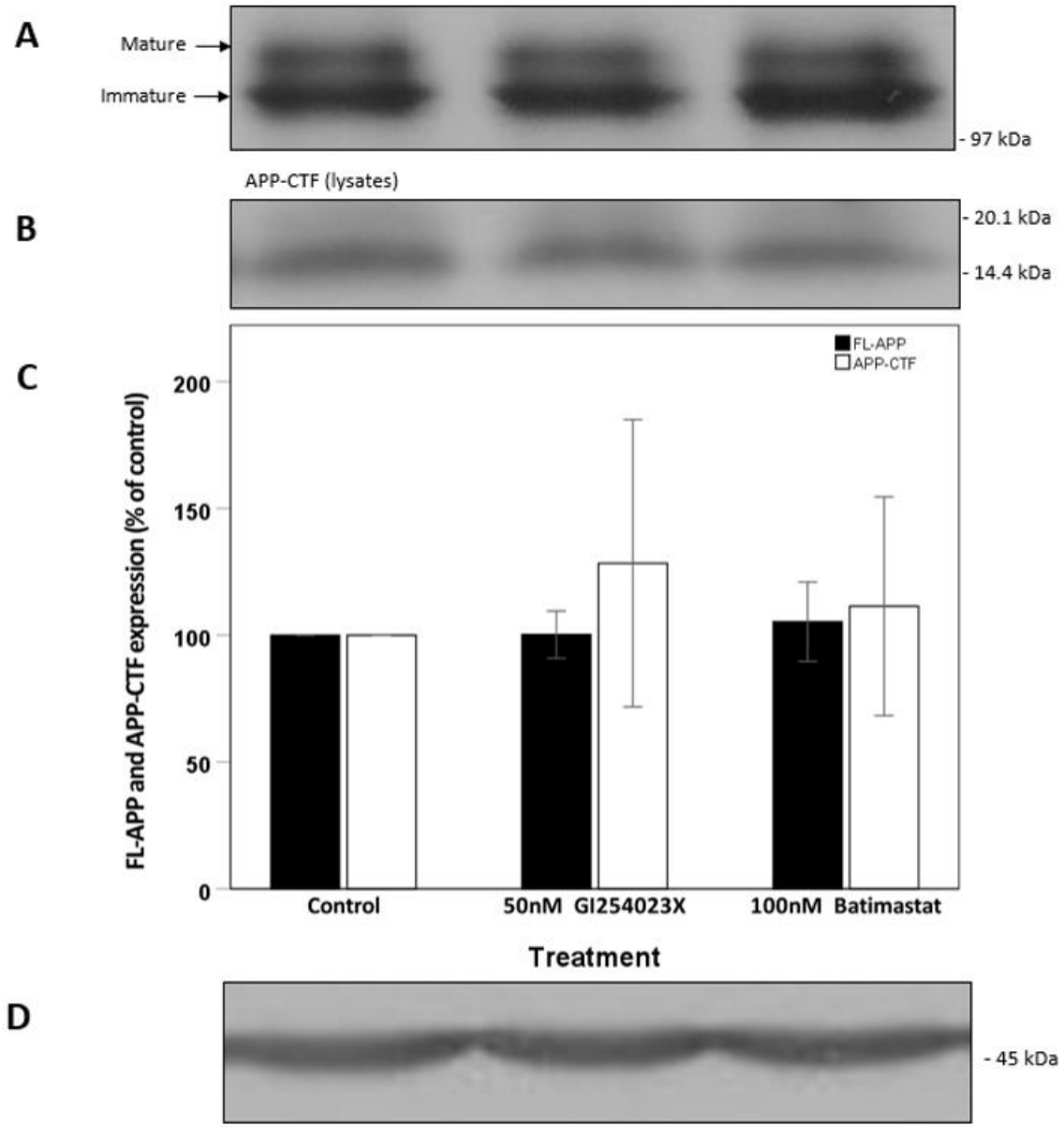

Figure 5.5. The effect of GI254023X (50 nM) and batimastat (100 nM) on FL-APP and APP-CTF levels in cell lysates following 24 h treatment of confluent SH-SY5Y cells. Confluent cells were transferred into UltraMEM and incubated in the absence or presence of the indicated drug concentrations for 24 h. Cell lysates were then prepared and equal protein amounts from each sample were immunoblotted (see Materials and Methods). **(A)** Detection of FL-APP using the anti-APP C-terminal antibody. **(B)** Detection of APP-CTF using the anti-APP C-terminal antibody. **(C)** Quantification of multiple APP immunoblots by densitometric analysis. **(D)** Detection of actin using the anti-actin antibody. Results are expressed as a percentage of no inhibitor control cell cultures and are means ± S.D. (n=3).

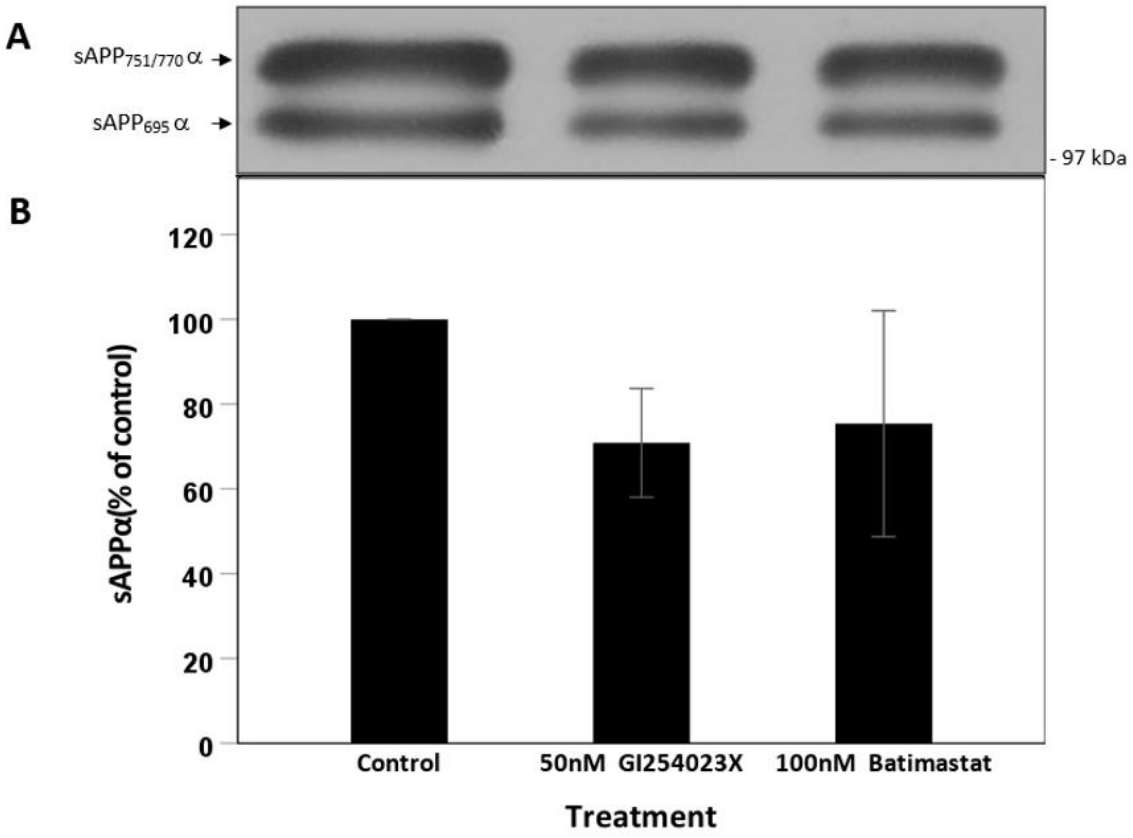

Figure 5.6. The effect of GI254023X (50 nM) and batimastat (100 nM) on sAPPα levels in conditioned medium following 24 h treatment of confluent SH-SY5Y cells. Confluent cells were transferred into UltraMEM and incubated in the absence or presence of the indicated drug concentrations for 24 h. Concentrated conditioned medium samples were then prepared and equal volumes from each sample were immunoblotted. **(A)** Detection of sAPPα using antibody 6E10. **(B)** Quantification of multiple 6E10 immunoblots by densitometric analysis. Results are expressed as a percentage of control cell cultures and are means ± S.D. (n=3).

From the preceding results, it was apparent that the effective concentration of GI254023X in SH-SY5Y cells was still much higher than the published IC50 value for the compound relative to ADAM10 (IC_{50} = 5.3 nM) (Ludwig *et al.*, 2005). It was noted that the latter value was determined using recombinant enzyme and would not, therefore, be impacted by any cell-associated factors such as permeability or interaction with other proteins. Therefore, it was postulated that even higher concentrations of the α-secretase inhibitors might be required to inhibit sAPPα production by ARPE-19 cells. To this end, we tested a batimastat concentration (5 μM) more in-line with previously published cell-based studies (Leriche *et al.*, 2016; Woods and Padmanabhan, 2013). Here, confluent ARPE-19 cells were, once more, transferred to UltraMEM and treated for 24 h in the absence or presence of 5 μM batimastat. Lysates were subsequently prepared and equal amounts of protein were

immunoblotted with the anti-APP C-terminal antibody. The results (Fig. 5.7A and C) demonstrated an increase in cell associated FL-APP following batimastat treatment (27.2 ± 12.7 %) and an 89.8 ± 1.5 % decrease in APP-CTF levels relative to controls (Fig. 5.7B and C).

Next the concentrated conditioned medium samples from 5 μM batimastat treated cells were immunoblotted with antibody 6E10. The results (Fig. 5.8) showed a 72.7 ± 7.8 % decrease in sAPPα production by ARPE-19 cells following batimastat treatment. As we had now identified an effective drug concentration, the effect of batimastat on sAPPβ levels in conditioned medium were also investigated by immunoblotting. The results (Fig. 5.9) showed that the inhibitor had no effect on the production of this fragment via the amyloidogenic processing of APP.

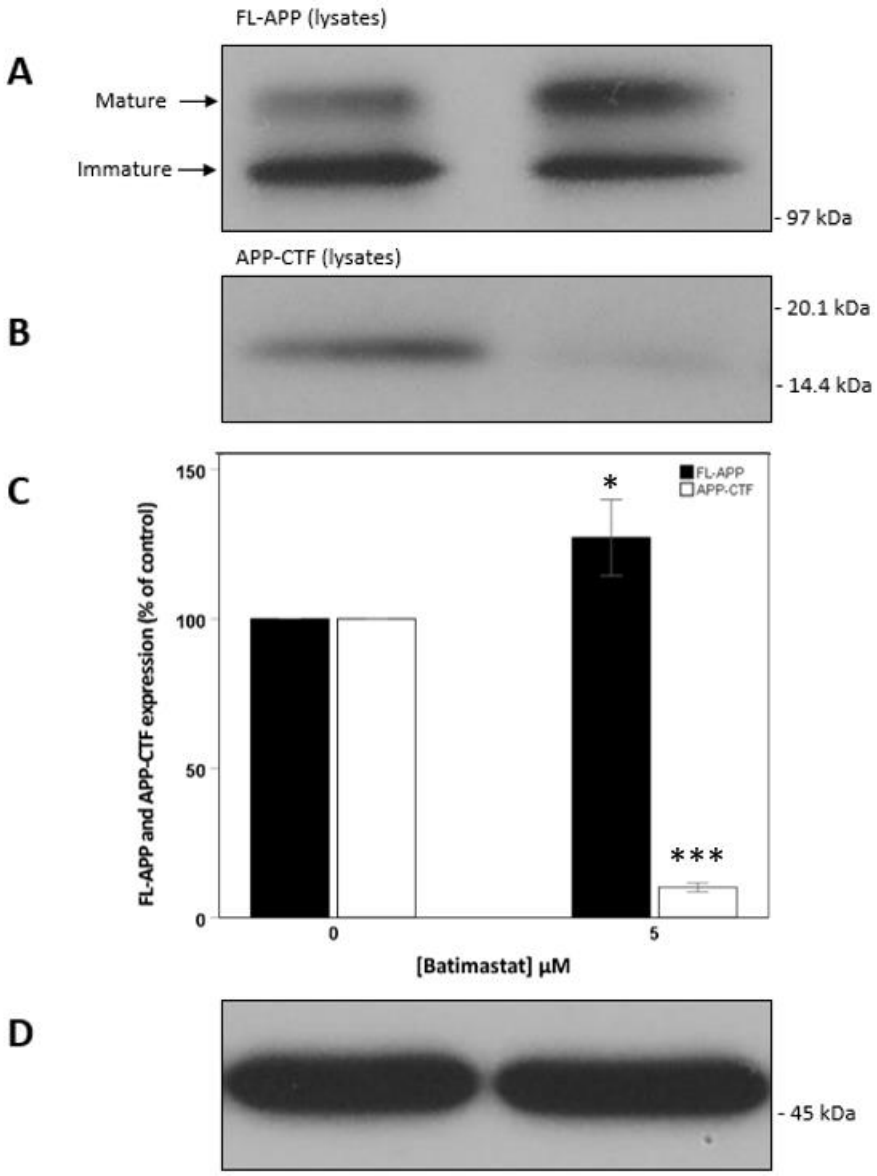

Figure 5.7. The effect of batimastat (5 µM) on FL-APP and APP-CTF levels in cell lysates following 24 h treatment of confluent ARPE-19 cells. Confluent cells were transferred into UltraMEM and incubated in the absence or presence of the indicated drug concentrations for 24 h. Cell lysates were then prepared and equal protein amounts from each sample were immunoblotted (see Materials and Methods). **(A)** Detection of mature and immature forms of FL-APP using the anti-APP C-terminal antibody. **(B)** Detection of APP-CTF using the anti-APP C-terminal antibody. **(C)** Quantification of multiple APP immunoblots by densitometric analysis. **(D)** Detection of actin using the anti-actin antibody. Results are expressed as a percentage of no inhibitor control cell cultures and are means ± S.D. (n=3). *, $p \leq 0.05$; ***, $p \leq 0.001$.

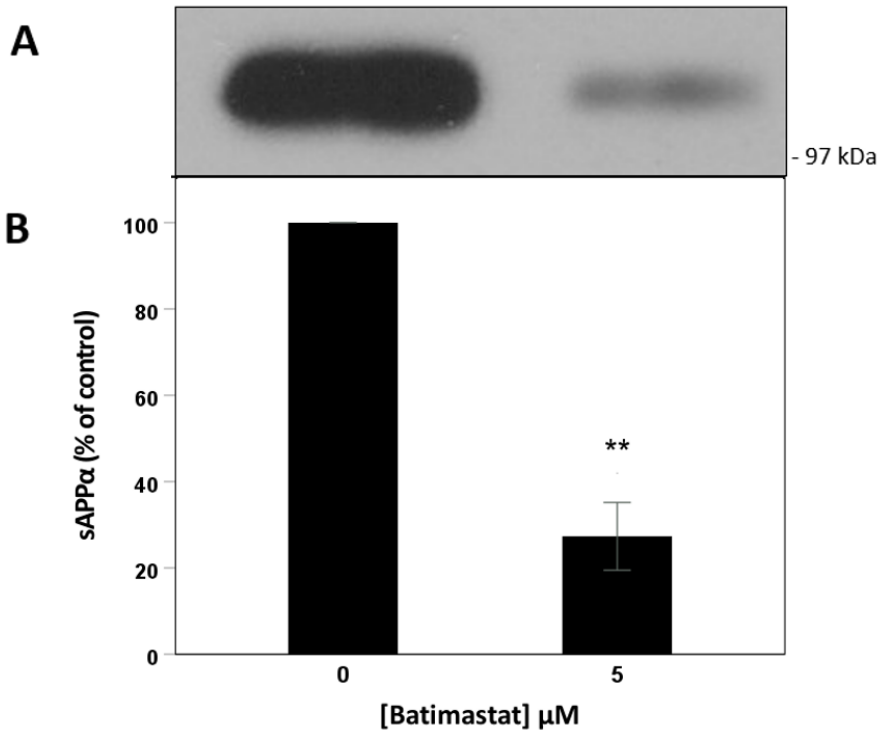

Figure 5.8. The effect of batimastat (5 μM) on sAPPα levels in conditioned medium following 24 h treatment of confluent ARPE-19 cells. Confluent cells were transferred into UltraMEM and incubated in the absence or presence of the indicated drug concentrations for 24 h. Concentrated conditioned medium samples were then prepared and equal volumes from each sample were immunoblotted. **(A)** Detection of sAPPα using antibody 6E10. **(B)** Quantification of multiple 6E10 immunoblots by densitometric analysis. Results are expressed as a percentage of control cell cultures and are means ± S.D. (n=3). **, $p \leq 0.01$.

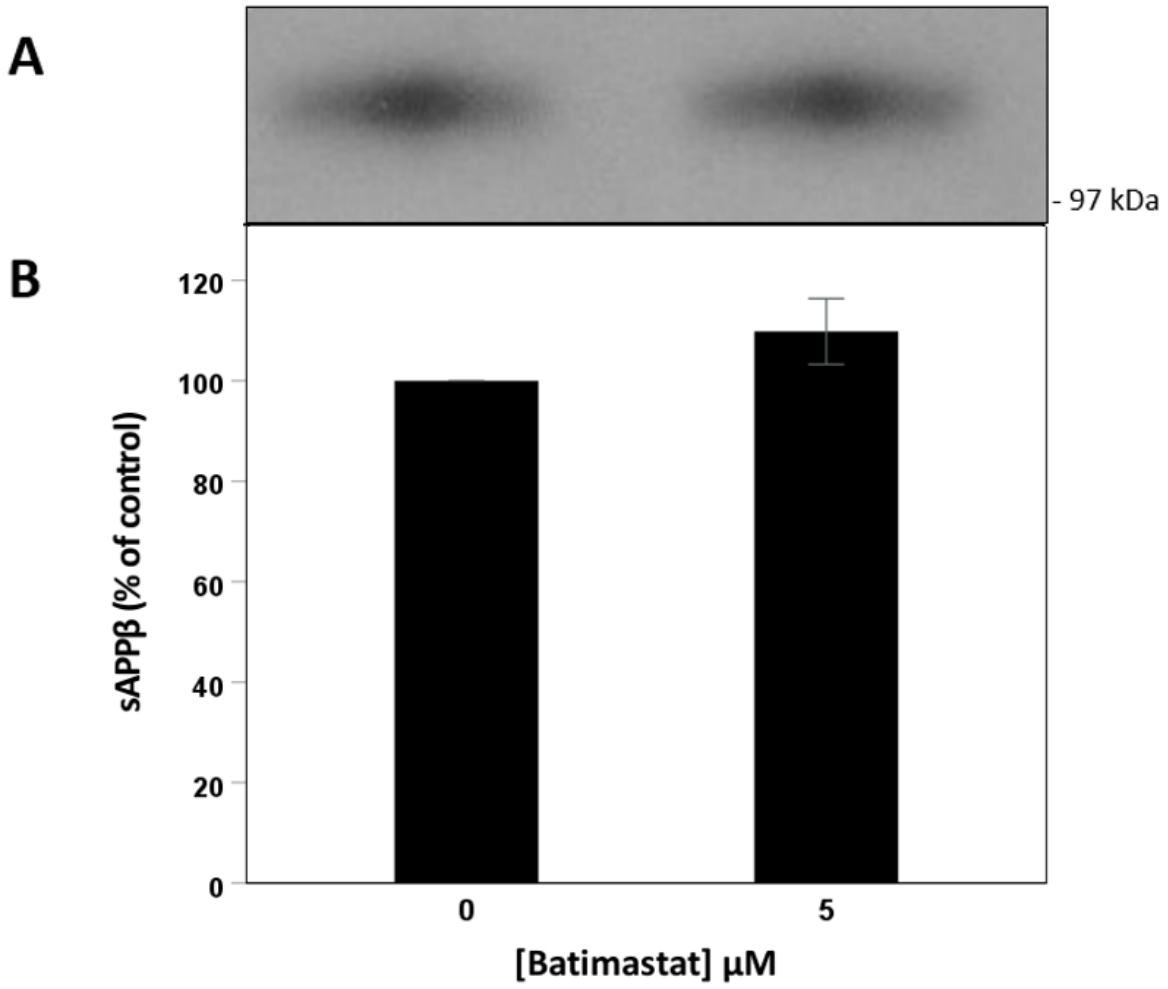

Figure 5.9. The effect of batimastat (5 μM) on sAPPβ levels in conditioned medium following 24 h treatment of confluent ARPE-19 cells. Confluent cells were transferred into UltraMEM and incubated in the absence or presence of the indicated drug concentrations for 24 h. Concentrated conditioned medium samples were then prepared and equal volumes from each sample were immunoblotted. **(A)** Detection of sAPPβ using the anti-sAPPβ antibody. **(B)** Quantification of multiple 6E10 immunoblots by densitometric analysis. Results are expressed as a percentage of control cell cultures and are means ± S.D. (n=3).

5.2. The effects of α-secretase inhibitor (batimastat) on ARPE-19 cell viability in the absence of UV-A treatment

Having confirmed an effective batimastat concentration (5 μM) in terms of inhibition of sAPPα generation, the effects of the drug on ARPE-19 viable cell numbers in the absence of UV-A treatment were examined. Initially, cells were grown to confluence in 96-well plates before changing the medium for UltraMEM and treating for 24 h with batimastat. An MTS assay was then used in order to determine

the relative numbers of viable cells between treatments (see Materials and Methods). The results (Fig. 5.10) confirmed that there was no effect of this concentration of drug on the viability of confluent cultures over 24 h.

Given that sAPPα is also known to promote cell proliferation (Demars *et al.*, 2011; Ohsawa *et al.*, 1999) we also investigated the ability of batimastat to inhibit cell proliferation over a seven-day period (adding the drug at the point of seeding). Cells were grown in DMEM:F12 and medium, together with batimastat, were replaced every 48 h. At the end of the seven-day growth period the relative numbers of viable cells were determined using the MTS assay. The results (Fig. 5.11) showed that batimastat did indeed decrease the viable cell number after seven days of incubation (a 49.2 ± 21.8 % decrease relative to control cell cultures). Thus, it would appear that any effects of batimastat in ARPE-19 cells were cytostatic rather than cytotoxic.

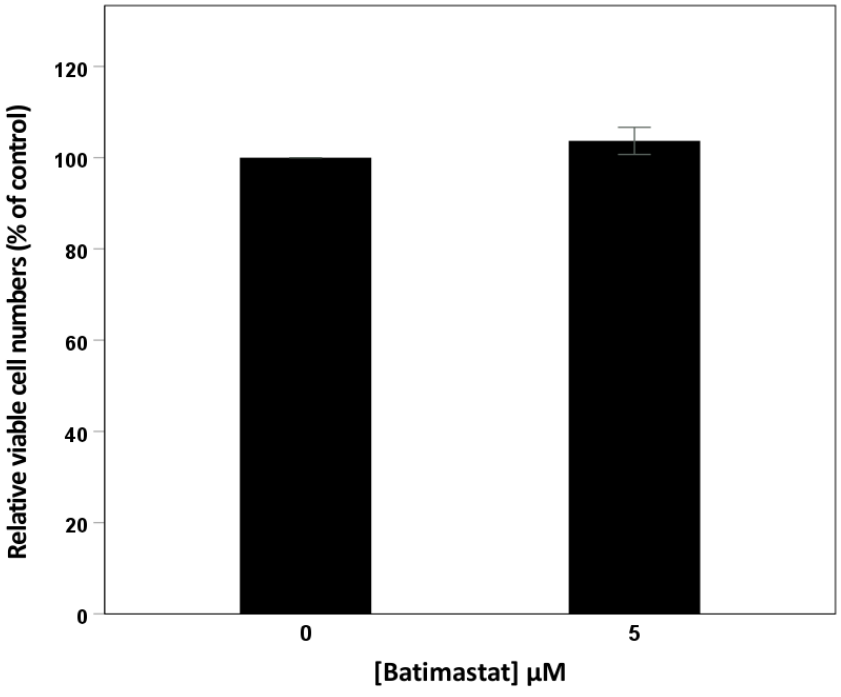

Figure 5.10. Relative viable cell numbers following 24 h treatment of confluent ARPE-19 cells with 5 µM batimastat. Confluent cells were treated for 24 h with 5 µM of batimastat in UltraMEM and then subjected to an MTS viability assay as described in the Materials and Methods section. Results are expressed as a percentage of no inhibitor control cell cultures and are means ± S.D. (n=4).

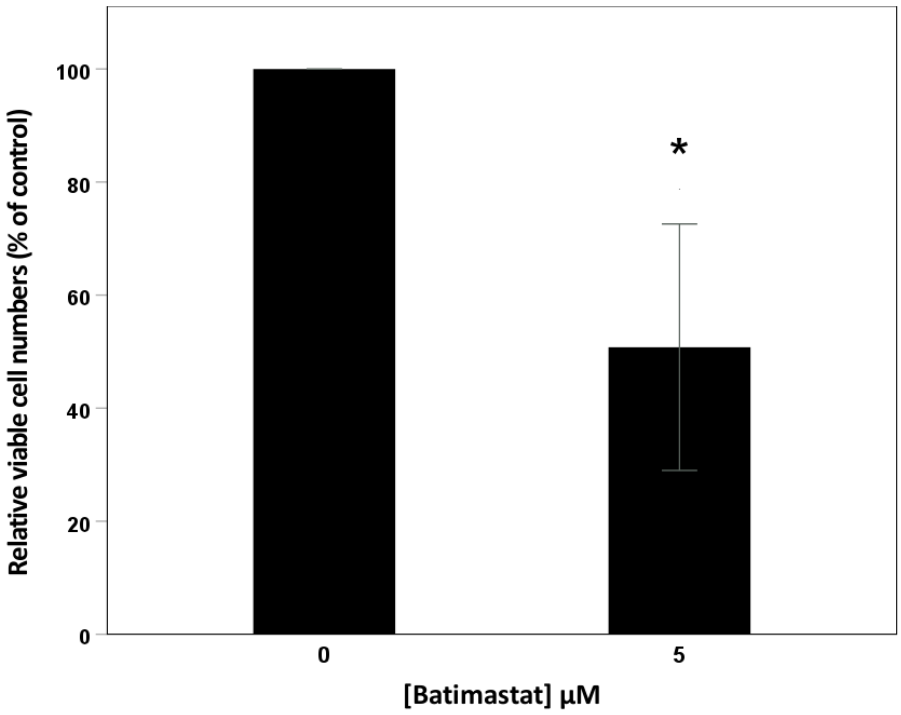

Figure 5.11. Relative viable cell numbers following seven days of ARPE-19 cell growth in the presence of 5 µM batimastat. ARPE-19 cells were seeded at an appropriate density to achieve confluence in 7 days. Cells were grown in complete growth medium DMEM:F12 and batimastat was added to the cultures at the point of seeding at a 5 µM final concentration. Medium was changed, and fresh inhibitor was added every 48 h until day 7 when cells were subjected to an MTS viability assay as described in the Materials and Methods section. Results are expressed as a percentage of no inhibitor control cell cultures and are means ± S.D. (n=4). *, $p \leq 0.05$.

5.3. The effects of α-secretase inhibitor (batimastat) on ARPE-19 cell viability following UV-A treatment

Given that batimastat effectively inhibited sAPPα production at 5µM without altering viable cell numbers over 24 h, this inhibitor concentration was then used to see if the compound would modify the resistance of ARPE-19 cells to UV-A treatment. To this end, T25cm^2 flasks of cells were grown to 80% confluence and pre-treated for 6h with 5 µM batimastat in UltraMEM. Following transfer to phenol red-free DMEM, the cells were exposed to UV-A for 50 min before being transferred back into UltraMEM (in the absence or presence of batimastat) for an 18 h recovery period. Viable cell numbers were then determined using Trypan blue counts as described in the Materials and Methods section. The results (Fig. 5.12) demonstrated that the 50 min exposure of cells to UV-A irradiation resulted in a 29.2 ± 5.2 % decrease in viable cell numbers relative to control cultures. Notably,

batimastat alone (i.e. without UV-A treatment did not affect viable cell counts (as observed in the preceding section) but also did not significantly alter the resistance of the ARPE-19 cells to UV-A treatment. These data indicate that inhibiting sAPPα production does not impact on cellular resistance to UV-A treatment.

In order to confirm the expected effects of batimastat on APP processing in the UV-A experiments, lysates and concentrated conditioned medium samples were prepared from the same treated cell samples. Following SDS-PAGE separation of equal amounts of lysate protein, the samples were immunoblotted with the anti-APP C-terminal antibody and the results (Fig. 5.13A) confirmed previous observations (Chapter 3, Fig. 3.3) that exposure of the cells to UV-A decreased FL-APP levels in lysates. Immunoblotting of the conditioned medium (Fig. 5.13C) likewise confirmed previous observations (Fig. 5.8) that 5 μM batimastat effectively inhibited sAPPα production.

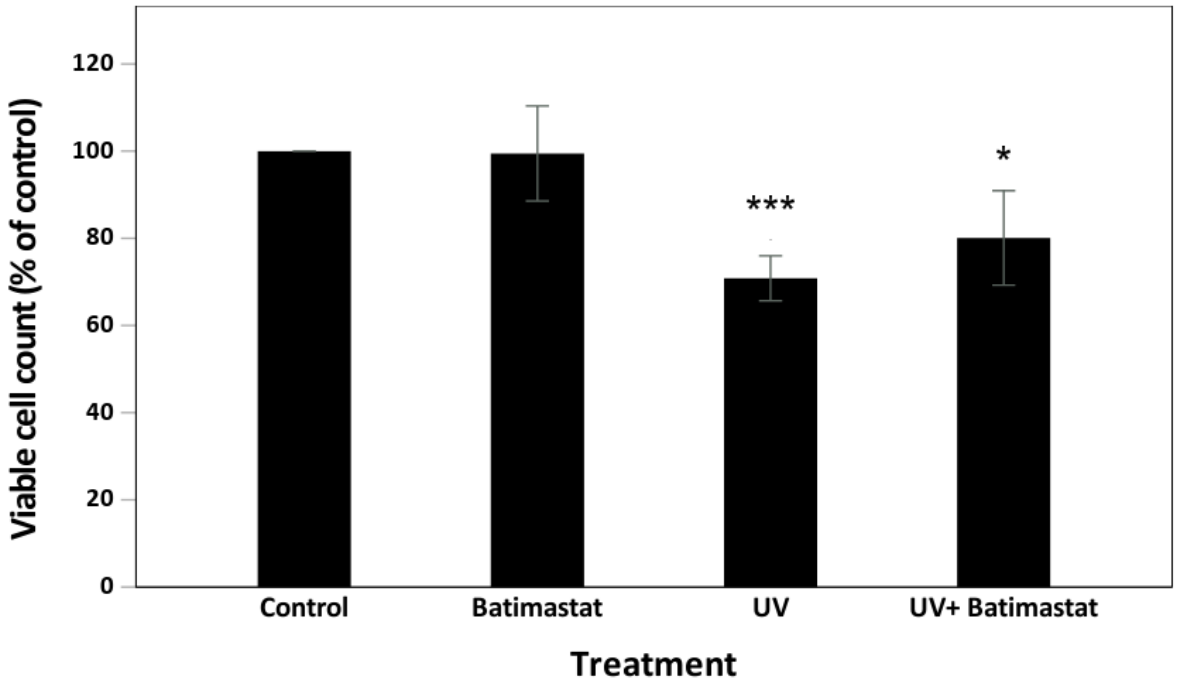

Figure 5.12. Inhibition of sAPPα production using batimastat does not alter the resistance of ARPE-19 cells to UV-A treatment. T25 cm^2 flasks of 80% confluent cells were preincubated for 6 h in UltraMEM +/- 5μM batimastat and then transferred into phenol red-free DMEM during UV exposure for 50 min. The cells were then transferred into UltraMEM +/- batimastat as indicated for an 18 h recovery period. Viable cell numbers were then determined using the Trypan blue assay as described in the Materials and Methods section. Results are expressed as a percentage of control cell cultures and are means ± S.D. (n=4). *, $p \leq 0.05$; ***, $p \leq 0.001$.

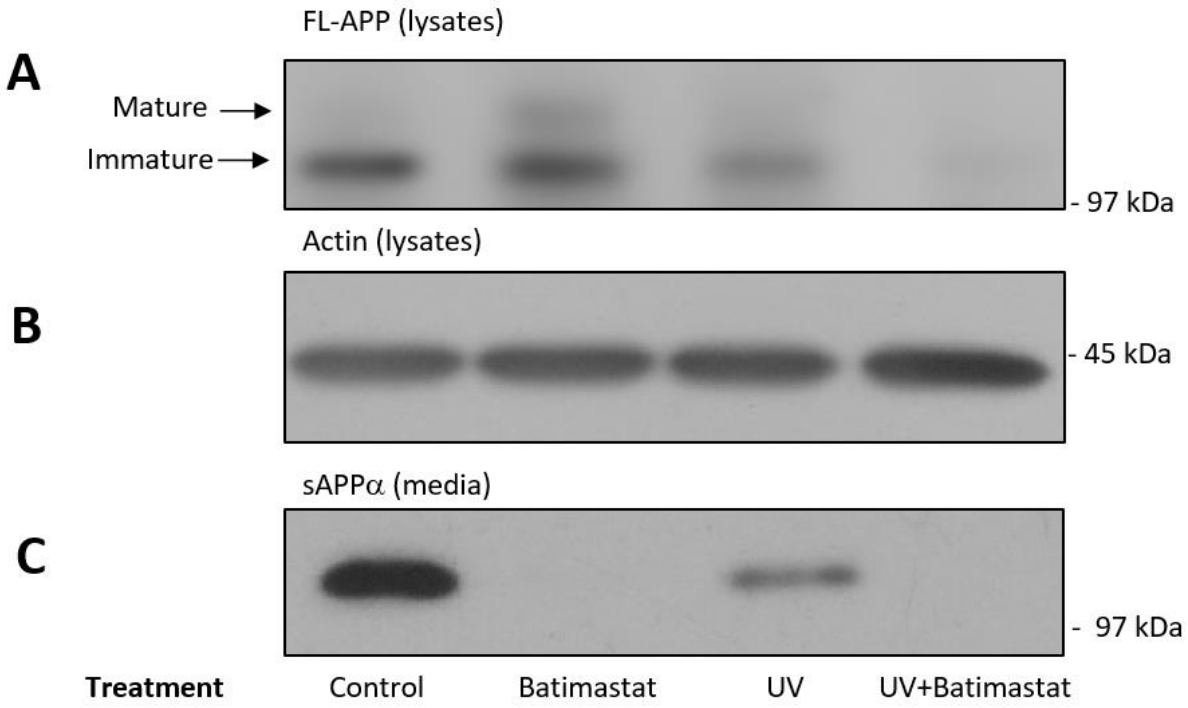

Figure 5.13. FL-APP expression and sAPPα production following UV-A and batimastat treatment of ARPE-19 cells. T25 cm^2 flasks of 80% confluent cells were preincubated for 6 h in UltraMEM +/- 5μM batimastat and then transferred into phenol red-free DMEM during UV exposure for 50 min. The cells were then transferred into UltraMEM +/- batimastat as indicated for an 18 h recovery period. Cell lysates and concentrated conditioned medium samples were then prepared and immunoblotted as described in the Materials and Methods section. **(A)** Detection of mature and immature forms of FL-APP in cell lysates using the anti-APP C-terminal antibody. **(B)** Detection of actin in cell lysates using the anti-actin antibody. **(C)** Detection of sAPPα in conditioned medium using the anti-APP 6E10 antibody.

5.4. Optimisation of β-secretase inhibitor concentrations

In order to study the effects of β-secretase cleavage products on ARPE-19 cell resistance to UV-A treatment, β-secretase inhibitor IV (Merck, Darmstadt, Germany) was employed. This compound is a selective BACE-1 inhibitor (BACE-1 IC_{50} = 15 nM, BACE-2 IC_{50} = 541 nM) (Stachel *et al.*, 2004). Initially, and taking into account the IC_{50} value of 15 nM, confluent T25cm^2 flasks of ARPE-19 cells were transferred into UltraMEM and treated for 24 h with a 0-100 nM concentration range of β-secretase inhibitor IV in order to investigate the effect of the drug on APP expression and proteolysis. Cell lysates were then prepared and equal amounts of protein were immunoblotted with the anti-APP C-terminal antibody. The results (Fig. 5.14 A and C) showed no significant changes in FL-APP levels but a dose-dependent increase in APP-CTF levels in cell lysates was observed (Fig. 5.14 B and C). Quantification

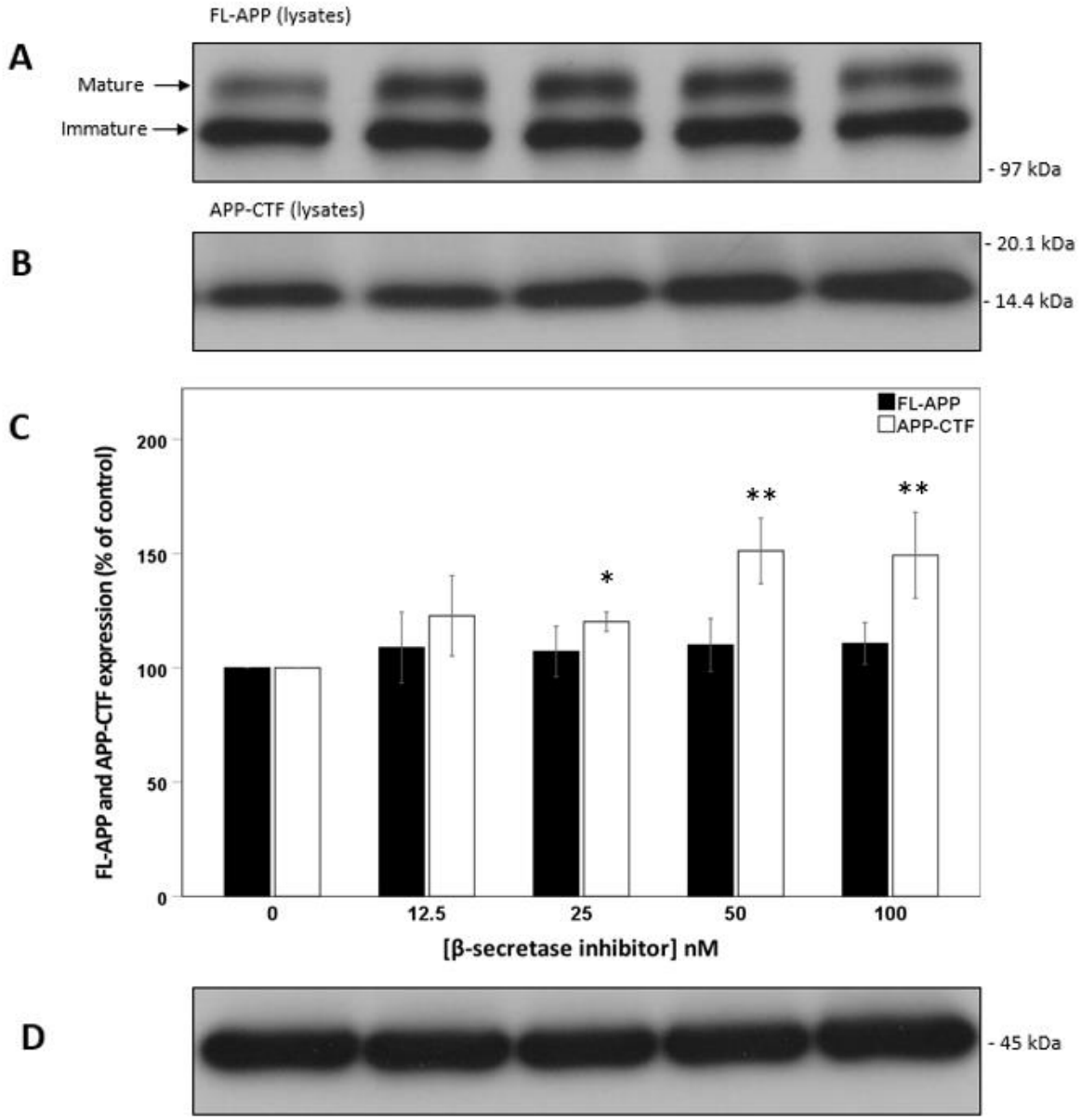

Figure 5.14. The effect of β-secretase inhibitor IV on FL-APP and APP-CTF levels in cell lysates following 24 h treatment of confluent ARPE-19 cells. Confluent cells were transferred into UltraMEM and incubated in the absence or presence of the indicated drug concentrations for 24 h. Cell lysates were then prepared and equal protein amounts from each sample were immunoblotted (see Materials and Methods). **(A)** Detection of mature and immature forms of FL-APP using the anti-APP C-terminal antibody. **(B)** Detection of APP-CTF using the anti-APP C-terminal antibody. **(C)** Quantification of multiple APP immunoblots by densitometric analysis. **(D)** Detection of actin using the anti-actin antibody. Results are expressed as a percentage of no inhibitor control cell cultures and are means ± S.D. (n=3). *, $p \leq 0.05$; **, $p \leq 0.01$.

of multiple blots revealed that APP-CTF levels increased by 20.2 ± 4.2, 51.2 ± 14.4 and 49.3 ± 18.8 % at inhibitor concentrations of 25, 50 and 100nM, respectively. This latter result was unexpected given that one would expect to see a decrease rather than increase in CTF levels following β-secretase inhibition.

Next the effects of β-secretase inhibitor IV on the generation of sAPPα were examined by immunoblotting equal volumes of concentrated conditioned medium samples with antibody 6E10. The results (Fig. 5.15) revealed that the compound did not alter sAPPα production as might be expected given the fact that only minor amounts of APP are cleaved by the reciprocal amyloidogenic pathway in non-diseased cells (Zhang and Song, 2013; Li *et al.*, 2006).

Finally, the effects of β-secretase inhibitor IV on the generation of sAPPβ by ARPE-19 cells were examined by immunoblotting the same medium samples with the anti-sAPPβ antibody. The results (Fig. 5.16) showed a dose-dependent decrease in the production of sAPPβ by 27.9 ± 3.9, 37.3 ± 6.4, 50.5 ± 7.9 and 67.3 ± 12.5 % following treatment with 12.5, 25, 50 and 100nM concentrations of the inhibitor, respectively.

Collectively, these data confirmed effective inhibition of sAPPβ production at the chosen drug concentrations with no corresponding effect on sAPPα production.

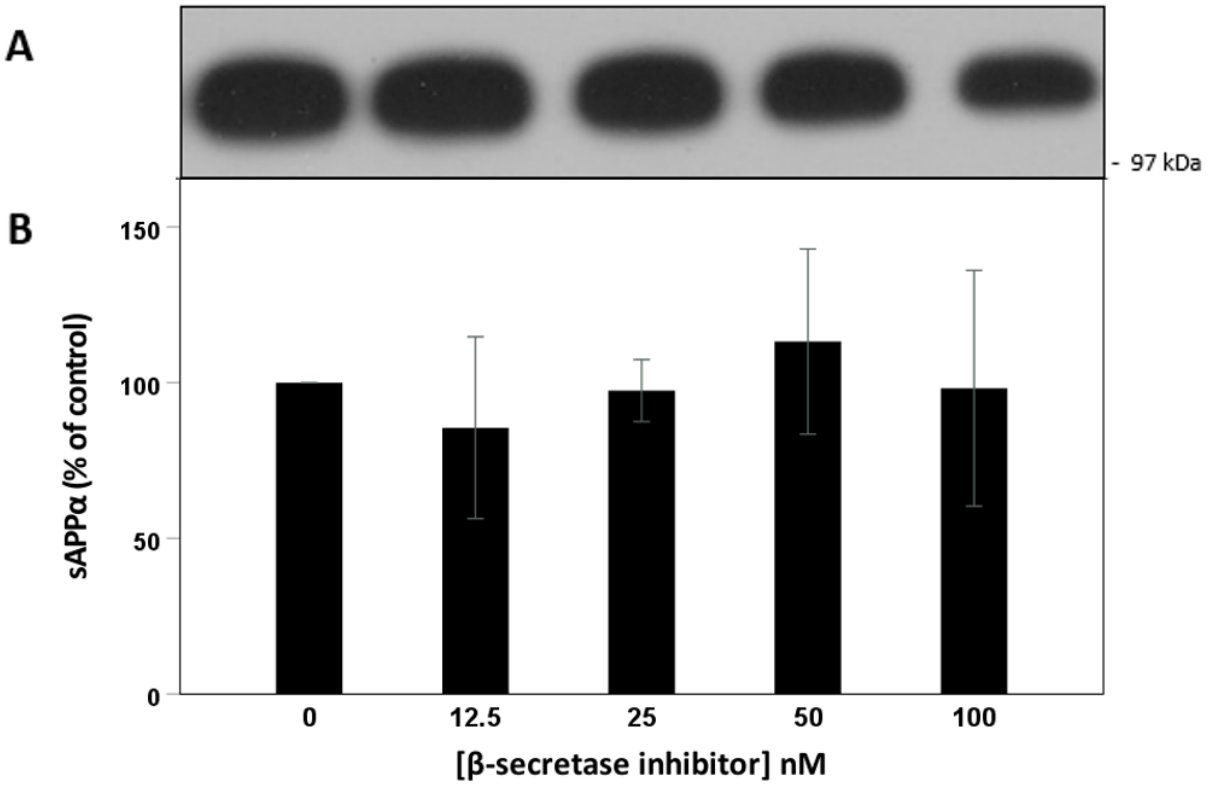

Figure 5.15. The effect of β-secretase inhibitor IV on sAPPα levels in conditioned medium following 24 h treatment of confluent ARPE-19 cells. Confluent cells were transferred into UltraMEM and incubated in the absence or presence of the indicated drug concentrations for 24 h. Concentrated conditioned medium samples were then prepared and equal volumes from each sample were immunoblotted. **(A)** Detection of sAPPα using antibody 6E10. **(B)** Quantification of multiple 6E10 immunoblots by densitometric analysis. Results are expressed as a percentage of control cell cultures and are means ± S.D. (n=3).

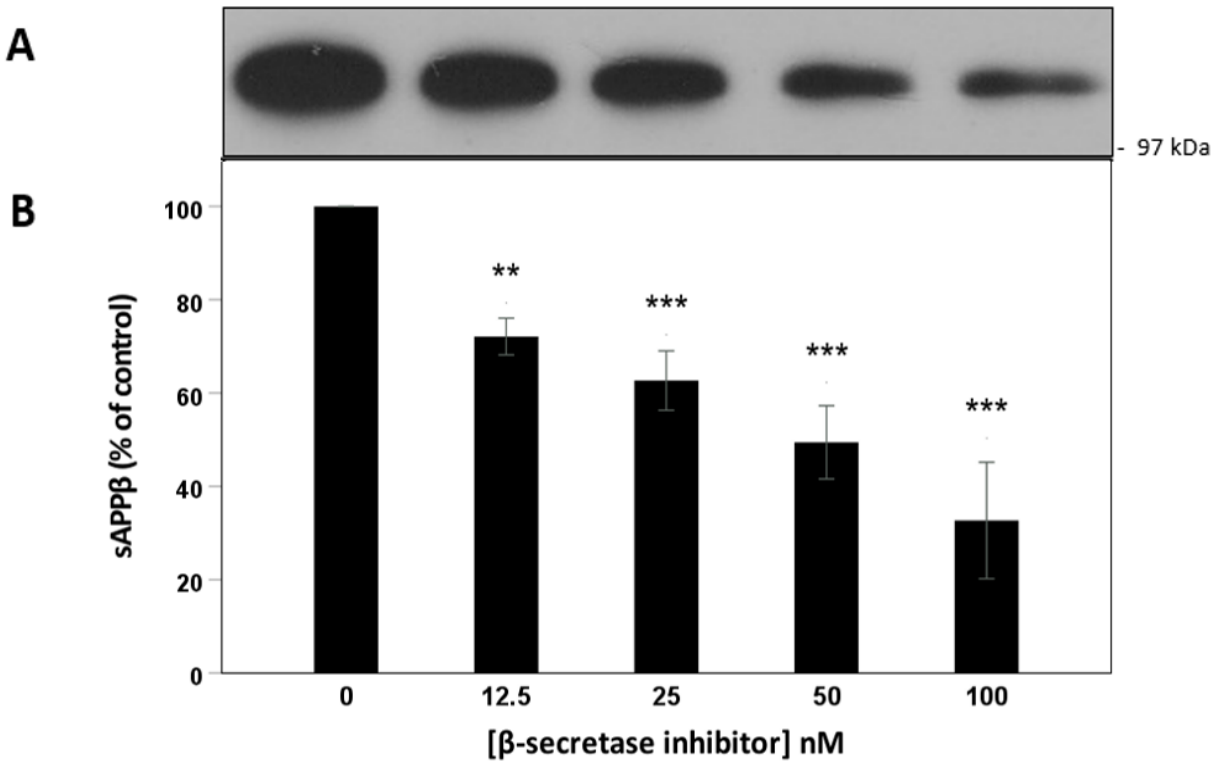

Figure 5.16. The effect of β-secretase inhibitor IV on sAPPβ levels in conditioned medium following 24 h treatment of confluent ARPE-19 cells. Confluent cells were transferred into UltraMEM and incubated in the absence or presence of the indicated drug concentrations for 24 h. Concentrated conditioned medium samples were then prepared and equal volumes from each sample were immunoblotted. **(A)** Detection of sAPPβ using the anti-sAPPβ antibody. **(B)** Quantification of multiple sAPPβ immunoblots by densitometric analysis. Results are expressed as a percentage of control cell cultures and are means ± S.D. (n=3). ***, $p \leq 0.001$.

5.5. The effects of β-secretase inhibitor on ARPE-19 cell viability in the absence of UV-A treatment

Having confirmed that all the concentrations (12.5, 25, 50 and 100 nM) of β-secretase inhibitor IV studied effectively inhibited sAPPβ production by ARPE-19 cells the effects of the drug on ARPE-19 viable cell numbers in the absence of UV-A treatment were examined. Initially, cells were grown to confluence in 96-well plates before changing the medium for UltraMEM and treating for 24 h with inhibitor IV. An MTS assay was then used in order to determine the relative numbers of viable cells between treatments (see Materials and Methods). The results (Fig. 5.17) showed that the drug did not alter the relative viable cell numbers except at the highest (100 nM) concentration at which point it marginally decreased relative viable cell numbers by 10.7 ± 8.2 % relative to control cultures.

We also investigated the ability of β-secretase inhibitor IV to inhibit cell proliferation over a seven-day period (adding the drug at the point of seeding). Cells were grown in DMEM:F12 and medium, together with β-secretase inhibitor IV, were replaced every 48 h. At the end of the seven-day growth period the relative numbers of viable cells were determined using the MTS assay. The results (Fig. 5.18) showed that inhibitor IV had minimal effects on cell proliferation over a seven-day period with a 21.5 ± 11.2 % increase (relative to control cultures) being observed at only one drug concentration (50 nM).

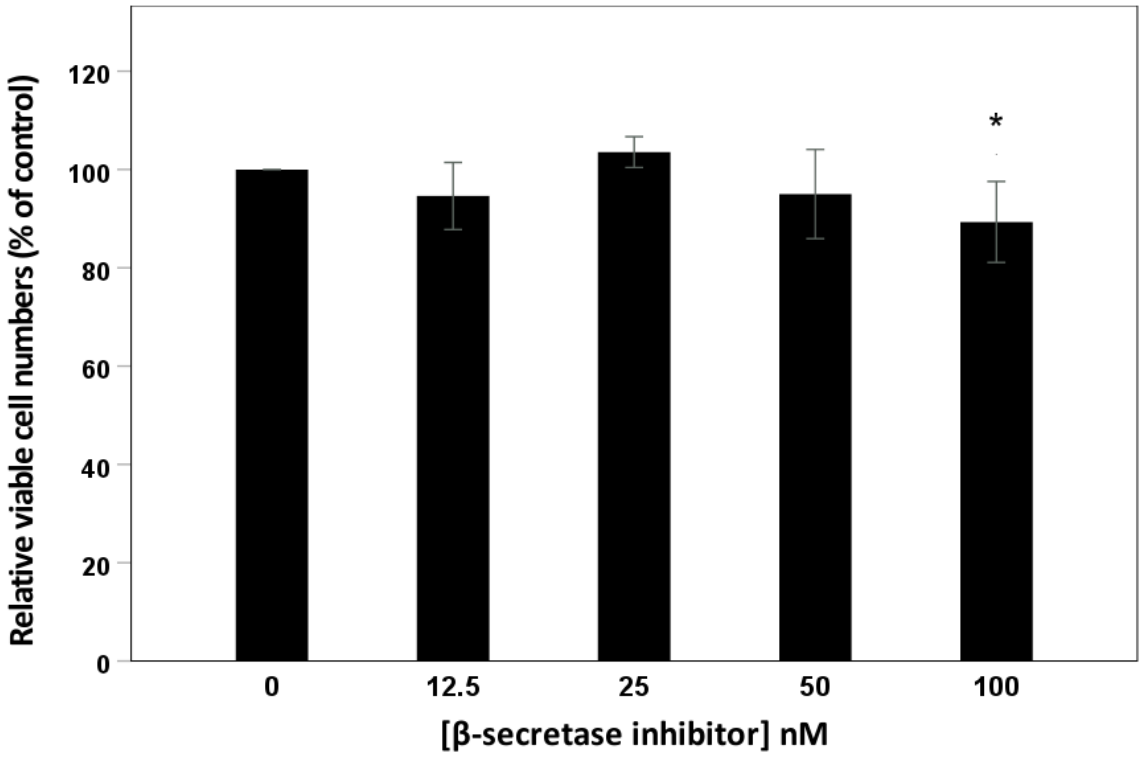

Figure 5.17. Relative viable cell numbers following 24 h treatment of confluent ARPE-19 cells with β-secretase inhibitor IV. Confluent cells were treated for 24 h with the indicated concentrations of inhibitor IV in UltraMEM and then subjected to an MTS viability assay as described in the Materials and Methods section. Results are expressed as a percentage of no inhibitor control cell cultures and are means ± S.D. (n=4). *, $p \leq 0.05$.

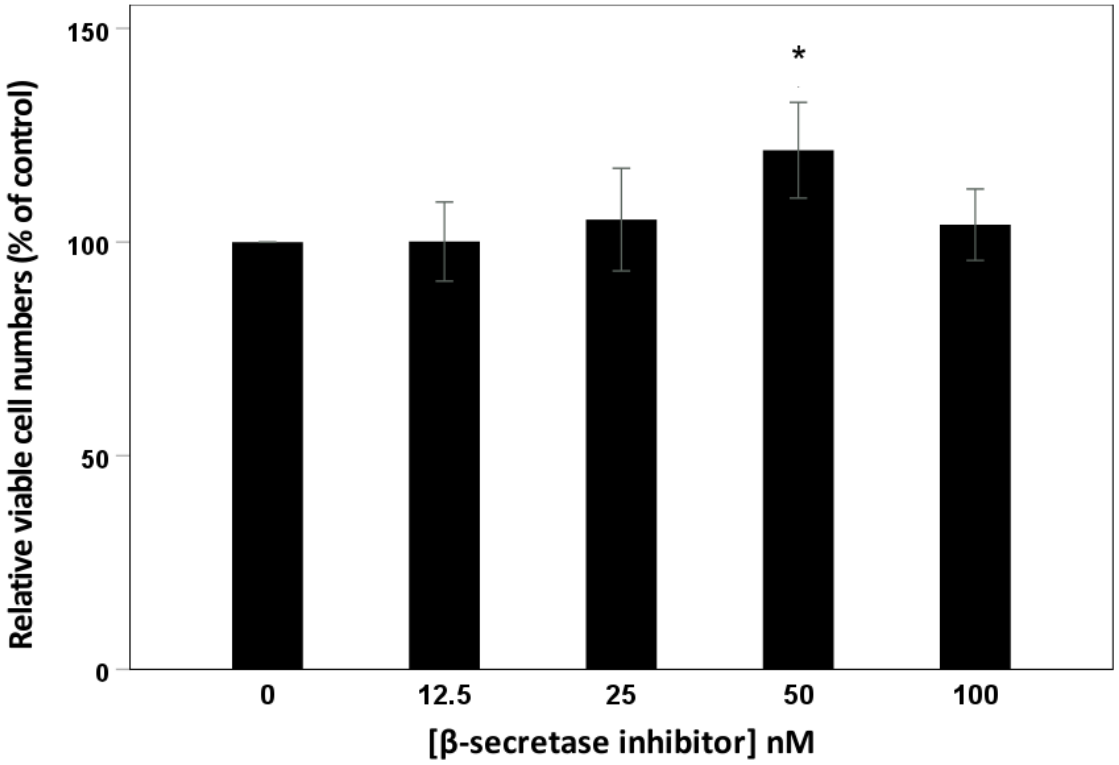

Figure 5.18. Relative viable cell numbers following seven days of ARPE-19 cell growth in the presence of β-secretase inhibitor IV. ARPE-19 cells were seeded at an appropriate density to achieve confluence in 7 days. Cells were grown in complete growth medium DMEM:F12 and inhibitor IV was added to the cultures at the point of seeding at the indicated concentrations. Medium was changed, and fresh inhibitor was added every 48 h until day 7 when cells were subjected to an MTS viability assay as described in the Materials and Methods section. Results are expressed as a percentage of no inhibitor control cell cultures and are means ± S.D. (n=4). *, $p \leq 0.05$.

5.6. The effects of β-secretase inhibitor on ARPE-19 cell viability following UV-A treatment

Given that the highest concentration of β-secretase inhibitor IV (100 nM) caused a slight but significant decrease in cell viability in the 24 h treatment of confluent cells (Fig. 5.17), the second highest concentration (50 nM) was adopted in order to investigate the potential effects of the drug on the resistance of ARPE-19 to UV-A treatment. Notably this concentration still dramatically reduced sAPPβ production (Fig. 5.16). T25 flasks of cells were grown to 80% confluence and pre-treated for 6h with 50 nM inhibitor IV in UltraMEM. Following transfer to phenol red-free DMEM, the cells were exposed to UV-A for 50 min before being transferred back into UltraMEM (in the absence or presence of inhibitor IV) for an 18 h recovery period. Viable cell numbers were then determined using Trypan blue counts as described in the Materials and Methods section. The results (Fig. 5.19) showed that, as

observed previously, UV-A exposure significantly decreased viable cell numbers (a reduction of 22.4 ± 3.4 % relative to control cultures). However, β-secretase inhibitor IV did not modify the susceptibility of the cells to UV-A treatment. Notably, the viable cell numbers in cultures treated with inhibitor IV in the absence of UV-A treatment increased relative to control cultures in this set of experiments (23.5 ± 12.2 % increase). Although it was not deemed statistically significant, this increase was not expected given that the 24 h treatment of confluent cells did not alter cell numbers at this concentration (Fig. 5.17). However, this might be explained looking at the effects of 50 nM inhibitor IV on actively growing cultures (Fig. 5.18) given that cells were treated with the inhibitor at 80% confluence in the UV experiment.

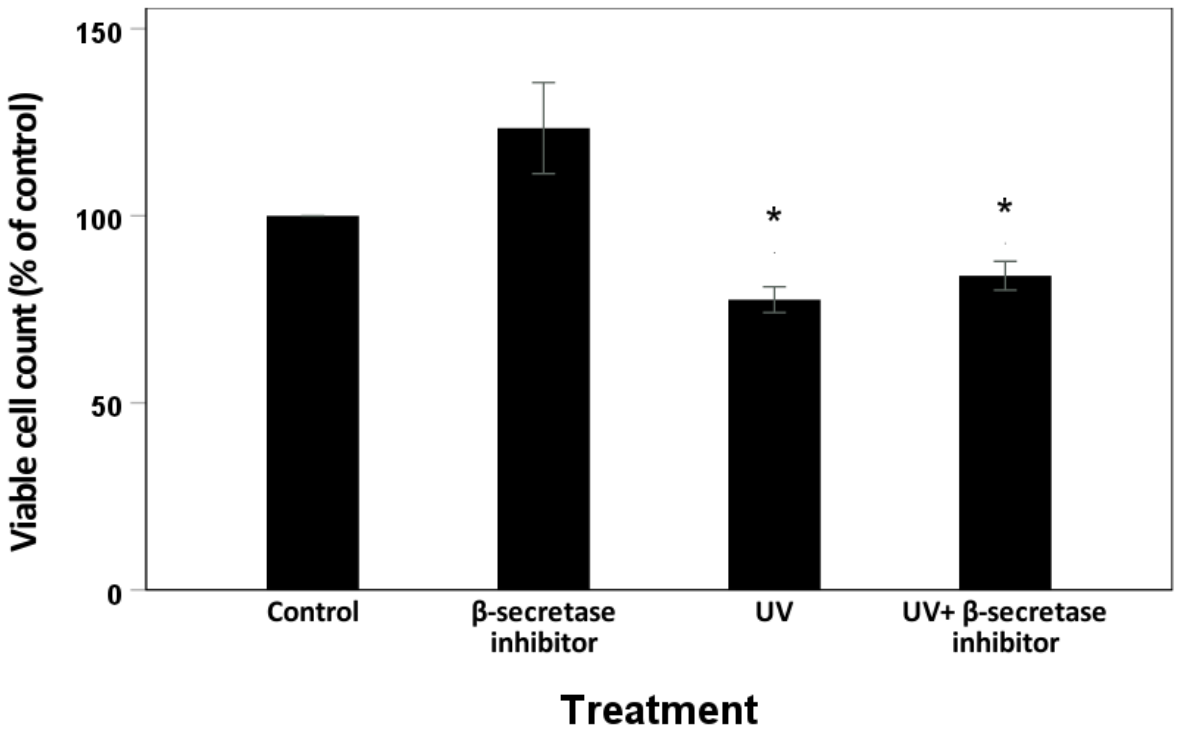

Fig. 5.19. Inhibition of sAPPβ production using β-secretase inhibitor IV does not alter the resistance of ARPE-19 cells to UV-A treatment. T25 cm^2 flasks of 80% confluent cells were preincubated for 6 h in UltraMEM +/- inhibitor IV (50 nM) and then transferred into phenol red-free DMEM during UV exposure for 50 min. The cells were then transferred into UltraMEM +/- inhibitor IV as indicated for an 18 h recovery period. Viable cell numbers were then determined using the Trypan blue assay as described in the Materials and Methods section. Results are expressed as a percentage of control cell cultures and are means ± S.D. (n=4 except with UV samples where n=3). *, $p \leq 0.05$.

In order to confirm the expected effects of β-secretase inhibitor IV on APP processing in the UV-A experiments, lysates and concentrated conditioned medium samples were prepared from the same treated cell samples. Following SDS-PAGE separation of equal amounts of lysate protein, the samples were immunoblotted with the anti-APP C-terminal antibody and the results (Fig. 5.20A) confirmed previous observations (Chapter 3, Fig. 3.3) that exposure of the cells to UV-A decreased FL-APP levels in lysates. Immunoblotting of the conditioned medium (Fig. 5.20C) likewise confirmed previous observations (Fig. 5.16) that 50 nM inhibitor IV effectively inhibited sAPPβ production.

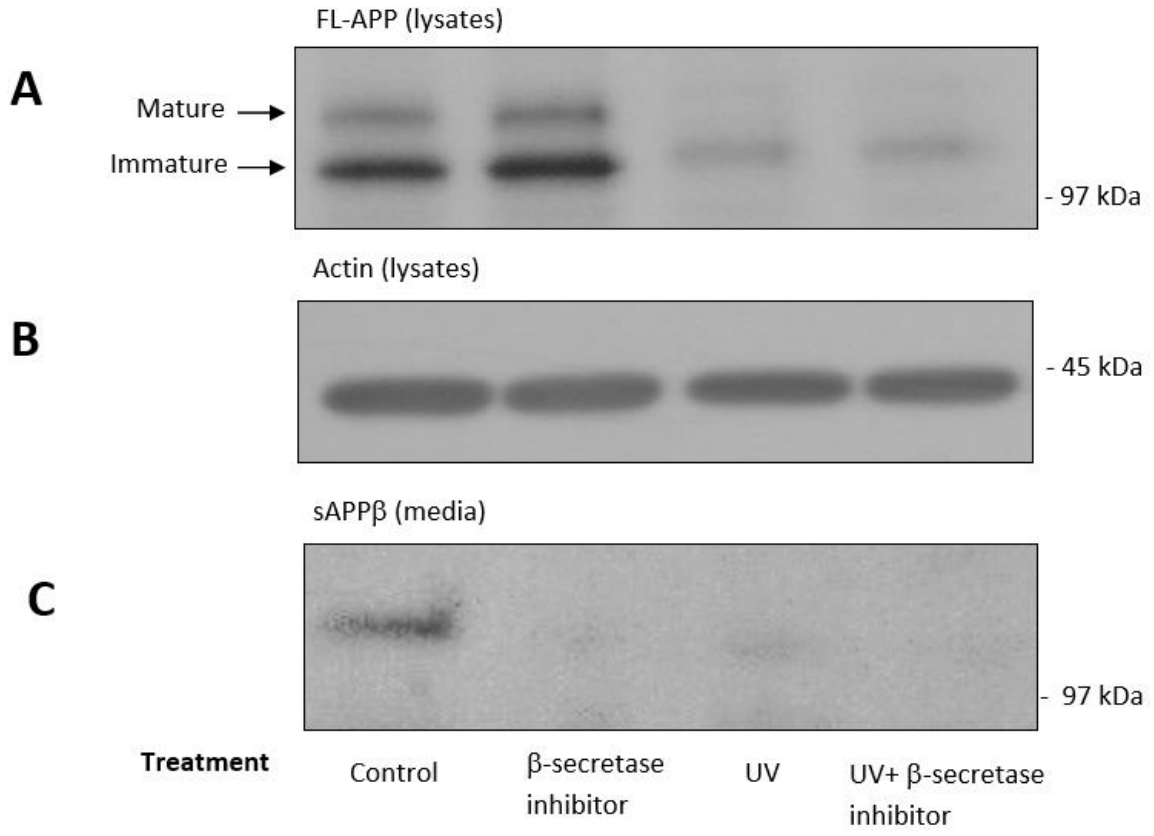

Figure 5.20. FL-APP expression and sAPPβ production following UV-A and β-secretase inhibitor IV treatment of ARPE-19 cells. T25 cm^2 flasks of 80% confluent cells were preincubated for 6 h in UltraMEM +/- 50 nM inhibitor IV and then transferred into phenol red-free DMEM during UV exposure for 50 min. The cells were then transferred into UltraMEM +/- inhibitor as indicated for an 18 h recovery period. Cell lysates and concentrated conditioned medium samples were then prepared and immunoblotted as described in the Materials and Methods section. **(A)** Detection of mature and immature forms of FL-APP in cell lysates using the anti-APP C-terminal antibody. **(B)** Detection of actin in cell lysates using the anti-actin antibody. **(C)** Detection of sAPPβ in conditioned medium using the anti-sAPPβ antibody.

5.7. Optimisation of γ-secretase inhibitor concentrations

In order to study the effects of blocking γ-secretase cleavage of APP-CTFs on ARPE-19 cell response to UV-A irradiation the selective γ-secretase inhibitor begacestat (GSI-953) (Tocris, Bristol, UK) was employed. This compound demonstrates a 14- to 16-fold selectivity towards the inhibition of APP-CTF cleavage relative to Notch-CTFs (Mayer *et al.*, 2008; Martone *et al.*, 2009). Initially the effects of begacestat on APP expression/proteolysis were investigated by transferring confluent T25cm^2 flasks of ARPE-19 cells into UltraMEM and treating for 24 h with a 0-100 nM concentration range of the inhibitor. This concentration range was selected on the basis that the IC_{50} value for begacestat relative to APP-CTFs is between 12.4 and 14.8 nM (Mayer *et al.*, 2008). Cell lysates were then prepared and subjected to immunoblotting using the anti-APP C-terminal antibody (see Materials and Methods). The results (Fig. 5.21A and C) showed no significant effects of the γ-secretase inhibitor on FL-APP levels. However, a dose-dependent increase in the levels of APP-CTF was observed and showed statistical significance at the concentrations of 25, 50 and 100 nM of the inhibitor (increases of 132.6 ± 48.1, 182.6 ± 92.4 and 232.4 ± 26.2 % respectively) (Fig 5.21B and C). This latter result was expected given that γ-secretase cleavage of the APP-CTFs should have been inhibited by the compound.

Next, the effects of begacestat on the generation of sAPPα were examined by immunoblotting equal volumes of concentrated conditioned medium samples with antibody 6E10. The results (Fig. 5.22) revealed that the compound had minimal effects on sAPPα with a slight increase (31.2 ± 9.5 % relative to controls) at the highest concentration (100 nM). However, this increase was not deemed statistically significant. Immunoblotting of the same samples with the anti-sAPPβ antibody (Fig. 5.23) similarly showed minimal effects of begacestat on the generation of sAPPβ with no significant difference being evident.

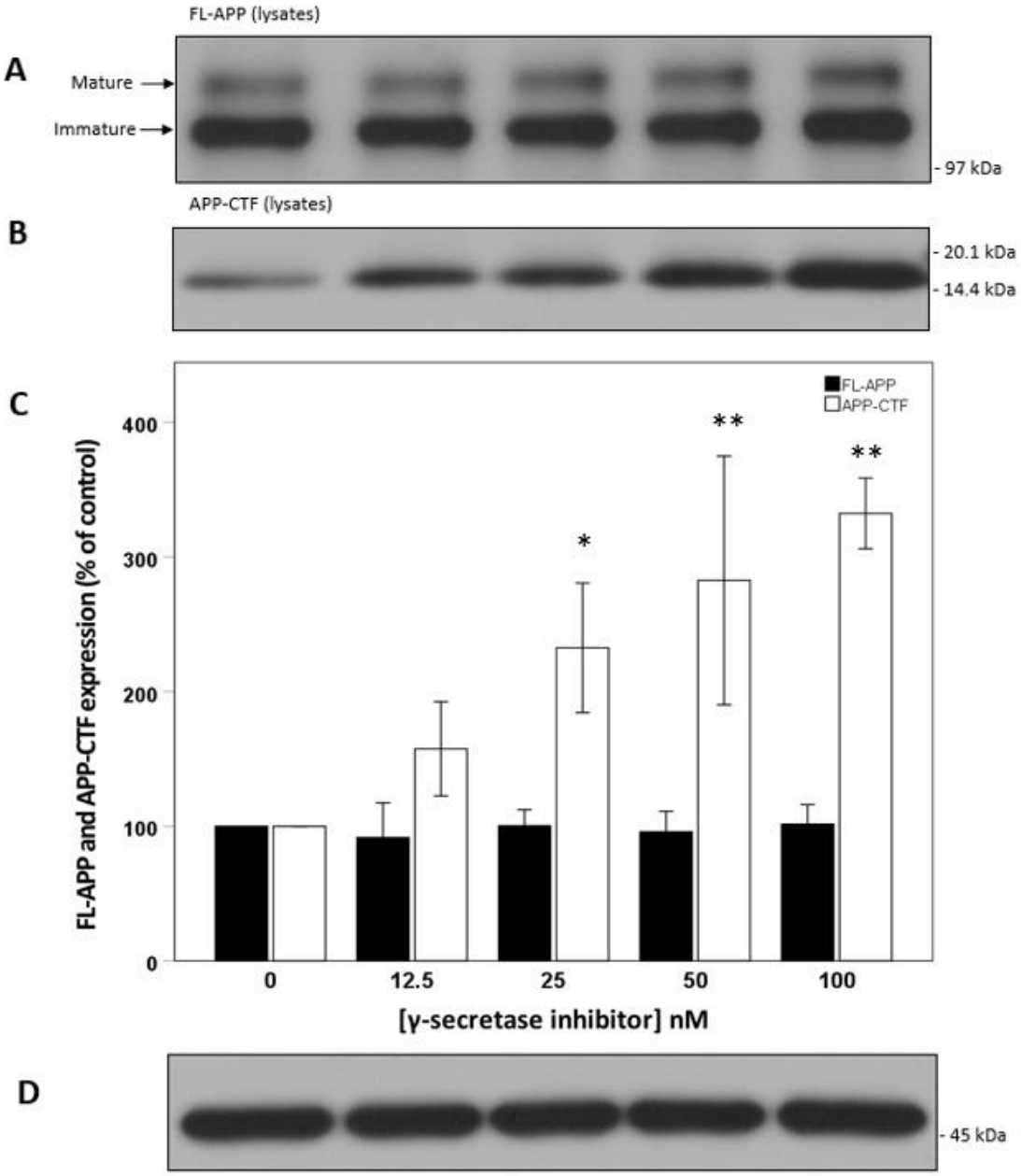

Figure 5.21. The effect of the γ-secretase inhibitor begacestat on FL-APP and APP-CTF levels in cell lysates following 24 h treatment of confluent ARPE-19 cells. Confluent cells were transferred into UltraMEM and incubated in the absence or presence of the indicated drug concentrations for 24 h. Cell lysates were then prepared and equal protein amounts from each sample were immunoblotted (see Materials and Methods). **(A)** Detection of mature and immature forms of FL-APP using the anti-APP C-terminal antibody. **(B)** Detection of APP-CTF using the anti-APP C-terminal antibody. **(C)** Quantification of multiple APP immunoblots by densitometric analysis. **(D)** Detection of actin using the anti-actin antibody. Results are expressed as a percentage of no inhibitor control cell cultures and are means ± S.D. (n=3). *, $p \leq 0.05$; **, $p \leq 0.01$.

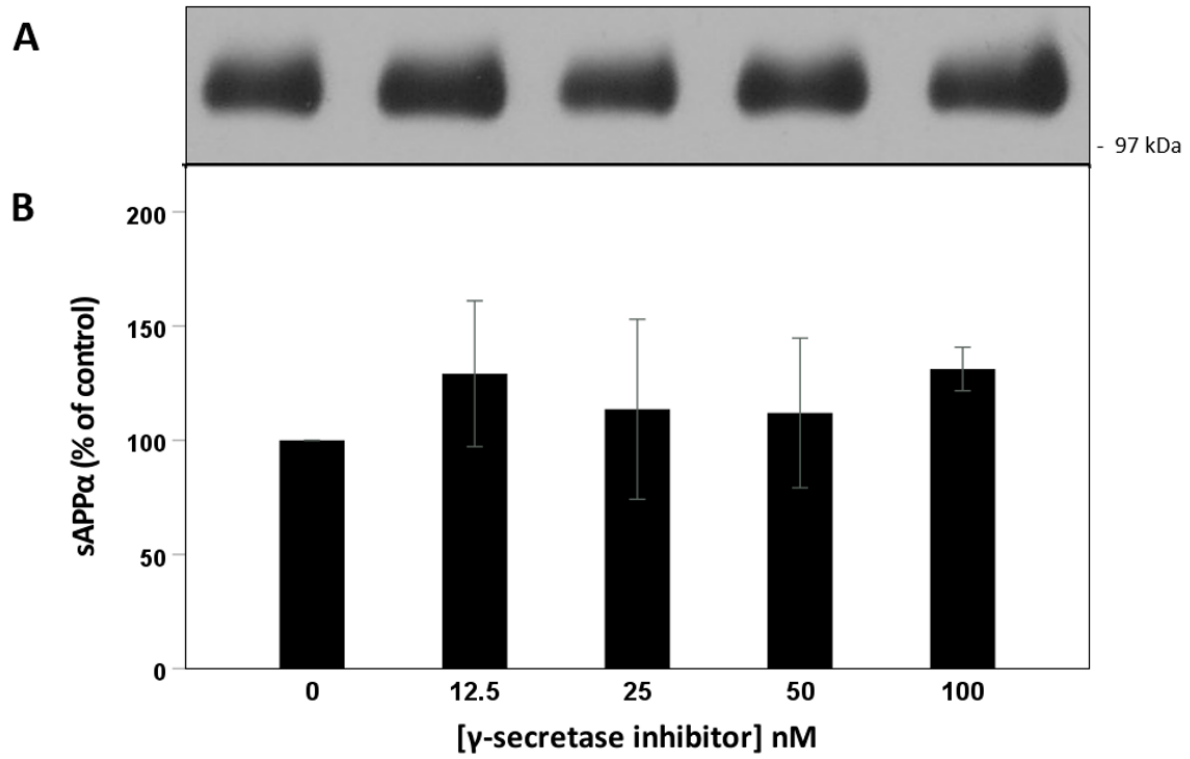

Figure 5.22. The effect of begacestat on sAPPα levels in conditioned medium following 24 h treatment of confluent ARPE-19 cells. Confluent cells were transferred into UltraMEM and incubated in the absence or presence of the indicated drug concentrations for 24 h. Concentrated conditioned medium samples were then prepared and equal volumes from each sample were immunoblotted. **(A)** Detection of sAPPα using antibody 6E10. **(B)** Quantification of multiple 6E10 immunoblots by densitometric analysis. Results are expressed as a percentage of control cell cultures and are means ± S.D. (n=3).

Collectively, these data confirmed effective inhibition of γ-secretase APP cleavage at the inhibitor concentrations employed starting from 25 nM and higher with an accumulation of APP-CTFs but only minor effects on FL-APP, sAPPα or sAPPβ levels.

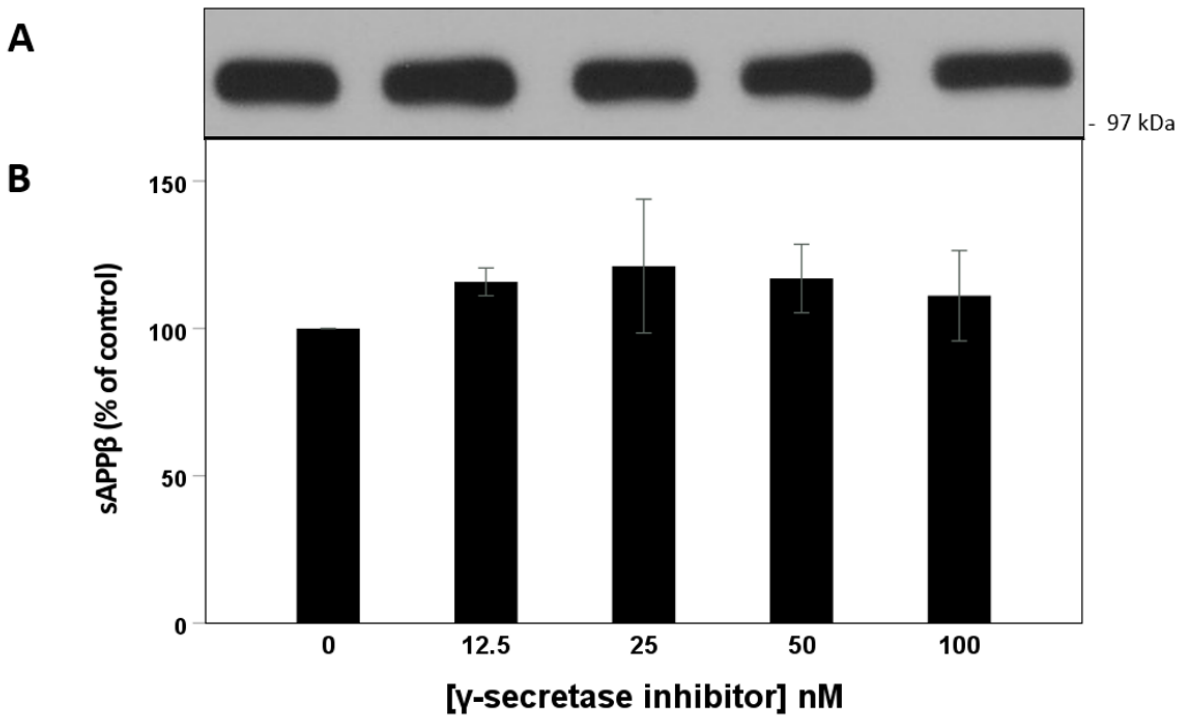

Figure 5.23. The effect of begacestat on sAPPβ levels in conditioned medium following 24 h treatment of confluent ARPE-19 cells. Confluent cells were transferred into UltraMEM and incubated in the absence or presence of the indicated drug concentrations for 24 h. Concentrated conditioned medium samples were then prepared and equal volumes from each sample were immunoblotted. **(A)** Detection of sAPPβ using the anti-sAPPβ antibody. **(B)** Quantification of multiple sAPPβ immunoblots by densitometric analysis. Results are expressed as a percentage of control cell cultures and are means ± S.D. (n=3).

5.8. The effects of γ-secretase inhibitor on ARPE-19 cell viability in the absence of UV-A treatment

Having confirmed that the following concentrations (25, 50 and 100 nM) of begacestat effectively inhibited γ-secretase cleavage of APP-CTFs in ARPE-19 cells, the effects of the drug on ARPE-19 viable cell numbers in the absence of UV-A treatment were examined. Initially, cells were grown to confluence in 96-well plates before changing the medium for UltraMEM and treating for 24 h with begacestat. An MTS assay was then used in order to determine the relative numbers of viable cells between treatments (see Materials and Methods). The results (Fig. 5.24) showed that the drug did actually slightly reduce cell viability although these effects could only be deemed statistically

significant at the lowest drug concentrations (12.5 nM) where viable cell numbers were reduced by 11.0 ± 3.5 relative to control cell cultures.

We also investigated the ability of begacestat to inhibit cell proliferation over a seven-day period (adding the drug at the point of seeding). Cells were grown in DMEM:F12 and medium, together with begacestat, were replaced every 48 h. At the end of the seven-day growth period the relative numbers of viable cells were determined using the MTS assay. The results (Fig. 5.25) showed that the γ-secretase inhibitor did effectively inhibit ARPE-19 cell proliferation over a seven-day growth period in a dose-dependent manner with relative viable cell numbers being reduced significantly by 22.1 ± 4.4 % at 100 nM inhibitor concentration.

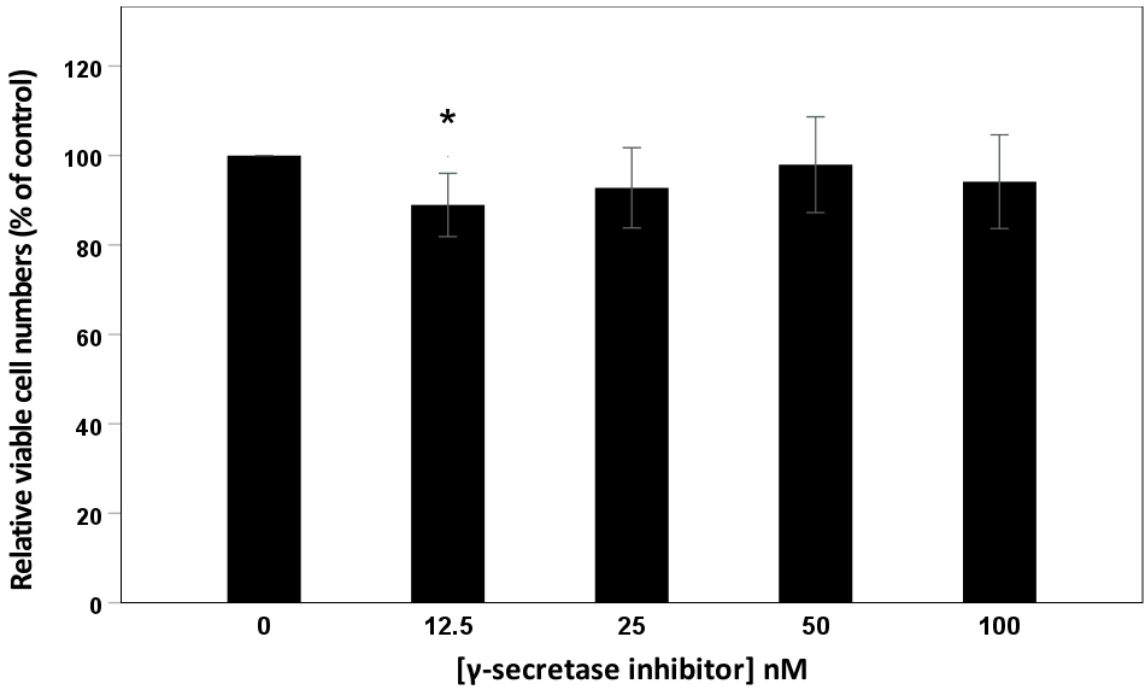

Figure 5.24. Relative viable cell numbers following 24 h treatment of confluent ARPE-19 cells with begacestat. Confluent cells were treated for 24 h with the indicated concentrations of begacestat in UltraMEM and then subjected to an MTS viability assay as described in the Materials and Methods section. Results are expressed as a percentage of no inhibitor control cell cultures and are means ± S.D. (n=4). *, $p \leq 0.05$.

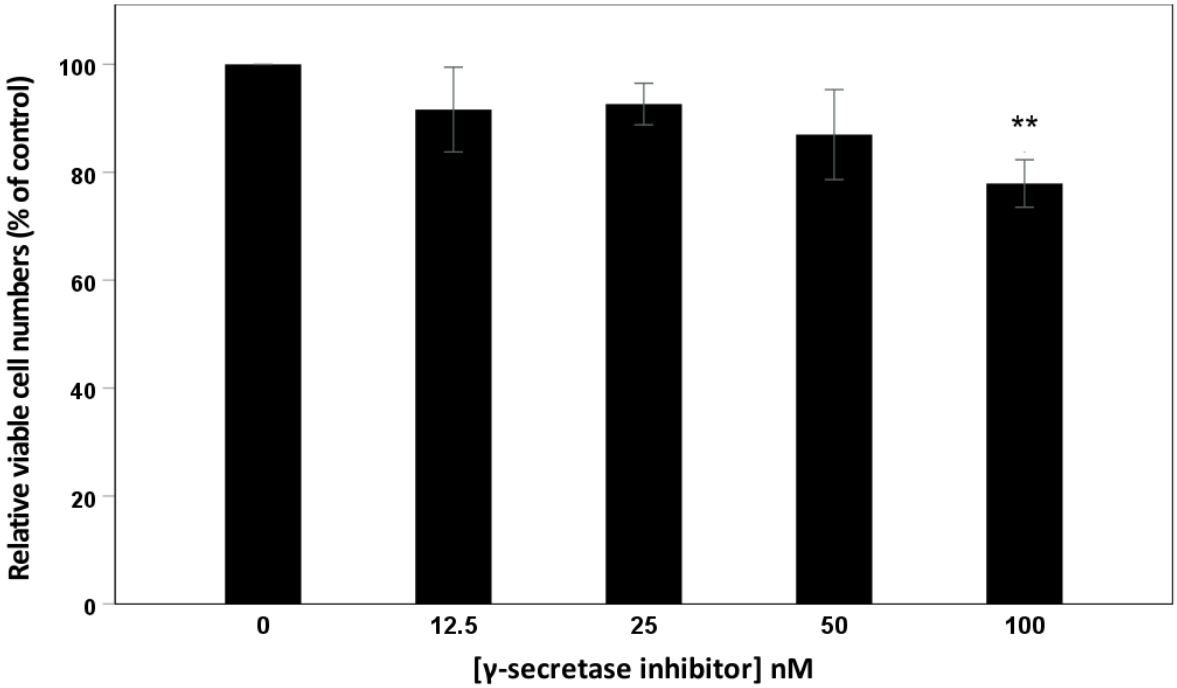

Figure 5.25. Relative viable cell numbers following seven days of ARPE-19 cell growth in the presence of begacestat. ARPE-19 cells were seeded at an appropriate density to achieve confluence in 7 days. Cells were grown in complete growth medium DMEM:F12 and begacestat was added to the cultures at the point of seeding at the indicated concentrations. Medium was changed, and fresh inhibitor was added every 48 h until day 7 when cells were subjected to an MTS viability assay as described in the Materials and Methods section. Results are expressed as a percentage of no inhibitor control cell cultures and are means ± S.D. (n=4). **, $p \leq 0.01$.

5.9. The effects of γ-secretase inhibitor on ARPE-19 cell viability following UV-A treatment

Given that the highest concentration of begacestat (100 nM) caused no significant reduction in viable cell numbers over a 24 h period (Fig. 5.24) this concentration of inhibitor was adopted in order to investigate the potential effects of the drug on the resistance of ARPE-19 cells to UV-A treatment. T25 flasks of cells were grown to 80% confluence and pre-treated for 6 h with 100 nM begacestat in UltraMEM. Following transfer to phenol red-free DMEM, the cells were exposed to UV-A for 50 min before being transferred back into UltraMEM (in the absence or presence of begacestat) for an 18 h recovery period. Viable cell numbers were then determined using Trypan blue counts as described in the Materials and Methods section. The results (Fig. 5.26) showed that, as observed previously, UV-A exposure significantly decreased viable cell numbers (a reduction of 28.7 ± 1.7 % relative to control cultures). Blocking APP-CTF proteolysis using the γ-secretase inhibitor did not

impact on cell viability in the absence of UV-A treatment. However, interestingly, the decline in cell numbers following UV-A exposure was partially abrogated by treatment with begacestat; here viable cell numbers were increased by 14.2 ± 4.1 **%** relative to the cells exposed to UV-A in the absence of the inhibitor.

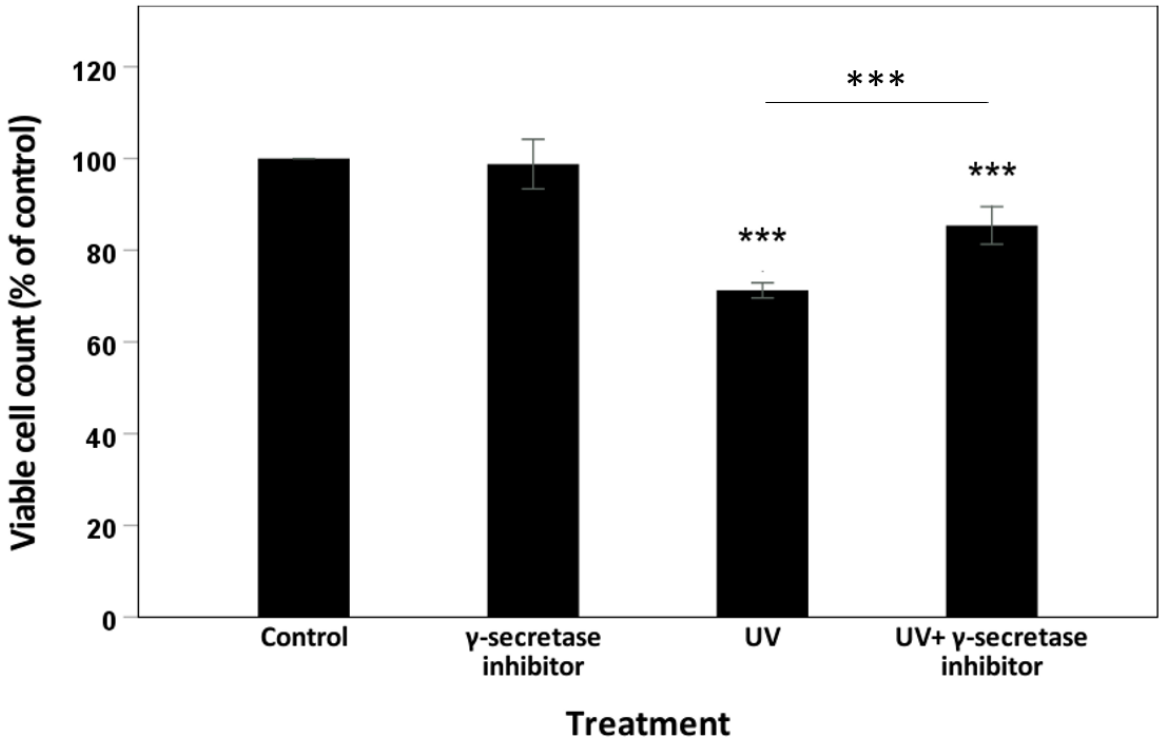

Fig. 5.26. Inhibition of γ-secretase-mediated APP-CTF cleavage using begacestat increases the resistance of ARPE-19 cells to UV-A treatment. T25 cm^2 flasks of 80% confluent cells were preincubated for 6 h in UltraMEM +/- begacestat (100 nM) and then transferred into phenol red-free DMEM during UV exposure for 50 min. The cells were then transferred into UltraMEM +/- begacestat as indicated for an 18 h recovery period. Viable cell numbers were then determined using the Trypan blue assay as described in the Materials and Methods section. Results are expressed as a percentage of control cell cultures and are means ± S.D. (n=4). ***, $p \leq 0.001$.

In order to confirm the expected effects of begacestat on APP-CTF processing in the UV-A experiments, lysates and concentrated conditioned medium samples were prepared from the same treated cell samples. Following SDS-PAGE separation of equal amounts of lysate protein, the samples were immunoblotted with the anti-APP C-terminal antibody and the results (Fig. 5.27A) confirmed previous observations (Chapter 3, Fig. 3.3) that exposure of the cells to UV-A decreased FL-APP levels in lysates. Using the same antibody, we were also able to confirm that APP-CTFs accumulated in the presence of the inhibitor regardless of whether cells were also treated with UV-A (Fig. 5.27B).

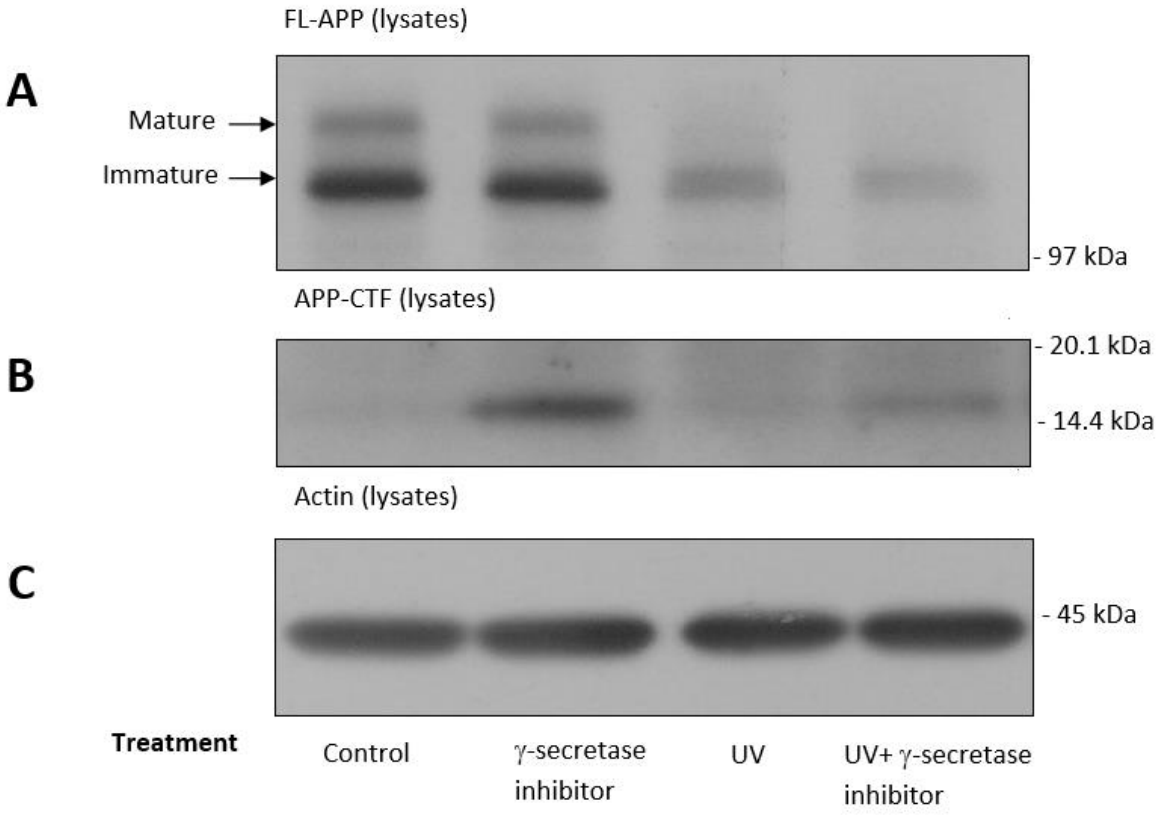

Figure 5.27. FL-APP and APP-CTF levels in cell lysates following UV-A and begacestat treatment of ARPE-19 cells. T25 cm^2 flasks of 80% confluent cells were preincubated for 6 h in UltraMEM +/- 100 nM begacestat and then transferred into phenol red-free DMEM during UV exposure for 50 min. The cells were then transferred into UltraMEM +/- inhibitor as indicated for an 18 h recovery period. Cell lysates were then prepared and immunoblotted as described in the Materials and Methods section. **(A)** Detection of mature and immature forms of FL-APP in cell lysates using the anti-APP C-terminal antibody. **(B)** Detection of APP-CTFs in cell lysates using the anti-APP C-terminal antibody. **(C)** Detection of actin in cell lysates using the anti-actin antibody.

5.10. Summary

In the current chapter, the effects of secretase inhibitors on ARPE-19 cell proliferation and resistance to UV-A exposure were examined.

Initial experiments using the α-secretase inhibitors GI254023X and batimastat at concentrations around the published IC_{50} values (relative to ADAM10) failed to significantly reduce sAPPα production by ARPE-19 cells and had only mild effects on the generation of the fragment by SH-SY5Y neuroblastoma cells. Eventually, a 5 μM batimastat concentration was shown to inhibit sAPPα production by ARPE-19 cells with a concomitant decrease in the levels of cell-associated APP-

CTFs but no significant effect on sAPPβ generation. The same batimastat concentration impaired cell proliferation over a seven-day period but had no effect on the viability of confluent ARPE-19 cells when treated for 24 h. Interestingly, the inhibition of sAPPα production did not modify the response of ARPE-19 cells to UV-A treatment.

β-secretase inhibitor IV successfully inhibited sAPPβ production by ARPE-19 cells in the concentration range 0-100 nM whilst having minimal effects on sAPPα production. Interestingly, the same compound caused an unexpected dose-dependent accumulation of APP-CTFs in cell lysates but did not alter levels of FL-APP. The inhibitor had minimal effects on relative viable cell numbers regardless of whether confluent cells were treated for 24 h or whether the drug was added to cells at the point of seeding. Furthermore, β-secretase inhibitor IV did not alter the resistance of ARPE-19 cells to UV-A treatment.

Finally, the APP-CTF specific γ-secretase inhibitor begacestat caused a dose-dependent accumulation of APP-CTFs in ARPE-19 cell lysates at concentrations in the range of 25-100 nM. No major effects of this drug on FL-APP, sAPPα or sAPPβ levels were observed. Minimal effects of begacestat on viable cell numbers were observed when confluent cells were treated with the drug for 24 h but a slight and dose-dependent decrease in relative viable cell numbers was observed when the drug was added to cells at the point of seeding which was statistically significant at the highest concentration applied (100 nM). These latter observations indicate that begacestat had a cytostatic rather than cytotoxic effect on ARPE-19 cells in the absence of UV-A treatment. Finally, begacestat was shown to partially protect ARPE-19 against the effects of UV-A treatment on viable cell numbers.

Collectively, these data suggest that neither α- nor β-secretase processing are important in modifying the response of ARPE-19 cells to UV-A treatment. The lack of effect of the β-secretase inhibitor in this respect also suggests that Aβ-peptide generation is not linked to the effects of UV-A on cell viability. In contrast, the fact that the γ-secretase inhibitor, begacestat, enhanced the resistance

of cells to UV-A treatment suggests that, rather than Aβ, APP intracellular domain (AICD) fragment formation may be mechanistically linked to the effects of UV-A on ARPE-19 cells.

Chapter 6

The protective effects of GLP-1 analogues in ARPE-19 cells

6. The protective effects of GLP-1 analogues in ARPE-19 cells

Glucagon-like peptide-1 (GLP-1) analogues are clinically used as type 2 diabetes drugs and have been shown to exert neurotrophic (Perry *et al.*, 2002b) and neuroprotective properties in cellular and animal models of neurodegenerative diseases such as Alzheimer's and Parkinson's disease (Harkavyi and Whitton, 2010; Sharma *et al.*, 2014; McClean and Hölscher, 2014). These effects are thought to be related to the stimulation of the GLP-1 receptor initiating a subsequent decrease in levels of Aβ and related cytotoxicity in cellular and animal models of neurodegenerative diseases (Li *et al.*, 2010; Perry *et al.*, 2003). Moreover, GLP-1 analogues might shift APP processing towards the non-amyloidogenic pathway by increasing expression levels of ADAM10 and thus releasing more of the neuroprotective sAPPα fragment (Ohtake *et al.*, 2014).

In addition, a number of studies have established a link between diabetes and AMD (Chen *et al.*, 2014; Hahn *et al.*, 2013; Leske *et al.*, 2006; Topouzis *et al.*, 2009), implicating diabetes as a risk factor for developing AMD. Hence, an effective treatment strategy against diabetes could have potential therapeutic value in AMD.

As such, in the current study, we sought to examine whether three GLP- 1 analogues (exendin-4, liraglutide and lixisenatide) were capable of protecting ARPE-19 cells against chemical stressors and UV-A irradiation.

6.1. The protective effects of GLP-1 analogues; hydrogen peroxide

Oxidative stress has been implicated in the pathology of AMD leading to the degeneration of photoreceptors and RPE cells (Pawlowska *et al.*, 2019; Beatty *et al.*, 2000). Moreover, Aβ aggregates present in neurodegenerative diseases such as AD have been shown to induce reactive oxygen species (ROS) production and contribute to oxidative damage (Sayre *et al.*, 2000; Cheignon *et al.*, 2018). These oxidative stress effects catalysed by Aβ oligomers have also been demonstrated in relation to AMD pathology (Aβ is a major constituent of drusen deposits in RPE cells) (Bruban *et al.*, 2009).

Given that GLP-1 analogues have been shown to protect cells against oxidative stress (Oh and Jun, 2017) and Aβ cytotoxicity (Li *et al.*, 2010), we decided in the current study to examine whether these drugs could protect ARPE-19 cells against hydrogen peroxide (H_2O_2) which has been employed in previous studies to cause oxidative stress *in vitro* (Coyle and Kader, 2007; Oraki Kohshour *et al.*, 2013).

Initially, it was necessary to determine suitably toxic concentrations of H_2O_2 and so confluent ARPE-19 cells were transferred into fresh complete growth medium and treated for 24 h in the presence of 0-500 μM H_2O_2 before quantifying relative viable cell numbers using an MTS assay (Materials and Methods). The results (Fig. 6.1) showed no significant effects on cell viability at the concentrations used apart from an unexpected trend towards an increase (by 27.2 ± 15.5 %) at the highest H_2O_2 concentration (500μM) (although it was not statistically significant).

This result raised the possibility that factors in the complete growth medium might have contributed to the elimination of H_2O_2 toxicity. Therefore, instead of adding the H_2O_2 to complete growth medium, UltraMEM reduced serum medium was employed. A 6 h pre-treatment incubation of the confluent cells in UltraMEM was also incorporated into this next set of experiments in order to take into account the pre-treatment with GLP-1 analogues that would be incorporated into subsequent experiments. The results (Fig. 6.2) showed significant reductions in relative viable cell numbers by 16.8 ± 5.7, 21.3 ± 5.0, 91.0 ± 6.7 and 95.0 ± 3.9 at concentrations of 350, 400, 450 and 500 μM H_2O_2, respectively.

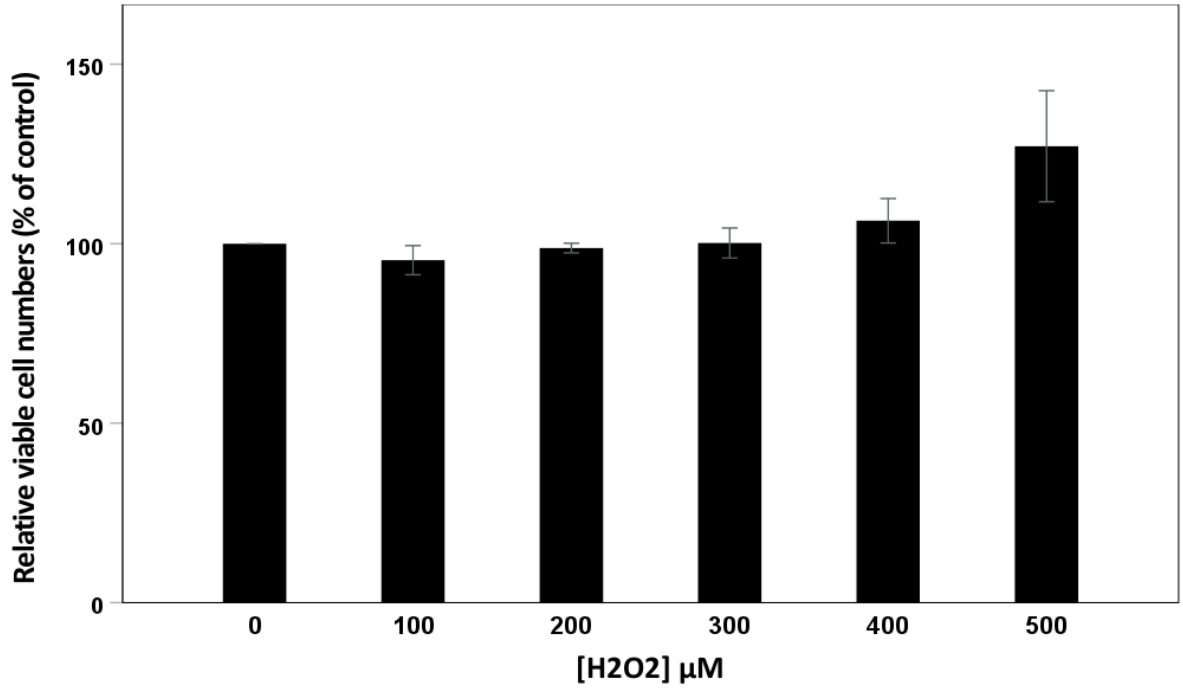

Figure 6.1. Relative viable cell numbers following 24 h treatment of confluent ARPE-19 cell cultures with H_2O_2 in complete growth medium. Confluent cells were treated for 24 h with the indicated concentrations of H_2O_2 in fresh complete growth medium and then subjected to an MTS viability assay as described in the Materials and Methods section. Results are expressed as a percentage of no hydrogen peroxide control cell cultures and are means ± S.D. (n=4).

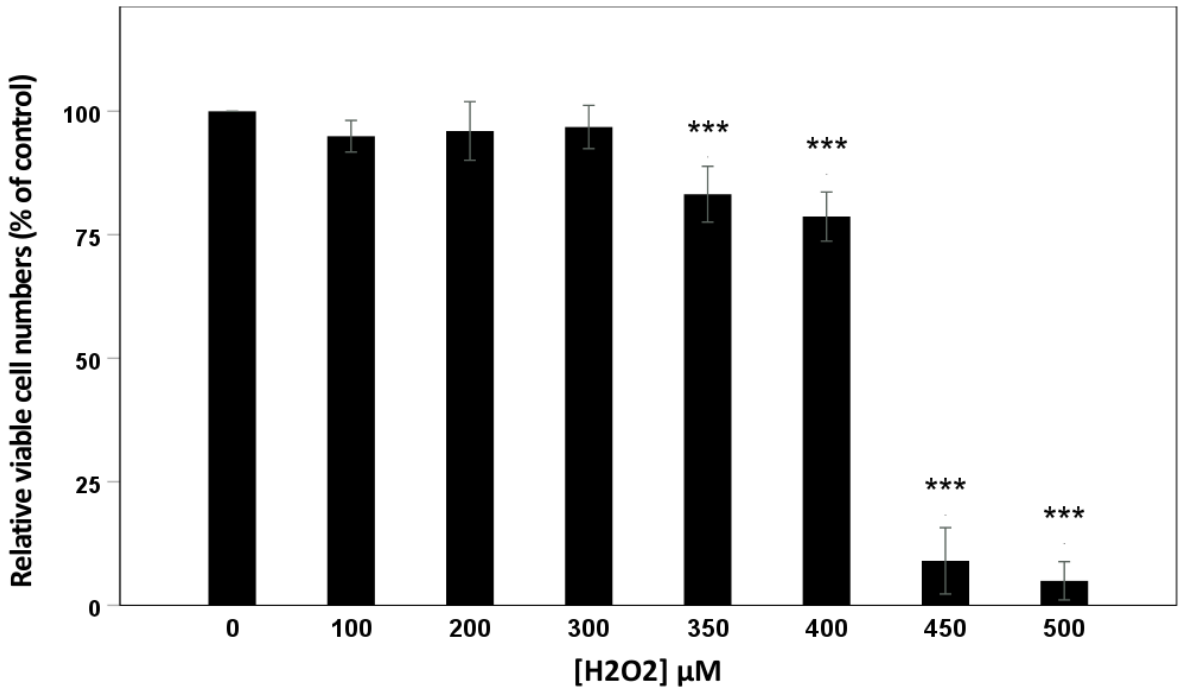

Figure 6.2. Relative viable cell numbers following 24 h treatment of confluent ARPE-19 cell cultures with H_2O_2 in reduced serum medium (UltraMEM). Confluent cells were transferred into UltraMEM for 6 h before adding H_2O_2 to the indicated final concentrations and culturing for a further 24 h after which the cells were subjected to an MTS viability assay as described in the Materials and Methods section. Results are expressed as a percentage of no hydrogen peroxide control cell cultures and are means ± S.D. (n=4). ***, $p \leq 0.001$.

Having determined suitable doses of H_2O_2 to use, we next examined the ability of GLP-1 analogues to protect against a 500 μM concentration of this chemical stressor. Again, cells were grown to confluence and transferred to UltraMEM for a 6 h pre-treatment incubation period in the presence of 0, 1, 10, 100 or 200 nM concentrations, initially, of exendin-4 (concentrations based on Sharma *et al.,* 2014; Jalewa *et al.,* 2016). Hydrogen peroxide (500 μM) was then added to the same medium (i.e. the medium was not changed) and the cells were incubated for a further 24 h before conducting an MTS assay. The results (Fig. 6.3) showed the previously determined toxic effect of 500 μM hydrogen peroxide on ARPE-19 cells. However, none of the exendin-4 concentrations had any effect on cell viability regardless of whether hydrogen peroxide was present.

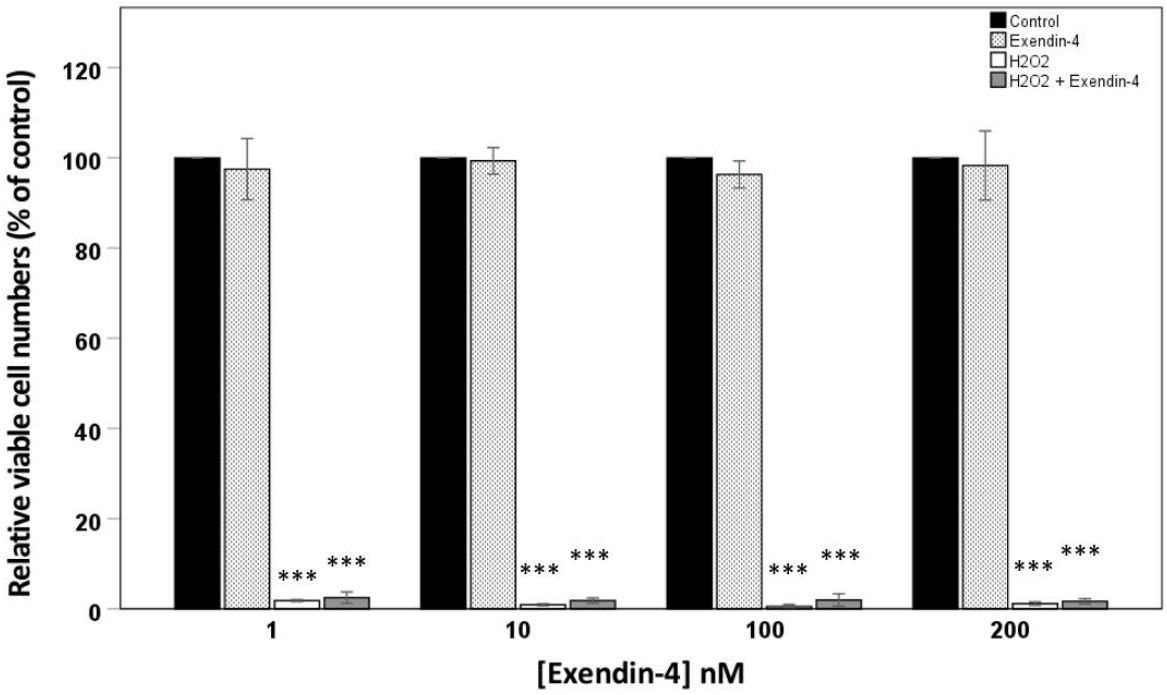

Figure 6.3. Lack of appreciable effect of exendin-4 on ARPE-19 cell viability in the absence or presence of 500 μM hydrogen peroxide. Confluent cells were transferred into UltraMEM containing the indicated concentrations of exendin-4 for 6 h before adding H_2O_2 (500 μM) to the same medium, incubating for a further 24 h and then conducting an MTS viability assay as described in the Materials and Methods section. Results are expressed as a percentage of no exendin-4 and no hydrogen peroxide control cell cultures and are means ± S.D. (n=3). ***, $p \leq 0.001$.

Similarly, the effects of the two other GLP-1 analogues, liraglutide and lixisenatide, were examined in relation to 500 μM H_2O_2. As observed previously for exendin-4, liraglutide also exhibited no increase in viable cell numbers regardless of whether hydrogen peroxide was present (Fig. 6.4). The results were also very similar for lixisenatide (Fig. 6.5) with no significant effect on relative viable cell numbers in the absence or presence of hydrogen peroxide.

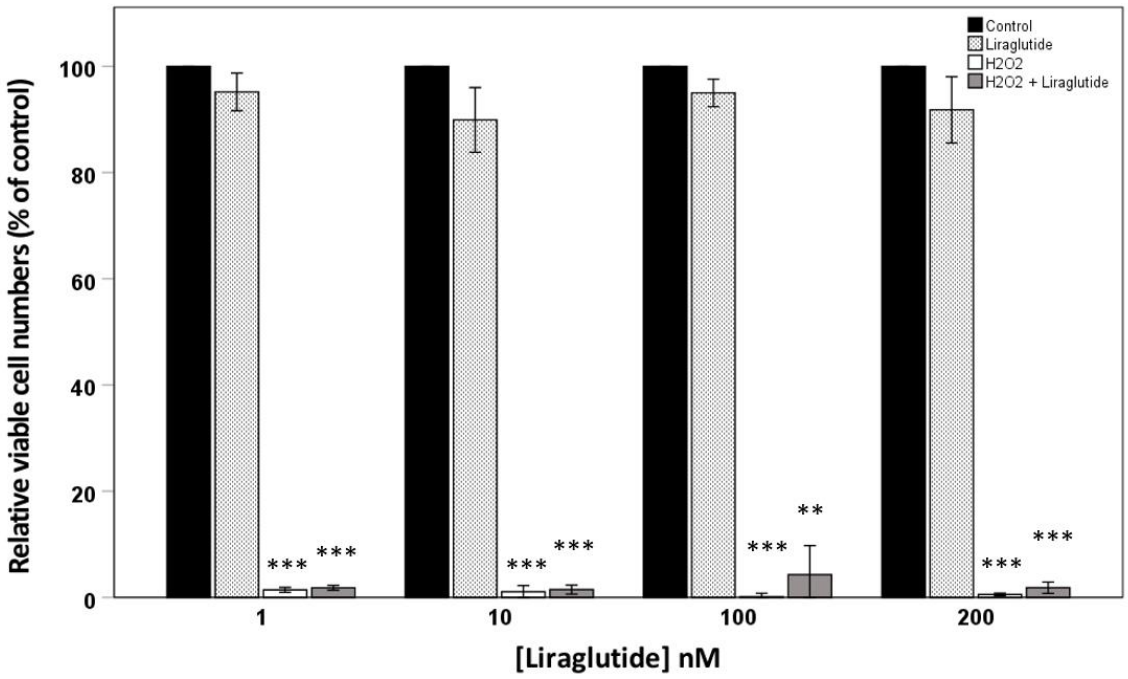

Figure 6.4. Lack of appreciable effect of liraglutide on ARPE-19 cell viability in the absence or presence of 500 μM hydrogen peroxide. Confluent cells were transferred into UltraMEM containing the indicated concentrations of liraglutide for 6 h before adding H_2O_2 (500 μM) to the same medium, incubating for a further 24 h and then conducting an MTS viability assay as described in the Materials and Methods section. Results are expressed as a percentage of no liraglutide and no hydrogen peroxide control cell cultures and are means ± S.D. (n=3). **, $p \leq 0.01$; ***, $p \leq 0.001$.

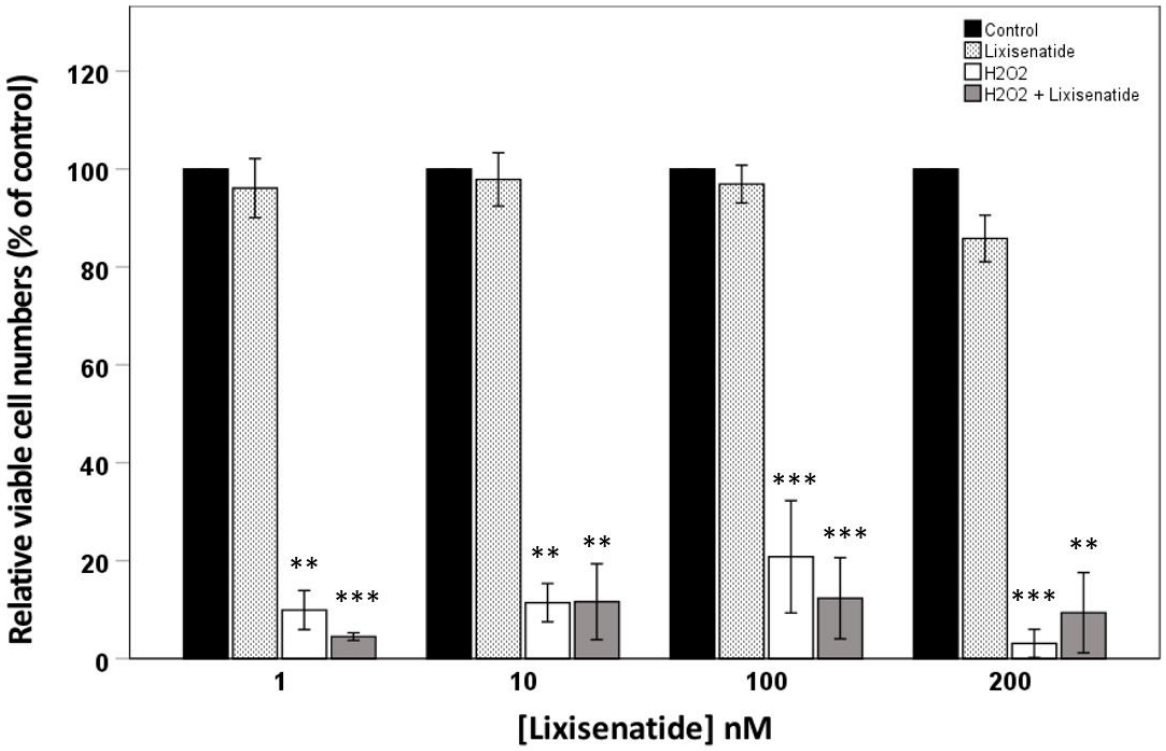

Figure 6.5. Lack of appreciable effect of lixisenatide on ARPE-19 cell viability in the absence or presence of 500 μM hydrogen peroxide. Confluent cells were transferred into UltraMEM containing the indicated concentrations of lixisenatide for 6 h before adding H_2O_2 (500 μM) to the same medium, incubating for a further 24 h and then conducting an MTS viability assay as described in the Materials and Methods section. Results are expressed as a percentage of no lixisenitide and no hydrogen peroxide control cell cultures and are means ± S.D. (n=3). **, $p \leq 0.01$; ***, $p \leq 0.001$.

Whilst none of the three GLP-1 analogues studied were able to protect ARPE-19 cells against the effects, on cell viability, of 500 μM H_2O_2 it was considered that such a high stressor concentration might simply overwhelm any potential protective effects of the drugs (given that 500 μM H_2O_2 resulted in near complete cytotoxicity). As such, the experiments in Figs 6.3, 6.4 and 6.5 were repeated using a lower (425 μM) H_2O_2 concentration under the pretense that this stressor concentration might yield a reduced, yet still appreciable, effect on cell viability. The results using exendin-4, liraglutide and lixisenatide (Figs 6.6., 6.7 and 6.8, respectively) did indeed show that the lower H_2O_2 concentration was less toxic than the previously employed 500 μM concentration. However, as observed previously, no protective effects of the three GLP-1 analogues were apparent in relation to H_2O_2 toxicity.

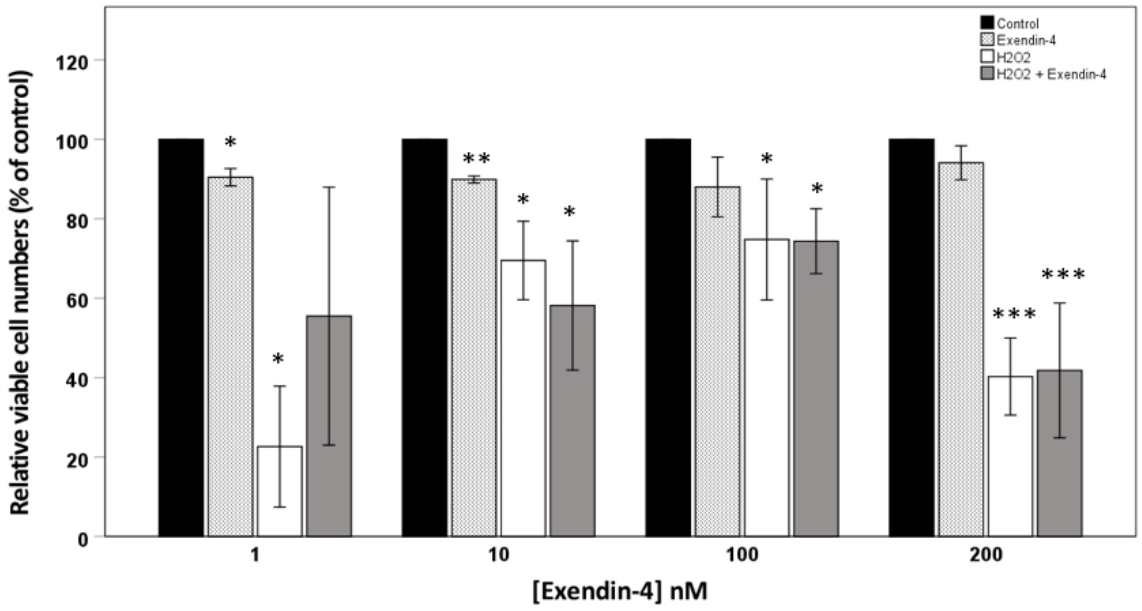

Figure 6.6. Lack of appreciable effect of exendin-4 on ARPE-19 cell viability in the absence or presence of 425 μM hydrogen peroxide. Confluent cells were transferred into UltraMEM containing the indicated concentrations of exendin-4 for 6 h before adding H_2O_2 (425 μM) to the same medium, incubating for a further 24 h and then conducting an MTS viability assay as described in the Materials and Methods section. Results are expressed as a percentage of no exendin-4 and no hydrogen peroxide control cell cultures and are means ± S.D. (n=3). *, $p \leq 0.05$; **, $p \leq 0.01$; ***, $p \leq 0.001$.

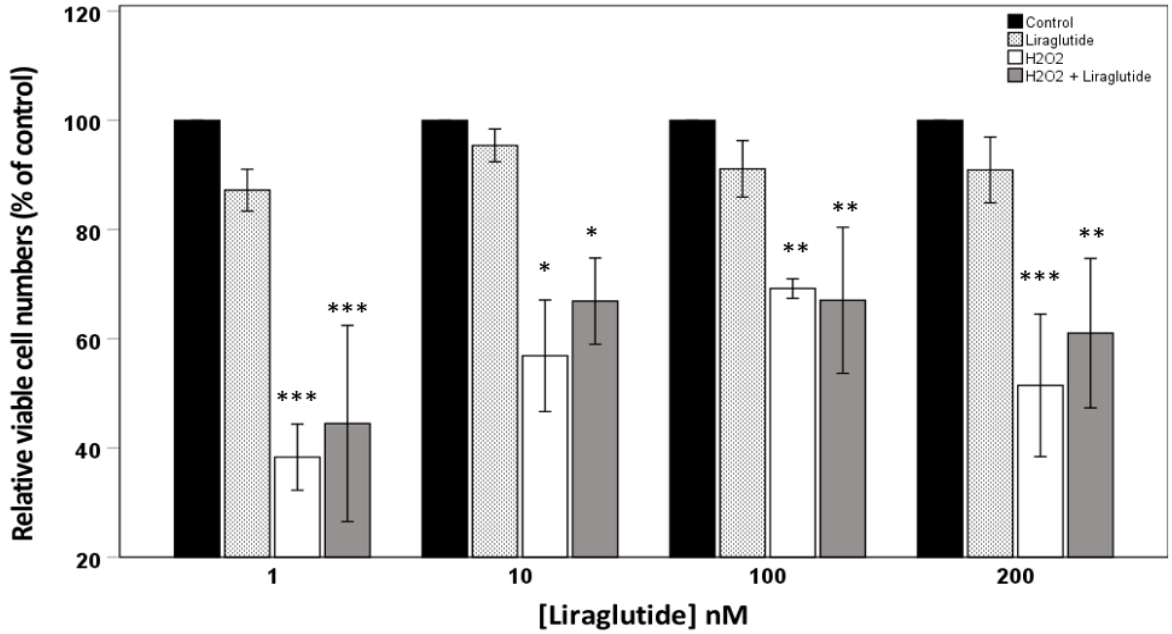

Figure 6.7. Lack of appreciable effect of liraglutide on ARPE-19 cell viability in the absence or presence of 425 μM hydrogen peroxide. Confluent cells were transferred into UltraMEM containing the indicated concentrations of liraglutide for 6 h before adding H_2O_2 (425 μM) to the same medium, incubating for a further 24 h and then conducting an MTS viability assay as described in the Materials and Methods section. Results are expressed as a percentage of no liraglutide and no hydrogen peroxide control cell cultures and are means ± S.D. (n=3). *, $p \leq 0.05$; **, $p \leq 0.01$; ***, $p \leq 0.001$.

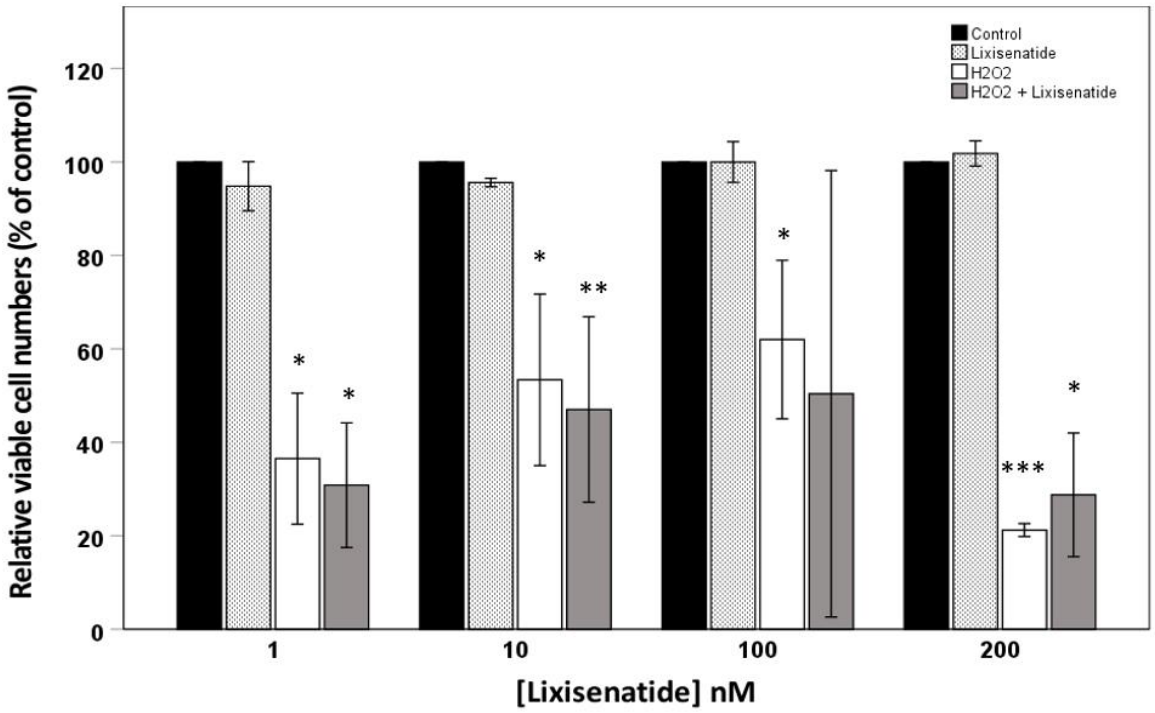

Figure 6.8. Lack of appreciable effect of lixisenatide on ARPE-19 cell viability in the absence or presence of 425 μM hydrogen peroxide. Confluent cells were transferred into UltraMEM containing the indicated concentrations of lixisenatide for 6 h before adding H_2O_2 (425 μM) to the same medium, incubating for a further 24 h and then conducting an MTS viability assay as described in the Materials and Methods section. Results are expressed as a percentage of no lixisenatide and no hydrogen peroxide control cell cultures and are means ± S.D. (n=3). *, $p \leq 0.05$; **, $p \leq 0.01$; ***, $p \leq 0.001$.

6.2. The protective effects of GLP-1 analogues; Aβ-peptide

Prior to determining whether GLP-1 analogues might protect ARPE-19 cells against Aβ-induced toxicity it was first necessary to determine peptide concentrations that yielded appropriate levels of cell toxicity. Previous studies had employed peptide concentration ranges between 1 and 25 μM with retinal pigment epithelial cells (Yoshida *et al.*, 2005; Masuda *et al.*, 2019). Therefore, in the current study, confluent ARPE-19 cells were transferred into UltraMEM and incubated for 24 h in the presence of 0-50 μM final concentrations of synthetic β-amyloid (1-42) peptide (GenScript, Piscataway, USA). Relative viable cell numbers were then determined using the MTS assay (Materials and Methods). The results (Fig. 6.9) showed minimal effects of the peptide on cell viability with only the highest (50 μM) peptide concentration showing any toxicity (an 8.7 ± 1.8 % decrease relative to control cultures).

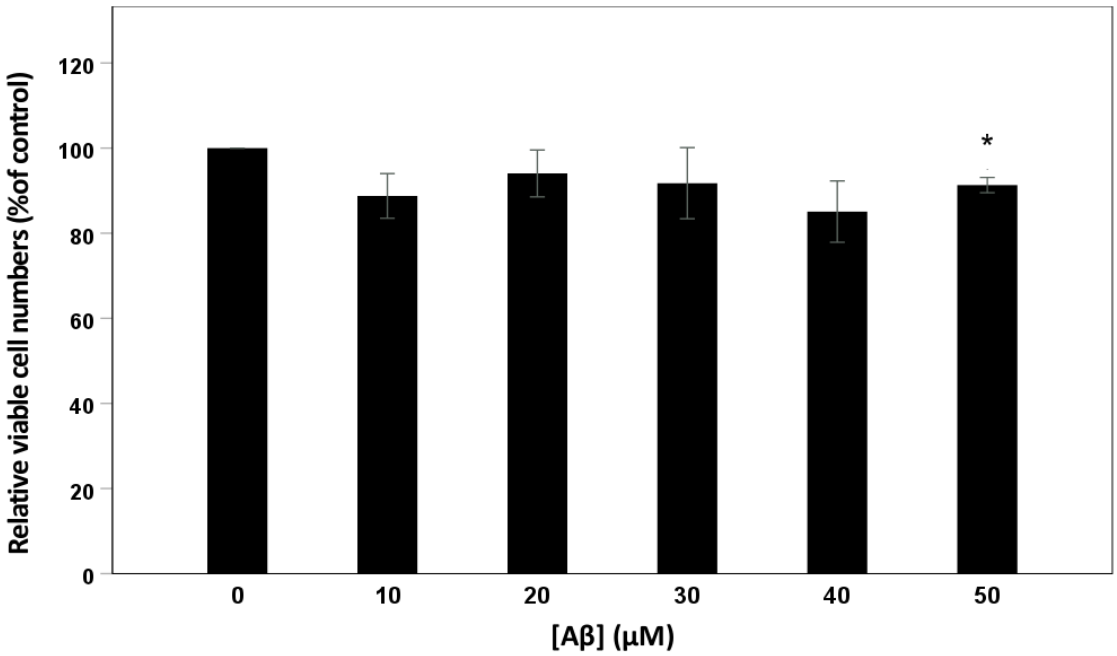

Figure 6.9. Lack of appreciable effect of Aβ-peptide (0-50 μM) on ARPE-19 cell viability. Confluent cells were treated for 24 h with the indicated concentrations of Aβ-peptide in UltraMEM and then subjected to an MTS viability assay as described in the Materials and Methods section. Results are expressed as a percentage of no Aβ-peptide control cell cultures and are means ± S.D. (n=3). *, $p \leq 0.05$.

These results were rather unexpected given the afore mentioned studies. However, another study by Chen *et al.* (2016) used higher concentrations in the millimolar range to attain significant effects in ARPE-19 cells. Unfortunately, given the economic considerations in the current study, such high concentrations of synthetic peptide were simply not viable and so it was decided not to continue with this aspect of the research.

6.3. The protective effects of GLP-1 analogues; UV-A

We next examined whether exendin-4, liraglutide or lixisenatide showed any protective effects in terms of preventing the UV-A-mediated reduction in viable cell numbers observed previously (Chapter 3, Fig. 3.1). Furthermore, the effect of the drugs on full-length APP levels and its metabolites were also monitored as we had previously shown changes in these proteins/fragments following UV-A irradiation of ARPE-19 cells (Chapter 3, Fig. 3.3, 3.4 and 3.5). These experiments were performed on cells in T25 cm^2 flasks as opposed to 96 well plates as in the preceding sections. Therefore, economic necessity dictated that only the highest GLP-1 analogue concentration (200 nM) was investigated in these experiments.

6.3.1. Exendin-4

Cells (80% confluent) were transferred into UltraMEM in the absence or presence of exendin-4 (200 nM) and cultured for 6 h. The UltraMEM was then removed and replaced with phenol red-free DMEM and the cells were irradiated with UV-A for 50 min as described in the Materials and Methods section before replacing the medium once more with UltraMEM +/- exendin-4 and culturing the cells for a further 18 h. Conditioned medium was then stored pending protein analysis and cells were released from the flasks by trypsinisation before counting using Trypan blue and freezing the remaining cells for later protein analysis. The cell viability results (Fig. 6.10) showed that, as previously observed (Chapter 3, Fig. 3.1), UV-A irradiation caused a significant decrease in viable cell counts (32.9 ± 8.1 %). Interestingly, exendin-4 caused a significant increase in viable cell numbers in the absence of UV-A treatment (18.8 ± 10.6 % increase) but the drug did not protect the cells against the effects of UV-A on cell viability.

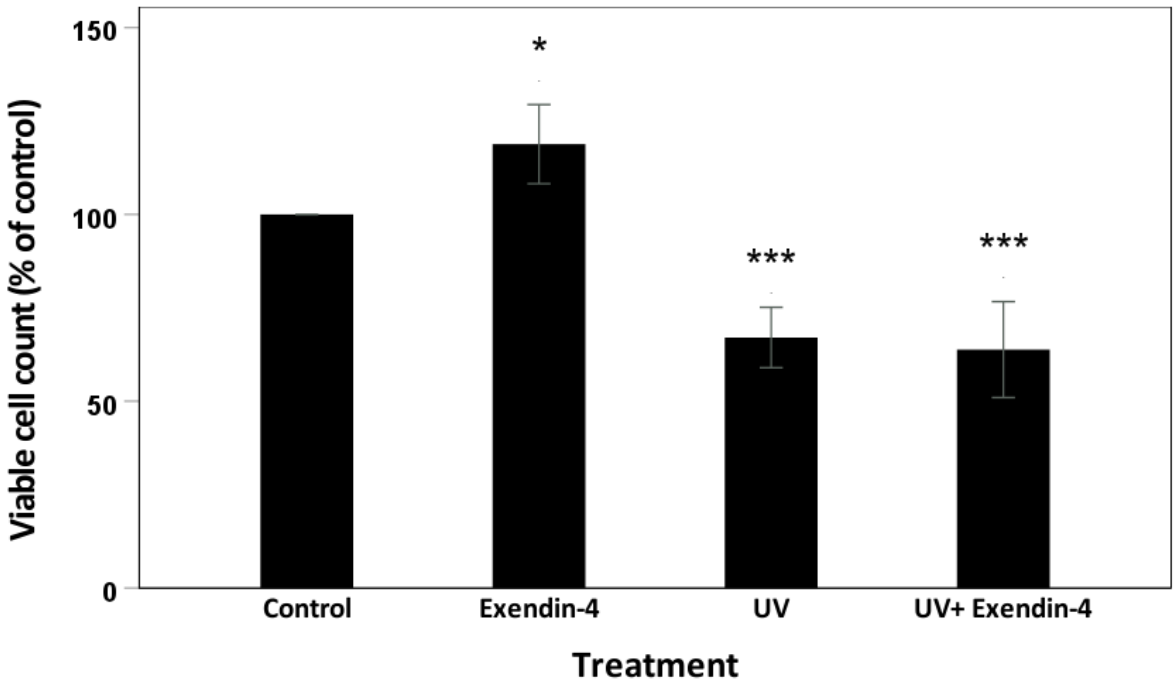

Figure 6.10. Exendin-4 does not protect ARPE-19 cells against UV-A-mediated decreases in cell viability. ARPE-19 cells (80% confluent) were pre-incubated for 6 h in UltraMEM in the absence or presence of 200 nM exendin-4 before exchanging the medium for phenol red-free DMEM and irradiating the cells with UV-A for 50 min (see Materials and Methods). The medium was then exchanged for fresh UltraMEM +/- exendin-4 and the cells were cultured for a further 18 h before analysing viable cell numbers using the Trypan blue assay. Results are expressed as a percentage of control cell cultures and are means ± S.D. (n=7). *, $p \leq 0.05$; **, $p \leq 0.01$; ***, $p \leq 0.001$.

Next, the treated cells were used to prepare lysates, from which the proteins were resolved by SDS-PAGE and immunoblotted using the anti-APP C-terminal antibody. The results (Fig. 6.11) showed the previously observed (Chapter 3, Fig. 3.3) decrease in full-length APP and APP-CTF levels following UV-A irradiation (decreased by 53.0 ± 29.3 and 60.5 ± 11.0 %, respectively relative to controls). Furthermore, exendin-4 did not impact on these UV-A mediated changes in FL-APP and APP-CTF levels.

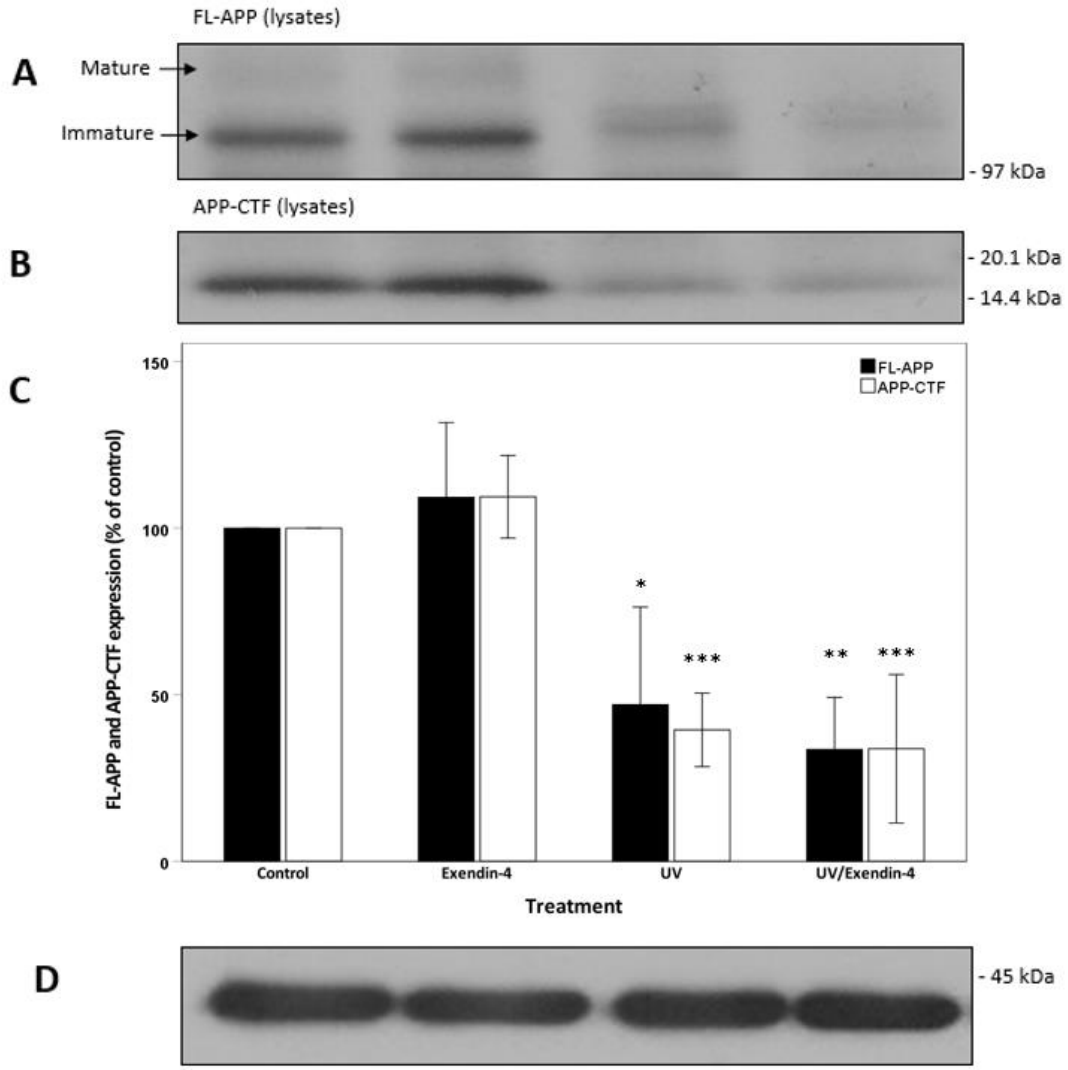

Figure 6.11. APP expression following UV-A and exendin-4 treatment of ARPE-19 cells. ARPE-19 cells (80% confluent) were pre-incubated for 6 h in UltraMEM in the absence or presence of 200 nM exendin-4 before exchanging the medium for phenol red-free DMEM and irradiating the cells with UV-A for 50 min (see Materials and Methods). The medium was then exchanged for fresh UltraMEM +/- exendin-4 and the cells were cultured for a further 18 h. Cell lysates were then prepared and proteins were resolved by SDS-PAGE and immunoblotted as described in the Materials and Methods section. **(A)** Detection of mature and immature forms of FL-APP using the anti-APP C-terminal antibody. **(B)** Detection of APP-CTF using the anti-APP C-terminal antibody. **(C)** Quantification of multiple APP immunoblots by densitometric analysis. **(D)** Detection of actin using the anti-actin antibody. Results are expressed as a percentage of control cell cultures and are means ± S.D. (n=4). *, $p \leq 0.05$; **, $p \leq 0.01$; ***, $p < 0.001$.

Conditioned medium samples from the exendin-4 experiments were concentrated and equal volumes were then immunoblotted with the anti-6E10 antibody in order to detect sAPPα. The results (Fig. 6.12A and B) showed an apparent decrease in sAPPα levels following UV-A treatment (by 28.5 ± 8.2 %) but, once the results were adjusted in order to take into account decreased cell numbers in cultures, this difference was no longer significant (Fig. 6.12C). Exendin-4 did not modify the amount of sAPPα produced regardless of whether cells were irradiated with UV-A.

The medium samples were also immunoblotted using the anti-sAPPβ antibody (Fig. 6.13) and, as observed previously, UV-A irradiation was shown to result in decreased sAPPβ production by cells whether or not the results were corrected in order to account for the decreased cell numbers present following irradiation (Fig. 6.13B and C). In UV-A-irradiated cells, there was no difference in sAPPβ production between those cells incubated in the presence or absence of exendin-4.

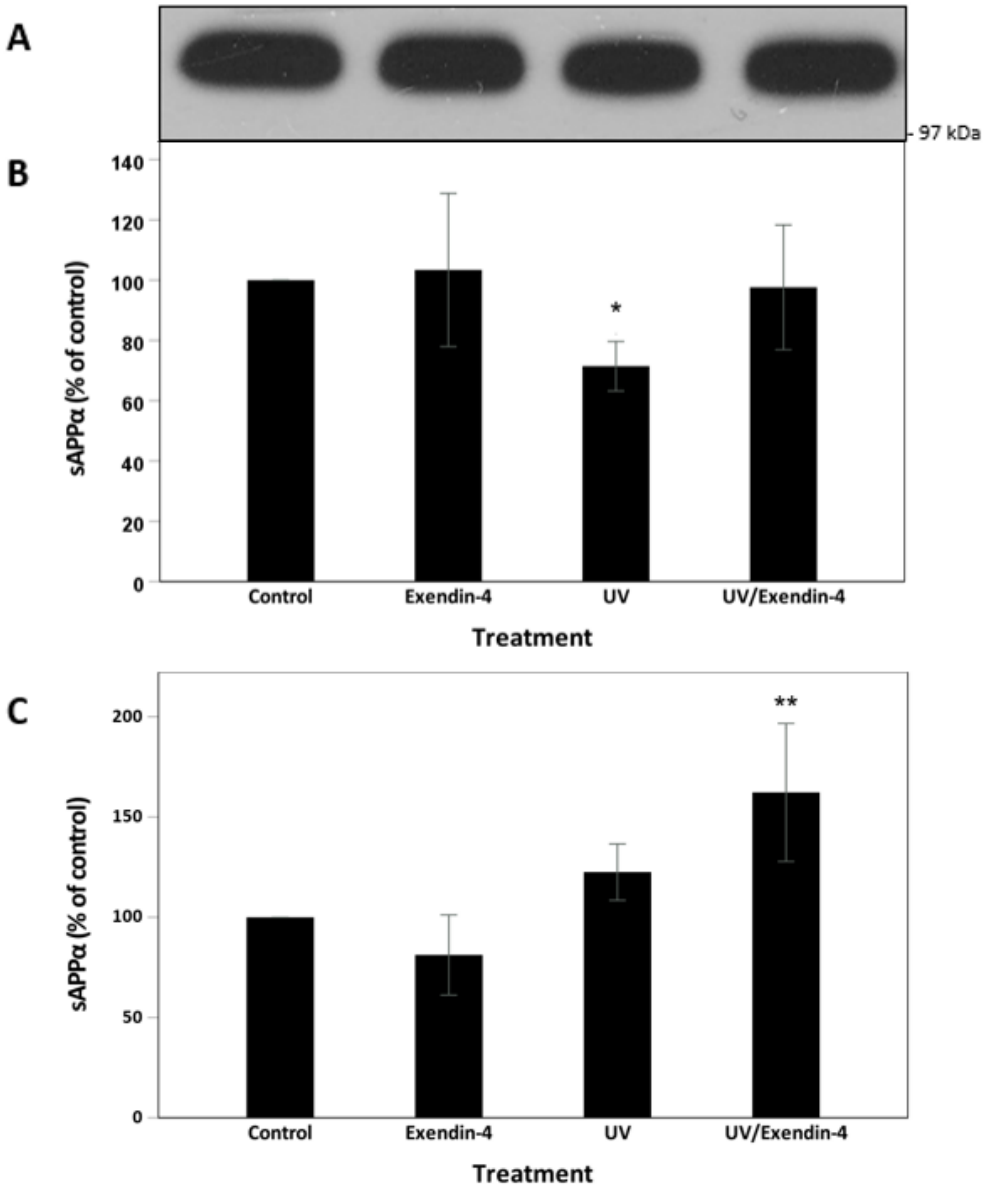

Figure 6.12. sAPPα production following UV-A and exendin-4 treatment of ARPE-19 cells. ARPE-19 cells (80% confluent) were pre-incubated for 6 h in UltraMEM in the absence or presence of 200 nM exendin-4 before exchanging the medium for phenol red-free DMEM and irradiating the cells with UV-A for 50 min (see Materials and Methods). The medium was then exchanged for fresh UltraMEM +/- exendin-4 and the cells were cultured for a further 18 h. Conditioned medium samples were concentrated as described in the Materials and Methods section and equal volumes were resolved by SDS-PAGE and immunoblotted (Materials and Methods). **(A)** Detection of sAPPα using antibody 6E10. **(B)** Quantification of multiple immunoblots by densitometric analysis showing uncorrected results. **(C)** Quantification of multiple immunoblots by densitometric analysis showing results corrected for observed changes in cell viability. Results are expressed as a percentage of control cell cultures and are means ± S.D. (n=4) except UV+Exendin-4 where n=3. *, $p \leq 0.05$; **, $p \leq 0.01$.

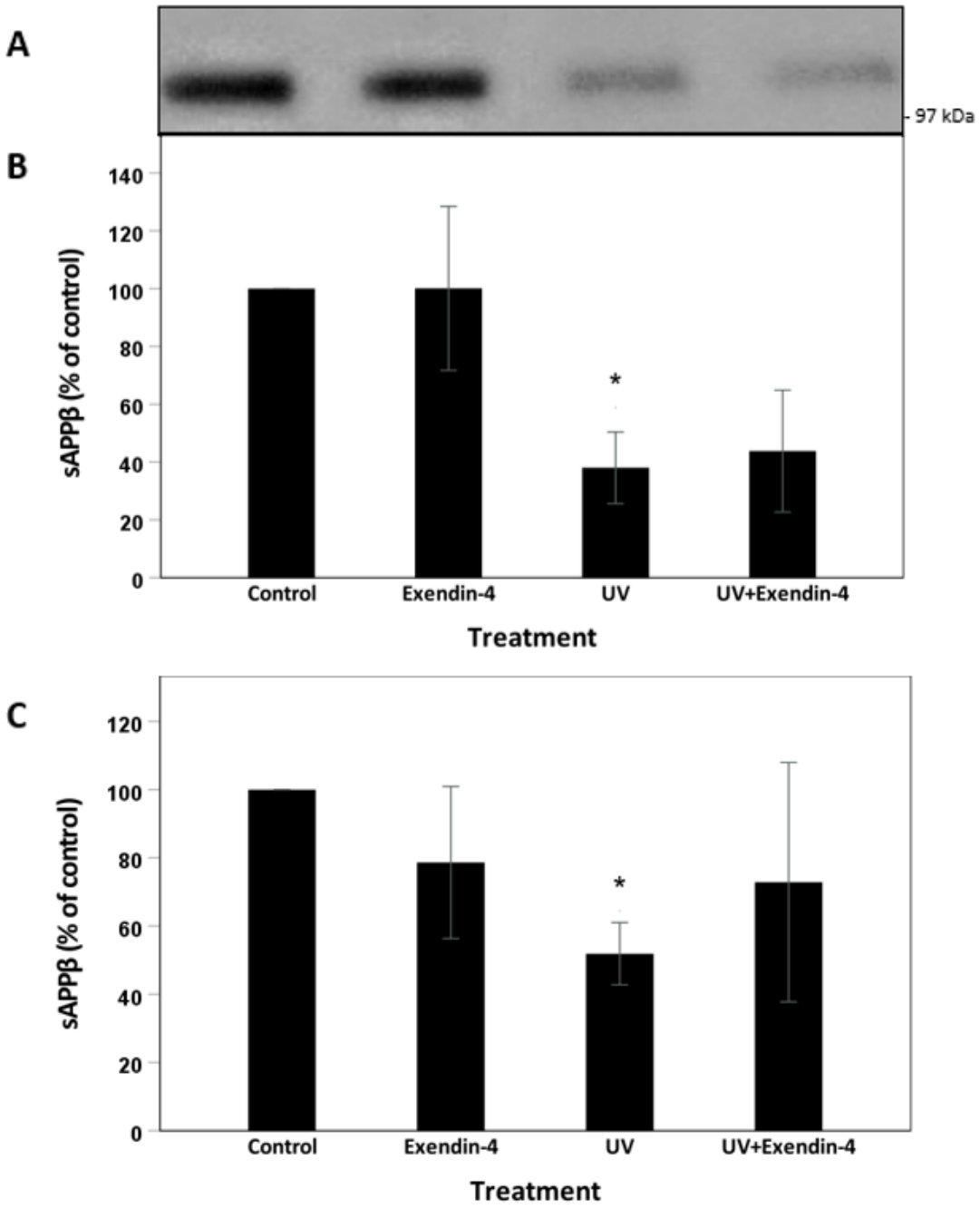

Figure 6.13. sAPPβ production following UV-A and exendin-4 treatment of ARPE-19 cells. ARPE-19 cells (80% confluent) were pre-incubated for 6 h in UltraMEM in the absence or presence of 200 nM exendin-4 before exchanging the medium for phenol red-free DMEM and irradiating the cells with UV-A for 50 min (see Materials and Methods). The medium was then exchanged for fresh UltraMEM +/- exendin-4 and the cells were cultured for a further 18 h. Conditioned medium samples were concentrated as described in the Materials and Methods section and equal volumes were resolved by SDS-PAGE and immunoblotted (Materials and Methods). **(A)** Detection of sAPPβ using the anti-sAPPβ antibody. **(B)** Quantification of multiple immunoblots by densitometric analysis showing uncorrected results. **(C)** Quantification of multiple immunoblots by densitometric analysis showing results corrected for observed changes in cell viability. Results are expressed as a percentage of control cell cultures and are means ± S.D. (n=3). *, $p \leq 0.05$.

6.3.2. Liraglutide

The experiments described in the preceding section were then repeated but using 200 nM liraglutide in place of the exendin-4. The Trypan blue cell viability assay results (Fig. 6.14) showed the previously observed decrease (Chapter 3, Fig. 3.1) in viable cell numbers following 50 min UV-A irradiation (by 23.4 ± 6.2 % relative to controls). Liraglutide treatment had no significant effect on cell viability in the absence of UV-A treatment. However, interestingly, liraglutide treatment was able to completely prevent UV-A-mediated decreases in cell viability resulting in the recovery of viable cell numbers to approximately control levels (98.6 ± 20.1 %).

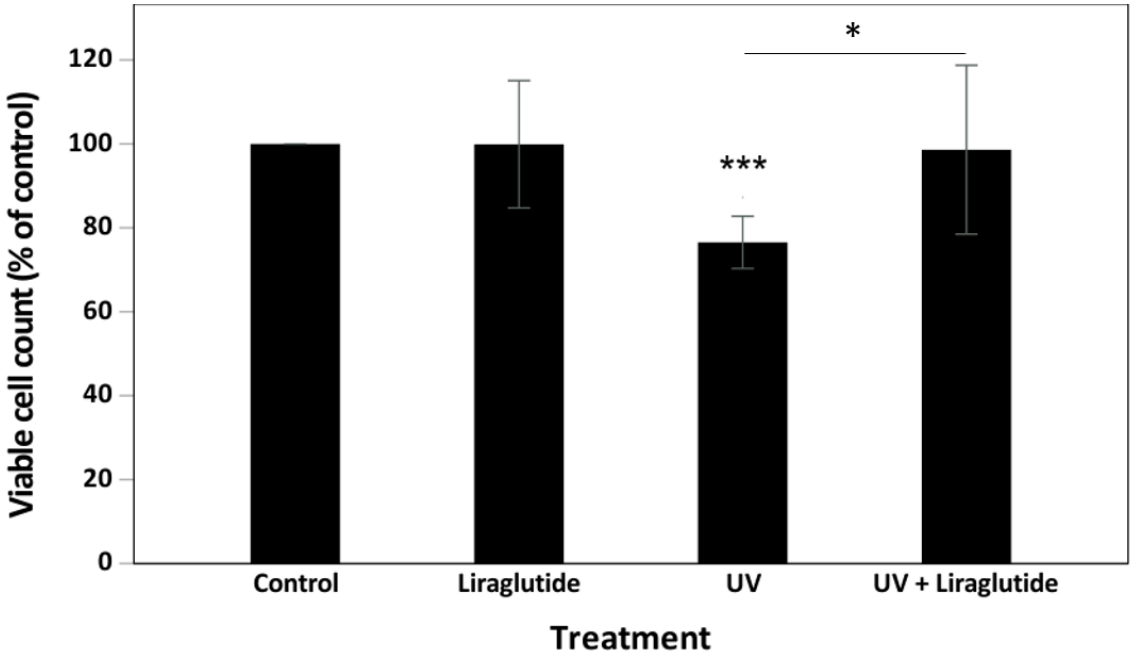

Figure 6.14. Liraglutide protects ARPE-19 cells against UV-A-mediated decreases in cell viability. ARPE-19 cells (80% confluent) were pre-incubated for 6 h in UltraMEM in the absence or presence of 200 nM liraglutide before exchanging the medium for phenol red-free DMEM and irradiating the cells with UV-A for 50 min (see Materials and Methods). The medium was then exchanged for fresh UltraMEM +/- liraglutide and the cells were cultured for a further 18 h before analysing viable cell numbers using the Trypan blue assay. Results are expressed as a percentage of control cell cultures and are means ± S.D. (n=11). *, $p \leq 0.05$; ***, $p \leq 0.001$.

Next, the treated cells were used to prepare lysates, from which the proteins were resolved by SDS-PAGE and immunoblotted using the anti-APP C-terminal antibody. The results (Fig. 6.15) showed the previously observed (Chapter 3, Fig. 3.3) decrease in full-length APP and APP-CTF levels

following UV-A irradiation (decreased by 51.8 ± 25.2 and 56.7 ± 9.9 %, respectively relative to controls). Furthermore, liraglutide did not impact on these UV-A mediated changes in FL-APP and APP-CTF levels.

Conditioned medium samples from the liraglutide experiments were concentrated and equal volumes were then immunoblotted with the anti-6E10 antibody in order to detect sAPPα. The results (Fig. 6.16A and B) showed an apparent decrease in sAPPα levels following UV-A treatment but this was, again, deemed insignificant when the results were corrected in order to account for the decreased cell numbers present following irradiation (Fig. 6.16C). In UV-A-irradiated cells, there was no difference in sAPPα production between those cells incubated in the presence or absence of liraglutide.

The same conditioned medium samples were also immunoblotted using the anti-sAPPβ antibody and the results (Fig. 6.17) demonstrated that sAPPβ production declined significantly in UV-A treated samples (57.0 ± 7.4 %) and in the co-treatment with liraglutide (56.5 ± 5.2%) and this decline persisted in both treatments after correction for viability results as observed previously (Chapter 3, Fig. 3.5). Liraglutide treatment alone did not affect the levels of this APP fragment.

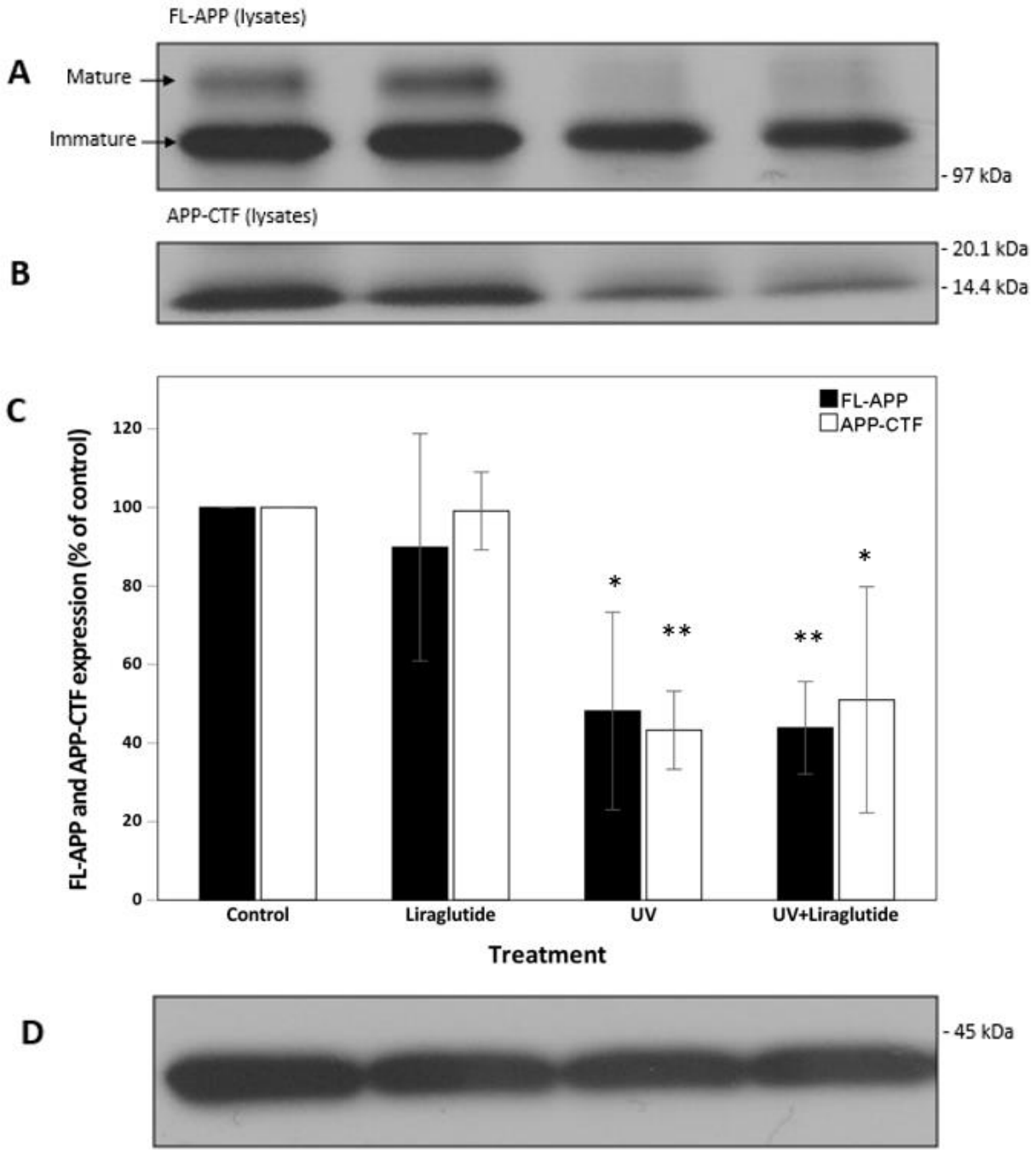

Figure 6.15. APP expression following UV-A and liraglutide treatment of ARPE-19 cells. ARPE-19 cells (80% confluent) were pre-incubated for 6 h in UltraMEM in the absence or presence of 200 nM liraglutide before exchanging the medium for phenol red-free DMEM and irradiating the cells with UV-A for 50 min (see Materials and Methods). The medium was then exchanged for fresh UltraMEM +/- liraglutide and the cells were cultured for a further 18 h. Cell lysates were then prepared and proteins were resolved by SDS-PAGE and immunoblotted as described in the Materials and Methods section. **(A)** Detection of mature and immature forms of FL-APP using the anti-APP C-terminal antibody. **(B)** Detection of APP-CTF using the anti-APP C-terminal antibody. **(C)** Quantification of multiple APP immunoblots by densitometric analysis. **(D)** Detection of actin using the anti-actin antibody. Results are expressed as a percentage of control cell cultures and are means ± S.D. (n=4). *, $p \leq 0.05$; **, $p \leq 0.01$.

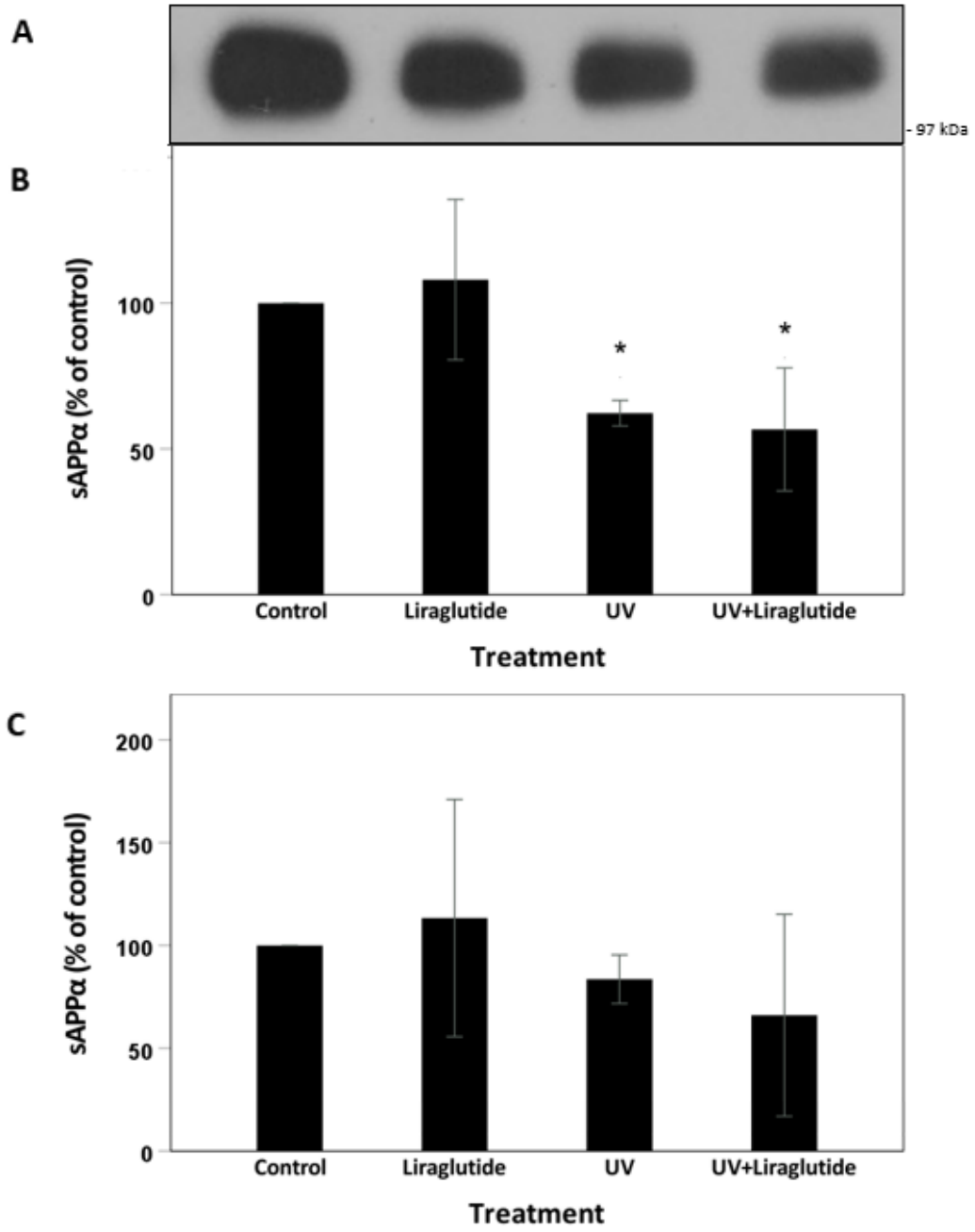

Figure 6.16. sAPPα production following UV-A and liraglutide treatment of ARPE-19 cells. ARPE-19 cells (80% confluent) were pre-incubated for 6 h in UltraMEM in the absence or presence of 200 nM liraglutide before exchanging the medium for phenol red-free DMEM and irradiating the cells with UV-A for 50 min (see Materials and Methods). The medium was then exchanged for fresh UltraMEM +/- liraglutide and the cells were cultured for a further 18 h. Conditioned medium samples were concentrated as described in the Materials and Methods section and equal volumes were resolved by SDS-PAGE and immunoblotted (Materials and Methods). **(A)** Detection of sAPPα using antibody 6E10. **(B)** Quantification of multiple immunoblots by densitometric analysis showing uncorrected results. **(C)** Quantification of multiple immunoblots by densitometric analysis showing results corrected for observed changes in cell viability. Results are expressed as a percentage of control cell cultures and are means ± S.D. (n=4). *, $p \leq 0.05$.

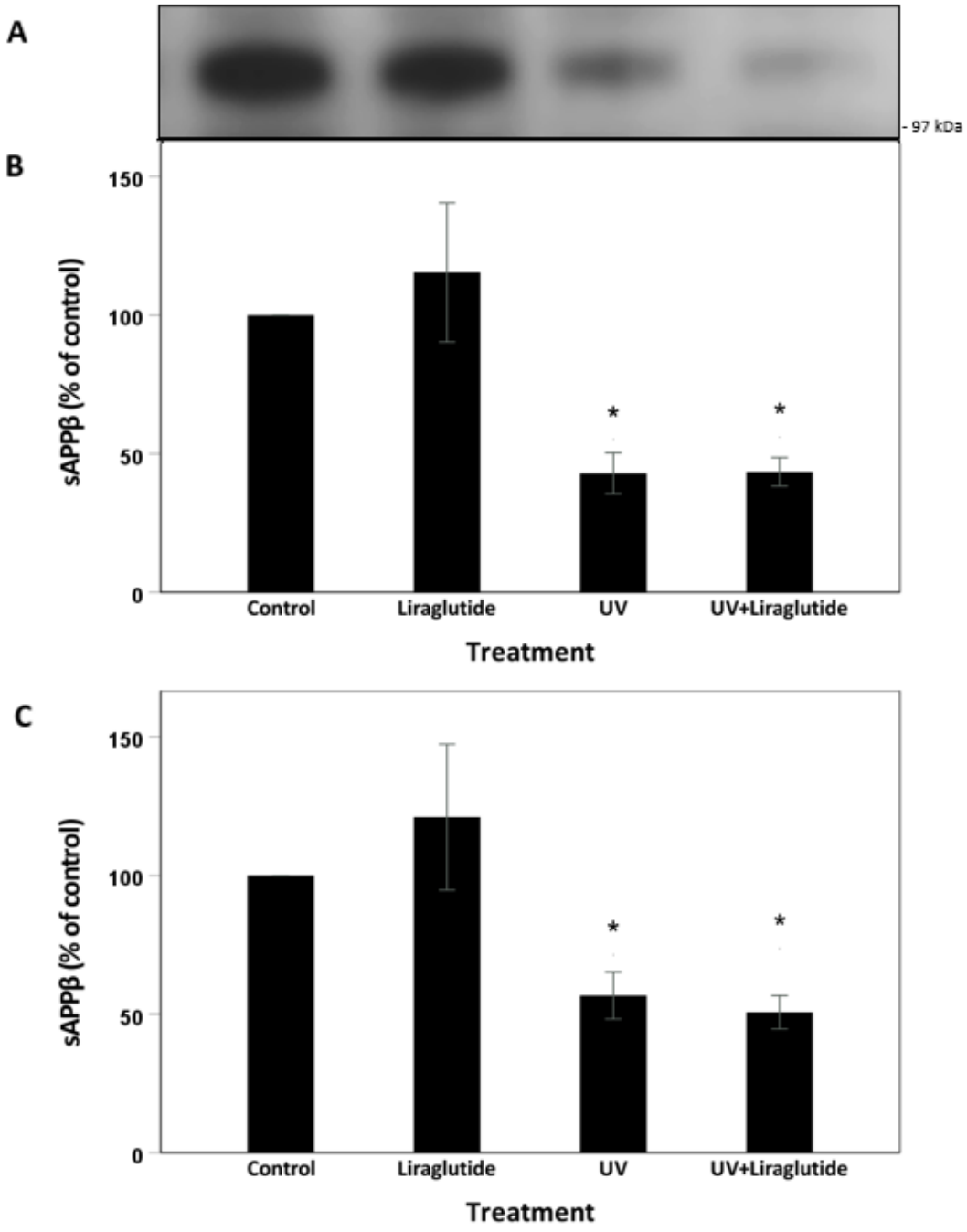

Figure 6.17. sAPPβ production following UV-A and liraglutide treatment of ARPE-19 cells. ARPE-19 cells (80% confluent) were pre-incubated for 6 h in UltraMEM in the absence or presence of 200 nM liraglutide before exchanging the medium for phenol red-free DMEM and irradiating the cells with UV-A for 50 min (see Materials and Methods). The medium was then exchanged for fresh UltraMEM +/- liraglutide and the cells were cultured for a further 18 h. Conditioned medium samples were concentrated as described in the Materials and Methods section and equal volumes were resolved by SDS-PAGE and immunoblotted (Materials and Methods). **(A)** Detection of sAPPβ using the anti-sAPPβ antibody. **(B)** Quantification of multiple immunoblots by densitometric analysis showing uncorrected results. **(C)** Quantification of multiple immunoblots by densitometric analysis showing results corrected for observed changes in cell viability. Results are expressed as a percentage of control cell cultures and are means ± S.D. (n=3). *, $p \leq 0.05$.

6.3.3. Lixisenatide

The preceding experiments were again repeated but this time using lixisenatide (200 nM). In this instance, the Trypan blue results (Fig. 6.18) showed that viable cell count decreased significantly following 50 min of UV-A exposure (21.5 ± 8.5 %). Interestingly, when cells were treated with lixisenatide and UV-A irradiation, the GLP-1 analogue was able to revert the viable cell count to that of controls (104.4 ± 9.2 %). It was also notable that lixisenatide treatment in the absence of UV irradiation lead to slight but significant increase in viable cell counts (by 12.2 ± 10.4 %) relative to controls.

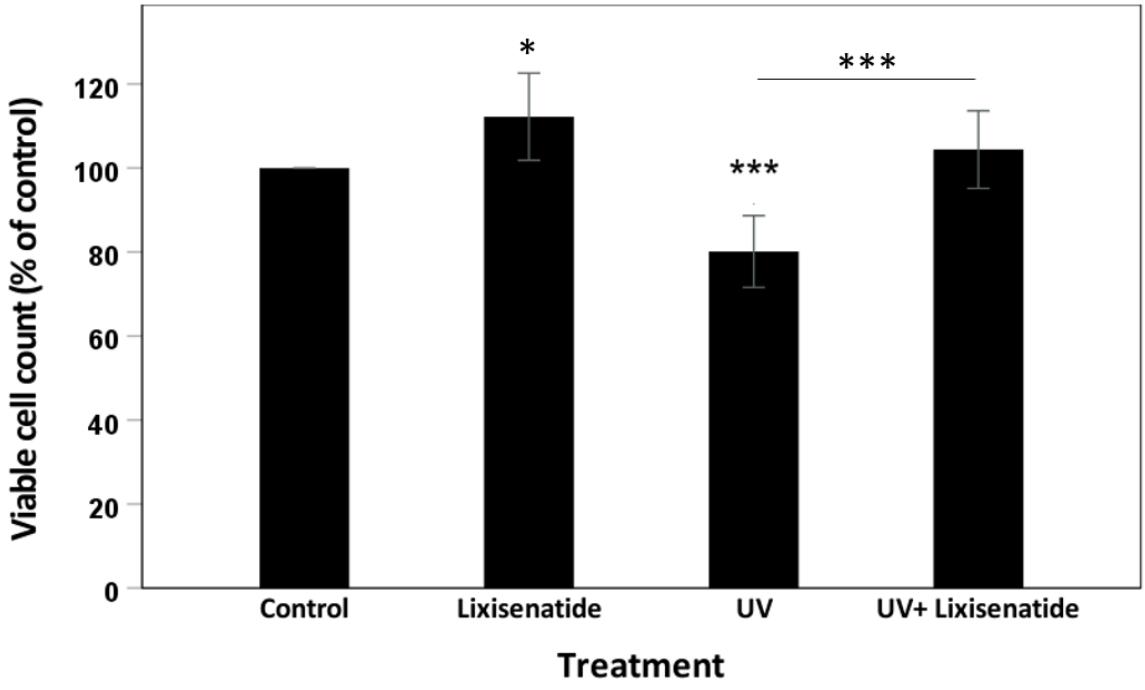

Figure 6.18. Lixisenatide protects ARPE-19 cells against UV-A-mediated decreases in cell viability. ARPE-19 cells (80% confluent) were pre-incubated for 6 h in UltraMEM in the absence or presence of 200 nM lixisenatide before exchanging the medium for phenol red-free DMEM and irradiating the cells with UV-A for 50 min (see Materials and Methods). The medium was then exchanged for fresh UltraMEM +/- lixisenatide and the cells were cultured for a further 18 h before analysing viable cell numbers using the Trypan blue assay. Results are expressed as a percentage of control cell cultures and are means ± S.D. (n=11). *, $p \leq 0.05$; ***, $p \leq 0.001$.

The cells harvested from the preceding experiment were then used to prepare lysates which were resolved by SDS-PAGE and immunoblotted using the anti-APP C-terminal antibody (Materials and Methods). The results (Fig. 6.19) showed that the expression levels of both FL-APP and APP-CTF decreased following UV-A treatment (by 41.5 ± 11.3 and 53.1 ± 21.3 % respectively, relative to the controls) as observed previously (Chapter 3, Fig. 3.3). Lixisenatide did not modify levels of APP/APP-CTF regardless of whether or not the cells were irradiated with UV-A.

When concentrated conditioned medium samples from the same experiment were immunoblotted with the anti-APP 6E10 antibody, previous results were confirmed in that, before correcting for cell numbers, there was an apparent decrease in sAPPα production by cells following UV-A irradiation (38.7 ± 11.2 %) (Fig. 6.20A and B). However, once the results were corrected in order to take into account the number of viable cells, this difference was rendered not significant (Fig. 6.20C). No modification of sAPPα generation following lixisenatide treatment was evident.

Immunoblotting the same medium samples in order to detect sAPPβ again showed a decrease in the production of this fragment following UV-A irradiation; a difference which persisted even after the results were corrected for cell numbers (a decrease of 42.5 ± 16.9 % relative to controls). Notably, lixisenatide treatment did not impact on sAPPβ levels in the presence or absence of UV-A light exposure.

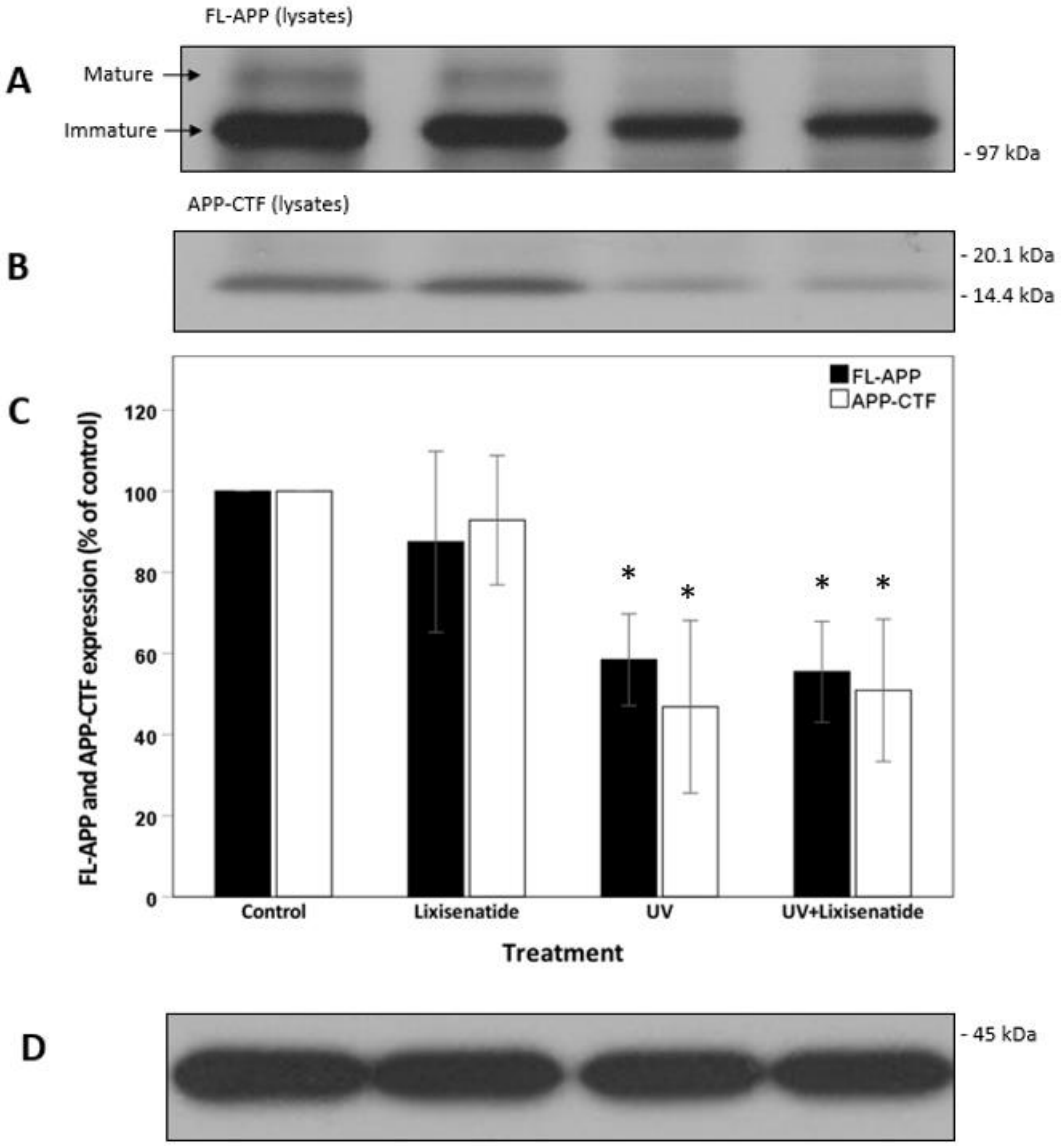

Figure 6.19. APP expression following UV-A and lixisenatide treatment of ARPE-19 cells. ARPE-19 cells (80% confluent) were pre-incubated for 6 h in UltraMEM in the absence or presence of 200 nM lixisenatide before exchanging the medium for phenol red-free DMEM and irradiating the cells with UV-A for 50 min (see Materials and Methods). The medium was then exchanged for fresh UltraMEM +/- lixisenatide and the cells were cultured for a further 18 h. Cell lysates were then prepared and proteins were resolved by SDS-PAGE and immunoblotted as described in the Materials and Methods section. **(A)** Detection of mature and immature forms of FL-APP using the anti-APP C-terminal antibody. **(B)** Detection of APP-CTF using the anti-APP C-terminal antibody. **(C)** Quantification of multiple APP immunoblots by densitometric analysis. **(D)** Detection of actin using the anti-actin antibody. Results are expressed as a percentage of control cell cultures and are means ± S.D. (n=4). *, $p \leq 0.05$.

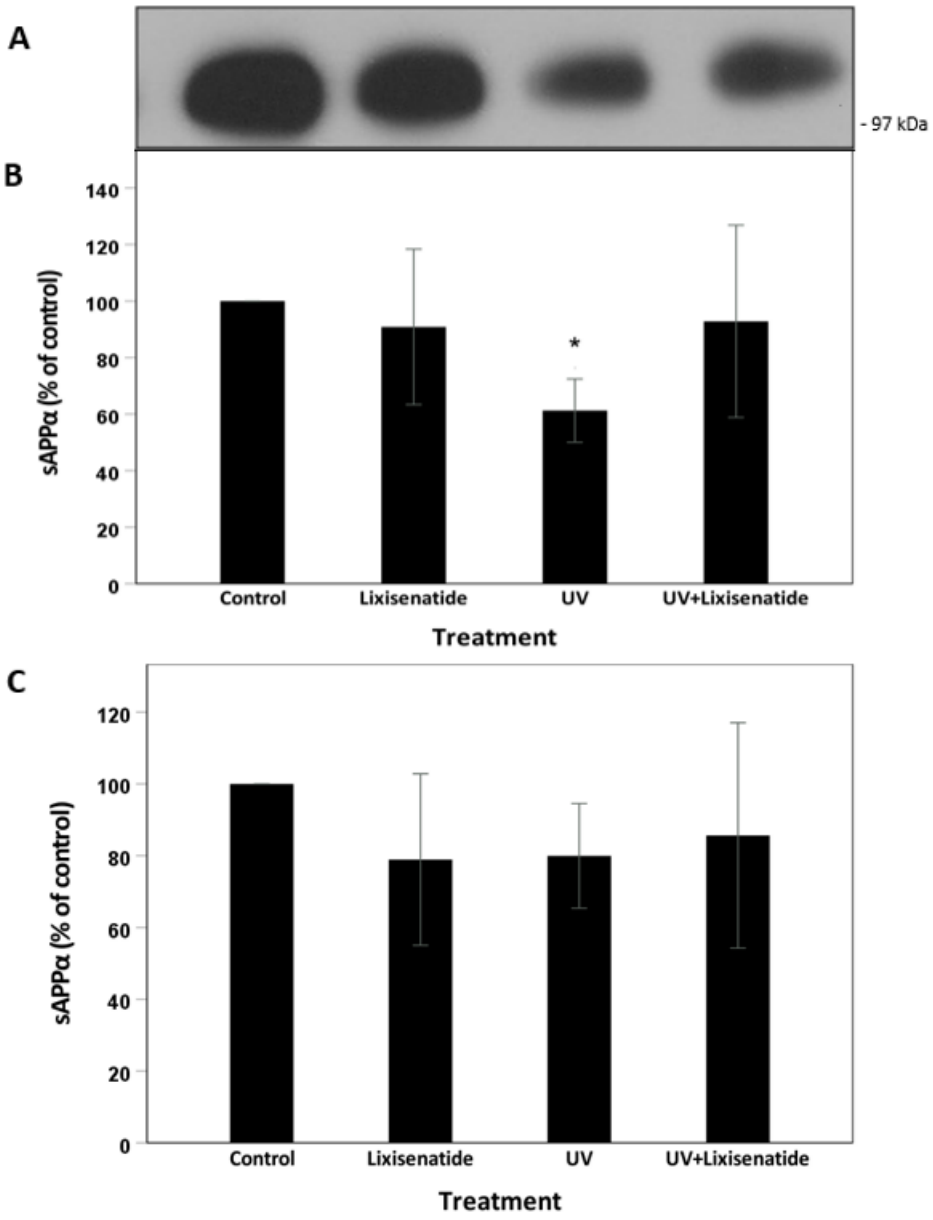

Figure 6.20. sAPPα production following UV-A and lixisenatide treatment of ARPE-19 cells. ARPE-19 cells (80% confluent) were pre-incubated for 6 h in UltraMEM in the absence or presence of 200 nM lixisenatide before exchanging the medium for phenol red-free DMEM and irradiating the cells with UV-A for 50 min (see Materials and Methods). The medium was then exchanged for fresh UltraMEM +/- lixisenatide and the cells were cultured for a further 18 h. Conditioned medium samples were concentrated as described in the Materials and Methods section and equal volumes were resolved by SDS-PAGE and immunoblotted (Materials and Methods). **(A)** Detection of sAPPα using antibody 6E10. **(B)** Quantification of multiple immunoblots by densitometric analysis showing uncorrected results. **(C)** Quantification of multiple immunoblots by densitometric analysis showing results corrected for observed changes in cell viability. Results are expressed as a percentage of control cell cultures and are means ± S.D. (n=4). *, $p \leq 0.05$.

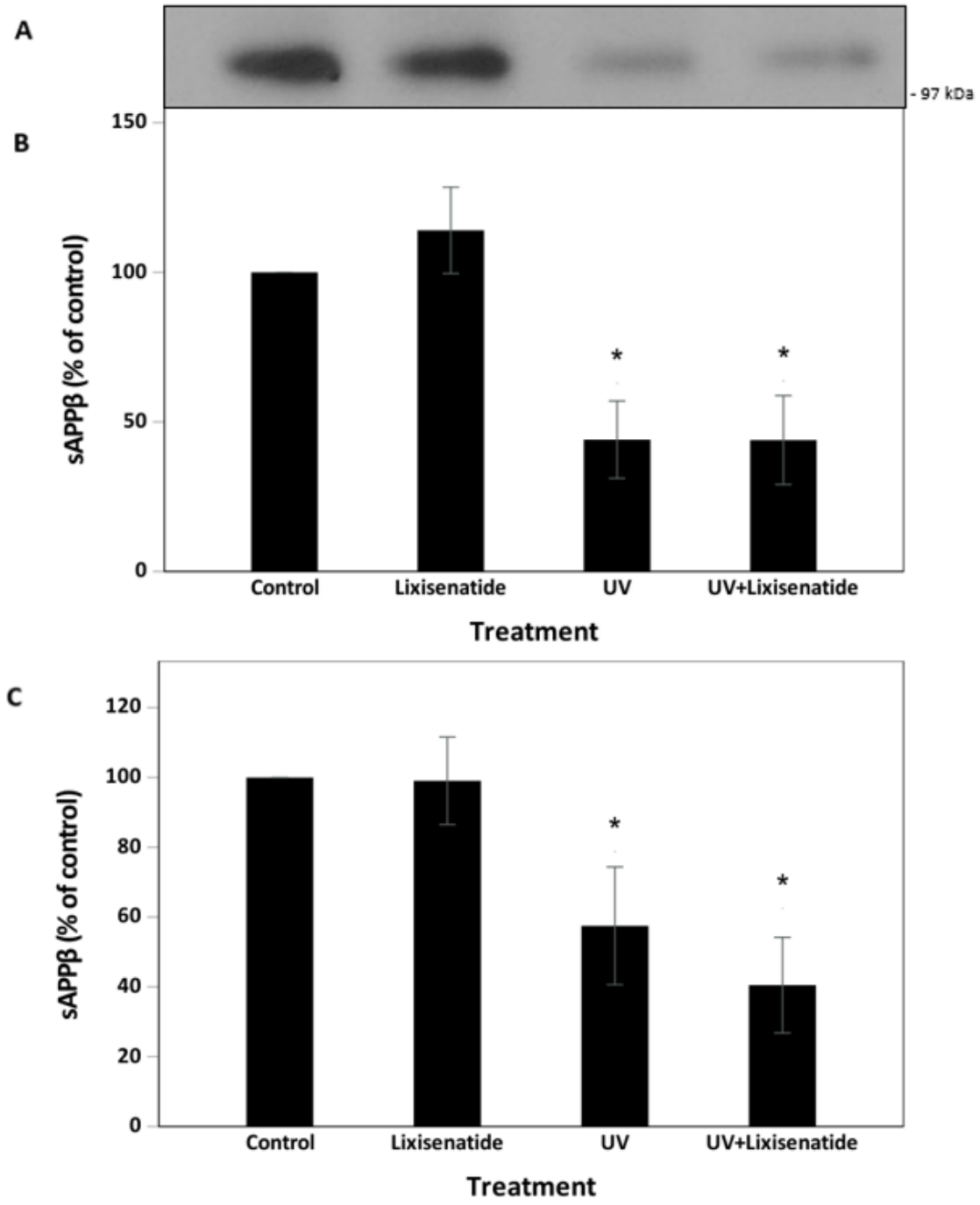

Figure 6.21. sAPPβ production following UV-A and lixisenatide treatment of ARPE-19 cells. ARPE-19 cells (80% confluent) were pre-incubated for 6 h in UltraMEM in the absence or presence of 200 nM lixisenatide before exchanging the medium for phenol red-free DMEM and irradiating the cells with UV-A for 50 min (see Materials and Methods). The medium was then exchanged for fresh UltraMEM +/- lixisenatide and the cells were cultured for a further 18 h. Conditioned medium samples were concentrated as described in the Materials and Methods section and equal volumes were resolved by SDS-PAGE and immunoblotted (Materials and Methods). **(A)** Detection of sAPPβ using the anti-sAPPβ antibody. **(B)** Quantification of multiple immunoblots by densitometric analysis showing uncorrected results. **(C)** Quantification of multiple immunoblots by densitometric analysis showing results corrected for observed changes in cell viability. Results are expressed as a percentage of control cell cultures and are means ± S.D. (n=4). *, $p \leq 0.05$.

6.4. Summary

In the current chapter, the effects of chemical stress and UV-A irradiation on ARPE-19 cells were examined alongside the ability of the GLP-1 analogues, exendin-4, liraglutide and lixisenatide, to protect cells against these toxic insults.

ARPE-19 cells were largely resistant to hydrogen peroxide up to 425 μM with only minor decreases in cell viability observed below this concentration. However, none of the three GLP-1 analogues tested were able to protect cells against 425 or 500 μM concentrations of this chemical stressor.

As far as Aβ-peptides were concerned, ARPE-19 cells proved remarkable resistance to these toxic entities and only a minor decrease in cell viability was observed even at a 50 μM concentration of these peptides. Unfortunately, one ramification for this result was that it was not economically viable to investigate whether the GLP-1 analogues were able to protect against Aβ-peptide-mediated toxicity.

In terms of UV-A irradiation of cells, liraglutide and lixisenatide but not exendin-4 were able to protect cells against the reduction in viable cell numbers associated with this treatment. The previously observed decreases in cell-associated levels of FL-APP and APP-CTFs associated with UV-A irradiation were again observed in this chapter as too was the lack of change in sAPPα generation but the UV-A-associated decrease in sAPPβ production by cells. However, it was clear that the ability of liraglutide and lixisenatide to prevent UV-A-associated decreases in cell viability was not mechanistically linked to APP metabolism as these compounds (and exendin-4) did not further modify FL-APP, APP-CTF, sAPPα or sAPPβ levels regardless of whether or not the cells were irradiated with UV-A.

Chapter 7

Discussion

7. Discussion

7.1. Introduction

Amyloid β has been found to be a major component of drusen deposits in AMD playing key roles in disease pathology including drusen formation, inflammation and oxidative stress leading to retinal degeneration (Ratnayaka *et al.*, 2015; Ohno-Matsui, 2011; Johnson *et al.*, 2002). This project aimed to investigate the role of APP and its proteolytic fragments from the amyloidogenic and non-amyloidogenic pathways in AMD using ARPE-19 as a cellular model of the disease and UV-A light as the stressor. Additionally, given the neuroprotective properties of GLP-1 analogues and its enhancement of the non-amyloidogenic pathway (Ohtake *et al.*, 2014; Perry *et al.*, 2003; McClean *et al.*, 2011), this study examined the possible use of GLP-1 analogues as drugs for the prevention or treatment of AMD.

7.2. Characterising the effects of UV-A on cell viability, p53 levels, and APP expression and processing in ARPE-19 cells

Initially, the effect of UV-A light exposure on ARPE-19 cell viability was assessed and a moderately toxic dose was used (consisting of 50 min irradiation of 80% confluent cells 8 cm away from the light source) which resulted in an approximately 30% decrease in viable cell counts (Fig. 3.1). The effects of this UV-A dose on p53 levels and APP expression/processing were characterised. UV-A light exposure resulted in a trend towards an increase in p53 levels (Fig. 3.2). However, due to variability between samples this increase was deemed insignificant. Although previous studies have consistently reported the role of p53 in the induction of apoptosis following UV-A exposure (Zhang, 2006; Santamaria *et al.*, 2002), a study by McFeat *et al.* (2013) demonstrated that, in contrast to UV-C, UV-A irradiation failed to induce p53 accumulation in mouse embryonic fibroblasts indicating that the induction of certain elements in the p53 pathway is wavelength specific.

In terms of APP, the results showed a significant decrease in FL-APP expression following UV-A irradiation (Fig. 3.3) which is in line with the previous findings of Almenar-Queralt *et al.* (2014) showing a decline in FL-APP protein levels following UV exposure in SH-SY5Y cells and various other

cell lines. The current results also demonstrated a greater decline of the mature (upper) protein band of FL-APP (Fig. 3.3A) possibly corresponding to increased shedding of the mature (post-translationally modified) protein by secretases at the cell surface. However, quantification of the secreted APP proteolytic fragments showed a significant decrease in both sAPPα and sAPPβ following UV-A irradiation. Interestingly, levels of sAPPα but not sAPPβ were normalised after correcting results to account for observed changes in cell viability. Although levels of sAPPα and sAPPβ following UV irradiation were not quantified in the literature to allow for direct comparison, levels of APP-CTFs were measured in Almenar-Queralt *et al.* (2014) and showed a significant decrease reportedly as the consequence of increased γ- secretase activity towards these fragments. The authors did also conclude that the activity of α-, β- and γ- secretases was enhanced by UV irradiation increasing the processing of full-length APP. By inference, this would mean that levels of the soluble fragments produced through α- and β- secretases would also increase which was not the case in the current study. That said, the near control levels of sAPPα observed after viability correction in the UV treated samples (Fig. 3.4C) may suggest an increased α-secretase activity as levels of the substrate (APP) expression were lower in UV treated cells compared to those of the control. Notably, results in the following chapters (Fig. 4.4 and Fig. 5.27) showed similar patterns to those observed in Almenar-Queralt *et al.* (2014) in terms of decreased levels of APP-CTFs following UV irradiation.

7.3. The effects of depleting full-length APP on ARPE-19 cell viability and resistance to UV-light

The data outlined in the previous section raised the possibility that APP might be linked to a cellular response to UV light in ARPE-19 cells. To examine this hypothesis, APP siRNA was utilised to deplete endogenous APP and subsequently monitor any changes in cell viability in the absence or presence of UV-A irradiation. The results showed that treatment of cells with APP siRNA (37.5 nM) did not affect cell viability (Fig. 4.3). Interestingly, however, treatment of cells with APP siRNA resulted in an increased cell resistance to UV-A irradiation. Viable cell counts increased significantly in APP siRNA and UV co-treated cells by approximately 20% compared to UV-A treated cells in the absence of APP

siRNA treatment (Fig. 4.3). This result might indicate that APP or some of its proteolytic fragments may be mediating the detrimental effects of UV-irradiation on cell viability.

7.4. The effects of exogenous sAPPα and sAPPβ on ARPE-19 cell proliferation

In the current study, ARPE-19 cells were co-cultured with HEK cell stable transfectants over-expressing FL-APP_{695}, $sAPP_{695}\alpha$ or $sAPP_{695}\beta$ in a transwell system. As expected, the results showed that cells incubated with the neuroprotective/trophic fragment sAPPα exogenously secreted from $sAPP_{695}\alpha$ HEK transfectants exhibited approximately 56 % higher numbers after a 7-day treatment compared to cells grown with HEK mock transfectants. On the other hand, no increase in viable cell counts was detected in cells cultured with HEK cells over-expressing FL-APP_{695} or $sAPP_{695}\beta$. Although FL-APP_{695} HEK transfectants also produce high concentrations of $sAPP_{695}\alpha$ compared to mock transfectants (Fig. 4.7C and D), $sAPP_{695}\alpha$ HEK transfectants produce approximately 2-fold higher concentrations of this fragment compared to FL-APP_{695} HEK transfectants (Fig. 4.7A and B) which might explain the lack of the proliferative effect of HEK cells over-expressing FL-APP_{695} in the co-culture experiment. Numerous studies have demonstrated the neuroprotective and neurotrophic roles of sAPPα not shared by the sAPPβ fragment (reviewed in Habib *et al.,* 2017). A study by Tackenberg and Nitsch (2019) showed that sAPPα and not sAPPβ was neuroprotective against Aβ-induced toxicity in mouse neuronal primary cultures and hippocampal slices. This neuroprotective role was related to the 16 additional amino acids at the C-terminus of sAPPα which are not present in sAPPβ (Barger and Harmon, 1997; Furukawa *et al.*, 1996b). Moreover, in the case of epithelial cells, (Pietrzik *et al.*, 1998) demonstrated that sAPPα acts as a local mediator of growth and proliferation in rat thyroid epithelial cells.

7.5. The effects of manipulating full-length APP and its proteolytic fragments on p53 expression in ARPE-19 cells

APP levels were manipulated by siRNA depletion of endogenous FL-APP in ARPE-19 cells and by over-expressing FL-APP_{695} or its fragments $sAPP_{695}\alpha$ and $sAPP_{695}\beta$ in HEK cells. p53 levels were

monitored in both cases and no significant changes were observed (Fig. 4.5 and Fig. 4.9). These results were unexpected given the previous findings in several studies showing a strong relationship between APP and p53 levels (Cuesta *et al.*, 2009b; Buizza *et al.*, 2013; Ozaki *et al.*, 2006; Li *et al.*, 2015). Cuesta *et al.* (2009) demonstrated that p53 inhibited APP gene expression and that UV-C exposure leads to a decline in APP levels through a p53-dependant mechanism in murine neuroblastoma cells (N2a-β). On the other hand, Ozaki *et al.* (2006) showed that over expression of APP in the human bone osteosarcoma epithelial cell line, U2OS, enhanced apoptosis through a p53 dependant pathway and this was related to AICD interaction with p53. The contradictions between these studies and the current study although not fully explainable, could be related to the differences in cell types employed.

7.6. The effects of α-secretase inhibitors on ARPE-19 cell proliferation and resistance to UV-A exposure

In the current study, the α-secretase inhibitors GI254023X and batimastat were applied to ARPE-19 cells. GI254023X was tested first because of its increased specificity towards ADAM10 (IC_{50} = 5.3 nM) relative to ADAM17 (IC_{50} = 541 nM). However, concentrations around the published IC_{50} (Ludwig *et al.*, 2005) failed to significantly reduce the production of sAPPα by ARPE-19 cells and only had a mild effect in SH-SY5Y cells. Similar results (lack of significant α-secretase inhibition) were achieved with batimastat at similarly low concentrations. This was explained by the fact that the published IC_{50} value was determined using recombinant enzyme and, therefore, did not consider any cell-associated factors such as permeability or interaction with other proteins. As such, a concentration of 5μM batimastat was tested on ARPE-19 cells which achieved the desired effect of significantly reducing sAPPα production (by approx. 70 %) (Fig. 5.8) with no significant effects on sAPPβ production (Fig. 5.9). This was accompanied by the accumulation of FL-APP, specifically the upper (mature) protein band, and a dramatic decrease in APP-CTF levels (by approx. 90 %) (Fig. 5.7) indicating the effective inhibition of α-secretase shedding which is responsible for the majority of APP processing in this cell line. The effective batimastat dose shown in the current study is in line with the

findings of Parkin *et al.* (2002) demonstrating that the batimastat IC_{50} for α-secretase is 1.2 μM in cell-based experiments.

The same effective concentration of batimastat (5μM) was tested for its effects on cell viability and growth in the absence or presence of UV-A irradiation. The results showed that the compound did indeed impair cell proliferation over a 7-day treatment of cells starting at the point of seeding (Fig. 5.11) with no significant effects on cell viability in a 24 h treatment of confluent cells (Fig. 5.10). It was, therefore, concluded that batimastat had cytostatic but not cytotoxic effects on ARPE-19 cells. The cytostatic effect of batimastat could be due to the lack of sAPPα which is consistent with the results of the co-culture experiment (Fig 4.7) emphasising the essential role of sAPPα in driving cell growth and proliferation and in line with the previously acknowledged trophic and proliferative roles of sAPPα (Demars *et al.*, 2011; Tsang *et al.*, 2018; Habib *et al.*, 2017). However, it should be mentioned that, due to lack of specificity, batimastat could be also inhibiting metalloproteinases other than ADAM10 at this high concentration (5μM) and, therefore, the cleavage of proteins essential for cell survival other than APP could be implicated including Notch which is cleaved by both ADAM10 and ADAM17 (Christian, 2012; Zolkiewska, 2008).

Finally, inhibition of sAPPα production using batimastat did not alter the resistance of cells to UV-A treatment. This indicated that the sAPPα fragment itself may not have a role to play in protecting cells against UV-induced damage in ARPE-19 cells. The question of whether sAPPα might harbour any protective effects against UV irradiation in ARPE-19 cells might be further clarified in future by adding conditioned medium from HEK cells over-expressing $sAPP_{695}α$ to UV-A irradiated ARPE-19 cells and monitoring any effects on cell viability but this was beyond the scope of the current study. In fact, a previous study by Copanaki *et al.* (2010) demonstrated that sAPPα was able to attenuate caspase-3 like activity, an apoptosis marker, following UV light exposure in PC12 cells indicating a protective effect of this fragment against UV-induced apoptosis although changes in cell viability were not directly quantified.

7.7. The effects of β-secretase inhibitor on ARPE-19 cell proliferation and resistance to UV-A exposure

BACE-1 is the first and rate-limiting enzyme in the production of the toxic Aβ fragment. β-secretase inhibitor IV, a selective BACE-1 inhibitor, was utilised in the current study to monitor the effects of inhibiting β-cleavage on the resistance of cells to UV-A light. Results demonstrated successful inhibition of sAPPβ production when the inhibitor was applied in the concentration range 0-100 nM (Fig. 5.16) which is in agreement with the published IC_{50} value relative to BACE-1 (15 nM) (Stachel *et al.*, 2004). No significant effects on sAPPα production were observed (Fig. 5.15) as expected given the specificity of the inhibitor to BACE-1. However, unexpectedly, the compound resulted in a dose-dependent accumulation of APP-CTFs with no significant effects on FL-APP levels (Fig. 5.14). Given the fact that sAPPα levels were not significantly altered, this increase in APP-CTFs could not be explained by a shift towards non-amyloidogenic processing of APP and, as yet, remains unresolved.

With regards to ARPE-19 cell viability and proliferation, β-secretase inhibitor IV had minimal effects following either a 24 h treatment of confluent cells or a 7-day treatment from the point of seeding (Fig. 5.17 and Fig. 5.18). The fact that the compound started demonstrating minor toxic effects at the highest concentration could be related to the inhibition of cleavage of any of the various substrates of BACE-1 as it is involved in the shedding of various type 1 transmembrane proteins (Hemming *et al.*, 2009).

Finally, β-secretase inhibitor IV did not modify the response of ARPE-19 cells to UV-A light which might indicate that the metabolites resulting from this pathway including sAPPβ and Aβ peptide are not linked to UV toxicity or protection. These results are in line with the findings of the co-culture experiment in which sAPPβ had no growth promoting properties and therefore no effect was expected when knocking the production of this fragment down.

7.8. The effects of γ-secretase inhibitor on ARPE-19 cell proliferation and resistance to UV-A exposure

γ-secretase cleavage is an essential step in APP processing following α- or β- cleavage. The resulting products of γ-secretase cleavage are Aβ or a shorter (p3) fragment for the amyloidogenic or non-amyloidogenic pathway, respectively, plus a common AICD for both pathways. Begacestat, a γ-secretase inhibitor demonstrating a 14- to 16-fold selectivity towards the inhibition of APP-CTFs cleavage relative to Notch-CTFs (Mayer *et al.*, 2008; Martone *et al.*, 2009) was utilised in the current study to inhibit γ-secretase cleavage of APP-CTFs. As expected, begacestat led to a dose dependant accumulation of APP-CTFs in the concentration range 0-100 nM (Fig. 5.21) which is in line with the published IC_{50} value for begacestat relative to APP-CTFs (between 12.4 and 14.8 nM) (Mayer *et al.*, 2008). No significant effects of begacestat on FL-APP levels were shown and only minor effects were observed relative to sAPPα or sAPPβ levels (Fig. 5.21, Fig. 5.22 and Fig. 5.23).

The effects on ARPE-19 cell viability were minimal when confluent cells were treated for 24 h with begacestat (Fig. 5.24), while more significant and dose-dependent decreases in viability occurred after a 7-day treatment of cells at the point of seeding (Fig. 5.25). This indicated that γ-secretase inhibition impaired cell growth (cytostatic) rather than causing toxicity. This effect could be related to the inhibition of APP-CTF processing but could also be an effect on Notch CTFs which might be inhibited at the high concentrations of begacestat employed. Notch receptors are widely expressed in a variety of tissues and they have roles in cell-cell signalling, cell fate and differentiation both during development and in the adult organism (Mao and Ito, 2017; Boyton and Altmann, 2006). Notably, Notch and APP are both cleaved in a similar manner by α- and γ-secretase activities (Lazarov and Demars, 2012). Notch cleavage also yields a soluble ectodomain and an intracellular domain (NICD) which, like the APP (AICD), regulates gene transcription (O'Brien and Wong, 2011). However, by taking into account the IC50 values of begacestat relative to APP-CTFs mentioned by Mayer *et al.* (2008) (between 12.4 and 14.8 nM) and the fact that begacestat is 14- to 16-fold more selective towards the inhibition of APP-CTF cleavage relative to Notch-CTFs, the lowest possible IC50 towards Notch would

be 173.6 nM which is still higher than the 100 nM used in our experiment. Therefore, the negative effects shown with begacestat on cell growth and proliferation are likely related to the inhibition of APP-CTFs processing rather than Notch-CTFs although an effect on other transmembrane protein fragments cleaved by γ-secretase cannot be completely excluded.

Interestingly, the inhibition of γ-secretase using begacestat (100 nM) did indeed modify the response of ARPE-19 cells to UV-A light. The number of viable cells was significantly higher in cells co-treated with UV-A and begacestat compared to cells treated with UV-A in the absence of the inhibitor (Fig. 5.26). Begacestat had no effect on viability in the absence of UV treatment in this experiment which is consistent with the results of the 24 h treatment of confluent cells (Fig. 5.24). The effect of begacestat increasing cell resistance to UV-A is likely related to the absence of gamma secretase cleavage products mainly those resulting from APP-CTFs cleavage including Aβ, p3 and the AICD given the specificity of begacestat to the inhibition of APP-CTFs cleavage over Notch. Furthermore, the lack of effect displayed when cells were treated with α- or β- secretase inhibitors in the presence of UV-A suggests that neither Aβ nor p3 are linked to the effects of UV-A on cell viability. However, a study by Kume *et al.* (2003) has shown that APP can be cleaved by γ-secretase independently without prior cleavage of α- or β- secretase. Moreover, it was observed in non-canonical cleavage of APP that γ-secretase can cleave APP directly after Meprin-β cleavage and without prior cleavage by α- or β-secretase (Andrew *et al.*, 2016; García-González *et al.*, 2019). Meprin-β cleaves APP at several sites including a position close to β-secretase cleavage site, thus producing sAPPβ with one or two additional amino acids and its complementary C-terminal fragment (β-CTF) with one or two less amino acids (Scharfenberg *et al.*, 2019; Andrew *et al.*, 2016). The β-CTF generated by Meprin-β cleavage can be then cleaved by γ-secretase to produce an N-terminally shorter Aβ species and the normal AICD (Bien *et al.*, 2012). This means that AICD production may not be completely blocked by the inhibition of α- or β- secretase which suggests that the AICD may be the fragment responsible for UV decreases in cell viability. Indeed, several studies have linked the AICD to the regulation of apoptosis and gene

expression (Müller *et al.*, 2008; Lu *et al.*, 2000; Giliberto *et al.*, 2008). A study by Kinoshita *et al.* (2002) demonstrated that the AICD can translocate to the nucleus and induce apoptosis in H4 neuroglioma cells by interaction with a histone acetyltransferase called Tip60. Another study by Giliberto *et al.* (2008) demonstrated a role for AICD in increasing neuronal sensitivity to toxic and apoptotic stimuli. Moreover, Ozaki *et al.* (2006) proved that the AICD enhances p53-mediated apoptosis by enhancing its transcriptional and pro-apoptotic activities.

Finally, the results of the APP siRNA and UV experiment (Chapter 4, Fig 4.3) showed a significant effect in protecting cells against UV-A light when the full-length protein (FL-APP) was knocked down using APP siRNA. It follows that depletion of FL-APP would also decrease levels of AICD thereby fitting the above hypothesis that it is this latter fragment that is responsible for mediating UV-A associated decreases in ARPE-19 cell viability.

7.9. GLP-1 analogues and the lack of protective effects against hydrogen peroxide

Previous studies have demonstrated protective effects of GLP-1 and its analogues in decreasing oxidative stress associated with the development of several chronic diseases such as diabetes, cancer and neurodegenerative diseases (Oh and Jun, 2017; Petersen *et al.*, 2016; Cai *et al.*, 2018). Given the link between diabetes and AMD (Chen *et al.*, 2014; Hahn *et al.*, 2013) and the similarity between AMD and AD in terms of the pathophysiology (Masuzzo *et al.*, 2016; Ratnayaka *et al.*, 2015), it was postulated that the diabetes drug GLP-1 analogues might prove effective in protecting retinal ARPE-19 cells through a similar mechanism to that observed in AD cell culture models (Li *et al.*, 2010; Jalewa *et al.*, 2016). Three GLP-1 analogues, exendin-4, liraglutide and lixisenatide, were employed in the current study to examine their effects on ARPE-19 cell viability and APP processing and whether they could protect cells against various stresses associated with AMD including oxidative stress and UV-A exposure.

Hydrogen peroxide was toxic to ARPE-19 cells in the current study at concentrations of 350 μM and above when the H_2O_2 was added in reduced serum medium (UltraMEM) (Fig. 6.2). However, the same concentrations did not induce any toxicity when the H_2O_2 was added to cells in complete growth medium (DMEM:F12) (Fig. 6.1). This might be explained by the presence of certain components in the complete growth medium that might have contributed to the degradation of H_2O_2. Indeed, several studies have emphasised the effect of components of the cell culture medium specifically the serum in affecting the response of cells to various treatments (Nass *et al.*, 2014; Halliwell, 2014; Arigony *et al.*, 2013). Mun *et al*. (2017) found that fetal bovine serum (FBS) added to cell culture medium significantly reduced ROS levels in *in vitro*-produced (IVP) porcine embryos. Moreover, treatment with FBS increased the levels of antioxidant transcript in these porcine embryonic cells (Mun *et al.*, 2017). Additionally, Tangtrongsup and Kisiday (2018) demonstrated antioxidant properties of FBS leading to reduced ROS production in mesenchymal stem cells.

None of the three GLP-1 analogues used in the current study showed any protective effects in relation to H_2O_2 toxicity. In contrast, a number of previous *in vitro* studies have shown a protective effect of GLP-1 analogues against oxidative stress and apoptosis induced by various stress factors in a variety of cell types (Wang *et al.*, 2013; Tomas *et al.*, 2011; Kimura *et al.*, 2009). Chang *et al.* (2013) demonstrated that pre-treatment with the GLP-1 analogue, exenatide, at concentrations of 0.1, 1 and 10 nM was able to protect rat cardiomyoblast H9c2 cells from H_2O_2-induced oxidative stress. Notably the H9c2 cells used in the study seemed more susceptible to H_2O_2 treatment (significant decreases in cell viability were observed following a 200 μM treatment for 6 h) than the ARPE-19 cells used in the current study where 350 μM H_2O_2 for 24 h was required for appreciable toxicity. It may well be possible that ARPE-19 cells have already very efficient inherent mechanisms imparting resistance to H_2O_2 toxicity that might not be activated significantly further through the addition of GLP-1 analogues.

7.10. GLP-1 analogues and their protective effects against UV-A light exposure

Interestingly the current study was able to demonstrate that liraglutide and lixisenatide but not exendin-4 were able to protect ARPE-19 cells from the toxic effects of UV-A irradiation (Fig 6.10, Fig. 6.14 and Fig 6.18); a stress factor known to be associated with AMD (Vojniković *et al.*, 2007; Chalam *et al.*, 2011). However, looking at the concentrations of FL-APP in the absence or presence of each of the GLP-1 analogues (Fig. 6.11, Fig. 6.15 and Fig. 6.19), it was evident that none of these drugs had significant effects on APP expression in ARPE-19 cells in the current study regardless of whether cells were irradiated with UV-A. Also, by analysing the level of the soluble fragment of the non-amyloidogenic pathway (sAPPα) (Fig. 6.12, Fig. 6.16 and Fig. 6.20) and the amyloidogenic pathway (sAPPβ) (Fig. 6.13, Fig. 6.17 and Fig. 6.21) as well as the APP-CTF (Fig. 6.11, Fig. 6.15 and Fig. 6.19) in the absence or presence of the GLP-1 analogues, results showed that these drugs did not significantly affect APP processing either. Therefore, it was concluded that neither liraglutide nor lixisenatide exerted their protective effects against UV-A light through the modification of APP expression or proteolysis.

In contrast, several previous studies have shown a connection between the protective effects of GLP-1 analogues and their effects on APP and its metabolites (Perry *et al.*, 2003; Ohtake *et al.*, 2014; Jantrapirom *et al.*, 2020). A study by Perry *et al.* (2003) demonstrated that GLP-1 can mitigate Aβ production in the brain *in vivo* and reduce the levels of APP in cultured neurons. Moreover, GLP-1 and its analogue, exendin-4, were able to protect cultured neurons from Aβ-induced toxicity (Perry *et al.*, 2003). Another study by Ohtake *et al.* (2014) demonstrated that subcutaneous injections of mice with exendin-4 (0.2 mg/kg five times) shifted APP processing towards the non-amyloidogenic pathway by increasing expression of ADAM10 in the mouse neocortex. Moreover, Jantrapirom *et al.* (2020) found that incubation of human neuroblastoma SH-SY5Y cells with 500 nM of liraglutide for 24 h can reduce the activity of BACE-1, thus decreasing the amyloidogenic processing of APP and reducing Aβ formation in insulin-resistant cells.

Notably, the above-mentioned studies were performed in neuronal cells which might react differently to GLP-1 and its analogues compared to non-neuronal cells given the specificity of the neuronal environment such as the existence of specific APP isoform (APP_{695}) only in the brain. Additionally, the concentrations of GLP-1 analogues used in the current study may not have been sufficient to induce significant effects on APP expression or proteolysis and it is possible that the protective effects of liraglutide and lixisenatide against UV-A light in ARPE-19 cells were mediated through a different cellular mechanism that was not investigated here. In fact, the variability in p53 levels following UV-A exposure (discussed in 7.2.) as well as the lack of relation between p53 and APP in the current study (discussed in 7.5.) has hindered the investigation of a possible mechanism of action of the GLP-1 analogues as to whether they could have manifested their protective effects against UV-A through the modulation of p53 levels.

7.11. Limitations

It is important to point out that there are limitations to the model of AMD utilised in the current study. RPE cells in this model were exposed to high doses of UV at a close distance which is not the case *in vivo*. Moreover, there are several protective anatomical structures in the human eye including the cornea, the intraocular lens, the aqueous humour and vitreous humour which all play a vital part in absorbing any excess of light photons thus protecting the retina from the damaging wavelengths of the UV spectrum (Walsh, 2009). These protective structures are all absent in this cell culture model where RPE cells are directly exposed to UV-A irradiation with minimal protection (i.e. only the flask walls and the DMEM free media). Similar limitations exist with regards to oxidative stress where cells are exposed to high doses of H_2O_2 with limited protective mechanisms and lack of access to dietary antioxidants (Widomska and Subczynski, 2019).

Other limitations include the timing of treatments with the secretase inhibitors. When studying the effects of the secretase inhibitors on APP expression and processing in the optimisation experiments, cells were treated for 24 h before harvesting cell lysates and media samples for

immunoblotting analysis. On the other hand, when studying the effects of these inhibitors on cell resistance to UV-A irradiation, cells were also treated for a total of 24 h but this was divided into a 6 h pre-incubation (before UV-A irradiation) and an 18 h post-incubation in UltraMEM in the presence or absence of the drug under examination. Although the immunoblots in Fig. 5.13, 5.20 and 5.27 confirmed the expected effects of the inhibitors on APP expression/processing, it is important to note that these effects might not have been fully attained at the point of irradiation (after only 6 h incubation with the drugs) and therefore this might have played a role in limiting the effects of these inhibitors in modifying the response of ARPE-19 cells to UV-A irradiation.

Similarly, when cells were treated with GLP-1 analogues alongside H_2O_2, they were pre-incubated with the drugs for 6 h and then H_2O_2 was added to the same medium and cells were further incubated for 24 h. This meant that cells were incubated for a total of 30 h with GLP-1 analogues before conducting an MTS assay. On the other hand, in the GLP-1 and UV-A treatment, cells were incubated with the drugs for 6 h before irradiation, however, they were subjected to an 18 h post-incubation with the drugs before harvesting cells and conducting Trypan Blue viable cell counts. That will add up as a 24 h incubation with GLP-1 analogues in the later experiment. These discrepancies in treatment times might have contributed to the inconsistencies observed with regards to the effects of GLP-1 analogues on cell viability in the absence of the stressors (Fig. 6.6 compared to Fig. 6.10) and (Fig. 6.5 compared to Fig. 6.18).

7.12. Concluding remarks and further research

The key findings of the current study are as follows:

1. UV-A light was shown to consistently decrease the expression of APP with a concomitant decrease in the production of sAPPβ but not sAPPα after correcting the results to account for decreases in cell viability.

2. FL-APP or some of its fragments may be detrimental to cells as depleting endogenous APP using APP siRNA significantly increased the resistance of ARPE-19 cells to UV-A irradiation restoring viable cell counts to approximately control levels.

3. sAPPα was important for ARPE-19 cell growth and proliferation as shown by the growth enhancement when ARPE-19 cells were co-cultured with HEK cells stably transfected with a construct encoding the fragment. The fact that sAPPα promotes ARPE-19 cell growth can also be inferred from the inhibitory effect of batimastat in this respect.

4. Whilst sAPPα promoted proliferation the inhibition of its production by batimastat did not seem to protect against the reductions in cell viability effected by UV-A irradiation.

5. sAPPβ did not share the growth promoting effects observed with sAPPα. This is also consistent with the lack of appreciable effects of the β-secretase inhibitor IV on cell growth.

6. The inhibition of sAPPβ generation using β-secretase inhibitor IV did not modify the reduction in cell viability effected by UV-A suggesting that this fragment (and possibly Aβ-peptides) are not mechanistically involved.

7. The fact that the γ-secretase inhibitor begacestat ablated the toxic effects of UV-A on ARPE-19 cells, together with point 6 (above), suggest that AICD generation may well be necessary for mediating the reductions in viability effected by UV-A. Although, as discussed, this hypothesis would require AICD generation without prior α- or β-secretase cleavage of APP given that neither batimastat nor β-secretase inhibitor IV exerted a similar effect.

8. Two of the tested GLP-1 analogues, liraglutide and lixisenatide, were able to increase cell resistance to UV-A light showing a significant restoration of viable cell numbers to control levels following UV-A exposure.

Future experiments in which ARPE1-9 cells are exposed to UV-A in the presence and absence of purified sAPP fragments or conditioned medium from the sAPP HEK stable transfectants used in the current study would further confirm the roles of these fragments in the proliferation and response of this retinal cell line to UV-A irradiation. Furthermore, the generation of stable transfections of ARPE-19 cells over-expressing FL-APP or the various APP fragments is also likely to prove useful in this respect. A possible way to confirm the role of the AICD in mediating cell toxicity from UV-A could be through the transfection of ARPE-19 cells with a construct expressing the AICD fragment and monitoring the effects on cell viability in the presence or absence of UV-A light. Moreover, using different types of SDS gels that allow the separation of low molecular weight protein fragments might be another approach to evaluate the role of the AICD in UV-A mediated toxicity by quantifying its concentrations while cells are treated with the various inhibitors alongside UV-A light.

The results in the current study provide an insight into the role played by APP and its metabolites in the pathophysiology of AMD. A possible treatment strategy could be through shifting APP processing towards the non-amyloidogenic pathway given the essential role played by the α-secretase generated fragment in maintaining the growth and proliferation of retinal pigment epithelial cells.

Finally, the results regarding GLP-1 analogues indicate that activating GLP-1 receptors in RPE cells might be of benefit in the protection of these cells from stress inducing reagents such as UV light. This result warrant further investigation of the cellular pathways which might be responsible for their cytoprotective effects against UV-A. Such studies might identify new drug targets for the prevention and treatment of retinal neurodegenerative diseases such as AMD.

Chapter 8

References

8. References

Ablonczy, Z., Dahrouj, M., Tang, P. H., Liu, Y., Sambamurti, K., Marmorstein, A. D. & Crosson, C. E. (2011) Human Retinal Pigment Epithelium Cells as Functional Models for the RPE In Vivo. *Investigative Ophthalmology & Visual Science,* 52(12)**,** 8614-8620.

Age-Related Eye Disease Study Research Group, G. (2000) Risk factors associated with age-related macular degeneration. A case-control study in the age-related eye disease study: Age-Related Eye Disease Study Report Number 3. *Ophthalmology,* 107(12)**,** 2224-32.

Allinson, T. M., Parkin, E. T., Turner, A. J. & Hooper, N. M. (2003) ADAMs family members as amyloid precursor protein alpha-secretases. *J Neurosci Res,* 74(3)**,** 342-52.

Almenar-Queralt, A., Falzone, T. L., Shen, Z., Lillo, C., Killian, R. L., Arreola, A. S., Niederst, E. D., Ng, K. S., Kim, S. N., Briggs, S. P., Williams, D. S. & Goldstein, L. S. (2014) UV irradiation accelerates amyloid precursor protein (APP) processing and disrupts APP axonal transport. *J Neurosci,* 34(9)**,** 3320-39.

Almkvist, O., Basun, H., Wagner, S. L., Rowe, B. A., Wahlund, L. O. & Lannfelt, L. (1997) Cerebrospinal fluid levels of alpha-secretase-cleaved soluble amyloid precursor protein mirror cognition in a Swedish family with Alzheimer disease and a gene mutation. *Arch Neurol,* 54(5)**,** 641-4.

Alvarez, E., Martínez, M. D., Roncero, I., Chowen, J. A., García-Cuartero, B., Gispert, J. D., Sanz, C., Vázquez, P., Maldonado, A., De Cáceres, J., Desco, M., Pozo, M. A. & Blázquez, E. (2005) The expression of GLP-1 receptor mRNA and protein allows the effect of GLP-1 on glucose metabolism in the human hypothalamus and brainstem. *J Neurochem,* 92(4)**,** 798-806.

Ambati, J., Atkinson, J. P. & Gelfand, B. D. (2013) Immunology of age-related macular degeneration. *Nature reviews. Immunology,* 13(6)**,** 438-451.

Ambati, J. & Fowler, B. J. (2012) Mechanisms of age-related macular degeneration. *Neuron,* 75(1)**,** 26-39.

Amour, A., Knight, C. G., English, W. R., Webster, A., Slocombe, P. M., Knäuper, V., Docherty, A. J. P., Becherer, J. D., Blobel, C. P. & Murphy, G. (2002) The enzymatic activity of ADAM8 and ADAM9 is not regulated by TIMPs. *FEBS Letters,* 524(1)**,** 154-158.

Anderson, D. H., Talaga, K. C., Rivest, A. J., Barron, E., Hageman, G. S. & Johnson, L. V. (2004) Characterization of beta amyloid assemblies in drusen: the deposits associated with aging and age-related macular degeneration. *Exp Eye Res,* 78(2)**,** 243-56.

Anderson, J. J., Holtz, G., Baskin, P. P., Wang, R., Mazzarelli, L., Wagner, S. L. & Menzaghi, F. (1999) Reduced cerebrospinal fluid levels of alpha-secretase-cleaved amyloid precursor protein in aged rats: correlation with spatial memory deficits. *Neuroscience,* 93(4)**,** 1409-20.

Andrew, R. J., Kellett, K. a. B., Thinakaran, G. & Hooper, N. M. (2016) A Greek Tragedy: The Growing Complexity of Alzheimer Amyloid Precursor Protein Proteolysis. *The Journal of biological chemistry,* 291(37)**,** 19235-19244.

Araki, W., Kitaguchi, N., Tokushima, Y., Ishii, K., Aratake, H., Shimohama, S., Nakamura, S. & Kimura, J. (1991) Trophic effect of beta-amyloid precursor protein on cerebral cortical neurons in culture. *Biochem Biophys Res Commun,* 181(1)**,** 265-71.

Arigony, A. L. V., De Oliveira, I. M., Machado, M., Bordin, D. L., Bergter, L., Prá, D. & Pêgas Henriques, J. A. (2013) The Influence of Micronutrients in Cell Culture: A Reflection on Viability and Genomic Stability. *BioMed Research International,* 2013**,** 597282.

Asai, M., Hattori, C., Szabo, B., Sasagawa, N., Maruyama, K., Tanuma, S. & Ishiura, S. (2003) Putative function of ADAM9, ADAM10, and ADAM17 as APP alpha-secretase. *Biochem Biophys Res Commun,* 301(1)**,** 231-5.

Athauda, D., Maclagan, K., Skene, S. S., Bajwa-Joseph, M., Letchford, D., Chowdhury, K., Hibbert, S., Budnik, N., Zampedri, L., Dickson, J., Li, Y., Aviles-Olmos, I., Warner, T. T., Limousin, P., Lees, A. J., Greig, N. H., Tebbs, S. & Foltynie, T. (2017) Exenatide once weekly versus placebo in Parkinson's disease: a randomised, double-blind, placebo-controlled trial. *Lancet (London, England),* 390(10103)**,** 1664-1675.

Aviles-Olmos, I., Dickson, J., Kefalopoulou, Z., Djamshidian, A., Kahan, J., Ell, P., Whitton, P., Wyse, R., Isaacs, T., Lees, A., Limousin, P. & Foltynie, T. (2014) Motor and cognitive advantages persist 12 months after exenatide exposure in Parkinson's disease. *J Parkinsons Dis,* 4(3)**,** 337-44.

Ayala, M., Strid, H., Jacobsson, U. & SöDerberg, P. G. (2007) p53 Expression and Apoptosis in the Lens after Ultraviolet Radiation Exposure. *Investigative Ophthalmology & Visual Science,* 48(9)**,** 4187-4191.

Barger, S. W. & Harmon, A. D. (1997) Microglial activation by Alzheimer amyloid precursor protein and modulation by apolipoprotein E. *Nature,* 388(6645)**,** 878-881.

Barnett, A. H. (2011) Lixisenatide: evidence for its potential use in the treatment of type 2 diabetes. *Core evidence,* 6**,** 67-79.

Bayer, T. A., Cappai, R., Masters, C. L., Beyreuther, K. & Multhaup, G. (1999) It all sticks together--the APP-related family of proteins and Alzheimer's disease. *Mol Psychiatry,* 4(6)**,** 524-8.

Beatty, S., Koh, H.-H., Phil, M., Henson, D. & Boulton, M. (2000) The Role of Oxidative Stress in the Pathogenesis of Age-Related Macular Degeneration. *Survey of Ophthalmology,* 45(2)**,** 115-134.

Bell, G. I., Santerre, R. F. & Mullenbach, G. T. (1983) Hamster preproglucagon contains the sequence of glucagon and two related peptides. *Nature,* 302(5910)**,** 716-8.

Bell, K. F., Zheng, L., Fahrenholz, F. & Cuello, A. C. (2008) ADAM-10 over-expression increases cortical synaptogenesis. *Neurobiol Aging,* 29(4)**,** 554-65.

Bertrand, E., Brouillet, E., Caillé, I., Bouillot, C., Cole, G. M., Prochiantz, A. & Allinquant, B. (2001) A Short Cytoplasmic Domain of the Amyloid Precursor Protein Induces Apoptosis In Vitro and In Vivo. *Molecular and Cellular Neuroscience,* 18(5)**,** 503-511.

Bien, J., Jefferson, T., Čaušević, M., Jumpertz, T., Munter, L., Multhaup, G., Weggen, S., Becker-Pauly, C. & Pietrzik, C. U. (2012) The Metalloprotease Meprin beta; Generates Amino Terminal-truncated Amyloid beta; Peptide Species *. *Journal of Biological Chemistry,* 287(40)**,** 33304-33313.

Blacker, M., Noe, M. C., Carty, T. J., Goodyer, C. G. & Leblanc, A. C. (2002) Effect of tumor necrosis factor-α converting enzyme (TACE) and metalloprotease inhibitor on amyloid precursor protein metabolism in human neurons. *Journal of Neurochemistry,* 83(6)**,** 1349-1357.

Bonilha, V. L. (2008) Age and disease-related structural changes in the retinal pigment epithelium. *Clinical ophthalmology (Auckland, N.Z.),* 2(2)**,** 413-424.

Borchelt, D. R., Thinakaran, G., Eckman, C. B., Lee, M. K., Davenport, F., Ratovitsky, T., Prada, C. M., Kim, G., Seekins, S., Yager, D., Slunt, H. H., Wang, R., Seeger, M., Levey, A. I., Gandy, S. E., Copeland, N. G., Jenkins, N. A., Price, D. L., Younkin, S. G. & Sisodia, S. S. (1996) Familial Alzheimer's disease-linked presenilin 1 variants elevate Abeta1-42/1-40 ratio in vitro and in vivo. *Neuron,* 17(5)**,** 1005-13.

Boyton, R. & Altmann, D. M. (2006) NOTCH. In: Laurent, G. J. & Shapiro, S. D. (eds.) *Encyclopedia of Respiratory Medicine.* Oxford: Academic Press.

Bridges, L. C. & Bowditch, R. D. (2005) ADAM-Integrin Interactions: potential integrin regulated ectodomain shedding activity. *Curr Pharm Des,* 11(7)**,** 837-47.

Brocker, C. N., Vasiliou, V. & Nebert, D. W. (2009) Evolutionary divergence and functions of the ADAM and ADAMTS gene families. *Hum Genomics,* 4(1)**,** 43-55.

Bruban, J., Glotin, A. L., Dinet, V., Chalour, N., Sennlaub, F., Jonet, L., An, N., Faussat, A. M. & Mascarelli, F. (2009) Amyloid-beta(1-42) alters structure and function of retinal pigmented epithelial cells. *Aging Cell,* 8(2)**,** 162-77.

Buffa, R., Capella, C., Fontana, P., Usellini, L. & Solcia, E. (1978) Types of endocrine cells in the human colon and rectum. *Cell Tissue Res,* 192(2)**,** 227-40.

Buizza, L., Prandelli, C., Bonini, S. A., Delbarba, A., Cenini, G., Lanni, C., Buoso, E., Racchi, M., Govoni, S., Memo, M. & Uberti, D. (2013) Conformational altered p53 affects neuronal function: relevance for the response to toxic insult and growth-associated protein 43 expression. *Cell Death & Disease,* 4(2)**,** e484-e484.

Buxbaum, J. D., Liu, K. N., Luo, Y., Slack, J. L., Stocking, K. L., Peschon, J. J., Johnson, R. S., Castner, B. J., Cerretti, D. P. & Black, R. A. (1998) Evidence that tumor necrosis factor alpha converting enzyme is involved in regulated alpha-secretase cleavage of the Alzheimer amyloid protein precursor. *J Biol Chem,* 273(43)**,** 27765-7.

Cai, D., Leem, J. Y., Greenfield, J. P., Wang, P., Kim, B. S., Wang, R., Lopes, K. O., Kim, S. H., Zheng, H., Greengard, P., Sisodia, S. S., Thinakaran, G. & Xu, H. (2003) Presenilin-1 regulates intracellular trafficking and cell surface delivery of beta-amyloid precursor protein. *J Biol Chem,* 278(5)**,** 3446-54.

Cai, H., Wang, Y., Mccarthy, D., Wen, H., Borchelt, D. R., Price, D. L. & Wong, P. C. (2001) BACE1 is the major beta-secretase for generation of Abeta peptides by neurons. *Nat Neurosci,* 4(3)**,** 233-4.

Cai, X., She, M., Xu, M., Chen, H., Li, J., Chen, X., Zheng, D., Liu, J., Chen, S., Zhu, J., Xu, X., Li, R., Li, J., Chen, S., Yang, X. & Li, H. (2018) GLP-1 treatment protects endothelial cells from oxidative stress-induced autophagy and endothelial dysfunction. *International Journal of Biological Sciences,* 14(12)**,** 1696-1708.

Caillé, I., Allinquant, B., Dupont, E., Bouillot, C., Langer, A., Müller, U. & Prochiantz, A. (2004) Soluble form of amyloid precursor protein regulates proliferation of progenitors in the adult subventricular zone. *Development,* 131(9)**,** 2173-81.

Chakravarthy, U., Williams, M. & Group, A. M. D. G. (2013) The Royal College of Ophthalmologists Guidelines on AMD: Executive Summary. *Eye (London, England),* 27(12)**,** 1429-1431.

Chalam, K. V., Khetpal, V., Rusovici, R. & Balaiya, S. (2011) A review: role of ultraviolet radiation in age-related macular degeneration. *Eye Contact Lens,* 37(4)**,** 225-32.

Chang, C. C., Lin, T. C., Ho, H. L., Kuo, C. Y., Li, H. H., Korolenko, T. A., Chen, W. J., Lai, T. J., Ho, Y. J. & Lin, C. L. (2018) GLP-1 Analogue Liraglutide Attenuates Mutant Huntingtin-Induced Neurotoxicity by Restoration of Neuronal Insulin Signaling. *Int J Mol Sci,* 19(9).

Chang, G., Zhang, D., Yu, H., Zhang, P., Wang, Y., Zheng, A. & Qin, S. (2013) Cardioprotective effects of exenatide against oxidative stress-induced injury. *Int J Mol Med,* 32(5)**,** 1011-1020.

Chasseigneaux, S. & Allinquant, B. (2012) Functions of Aβ, sAPPα and sAPPβ : similarities and differences. *Journal of Neurochemistry,* 120(s1)**,** 99-108.

Cheignon, C., Tomas, M., Bonnefont-Rousselot, D., Faller, P., Hureau, C. & Collin, F. (2018) Oxidative stress and the amyloid beta peptide in Alzheimer's disease. *Redox Biol,* 14**,** 450-464.

Chen, H., Liu, B., Lukas, T. J. & Neufeld, A. H. (2008) The aged retinal pigment epithelium/choroid: a potential substratum for the pathogenesis of age-related macular degeneration. *PLoS One,* 3(6)**,** e2339.

Chen, L., Bai, Y., Zhao, M. & Jiang, Y. (2016) TLR4 inhibitor attenuates amyloid-β-induced angiogenic and inflammatory factors in ARPE-19 cells: Implications for age-related macular degeneration. *Mol Med Rep,* 13(4)**,** 3249-3256.

Chen, X., Rong, S. S., Xu, Q., Tang, F. Y., Liu, Y., Gu, H., Tam, P. O., Chen, L. J., Brelén, M. E., Pang, C. P. & Zhao, C. (2014) Diabetes mellitus and risk of age-related macular degeneration: a systematic review and meta-analysis. *PLoS One,* 9(9)**,** e108196.

Choi, J. K., Lym, Y. L., Moon, J. W., Shin, H. J. & Cho, B. (2011) Diabetes Mellitus and Early Age-related Macular Degeneration. *Archives of Ophthalmology,* 129(2)**,** 196-199.

Chou, R.-H., Lee, C.-Y., Chong, L.-W., Chang, K.-H., Lin, C.-L., Yan, K.-S., Tsou, C. & Hsu, Y.-C. (2018) HBV infection increases the risk of macular degeneration: the roles of HBx-mediated sensitization of retinal pigment epithelial cells to UV and blue light irradiation. *Journal of Translational Medicine,* 16(1)**,** 221.

Christian, L. (2012) The ADAM family. *Fly,* 6(1)**,** 30-34.

Chua, L. M., Lim, M. L. & Wong, B. S. (2013) The Kunitz-protease inhibitor domain in amyloid precursor protein reduces cellular mitochondrial enzymes expression and function. *Biochem Biophys Res Commun,* 437(4)**,** 642-7.

Cissé, M. A., Sunyach, C., Lefranc-Jullien, S., Postina, R., Vincent, B. & Checler, F. (2005) The Disintegrin ADAM9 Indirectly Contributes to the Physiological Processing of Cellular Prion by Modulating ADAM10 Activity *. *Journal of Biological Chemistry,* 280(49)**,** 40624-40631.

Coburger, I., Dahms, S. O., Roeser, D., Guhrs, K. H., Hortschansky, P. & Than, M. E. (2013) Analysis of the overall structure of the multi-domain amyloid precursor protein (APP). *PLoS One,* 8(12)**,** e81926.

Coleman, H. R., Chan, C. C., Ferris, F. L., 3rd & Chew, E. Y. (2008) Age-related macular degeneration. *Lancet,* 372(9652)**,** 1835-45.

Copanaki, E., Chang, S., Vlachos, A., Tschäpe, J.-A., Müller, U. C., Kögel, D. & Deller, T. (2010) sAPPα antagonizes dendritic degeneration and neuron death triggered by proteasomal stress. *Molecular and Cellular Neuroscience,* 44(4)**,** 386-393.

Corrigan, F., Vink, R., Blumbergs, P. C., Masters, C. L., Cappai, R. & Van Den Heuvel, C. (2012) sAPPα rescues deficits in amyloid precursor protein knockout mice following focal traumatic brain injury. *J Neurochem,* 122(1)**,** 208-20.

Coyle, C. H. & Kader, K. N. (2007) Mechanisms of H2O2-induced oxidative stress in endothelial cells exposed to physiologic shear stress. *Asaio j,* 53(1)**,** 17-22.

Cuesta, A., Zambrano, A., López, E. & Pascual, A. (2009a) Thyroid hormones reverse the UV-induced repression of APP in neuroblastoma cells. *FEBS Letters,* 583(14)**,** 2401-2406.

Cuesta, A., Zambrano, A., Royo, M. & Pascual, A. (2009b) The tumour suppressor p53 regulates the expression of amyloid precursor protein (APP). *Biochem J,* 418(3)**,** 643-50.

Dawson, D. W., Volpert, O. V., Gillis, P., Crawford, S. E., Xu, H., Benedict, W. & Bouck, N. P. (1999) Pigment epithelium-derived factor: a potent inhibitor of angiogenesis. *Science,* 285(5425)**,** 245-8.

Day, C. (2018) Chapter 26 - New Therapies in Obesity. In: Weaver, J. U. (ed.) *Practical Guide to Obesity Medicine.* Elsevier.

De Jong, P. T. (2006) Age-related macular degeneration. *N Engl J Med,* 355(14)**,** 1474-85.

De Strooper, B. (2003) Aph-1, Pen-2, and Nicastrin with Presenilin Generate an Active γ-Secretase Complex. *Neuron,* 38(1)**,** 9-12.

De Strooper, B. & Annaert, W. (2000) Proteolytic processing and cell biological functions of the amyloid precursor protein. *Journal of Cell Science,* 113(11)**,** 1857-1870.

De Strooper, B., Annaert, W., Cupers, P., Saftig, P., Craessaerts, K., Mumm, J. S., Schroeter, E. H., Schrijvers, V., Wolfe, M. S., Ray, W. J., Goate, A. & Kopan, R. (1999) A presenilin-1-dependent gamma-secretase-like protease mediates release of Notch intracellular domain. *Nature,* 398(6727)**,** 518-22.

De Strooper, B., Vassar, R. & Golde, T. (2010) The secretases: enzymes with therapeutic potential in Alzheimer disease. *Nature reviews. Neurology,* 6(2)**,** 99-107.

Demars, M. P., Bartholomew, A., Strakova, Z. & Lazarov, O. (2011) Soluble amyloid precursor protein: a novel proliferation factor of adult progenitor cells of ectodermal and mesodermal origin. *Stem Cell Res Ther,* 2(4)**,** 36.

Deng, J., Habib, A., Obregon, D. F., Barger, S. W., Giunta, B., Wang, Y.-J., Hou, H., Sawmiller, D. & Tan, J. (2015) Soluble amyloid precursor protein alpha inhibits tau phosphorylation through modulation of GSK3β signaling pathway. *Journal of neurochemistry,* 135(3)**,** 630-637.

Dentchev, T., Milam, A. H., Lee, V. M., Trojanowski, J. Q. & Dunaief, J. L. (2003) Amyloid-beta is found in drusen from some age-related macular degeneration retinas, but not in drusen from normal retinas. *Mol Vis,* 9**,** 184-90.

Deuss, M., Reiss, K. & Hartmann, D. (2008) Part-time alpha-secretases: the functional biology of ADAM 9, 10 and 17. *Current Alzheimer research,* 5**,** 187-201.

Dillon, J. S., Tanizawa, Y., Wheeler, M. B., Leng, X. H., Ligon, B. B., Rabin, D. U., Yoo-Warren, H., Permutt, M. A. & Boyd, A. E., 3rd (1993) Cloning and functional expression of the human glucagon-like peptide-1 (GLP-1) receptor. *Endocrinology,* 133(4)**,** 1907-10.

Ding, X., Patel, M. & Chan, C. C. (2009) Molecular pathology of age-related macular degeneration. *Prog Retin Eye Res,* 28(1)**,** 1-18.

Dulin, F., Leveille, F., Ortega, J. B., Mornon, J. P., Buisson, A., Callebaut, I. & Colloc'h, N. (2008) P3 peptide, a truncated form of A beta devoid of synaptotoxic effect, does not assemble into soluble oligomers. *FEBS Lett,* 582(13)**,** 1865-70.

Dunn, K. C., Aotaki-Keen, A. E., Putkey, F. R. & Hjelmeland, L. M. (1996) ARPE-19, a human retinal pigment epithelial cell line with differentiated properties. *Exp Eye Res,* 62(2)**,** 155-69.

During, M. J., Cao, L., Zuzga, D. S., Francis, J. S., Fitzsimons, H. L., Jiao, X., Bland, R. J., Klugmann, M., Banks, W. A., Drucker, D. J. & Haile, C. N. (2003) Glucagon-like peptide-1 receptor is involved in learning and neuroprotection. *Nature Medicine,* 9(9)**,** 1173-1179.

Edwards, D. R., Handsley, M. M. & Pennington, C. J. (2008) The ADAM metalloproteinases. *Mol Aspects Med,* 29(5)**,** 258-89.

Elkinson, S. & Keating, G. M. (2013) Lixisenatide: first global approval. *Drugs,* 73(4)**,** 383-91.

Evans, J. R. (2001) Risk Factors for Age-related Macular Degeneration. *Progress in Retinal and Eye Research,* 20(2)**,** 227-253.

Exton, J. H. & Park, C. R. (1968) Control of Gluconeogenesis in Liver: II. EFFECTS OF GLUCAGON, CATECHOLAMINES, AND ADENOSINE 3',5'-MONOPHOSPHATE ON GLUCONEOGENESIS IN THE PERFUSED RAT LIVER. *Journal of Biological Chemistry,* 243(16)**,** 4189-4196.

Femminella, G. D., Frangou, E., Love, S. B., Busza, G., Holmes, C., Ritchie, C., Lawrence, R., Mcfarlane, B., Tadros, G., Ridha, B. H., Bannister, C., Walker, Z., Archer, H., Coulthard, E., Underwood, B. R., Prasanna, A., Koranteng, P., Karim, S., Junaid, K., Mcguinness, B., Nilforooshan, R., Macharouthu, A., Donaldson, A., Thacker, S., Russell, G., Malik, N., Mate, V., Knight, L., Kshemendran, S., Harrison, J., Brooks, D. J., Passmore, A. P., Ballard, C. & Edison, P. (2019) Evaluating the effects of the novel GLP-1 analogue liraglutide in Alzheimer's disease: study protocol for a randomised controlled trial (ELAD study). *Trials,* 20(1)**,** 191.

Fingleton, B. (2008) MMPs as therapeutic targets—Still a viable option? *Seminars in Cell & Developmental Biology,* 19(1)**,** 61-68.

Fischer, T., Senn, N. & Riedl, R. (2019) Design and Structural Evolution of Matrix Metalloproteinase Inhibitors. *Chemistry – A European Journal,* 25(34)**,** 7960-7980.

Fletcher, A. E., Bentham, G. C., Agnew, M., Young, I. S., Augood, C., Chakravarthy, U., De Jong, P. T., Rahu, M., Seland, J., Soubrane, G., Tomazzoli, L., Topouzis, F., Vingerling, J. R. & Vioque, J. (2008) Sunlight exposure, antioxidants, and age-related macular degeneration. *Arch Ophthalmol,* 126(10)**,** 1396-403.

Foltynie, T. & Aviles-Olmos, I. (2014) Exenatide as a potential treatment for patients with Parkinson's disease: First steps into the clinic. *Alzheimer's & Dementia,* 10(1S)**,** S38-S46.

Forest, D. L., Johnson, L. V. & Clegg, D. O. (2015) Cellular models and therapies for age-related macular degeneration. *Disease models & mechanisms,* 8(5)**,** 421-427.

Frost, S., Guymer, R., Aung, K. Z., Macaulay, S. L., Sohrabi, H. R., Bourgeat, P., Salvado, O., Rowe, C. C., Ames, D., Masters, C. L., Martins, R. N. & Kanagasingam, Y. (2016) Alzheimer's Disease and the Early Signs of Age-Related Macular Degeneration. *Curr Alzheimer Res,* 13(11)**,** 1259-1266.

Frykman, S., Hur, J. Y., Frånberg, J., Aoki, M., Winblad, B., Nahalkova, J., Behbahani, H. & Tjernberg, L. O. (2010) Synaptic and endosomal localization of active gamma-secretase in rat brain. *PLoS One,* 5(1)**,** e8948.

Furukawa, K., Barger, S. W., Blalock, E. M. & Mattson, M. P. (1996a) Activation of K+ channels and suppression of neuronal activity by secreted beta-amyloid-precursor protein. *Nature,* 379(6560)**,** 74-8.

Furukawa, K., Sopher, B. L., Rydel, R. E., Begley, J. G., Pham, D. G., Martin, G. M., Fox, M. & Mattson, M. P. (1996b) Increased activity-regulating and neuroprotective efficacy of alpha-secretase-derived secreted amyloid precursor protein conferred by a C-terminal heparin-binding domain. *J Neurochem,* 67(5)**,** 1882-96.

Gao, J., Liu, R., Cao, S., Cui, J., Wang, A., To, E. & Matsubara, J. (2015) NLRP3 Inflammasome: Activation and Regulation in Age-Related Macular Degeneration. *Mediators of Inflammation,* 2015**,** 11 pages.

Gao, X. & Talalay, P. (2004) Induction of phase 2 genes by sulforaphane protects retinal pigment epithelial cells against photooxidative damage. *Proc Natl Acad Sci U S A,* 101(28)**,** 10446-51.

García-González, L., Pilat, D., Baranger, K. & Rivera, S. (2019) Emerging Alternative Proteinases in APP Metabolism and Alzheimer's Disease Pathogenesis: A Focus on MT1-MMP and MT5-MMP. *Frontiers in Aging Neuroscience,* 11(244).

Gearing, A. J. H., Beckett, P., Christodoulou, M., Churchill, M., Clements, J., Davidson, A. H., Drummond, A. H., Galloway, W. A., Gilbert, R., Gordon, J. L., Leber, T. M., Mangan, M., Miller, K., Nayee, P., Owen, K., Patel, S., Thomas, W., Wells, G., Wood, L. M. & Woolley, K. (1994) Processing of tumour necrosis factor-α precursor by metalloproteinases. *Nature,* 370(6490)**,** 555-557.

Gejl, M., Gjedde, A., Egefjord, L., Møller, A., Hansen, S. B., Vang, K., Rodell, A., Brændgaard, H., Gottrup, H., Schacht, A., Møller, N., Brock, B. & Rungby, J. (2016) In Alzheimer's Disease, 6-Month Treatment with GLP-1 Analog Prevents Decline of Brain Glucose Metabolism: Randomized, Placebo-Controlled, Double-Blind Clinical Trial. *Frontiers in aging neuroscience,* 8**,** 108-108.

Giliberto, L., Zhou, D., Weldon, R., Tamagno, E., De Luca, P., Tabaton, M. & D'adamio, L. (2008) Evidence that the Amyloid beta Precursor Protein-intracellular domain lowers the stress threshold of neurons and has a "regulated" transcriptional role. *Molecular neurodegeneration,* 3**,** 12-12.

Glickman, R. D. (2011) Ultraviolet phototoxicity to the retina. *Eye Contact Lens,* 37(4)**,** 196-205.

Gold, M. & El Khoury, J. (2015) β-amyloid, microglia, and the inflammasome in Alzheimer's disease. *Semin Immunopathol,* 37(6)**,** 607-11.

Goldblum, D., Kipfer-Kauer, A., Sarra, G.-M., Wolf, S. & Frueh, B. E. (2007) Distribution of Amyloid Precursor Protein and Amyloid-β Immunoreactivity in DBA/2J Glaucomatous Mouse Retinas. *Investigative Ophthalmology & Visual Science,* 48(11)**,** 5085-5090.

Goodman, Y. & Mattson, M. P. (1994) Secreted forms of beta-amyloid precursor protein protect hippocampal neurons against amyloid beta-peptide-induced oxidative injury. *Exp Neurol,* 128(1)**,** 1-12.

Gough, M., Parr-Sturgess, C. & Parkin, E. (2011) Zinc Metalloproteinases and Amyloid Beta-Peptide Metabolism: The Positive Side of Proteolysis in Alzheimer's Disease. *Biochemistry Research International,* 2011**,** 721463.

Gralle, M., Botelho, M. G. & Wouters, F. S. (2009) Neuroprotective secreted amyloid precursor protein acts by disrupting amyloid precursor protein dimers. *The Journal of biological chemistry,* 284(22)**,** 15016-15025.

Gralle, M. & Ferreira, S. T. (2007) Structure and functions of the human amyloid precursor protein: the whole is more than the sum of its parts. *Prog Neurobiol,* 82(1)**,** 11-32.

Gupta, S. K., Murthy, G. V., Morrison, N., Price, G. M., Dherani, M., John, N., Fletcher, A. E. & Chakravarthy, U. (2007) Prevalence of early and late age-related macular degeneration in a rural population in northern India: the INDEYE feasibility study. *Invest Ophthalmol Vis Sci,* 48(3)**,** 1007-11.

Haapasalo, A. & Kovacs, D. M. (2011) The many substrates of presenilin/γ-secretase. *Journal of Alzheimer's disease : JAD,* 25(1)**,** 3-28.

Habib, A., Sawmiller, D. & Tan, J. (2017) Restoring Soluble Amyloid Precursor Protein α Functions as a Potential Treatment for Alzheimer's Disease. *J Neurosci Res,* 95(4)**,** 973-991.

Hageman, G. S., Luthert, P. J., Victor Chong, N. H., Johnson, L. V., Anderson, D. H. & Mullins, R. F. (2001) An Integrated Hypothesis That Considers Drusen as Biomarkers of Immune-Mediated Processes at the RPE-Bruch's Membrane Interface in Aging and Age-Related Macular Degeneration. *Progress in Retinal and Eye Research,* 20(6)**,** 705-732.

Hahn, P., Acquah, K., Cousins, S. W., Lee, P. P. & Sloan, F. A. (2013) Ten-year incidence of age-related macular degeneration according to diabetic retinopathy classification among medicare beneficiaries. *Retina,* 33(5)**,** 911-9.

Halliwell, B. (2014) Cell culture, oxidative stress, and antioxidants: avoiding pitfalls. *Biomed J,* 37(3)**,** 99-105.

Harkavyi, A. & Whitton, P. S. (2010) Glucagon-like peptide 1 receptor stimulation as a means of neuroprotection. *British journal of pharmacology,* 159(3)**,** 495-501.

Hayashi, Y., Kashiwagi, K., Ohta, J., Nakajima, M., Kawashima, T. & Yoshikawa, K. (1994) Alzheimer amyloid protein precursor enhances proliferation of neural stem cells from fetal rat brain. *Biochem Biophys Res Commun,* 205(1)**,** 936-43.

Hebsgaard, J., Pyke, C., Yildirim, E., Knudsen, L., Heegaard, S. & Kvist, P. (2018) Glucagon-like peptide-1 receptor expression in the human eye. *Diabetes, Obesity and Metabolism,* 20.

Hemming, M. L., Elias, J. E., Gygi, S. P. & Selkoe, D. J. (2009) Identification of beta-secretase (BACE1) substrates using quantitative proteomics. *PloS one,* 4(12)**,** e8477-e8477.

Hernández-Zimbrón, L. F., Zamora-Alvarado, R., Ochoa-De La Paz, L., Velez-Montoya, R., Zenteno, E., Gulias-Cañizo, R., Quiroz-Mercado, H. & Gonzalez-Salinas, R. (2018) Age-Related Macular Degeneration: New Paradigms for Treatment and Management of AMD. *Oxidative medicine and cellular longevity,* 2018**,** 8374647-8374647.

Hernandez, C., Bogdanov, P., Corraliza, L., Garcia-Ramirez, M., Sola-Adell, C., Arranz, J. A., Arroba, A. I., Valverde, A. M. & Simo, R. (2016) Topical Administration of GLP-1 Receptor Agonists Prevents Retinal Neurodegeneration in Experimental Diabetes. *Diabetes,* 65(1)**,** 172-87.

Hinnen, D. (2017) Glucagon-Like Peptide 1 Receptor Agonists for Type 2 Diabetes. *Diabetes spectrum : a publication of the American Diabetes Association,* 30(3)**,** 202-210.

Hiraoka, Y., Ohno, M., Yoshida, K., Okawa, K., Tomimoto, H., Kita, T. & Nishi, E. (2007) Enhancement of α-secretase cleavage of amyloid precursor protein by a metalloendopeptidase nardilysin. *Journal of Neurochemistry,* 102(5)**,** 1595-1605.

Ho, T., Vessey, K. A., Cappai, R., Dinet, V., Mascarelli, F., Ciccotosto, G. D. & Fletcher, E. L. (2012) Amyloid Precursor Protein Is Required for Normal Function of the Rod and Cone Pathways in the Mouse Retina. *PLOS ONE,* 7(1)**,** e29892.

Hooper, N. M., Karran, E. H. & Turner, A. J. (1997) Membrane protein secretases. *Biochemical Journal,* 321(2)**,** 265-279.

Hornof, M., Toropainen, E. & Urtti, A. (2005) Cell culture models of the ocular barriers. *European Journal of Pharmaceutics and Biopharmaceutics,* 60(2)**,** 207-225.

Hotoda, N., Koike, H., Sasagawa, N. & Ishiura, S. (2002) A secreted form of human ADAM9 has an α-secretase activity for APP. *Biochemical and Biophysical Research Communications,* 293(2)**,** 800-805.

Hui, H., Farilla, L., Merkel, P. & Perfetti, R. (2002) The short half-life of glucagon-like peptide-1 in plasma does not reflect its long-lasting beneficial effects. *Eur J Endocrinol,* 146(6)**,** 863-9.

Jalewa, J., Sharma, M. K. & Hölscher, C. (2016) Novel incretin analogues improve autophagy and protect from mitochondrial stress induced by rotenone in SH-SY5Y cells. *Journal of Neurochemistry,* 139(1)**,** 55-67.

Janes, P. W., Saha, N., Barton, W. A., Kolev, M. V., Wimmer-Kleikamp, S. H., Nievergall, E., Blobel, C. P., Himanen, J.-P., Lackmann, M. & Nikolov, D. B. (2005) Adam Meets Eph: An ADAM Substrate Recognition Module Acts as a Molecular Switch for Ephrin Cleavage In trans. *Cell,* 123(2)**,** 291-304.

Jantrapirom, S., Nimlamool, W., Chattipakorn, N., Chattipakorn, S., Temviriyanukul, P., Inthachat, W., Govitrapong, P. & Potikanond, S. (2020) Liraglutide Suppresses Tau Hyperphosphorylation, Amyloid Beta Accumulation through Regulating Neuronal Insulin Signaling and BACE-1 Activity. *International journal of molecular sciences,* 21(5)**,** 1725.

Jin, L. W., Ninomiya, H., Roch, J. M., Schubert, D., Masliah, E., Otero, D. A. & Saitoh, T. (1994) Peptides containing the RERMS sequence of amyloid beta/A4 protein precursor bind cell surface and promote neurite extension. *J Neurosci,* 14(9)**,** 5461-70.

Johnson, L. V., Leitner, W. P., Rivest, A. J., Staples, M. K., Radeke, M. J. & Anderson, D. H. (2002) The Alzheimer's A beta -peptide is deposited at sites of complement activation in pathologic deposits associated with aging and age-related macular degeneration. *Proceedings of the National Academy of Sciences of the United States of America,* 99(18)**,** 11830-11835.

Jorissen, E., Prox, J., Bernreuther, C., Weber, S., Schwanbeck, R., Serneels, L., Snellinx, A., Craessaerts, K., Thathiah, A., Tesseur, I., Bartsch, U., Weskamp, G., Blobel, C. P., Glatzel, M., De Strooper, B. & Saftig, P. (2010) The Disintegrin/Metalloproteinase ADAM10 Is Essential for the Establishment of the Brain Cortex. *The Journal of Neuroscience,* 30(14)**,** 4833-4844.

Kaarniranta, K., Salminen, A., Haapasalo, A., Soininen, H. & Hiltunen, M. (2011) Age-related macular degeneration (AMD): Alzheimer's disease in the eye? *J Alzheimers Dis,* 24(4)**,** 615-31.

Kauppinen, A., Paterno, J. J., Blasiak, J., Salminen, A. & Kaarniranta, K. (2016) Inflammation and its role in age-related macular degeneration. *Cellular and molecular life sciences : CMLS,* 73(9)**,** 1765-1786.

Kaur, G. & Dufour, J. M. (2012) Cell lines: Valuable tools or useless artifacts. *Spermatogenesis,* 2(1)**,** 1-5.

Kimball, C. P. & Murlin, J. R. (1923) AQUEOUS EXTRACTS OF PANCREAS: III. SOME PRECIPITATION REACTIONS OF INSULIN. *Journal of Biological Chemistry,* 58(1)**,** 337-346.

Kimura, R., Okouchi, M., Fujioka, H., Ichiyanagi, A., Ryuge, F., Mizuno, T., Imaeda, K., Okayama, N., Kamiya, Y., Asai, K. & Joh, T. (2009) Glucagon-like peptide-1 (GLP-1) protects against methylglyoxal-induced PC12 cell apoptosis through the PI3K/Akt/mTOR/GCLc/redox signaling pathway. *Neuroscience,* 162(4)**,** 1212-9.

Kinoshita, A., Fukumoto, H., Shah, T., Whelan, C. M., Irizarry, M. C. & Hyman, B. T. (2003) Demonstration by FRET of BACE interaction with the amyloid precursor protein at the cell surface and in early endosomes. *J Cell Sci,* 116(Pt 16)**,** 3339-46.

Kinoshita, A., Whelan, C. M., Berezovska, O. & Hyman, B. T. (2002) The γ secretase-generated carboxyl-terminal domain of the amyloid precursor protein induces apoptosis via Tip60 in H4 cells. *Journal of Biological Chemistry,* 277(32)**,** 28530-28536.

Kipfer-Kauer, A., Mckinnon, S. J., Frueh, B. E. & Goldblum, D. (2010) Distribution of amyloid precursor protein and amyloid-beta in ocular hypertensive C57BL/6 mouse eyes. *Current eye research,* 35(9)**,** 828-834.

Kirfel, G., Borm, B., Rigort, A. & Herzog, V. (2002) The secretory beta-amyloid precursor protein is a motogen for human epidermal keratinocytes. *Eur J Cell Biol,* 81(12)**,** 664-76.

Klaver, C. C. W., Ott, A., Hofman, A., Assink, J. J. M., Breteler, M. M. B. & De Jong, P. T. V. M. (1999) Is Age-related Maculopathy Associated with Alzheimer's Disease?: The Rotterdam Study. *American Journal of Epidemiology,* 150(9)**,** 963-968.

Klein, R., Klein, B. E., Tomany, S. C., Meuer, S. M. & Huang, G. H. (2002) Ten-year incidence and progression of age-related maculopathy: The Beaver Dam eye study. *Ophthalmology,* 109(10)**,** 1767-79.

Koike, H., Tomioka, S., Sorimachi, H., Saido, T. C., Maruyama, K., Okuyama, A., Fujisawa-Sehara, A., Ohno, S., Suzuki, K. & Ishiura, S. (1999) Membrane-anchored metalloprotease MDC9 has an alpha-secretase activity responsible for processing the amyloid precursor protein. *Biochem J,* 343 Pt 2**,** 371-5.

Koyama, Y., Matsuzaki, S., Gomi, F., Yamada, K., Katayama, T., Sato, K., Kumada, T., Fukuda, A., Matsuda, S., Tano, Y. & Tohyama, M. (2008) Induction of Amyloid β Accumulation by ER Calcium Disruption and Resultant Upregulation of Angiogenic Factors in ARPE19 Cells. *Investigative Ophthalmology & Visual Science,* 49(6)**,** 2376-2383.

Krentz, A. J. (2018) Chapter 33 - Evolution of Glucose-Lowering Drugs for Type 2 Diabetes: A New Era of Cardioprotection. In: Bagchi, D. & Nair, S. (eds.) *Nutritional and Therapeutic Interventions for Diabetes and Metabolic Syndrome (Second Edition).* Academic Press.

Kreymann, B., Williams, G., Ghatei, M. A. & Bloom, S. R. (1987) Glucagon-like peptide-1 7-36: a physiological incretin in man. *Lancet,* 2(8571)**,** 1300-4.

Krishnan, T., Ravindran, R. D., Murthy, G. V., Vashist, P., Fitzpatrick, K. E., Thulasiraj, R. D., John, N., Maraini, G., Camparini, M., Chakravarthy, U. & Fletcher, A. E. (2010) Prevalence of early and late age-related macular degeneration in India: the INDEYE study. *Invest Ophthalmol Vis Sci,* 51(2)**,** 701-7.

Kuhn, P.-H., Wang, H., Dislich, B., Colombo, A., Zeitschel, U., Ellwart, J. W., Kremmer, E., Roßner, S. & Lichtenthaler, S. F. (2010) ADAM10 is the physiologically relevant, constitutive α-secretase of the amyloid precursor protein in primary neurons. *The EMBO Journal,* 29(17)**,** 3020-3032.

Kume, H., Sekijima, Y., Maruyama, K. & Kametani, F. (2003) gamma-Secretase can cleave amyloid precursor protein fragments independent of alpha- and beta-secretase pre-cutting. *Int J Mol Med,* 12(1)**,** 57-60.

Kwak, Y. D., Brannen, C. L., Qu, T., Kim, H. M., Dong, X., Soba, P., Majumdar, A., Kaplan, A., Beyreuther, K. & Sugaya, K. (2006) Amyloid precursor protein regulates differentiation of human neural stem cells. *Stem Cells Dev,* 15(3)**,** 381-9.

Lammich, S., Kojro, E., Postina, R., Gilbert, S., Pfeiffer, R., Jasionowski, M., Haass, C. & Fahrenholz, F. (1999) Constitutive and regulated alpha-secretase cleavage of Alzheimer's amyloid precursor protein by a disintegrin metalloprotease. *Proc Natl Acad Sci U S A,* 96(7)**,** 3922-7.

Lannfelt, L., Basun, H., Wahlund, L. O., Rowe, B. A. & Wagner, S. L. (1995) Decreased alpha-secretase-cleaved amyloid precursor protein as a diagnostic marker for Alzheimer's disease. *Nat Med,* 1(8)**,** 829-32.

Laßek, M., Weingarten, J., Wegner, M. & Volknandt, W. (2016) The Amyloid Precursor Protein—A Novel Player within the Molecular Array of Presynaptic Nanomachines. *Frontiers in Synaptic Neuroscience,* 7(21).

Latonen, L. & Laiho, M. (2005) Cellular UV damage responses—Functions of tumor suppressor p53. *Biochimica et Biophysica Acta (BBA) - Reviews on Cancer,* 1755(2)**,** 71-89.

Laudon, H., Hansson, E. M., Melén, K., Bergman, A., Farmery, M. R., Winblad, B., Lendahl, U., Von Heijne, G. & Näslund, J. (2005) A nine-transmembrane domain topology for presenilin 1. *J Biol Chem,* 280(42)**,** 35352-60.

Lavoie, M. J., Fraering, P. C., Ostaszewski, B. L., Ye, W., Kimberly, W. T., Wolfe, M. S. & Selkoe, D. J. (2003) Assembly of the gamma-secretase complex involves early formation of an intermediate subcomplex of Aph-1 and nicastrin. *J Biol Chem,* 278(39)**,** 37213-22.

Lazarov, O. & Demars, M. (2012) All in the Family: How the APPs Regulate Neurogenesis. *Frontiers in Neuroscience,* 6(81).

Leblanc, A. C., Koutroumanis, M. & Goodyer, C. G. (1998) Protein kinase C activation increases release of secreted amyloid precursor protein without decreasing Abeta production in human primary neuron cultures. *J Neurosci,* 18(8)**,** 2907-13.

Leriche, G., Chen, A. C., Kim, S., Selkoe, D. J. & Yang, J. (2016) Fluorescent Analogue of Batimastat Enables Imaging of α-Secretase in Living Cells. *ACS chemical neuroscience,* 7(1)**,** 40-45.

Leske, M. C., Wu, S. Y., Hennis, A., Nemesure, B., Yang, L., Hyman, L. & Schachat, A. P. (2006) Nine-year incidence of age-related macular degeneration in the Barbados Eye Studies. *Ophthalmology,* 113(1)**,** 29-35.

Li, M., Pehar, M., Liu, Y., Bhattacharyya, A., Zhang, S.-C., O'riordan, K. J., Burger, C., D'adamio, L. & Puglielli, L. (2015) The amyloid precursor protein (APP) intracellular domain regulates translation of p44, a short isoform of p53, through an IRES-dependent mechanism. *Neurobiology of aging,* 36(10)**,** 2725-2736.

Li, Y., Duffy, K. B., Ottinger, M. A., Ray, B., Bailey, J. A., Holloway, H. W., Tweedie, D., Perry, T., Mattson, M. P., Kapogiannis, D., Sambamurti, K., Lahiri, D. K. & Greig, N. H. (2010) GLP-1

receptor stimulation reduces amyloid-beta peptide accumulation and cytotoxicity in cellular and animal models of Alzheimer's disease. *Journal of Alzheimer's disease : JAD,* 19(4)**,** 1205-1219.

Li, Y., Perry, T., Kindy, M. S., Harvey, B. K., Tweedie, D., Holloway, H. W., Powers, K., Shen, H., Egan, J. M., Sambamurti, K., Brossi, A., Lahiri, D. K., Mattson, M. P., Hoffer, B. J., Wang, Y. & Greig, N. H. (2009) GLP-1 receptor stimulation preserves primary cortical and dopaminergic neurons in cellular and rodent models of stroke and Parkinsonism. *Proc Natl Acad Sci U S A,* 106(4)**,** 1285-90.

Li, Y., Wang, Y., Zhang, W., Jiang, L., Zhou, W., Liu, Z., Li, S. & Lu, H. (2018) Overexpression of Amyloid Precursor Protein Promotes the Onset of Seborrhoeic Keratosis and is Related to Skin Ageing. *Acta Derm Venereol,* 98(6)**,** 594-600.

Li, Y., Zhou, W., Tong, Y., He, G. & Song, W. (2006) Control of APP processing and Abeta generation level by BACE1 enzymatic activity and transcription. *Faseb j,* 20(2)**,** 285-92.

Lichtenthaler, S. F. (2011) α-secretase in Alzheimer's disease: molecular identity, regulation and therapeutic potential. *J Neurochem,* 116(1)**,** 10-21.

Lorenz, M., Pfeiffer, C., Steinsträsser, A., Becker, R. H., Rütten, H., Ruus, P. & Horowitz, M. (2013) Effects of lixisenatide once daily on gastric emptying in type 2 diabetes--relationship to postprandial glycemia. *Regul Pept,* 185**,** 1-8.

Lowery, L. A. & Van Vactor, D. (2009) The trip of the tip: understanding the growth cone machinery. *Nature reviews. Molecular cell biology,* 10(5)**,** 332-343.

Lu, D. C., Rabizadeh, S., Chandra, S., Shayya, R. F., Ellerby, L. M., Ye, X., Salvesen, G. S., Koo, E. H. & Bredesen, D. E. (2000) A second cytotoxic proteolytic peptide derived from amyloid β-protein precursor. *Nature Medicine,* 6(4)**,** 397-404.

Ludwig, A., Hundhausen, C., Lambert, M. H., Broadway, N., Andrews, R. C., Bickett, D. M., Leesnitzer, M. A. & Becherer, J. D. (2005) Metalloproteinase inhibitors for the disintegrin-like metalloproteinases ADAM10 and ADAM17 that differentially block constitutive and phorbol ester-inducible shedding of cell surface molecules. *Comb Chem High Throughput Screen,* 8(2)**,** 161-71.

Luibl, V., Isas, J. M., Kayed, R., Glabe, C. G., Langen, R. & Chen, J. (2006) Drusen deposits associated with aging and age-related macular degeneration contain nonfibrillar amyloid oligomers. *The Journal of clinical investigation,* 116(2)**,** 378-385.

Luo, W.-J., Wang, H., Li, H., Kim, B. S., Shah, S., Lee, H.-J., Thinakaran, G., Kim, T.-W., Yu, G. & Xu, H. (2003) PEN-2 and APH-1 Coordinately Regulate Proteolytic Processing of Presenilin 1. *Journal of Biological Chemistry,* 278(10)**,** 7850-7854.

Maminishkis, A., Chen, S., Jalickee, S., Banzon, T., Shi, G., Wang, F. E., Ehalt, T., Hammer, J. A. & Miller, S. S. (2006) Confluent monolayers of cultured human fetal retinal pigment epithelium exhibit morphology and physiology of native tissue. *Invest Ophthalmol Vis Sci,* 47(8)**,** 3612-24.

Mao, H. & Ito, Y. (2017) 4.19 Growth Factors and Protein-Modified Surfaces and Interfaces☆. In: Ducheyne, P. (ed.) *Comprehensive Biomaterials II.* Oxford: Elsevier.

Marambaud, P., Shioi, J., Serban, G., Georgakopoulos, A., Sarner, S., Nagy, V., Baki, L., Wen, P., Efthimiopoulos, S., Shao, Z., Wisniewski, T. & Robakis, N. K. (2002) A presenilin-1/γ-secretase cleavage releases the E-cadherin intracellular domain and regulates disassembly of adherens junctions. *The EMBO Journal,* 21(8)**,** 1948-1956.

Martone, R. L., Zhou, H., Atchison, K., Comery, T., Xu, J. Z., Huang, X., Gong, X., Jin, M., Kreft, A., Harrison, B., Mayer, S. C., Aschmies, S., Gonzales, C., Zaleska, M. M., Riddell, D. R., Wagner, E., Lu, P., Sun, S. C., Sonnenberg-Reines, J., Oganesian, A., Adkins, K., Leach, M. W., Clarke, D. W., Huryn, D., Abou-Gharbia, M., Magolda, R., Bard, J., Frick, G., Raje, S., Forlow, S. B., Balliet, C., Burczynski, M. E., Reinhart, P. H., Wan, H. I., Pangalos, M. N. & Jacobsen, J. S. (2009) Begacestat (GSI-953): a novel, selective thiophene sulfonamide inhibitor of amyloid

precursor protein gamma-secretase for the treatment of Alzheimer's disease. *J Pharmacol Exp Ther,* 331(2)**,** 598-608.
Masuda, N., Tsujinaka, H., Hirai, H., Yamashita, M., Ueda, T. & Ogata, N. (2019) Effects of concentration of amyloid β (Aβ) on viability of cultured retinal pigment epithelial cells. *BMC Ophthalmol,* 19(1)**,** 70.
Masuzzo, A., Dinet, V., Cavanagh, C., Mascarelli, F. & Krantic, S. (2016) Amyloidosis in Retinal Neurodegenerative Diseases. *Frontiers in Neurology,* 7(127).
Mathenge, W. (2014) Age-related macular degeneration. *Community eye health,* 27(87)**,** 49-50.
Mathenge, W., Bastawrous, A., Foster, A. & Kuper, H. (2012) The Nakuru posterior segment eye disease study: methods and prevalence of blindness and visual impairment in Nakuru, Kenya. *Ophthalmology,* 119(10)**,** 2033-9.
Mattson, M. P., Cheng, B., Culwell, A. R., Esch, F. S., Lieberburg, I. & Rydel, R. E. (1993) Evidence for excitoprotective and intraneuronal calcium-regulating roles for secreted forms of the β-amyloid precursor protein. *Neuron,* 10(2)**,** 243-254.
Mayer, S. C., Kreft, A. F., Harrison, B., Abou-Gharbia, M., Antane, M., Aschmies, S., Atchison, K., Chlenov, M., Cole, D. C., Comery, T., Diamantidis, G., Ellingboe, J., Fan, K., Galante, R., Gonzales, C., Ho, D. M., Hoke, M. E., Hu, Y., Huryn, D., Jain, U., Jin, M., Kremer, K., Kubrak, D., Lin, M., Lu, P., Magolda, R., Martone, R., Moore, W., Oganesian, A., Pangalos, M. N., Porte, A., Reinhart, P., Resnick, L., Riddell, D. R., Sonnenberg-Reines, J., Stock, J. R., Sun, S. C., Wagner, E., Wang, T., Woller, K., Xu, Z., Zaleska, M. M., Zeldis, J., Zhang, M., Zhou, H. & Jacobsen, J. S. (2008) Discovery of begacestat, a Notch-1-sparing gamma-secretase inhibitor for the treatment of Alzheimer's disease. *J Med Chem,* 51(23)**,** 7348-51.
Mayo, K. E., Miller, L. J., Bataille, D., Dalle, S., Göke, B., Thorens, B. & Drucker, D. J. (2003) International Union of Pharmacology. XXXV. The glucagon receptor family. *Pharmacol Rev,* 55(1)**,** 167-94.
Mcclean, P. L. & Hölscher, C. (2014) Lixisenatide, a drug developed to treat type 2 diabetes, shows neuroprotective effects in a mouse model of Alzheimer's disease. *Neuropharmacology,* 86**,** 241-58.
Mcclean, P. L., Parthsarathy, V., Faivre, E. & Hölscher, C. (2011) The Diabetes Drug Liraglutide Prevents Degenerative Processes in a Mouse Model of Alzheimer's Disease. *The Journal of Neuroscience,* 31(17)**,** 6587-6594.
Mcfeat, G. D., Allinson, S. L. & Mcmillan, T. J. (2013) Characterisation of the p53-mediated cellular responses evoked in primary mouse cells following exposure to ultraviolet radiation. *PLoS One,* 8(9)**,** e75800.
Meloni, A. R., Deyoung, M. B., Lowe, C. & Parkes, D. G. (2013) GLP-1 receptor activated insulin secretion from pancreatic β-cells: mechanism and glucose dependence. *Diabetes, obesity & metabolism,* 15(1)**,** 15-27.
Meziane, H., Dodart, J. C., Mathis, C., Little, S., Clemens, J., Paul, S. M. & Ungerer, A. (1998) Memory-enhancing effects of secreted forms of the beta-amyloid precursor protein in normal and amnestic mice. *Proc Natl Acad Sci U S A,* 95(21)**,** 12683-8.
Mileusnic, R., Lancashire, C. L. & Rose, S. P. (2004) The peptide sequence Arg-Glu-Arg, present in the amyloid precursor protein, protects against memory loss caused by A beta and acts as a cognitive enhancer. *Eur J Neurosci,* 19(7)**,** 1933-8.
Mills, J. & Reiner, P. B. (1999) Regulation of Amyloid Precursor Protein Cleavage. *Journal of Neurochemistry,* 72(2)**,** 443-460.
Milward, E. A., Papadopoulos, R., Fuller, S. J., Moir, R. D., Small, D., Beyreuther, K. & Masters, C. L. (1992) The amyloid protein precursor of Alzheimer's disease is a mediator of the effects of nerve growth factor on neurite outgrowth. *Neuron,* 9(1)**,** 129-37.
Mohan, M. J., Seaton, T., Mitchell, J., Howe, A., Blackburn, K., Burkhart, W., Moyer, M., Patel, I., Waitt, G. M., Becherer, J. D., Moss, M. L. & Milla, M. E. (2002) The Tumor Necrosis Factor-α

Converting Enzyme (TACE): A Unique Metalloproteinase with Highly Defined Substrate Selectivity. *Biochemistry,* 41(30)**,** 9462-9469.
Morin, P. J., Abraham, C. R., Amaratunga, A., Johnson, R. J., Huber, G., Sandell, J. H. & Fine, R. E. (1993) Amyloid precursor protein is synthesized by retinal ganglion cells, rapidly transported to the optic nerve plasma membrane and nerve terminals, and metabolized. *J Neurochem,* 61(2)**,** 464-73.
Müller, T., Concannon, C. G., Ward, M. W., Walsh, C. M., Tirniceriu, A. L., Tribl, F., Kögel, D., Prehn, J. H. M. & Egensperger, R. (2007) Modulation of Gene Expression and Cytoskeletal Dynamics by the Amyloid Precursor Protein Intracellular Domain (AICD). *Molecular Biology of the Cell,* 18(1)**,** 201-210.
Muller, T., Meyer, H. E., Egensperger, R. & Marcus, K. (2008) The amyloid precursor protein intracellular domain (AICD) as modulator of gene expression, apoptosis, and cytoskeletal dynamics-relevance for Alzheimer's disease. *Prog Neurobiol,* 85(4)**,** 393-406.
Müller, T., Meyer, H. E., Egensperger, R. & Marcus, K. (2008) The amyloid precursor protein intracellular domain (AICD) as modulator of gene expression, apoptosis, and cytoskeletal dynamics—Relevance for Alzheimer's disease. *Progress in Neurobiology,* 85(4)**,** 393-406.
Müller, T. D., Finan, B., Bloom, S. R., D'alessio, D., Drucker, D. J., Flatt, P. R., Fritsche, A., Gribble, F., Grill, H. J., Habener, J. F., Holst, J. J., Langhans, W., Meier, J. J., Nauck, M. A., Perez-Tilve, D., Pocai, A., Reimann, F., Sandoval, D. A., Schwartz, T. W., Seeley, R. J., Stemmer, K., Tang-Christensen, M., Woods, S. C., Dimarchi, R. D. & Tschöp, M. H. (2019) Glucagon-like peptide 1 (GLP-1). *Molecular metabolism,* 30**,** 72-130.
Mullins, R. F., Russell, S. R., Anderson, D. H. & Hageman, G. S. (2000) Drusen associated with aging and age-related macular degeneration contain proteins common to extracellular deposits associated with atherosclerosis, elastosis, amyloidosis, and dense deposit disease. *Faseb j,* 14(7)**,** 835-46.
Multhaup, G., Huber, O., Buée, L. & Galas, M.-C. (2015) Amyloid Precursor Protein (APP) Metabolites APP Intracellular Fragment (AICD), Aβ42, and Tau in Nuclear Roles. *The Journal of biological chemistry,* 290(39)**,** 23515-23522.
Mun, S.-E., Sim, B.-W., Yoon, S.-B., Jeong, P.-S., Yang, H.-J., Choi, S.-A., Park, Y.-H., Kim, Y.-H., Kang, P., Jeong, K.-J., Lee, Y., Jin, Y. B., Song, B.-S., Kim, J.-S., Huh, J.-W., Lee, S.-R., Choo, Y.-K., Kim, S.-U. & Chang, K.-T. (2017) Dual effect of fetal bovine serum on early development depends on stage-specific reactive oxygen species demands in pigs. *PLOS ONE,* 12(4)**,** e0175427.
Murphy, R. F., Elmore, D. T. & Buchanan, K. D. (1971) Isolation of glucagon-like immunoreactivity of gut by affinity chromatography. *Biochem J,* 125(3)**,** 61p-62p.
Nass, N., Weissenberg, K., Somoza, V., Ruhs, S., Silber, R. E. & Simm, A. (2014) Cell culture condition-dependent impact of AGE-rich food extracts on kinase activation and cell survival on human fibroblasts. *Int J Food Sci Nutr,* 65(2)**,** 219-25.
Naus, S., Reipschläger, S., Wildeboer, D., Lichtenthaler, S. F., Mitterreiter, S., Guan, Z., Moss, M. L. & Bartsch, J. W. (2006) Identification of candidate substrates for ectodomain shedding by the metalloprotease-disintegrin ADAM8. 387(3)**,** 337-346.
Nhan, H. S., Chiang, K. & Koo, E. H. (2015) The multifaceted nature of amyloid precursor protein and its proteolytic fragments: friends and foes. *Acta neuropathologica,* 129(1)**,** 1-19.
Nikolaev, A., Mclaughlin, T., O'leary, D. D. & Tessier-Lavigne, M. (2009) APP binds DR6 to trigger axon pruning and neuron death via distinct caspases. *Nature,* 457(7232)**,** 981-9.
Ning, A., Cui, J., To, E., Ashe, K. H. & Matsubara, J. (2008) Amyloid-β Deposits Lead to Retinal Degeneration in a Mouse Model of Alzheimer Disease. *Investigative Ophthalmology & Visual Science,* 49(11)**,** 5136-5143.
Nowak, M., Gnitecki, W. & Jurowski, P. (2005) [The role of retinal oxygen metabolism in origin of age-related macular degeneration (AMD)]. *Klin Oczna,* 107(10-12)**,** 715-8.
Nozaki, M., Raisler, B. J., Sakurai, E., Sarma, J. V., Barnum, S. R., Lambris, J. D., Chen, Y., Zhang, K., Ambati, B. K., Baffi, J. Z. & Ambati, J. (2006) Drusen complement components C3a and C5a

promote choroidal neovascularization. *Proceedings of the National Academy of Sciences of the United States of America,* 103(7)**,** 2328-2333.
Nussenblatt, R. B. & Ferris, F., 3rd (2007) Age-related macular degeneration and the immune response: implications for therapy. *American journal of ophthalmology,* 144(4)**,** 618-626.
O'brien, R. J. & Wong, P. C. (2011) Amyloid precursor protein processing and Alzheimer's disease. *Annual review of neuroscience,* 34**,** 185-204.
Obregon, D., Hou, H., Deng, J., Giunta, B., Tian, J., Darlington, D., Shahaduzzaman, M., Zhu, Y., Mori, T., Mattson, M. P. & Tan, J. (2012) Soluble amyloid precursor protein-α modulates β-secretase activity and amyloid-β generation. *Nat Commun,* 3**,** 777.
Oh, Y. S. & Jun, H.-S. (2017) Effects of Glucagon-Like Peptide-1 on Oxidative Stress and Nrf2 Signaling. *International journal of molecular sciences,* 19(1)**,** 26.
Ohno-Matsui, K. (2011) Parallel findings in age-related macular degeneration and Alzheimer's disease. *Prog Retin Eye Res,* 30(4)**,** 217-38.
Ohsawa, I., Takamura, C., Morimoto, T., Ishiguro, M. & Kohsaka, S. (1999) Amino-terminal region of secreted form of amyloid precursor protein stimulates proliferation of neural stem cells. *European Journal of Neuroscience,* 11(6)**,** 1907-1913.
Ohtake, N., Saito, M., Eto, M. & Seki, K. (2014) Exendin-4 promotes the membrane trafficking of the AMPA receptor GluR1 subunit and ADAM10 in the mouse neocortex. *Regul Pept,* 190-191**,** 1-11.
Ong, S. S., Proia, A. D., Whitson, H. E., Farsiu, S., Doraiswamy, P. M. & Lad, E. M. (2019) Ocular amyloid imaging at the crossroad of Alzheimer's disease and age-related macular degeneration: implications for diagnosis and therapy. *Journal of Neurology,* 266(7)**,** 1566-1577.
Oraki Kohshour, M., Najafi, L., Heidari, M. & Ghaffari Sharaf, M. (2013) Antiproliferative Effect of H2O2 against Human Acute Myelogenous Leukemia KG1 Cell Line. *Journal of Acupuncture and Meridian Studies,* 6(3)**,** 134-141.
Orskov, C., Holst, J. J., Poulsen, S. S. & Kirkegaard, P. (1987) Pancreatic and intestinal processing of proglucagon in man. *Diabetologia,* 30(11)**,** 874-81.
Orskov, C. & Nielsen, J. H. (1988) Truncated glucagon-like peptide-1 (proglucagon 78-107 amide), an intestinal insulin-releasing peptide, has specific receptors on rat insulinoma cells (RIN 5AH). *FEBS Lett,* 229(1)**,** 175-8.
Owen, C. G., Jarrar, Z., Wormald, R., Cook, D. G., Fletcher, A. E. & Rudnicka, A. R. (2012) The estimated prevalence and incidence of late stage age related macular degeneration in the UK. *British Journal of Ophthalmology,* 96(5)**,** 752.
Ozaki, T., Li, Y., Kikuchi, H., Tomita, T., Iwatsubo, T. & Nakagawara, A. (2006) The intracellular domain of the amyloid precursor protein (AICD) enhances the p53-mediated apoptosis. *Biochemical and Biophysical Research Communications,* 351(1)**,** 57-63.
Panagaki, T., Michael, M. & Hölscher, C. (2017) Liraglutide restores chronic ER stress, autophagy impairments and apoptotic signalling in SH-SY5Y cells. *Scientific Reports,* 7(1)**,** 16158.
Park, M. K. (2016) Subchapter 17C - Glucagon-Like Peptide-1. In: Takei, Y., Ando, H. & Tsutsui, K. (eds.) *Handbook of Hormones.* San Diego: Academic Press.
Parkin, E. & Harris, B. (2009) A disintegrin and metalloproteinase (ADAM)-mediated ectodomain shedding of ADAM10. *J Neurochem,* 108(6)**,** 1464-79.
Parkin, E. T., Trew, A., Christie, G., Faller, A., Mayer, R., Turner, A. J. & Hooper, N. M. (2002) Structure−Activity Relationship of Hydroxamate-Based Inhibitors on the Secretases that Cleave the Amyloid Precursor Protein, Angiotensin Converting Enzyme, CD23, and Pro-Tumor Necrosis Factor-α. *Biochemistry,* 41(15)**,** 4972-4981.
Parmet, S., Lynm, C. & Glass, R. M. (2006) Age-Related Macular Degeneration. *JAMA,* 295(20)**,** 2438-2438.
Parvathy, S., Hussain, I., Karran, E. H., Turner, A. J. & Hooper, N. M. (1998) Alzheimer's amyloid precursor protein alpha-secretase is inhibited by hydroxamic acid-based zinc

metalloprotease inhibitors: similarities to the angiotensin converting enzyme secretase. *Biochemistry,* 37(6)**,** 1680-5.

Parvathy, S., Hussain, I., Karran, E. H., Turner, A. J. & Hooper, N. M. (1999) Cleavage of Alzheimer's amyloid precursor protein by alpha-secretase occurs at the surface of neuronal cells. *Biochemistry,* 38(30)**,** 9728-34.

Pascolini, D. & Mariotti, S. P. (2012) Global estimates of visual impairment: 2010. *Br J Ophthalmol,* 96(5)**,** 614-8.

Patzelt, C., Tager, H. S., Carroll, R. J. & Steiner, D. F. (1979) Identification and processing of proglucagon in pancreatic islets. *Nature,* 282(5736)**,** 260-6.

Pawlowska, E., Szczepanska, J., Koskela, A., Kaarniranta, K. & Blasiak, J. (2019) Dietary Polyphenols in Age-Related Macular Degeneration: Protection against Oxidative Stress and Beyond. *Oxidative Medicine and Cellular Longevity,* 2019**,** 9682318.

Pennington, K. L. & Deangelis, M. M. (2016) Epidemiology of age-related macular degeneration (AMD): associations with cardiovascular disease phenotypes and lipid factors. *Eye and vision (London, England),* 3**,** 34-34.

Perazella, M. A. & Shirali, A. (2014) 37 - Kidney Disease Caused by Therapeutic Agents. In: Gilbert, S. J. & Weiner, D. E. (eds.) *National Kidney Foundation Primer on Kidney Diseases (Sixth Edition).* Philadelphia: W.B. Saunders.

Perry, T., Haughey, N. J., Mattson, M. P., Egan, J. M. & Greig, N. H. (2002a) Protection and Reversal of Excitotoxic Neuronal Damage by Glucagon-Like Peptide-1 and Exendin-4. *Journal of Pharmacology and Experimental Therapeutics,* 302(3)**,** 881-888.

Perry, T., Lahiri, D. K., Chen, D., Zhou, J., Shaw, K. T., Egan, J. M. & Greig, N. H. (2002b) A novel neurotrophic property of glucagon-like peptide 1: a promoter of nerve growth factor-mediated differentiation in PC12 cells. *J Pharmacol Exp Ther,* 300(3)**,** 958-66.

Perry, T., Lahiri, D. K., Sambamurti, K., Chen, D., Mattson, M. P., Egan, J. M. & Greig, N. H. (2003) Glucagon-like peptide-1 decreases endogenous amyloid-beta peptide (Abeta) levels and protects hippocampal neurons from death induced by Abeta and iron. *J Neurosci Res,* 72(5)**,** 603-12.

Petersen, K. E., Rakipovski, G., Raun, K. & Lykkesfeldt, J. (2016) Does Glucagon-like Peptide-1 Ameliorate Oxidative Stress in Diabetes? Evidence Based on Experimental and Clinical Studies. *Current diabetes reviews,* 12(4)**,** 331-358.

Pietrzik, C. U., Hoffmann, J., Stöber, K., Chen, C. Y., Bauer, C., Otero, D. A., Roch, J. M. & Herzog, V. (1998) From differentiation to proliferation: the secretory amyloid precursor protein as a local mediator of growth in thyroid epithelial cells. *Proceedings of the National Academy of Sciences of the United States of America,* 95(4)**,** 1770-1775.

Pirttila, T., Kim, K. S., Mehta, P. D., Frey, H. & Wisniewski, H. M. (1994) Soluble amyloid beta-protein in the cerebrospinal fluid from patients with Alzheimer's disease, vascular dementia and controls. *J Neurol Sci,* 127(1)**,** 90-5.

Plestina-Borjan, I. & Klinger-Lasić, M. (2007) Long-term exposure to solar ultraviolet radiation as a risk factor for age-related macular degeneration. *Collegium antropologicum,* 31 Suppl 1**,** 33-8.

Plummer, S., Van Den Heuvel, C., Thornton, E., Corrigan, F. & Cappai, R. (2016) The Neuroprotective Properties of the Amyloid Precursor Protein Following Traumatic Brain Injury. *Aging Dis,* 7(2)**,** 163-79.

Postina, R., Schroeder, A., Dewachter, I., Bohl, J., Schmitt, U., Kojro, E., Prinzen, C., Endres, K., Hiemke, C., Blessing, M., Flamez, P., Dequenne, A., Godaux, E., Van Leuven, F. & Fahrenholz, F. (2004) A disintegrin-metalloproteinase prevents amyloid plaque formation and hippocampal defects in an Alzheimer disease mouse model. *J Clin Invest,* 113(10)**,** 1456-64.

Prakasam, A., Muthuswamy, A., Ablonczy, Z., Greig, N. H., Fauq, A., Rao, K. J., Pappolla, M. A. & Sambamurti, K. (2010) Differential accumulation of secreted AbetaPP metabolites in ocular fluids. *Journal of Alzheimer's disease : JAD,* 20(4)**,** 1243-1253.

Prasad, T., Zhu, P., Verma, A., Chakrabarty, P., Rosario, A. M., Golde, T. E. & Li, Q. (2017) Amyloid β peptides overexpression in retinal pigment epithelial cells via AAV-mediated gene transfer mimics AMD-like pathology in mice. *Sci Rep,* 7(1)**,** 3222.

Prokop, S., Shirotani, K., Edbauer, D., Haass, C. & Steiner, H. (2004) Requirement of PEN-2 for Stabilization of the Presenilin N-/C-terminal Fragment Heterodimer within the γ-Secretase Complex. *Journal of Biological Chemistry,* 279(22)**,** 23255-23261.

Puddu, A., Sanguineti, R., Montecucco, F. & Viviani, G. L. (2013) Retinal pigment epithelial cells express a functional receptor for glucagon-like peptide-1 (GLP-1). *Mediators of inflammation,* 2013**,** 975032-975032.

Quast, T., Wehner, S., Kirfel, G., Jaeger, K., De Luca, M. & Herzog, V. (2003) sAPP as a regulator of dendrite motility and melanin release in epidermal melanocytes and melanoma cells. *FASEB journal : official publication of the Federation of American Societies for Experimental Biology,* 17(12)**,** 1739-1741.

Ramnanan, C. J., Edgerton, D. S., Kraft, G. & Cherrington, A. D. (2011) Physiologic action of glucagon on liver glucose metabolism. *Diabetes, obesity & metabolism,* 13 Suppl 1(Suppl 1)**,** 118-125.

Ramos, T. V., Mathew, A. J., Thompson, M. L. & Ehrhardt, R. O. (2014) Standardized Cryopreservation of Human Primary Cells. *Current Protocols in Cell Biology,* 64(1)**,** A.3I.1-A.3I.8.

Ratnayaka, J. A., Serpell, L. C. & Lotery, A. J. (2015) Dementia of the eye: the role of amyloid beta in retinal degeneration. *Eye (London, England),* 29(8)**,** 1013-1026.

Ratner, R. E., Rosenstock, J., Boka, G. & Investigators, D. R. I. S. (2010) Dose-dependent effects of the once-daily GLP-1 receptor agonist lixisenatide in patients with Type 2 diabetes inadequately controlled with metformin: a randomized, double-blind, placebo-controlled trial. *Diabetic medicine : a journal of the British Diabetic Association,* 27(9)**,** 1024-1032.

Rattner, A. & Nathans, J. (2006) Macular degeneration: recent advances and therapeutic opportunities. *Nature Reviews Neuroscience,* 7(11)**,** 860-872.

Ring, S., Weyer, S. W., Kilian, S. B., Waldron, E., Pietrzik, C. U., Filippov, M. A., Herms, J., Buchholz, C., Eckman, C. B., Korte, M., Wolfer, D. P. & Müller, U. C. (2007) The secreted beta-amyloid precursor protein ectodomain APPs alpha is sufficient to rescue the anatomical, behavioral, and electrophysiological abnormalities of APP-deficient mice. *J Neurosci,* 27(29)**,** 7817-26.

Roberts, J. E. (2001) Ocular phototoxicity. *Journal of Photochemistry and Photobiology B: Biology,* 64(2)**,** 136-143.

Roberts, J. E. (2011) Ultraviolet radiation as a risk factor for cataract and macular degeneration. *Eye Contact Lens,* 37(4)**,** 246-9.

Roch, J. M., Masliah, E., Roch-Levecq, A. C., Sundsmo, M. P., Otero, D. A., Veinbergs, I. & Saitoh, T. (1994) Increase of synaptic density and memory retention by a peptide representing the trophic domain of the amyloid beta/A4 protein precursor. *Proceedings of the National Academy of Sciences of the United States of America,* 91(16)**,** 7450-7454.

Roghani, M., Becherer, J. D., Moss, M. L., Atherton, R. E., Erdjument-Bromage, H., Arribas, J., Blackburn, R. K., Weskamp, G., Tempst, P. & Blobel, C. P. (1999) Metalloprotease-disintegrin MDC9: intracellular maturation and catalytic activity. *J Biol Chem,* 274(6)**,** 3531-40.

Sagane, K., Yamazaki, K., Mizui, Y. & Tanaka, I. (1999) Cloning and chromosomal mapping of mouse ADAM11, ADAM22 and ADAM23. *Gene,* 236(1)**,** 79-86.

Saitoh, T., Sundsmo, M., Roch, J. M., Kimura, N., Cole, G., Schubert, D., Oltersdorf, T. & Schenk, D. B. (1989) Secreted form of amyloid beta protein precursor is involved in the growth regulation of fibroblasts. *Cell,* 58(4)**,** 615-22.

Salvi, S. M., Akhtar, S. & Currie, Z. (2006) Ageing changes in the eye. *Postgraduate medical journal,* 82(971)**,** 581-587.

Sambamurti, K., Venugopal, C., Suram, A., Pappolla, M., Rohrer, B. & Annamalai, P. (2007) Amyloid Precursor Protein Metabolism in Retinal Degeneration. *Investigative Ophthalmology & Visual Science,* 48(13)**,** 26-26.

Santamaria, A. B., Davis, D. W., Nghiem, D. X., Mcconkey, D. J., Ullrich, S. E., Kapoor, M., Lozano, G. & Ananthaswamy, H. N. (2002) p53 and Fas ligand are required for psoralen and UVA-induced apoptosis in mouse epidermal cells. *Cell Death & Differentiation,* 9(5)**,** 549-560.

Sayre, L. M., Perry, G., Harris, P. L., Liu, Y., Schubert, K. A. & Smith, M. A. (2000) In situ oxidative catalysis by neurofibrillary tangles and senile plaques in Alzheimer's disease: a central role for bound transition metals. *J Neurochem,* 74(1)**,** 270-9.

Scharfenberg, F., Armbrust, F., Marengo, L., Pietrzik, C. & Becker-Pauly, C. (2019) Regulation of the alternative β-secretase meprin β by ADAM-mediated shedding. *Cellular and molecular life sciences : CMLS,* 76(16)**,** 3193-3206.

Scripsema, N. K., Hu, D. N. & Rosen, R. B. (2015) Lutein, Zeaxanthin, and meso-Zeaxanthin in the Clinical Management of Eye Disease. *J Ophthalmol,* 2015**,** 865179.

Seals, D. F. & Courtneidge, S. A. (2003) The ADAMs family of metalloproteases: multidomain proteins with multiple functions. *Genes Dev,* 17(1)**,** 7-30.

Seegar, T. C. M., Killingsworth, L. B., Saha, N., Meyer, P. A., Patra, D., Zimmerman, B., Janes, P. W., Rubinstein, E., Nikolov, D. B., Skiniotis, G., Kruse, A. C. & Blacklow, S. C. (2017) Structural Basis for Regulated Proteolysis by the α-Secretase ADAM10. *Cell,* 171(7)**,** 1638-1648.e7.

Segeritz, C.-P. & Vallier, L. (2017) Cell Culture: Growing Cells as Model Systems In Vitro. *Basic Science Methods for Clinical Researchers***,** 151-172.

Sekar, R., Singh, K., Arokiaraj, A. W. R. & Chow, B. K. C. (2016) Chapter Seven - Pharmacological Actions of Glucagon-Like Peptide-1, Gastric Inhibitory Polypeptide, and Glucagon. In: Jeon, K. W. & Galluzzi, L. (eds.) *International Review of Cell and Molecular Biology.* Academic Press.

Shah, S., Lee, S. F., Tabuchi, K., Hao, Y. H., Yu, C., Laplant, Q., Ball, H., Dann, C. E., 3rd, Südhof, T. & Yu, G. (2005) Nicastrin functions as a gamma-secretase-substrate receptor. *Cell,* 122(3)**,** 435-47.

Shahandeh, A., Purushothuman, S., Martin, K., Graham, M., Johnstone, D. & Milward, E. (2015) Anti-Oxidant Phytochemicals As Potential Treatments For Age-Related Macular Degeneration. *Journal of Antioxidant Activity,* 1**,** 26-38.

Sharma, M. K., Jalewa, J. & Hölscher, C. (2014) Neuroprotective and anti-apoptotic effects of liraglutide on SH-SY5Y cells exposed to methylglyoxal stress. *Journal of Neurochemistry,* 128(3)**,** 459-471.

Shu, X., Zhang, Y., Li, M., Huang, X., Yang, Y., Zeng, J., Zhao, Y., Wang, X., Zhang, W. & Ying, Y. (2019) Topical ocular administration of the GLP-1 receptor agonist liraglutide arrests hyperphosphorylated tau-triggered diabetic retinal neurodegeneration via activation of GLP-1R/Akt/GSK3β signaling. *Neuropharmacology,* 153**,** 1-12.

Sisodia, S. S. (1992) Beta-amyloid precursor protein cleavage by a membrane-bound protease. *Proceedings of the National Academy of Sciences of the United States of America,* 89(13)**,** 6075-6079.

Sisodia, S. S., Koo, E. H., Beyreuther, K., Unterbeck, A. & Price, D. L. (1990) Evidence that beta-amyloid protein in Alzheimer's disease is not derived by normal processing. *Science,* 248(4954)**,** 492-5.

Slack, B. E., Ma, L. K. & Seah, C. C. (2001) Constitutive shedding of the amyloid precursor protein ectodomain is up-regulated by tumour necrosis factor-alpha converting enzyme. *Biochem J,* 357(Pt 3)**,** 787-94.

Smith-Swintosky, V. L., Pettigrew, L. C., Craddock, S. D., Culwell, A. R., Rydel, R. E. & Mattson, M. P. (1994) Secreted forms of beta-amyloid precursor protein protect against ischemic brain injury. *Journal of neurochemistry,* 63(2)**,** 781-784.

Sonia, T. A. & Sharma, C. P. (2014) 1 - Diabetes mellitus – an overview. In: Sonia, T. A. & Sharma, C. P. (eds.) *Oral Delivery of Insulin.* Woodhead Publishing.

Sosa, L. J., Cáceres, A., Dupraz, S., Oksdath, M., Quiroga, S. & Lorenzo, A. (2017) The physiological role of the amyloid precursor protein as an adhesion molecule in the developing nervous system. *Journal of Neurochemistry,* 143(1)**,** 11-29.

Stachel, S. J., Coburn, C. A., Steele, T. G., Jones, K. G., Loutzenhiser, E. F., Gregro, A. R., Rajapakse, H. A., Lai, M. T., Crouthamel, M. C., Xu, M., Tugusheva, K., Lineberger, J. E., Pietrak, B. L., Espeseth, A. S., Shi, X. P., Chen-Dodson, E., Holloway, M. K., Munshi, S., Simon, A. J., Kuo, L. & Vacca, J. P. (2004) Structure-based design of potent and selective cell-permeable inhibitors of human beta-secretase (BACE-1). *J Med Chem,* 47(26)**,** 6447-50.

Streilein, J. W. (2003) Ocular immune privilege: therapeutic opportunities from an experiment of nature. *Nat Rev Immunol,* 3(11)**,** 879-89.

Sun, X., Chen, W.-D. & Wang, Y.-D. (2015) β-Amyloid: the key peptide in the pathogenesis of Alzheimer's disease. *Frontiers in pharmacology,* 6**,** 221-221.

Tackenberg, C. & Nitsch, R. M. (2019) The secreted APP ectodomain sAPPα, but not sAPPβ, protects neurons against Aβ oligomer-induced dendritic spine loss and increased tau phosphorylation. *Molecular Brain,* 12(1)**,** 27.

Tanabe, C., Hotoda, N., Sasagawa, N., Sehara-Fujisawa, A., Maruyama, K. & Ishiura, S. (2007) ADAM19 is tightly associated with constitutive Alzheimer's disease APP alpha-secretase in A172 cells. *Biochem Biophys Res Commun,* 352(1)**,** 111-7.

Tangtrongsup, S. & Kisiday, J. D. (2018) Modulating the oxidative environment during mesenchymal stem cells chondrogenesis with serum increases collagen accumulation in agarose culture. *J Orthop Res,* 36(1)**,** 506-514.

Taylor, C. J., Ireland, D. R., Ballagh, I., Bourne, K., Marechal, N. M., Turner, P. R., Bilkey, D. K., Tate, W. P. & Abraham, W. C. (2008) Endogenous secreted amyloid precursor protein-alpha regulates hippocampal NMDA receptor function, long-term potentiation and spatial memory. *Neurobiol Dis,* 31(2)**,** 250-60.

Thinakaran, G. & Koo, E. H. (2008) Amyloid Precursor Protein Trafficking, Processing, and Function. *Journal of Biological Chemistry,* 283(44)**,** 29615-29619.

Thumann, G., Dou, G., Wang, Y. & Hinton, D. R. (2013) Chapter 16 - Cell Biology of the Retinal Pigment Epithelium. In: Ryan, S. J., Sadda, S. R., Hinton, D. R., Schachat, A. P., Sadda, S. R., Wilkinson, C. P., Wiedemann, P. & Schachat, A. P. (eds.) *Retina (Fifth Edition).* London: W.B. Saunders.

Tomas, E., Stanojevic, V. & Habener, J. F. (2011) GLP-1-derived nonapeptide GLP-1(28–36)amide targets to mitochondria and suppresses glucose production and oxidative stress in isolated mouse hepatocytes. *Regulatory Peptides,* 167(2)**,** 177-184.

Topouzis, F., Anastasopoulos, E., Augood, C., Bentham, G. C., Chakravarthy, U., De Jong, P. T., Rahu, M., Seland, J., Soubrane, G., Tomazzoli, L., Vingerling, J. R., Vioque, J., Young, I. S. & Fletcher, A. E. (2009) Association of diabetes with age-related macular degeneration in the EUREYE study. *Br J Ophthalmol,* 93(8)**,** 1037-41.

Tousseyn, T., Thathiah, A., Jorissen, E., Raemaekers, T., Konietzko, U., Reiss, K., Maes, E., Snellinx, A., Serneels, L., Nyabi, O., Annaert, W., Saftig, P., Hartmann, D. & De Strooper, B. (2009) ADAM10, the Rate-limiting Protease of Regulated Intramembrane Proteolysis of Notch and Other Proteins, Is Processed by ADAMS-9, ADAMS-15, and the γ-Secretase*. *Journal of Biological Chemistry,* 284(17)**,** 11738-11747.

Tsang, J. Y. S., Lee, M. A., Chan, T.-H., Li, J., Ni, Y.-B., Shao, Y., Chan, S.-K., Cheungc, S.-Y., Lau, K.-F. & Tse, G. M. K. (2018) Proteolytic cleavage of amyloid precursor protein by ADAM10 mediates proliferation and migration in breast cancer. *EBioMedicine,* 38**,** 89-99.

Unger, R. H., Ohneda, A., Valverde, I., Eisentraut, A. M. & Exton, J. (1968) Characterization of the responses of circulating glucagon-like immunoreactivity to intraduodenal and intravenous administration of glucose. *J Clin Invest,* 47(1)**,** 48-65.

Valiente, M. & Marin, O. (2010) Neuronal migration mechanisms in development and disease. *Curr Opin Neurobiol,* 20(1)**,** 68-78.

Vandenbroucke, R. E. & Libert, C. (2014) Is there new hope for therapeutic matrix metalloproteinase inhibition? *Nature Reviews Drug Discovery,* 13(12)**,** 904-927.

Vassar, R., Bennett, B. D., Babu-Khan, S., Kahn, S., Mendiaz, E. A., Denis, P., Teplow, D. B., Ross, S., Amarante, P., Loeloff, R., Luo, Y., Fisher, S., Fuller, J., Edenson, S., Lile, J., Jarosinski, M. A., Biere, A. L., Curran, E., Burgess, T., Louis, J. C., Collins, F., Treanor, J., Rogers, G. & Citron, M. (1999) Beta-secretase cleavage of Alzheimer's amyloid precursor protein by the transmembrane aspartic protease BACE. *Science,* 286(5440)**,** 735-41.

Verma, R. P. (2012) Hydroxamic Acids as Matrix Metalloproteinase Inhibitors. In: Gupta, S. P. (ed.) *Matrix Metalloproteinase Inhibitors: Specificity of Binding and Structure-Activity Relationships.* Basel: Springer Basel.

Vojniković, B., Njirić, S., Čoklo, M. & Spanjol, J. (2007) Ultraviolet sun radiation and incidence of age-related macular degeneration on Croatian Island Rab. *Collegium antropologicum,* 31 Suppl 1**,** 43-4.

Walsh, K. *UV radiation and the Eye*. 2009.

Walter, J. & Haass, C. (2000) Posttranslational modifications of amyloid precursor protein : ectodomain phosphorylation and sulfation. *Methods Mol Med,* 32**,** 149-68.

Wang, D., Luo, P., Wang, Y., Li, W., Wang, C., Sun, D., Zhang, R., Su, T., Ma, X., Zeng, C., Wang, H., Ren, J. & Cao, F. (2013) Glucagon-like peptide-1 protects against cardiac microvascular injury in diabetes via a cAMP/PKA/Rho-dependent mechanism. *Diabetes,* 62(5)**,** 1697-708.

Wang, J., Zhu, C., Xu, Y., Liu, B., Wang, M. & Wu, K. (2011) Development and Expression of Amyloid-β Peptide 42 in Retinal Ganglion Cells in Rats. *The Anatomical Record,* 294(8)**,** 1401-1405.

Wang, R., Tang, P., Wang, P., Boissy, R. E. & Zheng, H. (2006) Regulation of tyrosinase trafficking and processing by presenilins: Partial loss of function by familial Alzheimer's disease mutation. *Proceedings of the National Academy of Sciences of the United States of America,* 103(2)**,** 353-358.

Wehner, S., Siemes, C., Kirfel, G. & Herzog, V. (2004) Cytoprotective function of sAppalpha in human keratinocytes. *Eur J Cell Biol,* 83(11-12)**,** 701-8.

Wei, Y. & Mojsov, S. (1995) Tissue-specific expression of the human receptor for glucagon-like peptide-I: brain, heart and pancreatic forms have the same deduced amino acid sequences. *FEBS Lett,* 358(3)**,** 219-24.

Weidemann, A., Konig, G., Bunke, D., Fischer, P., Salbaum, J. M., Masters, C. L. & Beyreuther, K. (1989) Identification, biogenesis, and localization of precursors of Alzheimer's disease A4 amyloid protein. *Cell,* 57(1)**,** 115-26.

Weskamp, G., Cai, H., Brodie, T. A., Higashyama, S., Manova, K., Ludwig, T. & Blobel, C. P. (2002) Mice lacking the metalloprotease-disintegrin MDC9 (ADAM9) have no evident major abnormalities during development or adult life. *Molecular and cellular biology,* 22(5)**,** 1537-1544.

Widomska, J. & Subczynski, W. K. (2019) Mechanisms enhancing the protective functions of macular xanthophylls in the retina during oxidative stress. *Experimental eye research,* 178**,** 238-246.

Wolfe, M. S., Xia, W., Ostaszewski, B. L., Diehl, T. S., Kimberly, W. T. & Selkoe, D. J. (1999) Two transmembrane aspartates in presenilin-1 required for presenilin endoproteolysis and γ-secretase activity. *Nature,* 398(6727)**,** 513-517.

Wong, W. L., Su, X., Li, X., Cheung, C. M. G., Klein, R., Cheng, C.-Y. & Wong, T. Y. (2014) Global prevalence of age-related macular degeneration and disease burden projection for 2020 and 2040: a systematic review and meta-analysis. *The Lancet Global Health,* 2(2)**,** e106-e116.

Woods, N. K. & Padmanabhan, J. (2013) Inhibition of amyloid precursor protein processing enhances gemcitabine-mediated cytotoxicity in pancreatic cancer cells. *J Biol Chem,* 288(42)**,** 30114-24.

Yan, R., Munzner, J. B., Shuck, M. E. & Bienkowski, M. J. (2001) BACE2 functions as an alternative alpha-secretase in cells. *J Biol Chem,* 276(36)**,** 34019-27.

Yoshida, T., Ohno-Matsui, K., Ichinose, S., Sato, T., Iwata, N., Saido, T. C., Hisatomi, T., Mochizuki, M. & Morita, I. (2005) The potential role of amyloid beta in the pathogenesis of age-related macular degeneration. *The Journal of clinical investigation,* 115(10)**,** 2793-2800.

Yoshikai, S.-I., Sasaki, H., Doh-Ura, K., Furuya, H. & Sakaki, Y. (1990) Genomic organization of the human amyloid beta-protein precursor gene. *Gene,* 87(2)**,** 257-263.

Youn, H.-Y., Mccanna, D. J., Sivak, J. G. & Jones, L. W. (2011) In vitro ultraviolet-induced damage in human corneal, lens, and retinal pigment epithelial cells. *Molecular vision,* 17**,** 237-246.

Young, R. W. (1987) Pathophysiology of age-related macular degeneration. *Survey of Ophthalmology,* 31(5)**,** 291-306.

Zarbin, M. A. & Rosenfeld, P. J. (2010) Pathway-based therapies for age-related macular degeneration: an integrated survey of emerging treatment alternatives. *Retina,* 30(9)**,** 1350-67.

Zhang, H. (2006) p53 plays a central role in UVA and UVB induced cell damage and apoptosis in melanoma cells. *Cancer Lett,* 244(2)**,** 229-38.

Zhang, P., Shen, M., Fernandez-Patron, C. & Kassiri, Z. (2016) ADAMs family and relatives in cardiovascular physiology and pathology. *Journal of Molecular and Cellular Cardiology,* 93**,** 186-199.

Zhang, X., Li, Y., Xu, H. & Zhang, Y.-W. (2014) The γ-secretase complex: from structure to function. *Frontiers in Cellular Neuroscience,* 8(427).

Zhang, X. & Song, W. (2013) The role of APP and BACE1 trafficking in APP processing and amyloid-β generation. *Alzheimer's Research & Therapy,* 5(5)**,** 46.

Zhou, H., Zhang, H., Yu, A. & Xie, J. (2018) Association between sunlight exposure and risk of age-related macular degeneration: a meta-analysis. *BMC Ophthalmology,* 18(1)**,** 331.

Zhou, R. & Caspi, R. R. (2010) Ocular immune privilege. *F1000 biology reports,* 2**,** 3.

Zolkiewska, A. (2008) ADAM proteases: ligand processing and modulation of the Notch pathway. *Cellular and molecular life sciences : CMLS,* 65(13)**,** 2056-2068.

Zou, J., Zhu, F., Liu, J., Wang, W., Zhang, R., Garlisi, C. G., Liu, Y.-H., Wang, S., Shah, H., Wan, Y. & Umland, S. P. (2004) Catalytic Activity of Human ADAM33*. *Journal of Biological Chemistry,* 279(11)**,** 9818-9830.

Books:

Green W.R. 1996. Ophthalmic Pathology, Volume 2, Chapter 9-Retina, pp 982-1047 W.B. Saunders Company.

White J., Bridges L., DeSimone D., Tomczuk M., and Wolfsberf T. 2005. Introduction to the ADAM Family, vol. 4, Springer, Dordrecht, The Netherlands.

Websites:

Elshatory, Y., Feldman, B., Tripathy, K., Kim, L. and Shah, V., 2019. *Age-Related Macular Degeneration - Eyewiki*. [online] Eyewiki.aao.org. Available at: <https://eyewiki.aao.org/Age-related_macular_degeneration#cite_note-Guymer_and_Bird_.282006.29-24> [Accessed 21 April 2020].

NHS.uk. 2020. *Age-Related Macular Degeneration (AMD) - Symptoms*. [online] Available at: <https://www.nhs.uk/conditions/age-related-macular-degeneration-amd/symptoms/> [Accessed 20 April 2020].

Nice.org.uk. 2020. *Recommendations | Age-Related Macular Degeneration | Guidance | NICE*. [online] Available at: <https://www.nice.org.uk/guidance/ng82/chapter/recommendations#table-1-age-related-macular-degeneration-classification> [Accessed 20 April 2020].